The role of *Ppargc1αlpha* in neuronal survival and myelination in the neocortex

A dissertation presented

by

Youshan Melissa Lin

to

The Division of Medical Sciences

in partial fulfillment of the requirements

for the degree of

Doctor of Philosophy

in the subject of

Human Biology and Translational Medicine

Harvard University

Cambridge, Massachusetts

December 2013

Professor Paola Arlotta Youshan Melissa Lin

The role of *Ppargc1αlpha* in neuronal survival and myelination in the neocortex

Abstract

The mammalian neocortex contains diverse neuronal and glial cell types. Among them lies an important subclass, the subcerebral projection neurons (SCPN) that project to distant targets like the spinal cord. Aiming at identifiying molecular controls over the postnatal development of SCPN, I focus my investigations on the role of *Ppargc1α* because its function remains relatively unknown in the brain while it is important for metabolism and survival in other tissue systems.

Ppargc1α function in neuronal survival has been studied within the context of acute cellular stress but its developmental function remains unexplored. Work presented in this dissertation began by studying whether *Ppargc1α* is required for neuronal survival, either in the native cellular state without acute stress, or in the context of aging. Focusing on the neocortex, I found that absence of *Ppargc1α* does not cause cortical abnormalities or enhanced cell death. Moreover, I found lesions in the internal capsule (IC) within the axonal path of SCPN and myelin-positive vacuoles in the *Ppargc1α* null neocortex. Analysis of newly generated conditional null mutants for *Ppargc1α* in the dorsal telencephalon revealed that conditional loss of *Ppargc1α* generates myelin-positive neocortical vacuoles but not IC-localized lesions. Thus, *Ppargc1α* is required for myelin-positive neocortical vacuoles but not for neuronal survival and IC-localized lesion formation.

Considering the role of *Ppargc1α* in metabolism, I discovered that neuron-specific *Ppargc1α* is required for proper neocortical myelination. I found that *Ppargc1α* is restricted to neurons and is excluded from oligodendrocytes in the neocortex. Interestingly, the absence of *Ppargc1α* in neurons or in the dorsal forebrain caused hypomyelination across all cortical layers. Aging studies of mutants at 18 months further revealed that these hypomyelination defects are not due to a delay in myelination because they persist with age. Overexpression of *Ppargc1α* did not result in ectopic myelination. Therefore, neuron-specific *Ppargc1α* is required but not sufficient for neocortical myelination. Moreover, loss of *Ppargc1α* leads to decreased neuronal metabolism, suggesting that secreted metabolites can act as mediators for neuron-specific *Ppargc1α* to interact with oligodendrocytes to control myelination. Together, these data support a novel function for *Ppargc1α* in myelination and implicate it in neuron-to-glia communications.

Table of Contents

Figures and Tables

List of Abbreviations

AEP	Anterior entopeduncular area
ALS	Amyotrophic lateral sclerosis
BAT	Brown adipose tissue
CfuPN	Corticofugal projection neuron(s)
CGE	Caudal ganglionic eminence
CLN	Cortical-like neurons
CNS	Central nervous system
CP	Cortical plate
CPN	Callosal projection neuron(s)
CSMN	Corticospinal motor neuron(s)
CThPN	Corticothalamic projection neuron(s)
CTPN	Corticotectal projection neuron(s)
dd H_2O	Deionised water
DIG-UTP	Digoxigenin-UTP
DIV	Day of differentiation
DRIP	Vitamin D receptor interacting protein
DTP	Dorsal telencephalic progenitors
E	Embryonic day
FACS	Fluorescence activated cell sorting
HAT	Histone acetyletransferase
HD	Huntington's disease
HSP	Hereditary spastic paraplegia
IACUC	Institutional animal care and use committee
IC	Internal capsule
ICC	Immunocytochemistry
ICE	Inducible cassette exchange
IHC	Immunohistochemistry
IN	Interneurons
iPSC	Induced pluripotent stem cells
IRES	Internal ribosomal entry site
ISH	*In situ* hybridization
LC-MS	High performance liquid chromatography and mass spectrometry
LGE	Lateral ganglionic eminence
MEF	Mouse embryonic fibroblasts
mESC	Mouse embryonic stem cells
MGE	Medial ganglionic eminence
miPSC	Mouse induced pluripotent stem cells
MOI	Multiplicity of infection
MZ	Marginal zone
NAA	N-acetylaspartate
P	Postnatal day
PBS	Phosphate buffer saline
PCR	Polymerase chain reaction

PD	Parkinson's disease
PFA	Paraformaldehyde
PLS	Primary lateral sclerosis
PN	Projection neuron(s)
PNS	Peripheral nervous system
PP	Preplate
qPCR	Quantitative PCR
ROS	Reactive oxygen species
r.t.	Room temperature
RT-PCR	Reverse transcriptase PCR
SC	Spinal cord
SCI	Spinal cord injury
SCPN	Subcerebral projection neuron(s)
SP	Subplate
SVZ	Subventricular zone
TCPN	Thalamocortical projection neuron(s)
Th	Thalamus
TRAP	Thyroid hormone receptor-associated proteins
VZ	Ventricular zone

Acknowledgements

First and foremost, I would like to thank my advisor and mentor, Paola Arlotta, for her unwavering support over the last four years. She has taught me not only the rigor of the scientific method but also the importance of perseverance and hard work. She has been an inspiration.

Secondly, I am privileged to have my fellow lab members share this PhD journey. I am fortunate to work with Dr. Giulio Srubek Tomassy. I thank him for his inspiring enthusiasm for science and for sharing his encyclopedic knowledge of cortical development. I also thank him for our countless conversations in the lab about science and life in general. I would also like to thank Dr. Hsu-Hsin Chen for her scientific insights in the directed differentiation project, without which, the project would not have been possible. I would like to thank Dr. Simona Lodato whom I have known for the longest time in the lab. I thank her for being an inspiration, for the countless late-night pizzas and light-hearted moments in the lab that are just as important as the scientific discoveries we made together. I would like to thank Dr. Bradley J. Molyneaux for inspiring me with his passion for research and medicine. I would also like to thank Dr. Caroline Rouaux for sharing her expertise and advice on reprogramming. I am also grateful to Dr. William Hendriks for being a great project partner and for his faith and encouragement. I am extremely thankful to Zachary Trayes-Gibson for being a great lab manager and for his invaluable help on so many occasions. I also thank Amanda Merlino for her help in my experiments. I would like to extend my gratitude to Drs. Emanuela Zuccaro, Boyan Bonev and Juliana Brown. I also like to thank members of the Arlotta lab: Ryoji Amamoto, Mohammed Mostajo Radji and James Harris and I wish them all the best. I am grateful to have worked with Edward Stronge and Travis Hallett, who have been kind, understanding and extremely inquisitive individuals. They have taught me much more than I have imparted to them. I also thank Celia Shneider for her help on many occasions.

Third, I am very fortunate to have Professor Connie Cepko to be my program advisor as well as thesis committee chairperson over the past five years. My PhD journey would not have been the same without her wisdom and mentorship on both academic and personal levels. I am also grateful to other members of my thesis committee, Professors Joshua Sanes and Qiufu Ma, for their time, wisdom and advice over the past four years. I would also like to thank Professors Connie Cepko, Thomas Michel, Patricia D'Amore and Jordan Kreidberg for their leadership in the Leder Program. I am also thankful to Professor David Van Vactor for his leadership in the BBS program and my wonderful coordinators from the BBS office: Daniel Gonzalez, Maria Bollinger and especially Kate Hodgins who knows practically everything there is to know. I would also like to thank Professor David Cardozo, Leah Simons and Megan Kastner from the Division of Medical Sciences for their continual support and help on many occasions. I also thank Ellen Fox from the GSAS Student Services Office and GSAS Dean Garth McCavana for their support. I would also like to thank Professors David Van Vactor, Michela Fagiolini and Mark Zervas for taking the time to be on my thesis defense committee and for their advice. I also thank A*STAR for the many opportunities that they have given me as well as their generous sponsorship. I thank Jamie Tan for being a wonderful scholarship officer.

I close by expressing my gratitude to my undergraduate thesis advisor-turned-lifelong mentor Professor Volker Vogt from Cornell University. He is not only an inspiration in the

academic arena but one of the kindest and wisest people that I am fortunate to have met and befriended. I owe much to him and thank him for his support and encouragement during challenging times. To all my beloved friends who have accompanied me on this journey, especially my housemates Alvin and Huilin, Qunya, Khian Hong, ChenLi, Xuyu, Luhan, Joyce, Eileen, Chewie and Poyi, thank you so much for your support and for all the precious memories. Last but not least, I thank my Mum, Dad and sister for all their love, patience, kindness and understanding. I also thank my fiancé Michael who have been my pillar of support through these years, without whom I would not have come so far. Most importantly, I thank God for all the grace he has given me to begin and finish this endeavor. Thank you!

Dedicated to all my loved ones

Chapter 1:

Introduction

1.1. Overview.

The mammalian neocortex is a complex yet highly organized brain structure involved in higher-order functions like cognition, motor behavior and sensory perception (1-3). Comprising six radially organized layers, it contains a diversity of neuronal and glial cell types (1). Cortical neurons can be broadly categorized into two classes, namely inhibitory GABAergic interneurons (IN) that make local connections and the excitatory glutamatergic projection neurons (PN) that connect to distant intracortical, subcortical and subcerebral targets (1, 4). Cortical PN are classified into different subtypes based on their birthdates, laminar positions, axonal targets as well as molecular identities (1). Among the cortical PN, subcerebral projection neurons (SCPN) connect layer Vb to targets in the pons, superior colliculus and the spinal cord (1). SCPN in layer V, together with PN projecting to subcortical targets such as corticothalamic PN (CThPN) in layer VI, are collectively referred to as corticofugal PN (CfuPN) (1).

The molecular signals that govern SCPN development are not fully elucidated, with regard to their fate specification during early embryonic development as well as their maturation and maintenance of cell identity at later stages of differentiation during postnatal ages through to adulthood. To address this, a series of neuronal subtype-specific genes that mark SCPN *in vivo* has been identified (5). Notably, it was discovered that the transcription factor *Forebrain Embryonic Zinc Finger 2* (*Fezf2*) is necessary for the birth and early differentiation of all SCPN (6-9). It is also sufficient to "fate-switch" cortical progenitors fated to form upper layer callosal PN (CPN) to generate deep layer CfuPN, including CSMN (6-9). Moreover, our laboratory has recently demonstrated in two distinct studies that *Fezf2* is sufficient not only to direct the differentiation of non-cortical striatal progenitors to CfuPN *in vivo* (10), but also to instruct upper layer CPN to postmitotically lineage reprogram into deep layer CfuPN and change their

axonal connectivity from interhemispheric, intracortical projections to corticofugal projections directed below the cortex (11). Given the central role played by *Fezf2* in SCPN-specification and differentiation, our laboratory has investigated the molecular mechanisms mediating *Fezf2* function and has identified a second array of SCPN-specific genes that are acutely triggered or repressed by *Fezf2* (Lodato *et al.*, unpublished).

Here, I follow the hypothesis that mining the previously described dataset of SCPN-specific genes (5) and the newly defined database of *Fezf2* target genes (Lodato *et al.*, unpublished) will allow me to select molecules that are expressed exclusively in SCPN and are downstream targets mediating *Fezf2* action. Identifying and studying these molecular signals is critical to enriching our current understanding of SCPN/CSMN development, particularly for survival during later stages of differentiation from postnatal ages to adulthood where much remains unknown. Building on this prior work, I chose to broadly investigate the functional role of transcriptional co-activator *Peroxisome Proliferative-Activated Receptor Gamma, Co-activator 1 Alpha* (*Ppargc1α*) in the postnatal differentiation of SCPN and to specifically answer the following questions:

(1) Is *Ppargc1α* cell-intrinsically important in SCPN to act as a novel regulator that control subtype-selective survival during postnatal development? Initial studies in the context of neurodegenerative diseases and acute cellular stress have implicated *Ppargc1α* in neuronal survival. Yet, it is unclear if the developmental function of *Ppargc1α* in the nervous system, particularly in SCPN, maintains cell survival in the absence of acute cellular stress or in conjunction with chronic stress caused by aging. In Chapter 2, I studied whether *Ppargc1α* is cell-autonomously necessary in SCPN to govern their survival *in vivo*.

In addition, is *Ppargc1α* cell-intrinsically critical in SCPN to prevent the formation of spongiform-like lesions in the striatum? Previous studies have shown that the global loss of *Ppargc1α* leads to spongiform-like lesions in the white matter of the striatum. Since SCPN/CSMN project through the internal capsule of the striatum, in chapter 2, I elucidated if *Ppargc1α* is cell-autonomously required in SCPN to govern the development of these lesions. Knowing the cellular origins of these spongiform-like lesions will allow us to better understand the disease mechanisms behind their formation.

(2) Is *Ppargc1α* cell-intrinsically crucial in SCPN to establish a proper neocortical myelination pattern? In Chapter 3, I investigated whether *Ppargc1α* is cell-autonomously necessary in SCPN to establish a correct myelination pattern in the neocortex and whether it is sufficient to induce ectopic myelination. This study is significant because it purports a novel function for *Ppargc1α* in SCPN by implicating it in neocortical myelination and broadly in neuron-to-glia interactions. It is especially interesting because it questions whether and how a transcriptional co-activator restricted to neurons can regulate a process like myelination that is exclusively executed by another cell type – the oligodendrocytes.

Besides the role of *Ppargc1α* in the postnatal differentiation of SCPN, I have also dedicated a component of my thesis to test the extent to which cell-intrinsic developmental signals that direct SCPN-specification and development in the embryo can be utilized to selectively generate deep layer CfuPN, including SCPN/CSMN, from pluripotent mouse embryonic stem cells (mESC) and mouse induced pluripotent stem cells (miPSC) *in vitro*. Since the main focus of my dissertation is the role of *Ppargc1α* in the postnatal differentiation of SCPN, I have included this work in the Appendix (Chapter 6). There, I elucidated if *Fezf2* overexpression in mESC-derived dorsal telencephalic progenitors (DTP) and cortical-like

neurons (CLN) can preferentially instruct them to differentiate into CfuPN, including SCPN, *in vitro*. If successful, it will be the first study *in vitro* demonstrating that a single transcription factor *Fezf2* can direct mESC-derived cells to resemble CfuPN or even SCPN, in terms of their molecular identities as well as axonal connectivity. Achieving this is important for future applications like chemical screens as well as disease modeling, among others.

1.2. Molecular development of SCPN in the mammalian neocortex.

1.2.1. Neocortical progenitors generate the six-layer mammalian neocortex in an "inside-out" manner.

The mammalian telencephalon, originates from the evagination of the two cerebral hemispheres at the anterior aspect of the neural tube that encompasses the lateral ventricles (1, 2, 12). The mammalian cerebral cortex is formed from the dorsal side of the rostral telencephalon during early stages of embryonic development (1, 2, 12). Being the major part of the cerebral cortex, the mammalian neocortex is a six-layered structure that first comprises the ventricular zone (VZ), a thin proliferative neuroepithelium that lies immediately adjacent to the dorsal wall of the lateral ventricles (1, 2, 12). As neurogenesis progresses, the subventricular zone (SVZ), another propagating layer, forms above or superficial to the VZ (1, 2, 12). Neocortical progenitors located in the VZ and SVZ produce diverse postmitotic PN populations, which migrate radially to occupy different neocortical layers, in a temporal order that is tightly governed from embryonic day (E) 11.5 to E17.5 in the mouse (1, 13-15). The earliest born postmitotic neurons are generated around E10.5 in the mouse and they migrate to form a layer above the VZ, known as the preplate (PP) at E11.5 (1). A day later at E12.5, the PP is split into the more superficial marginal zone (MZ) and the more deeply located subplate (SP) by the expanding cortical plate (CP) from which the multilayered neocortex arises (1). The CP consists of postmitotic neurons from VZ and SVZ that migrate in such a manner that later born neurons arriving at the CP migrate past earlier born neurons to occupy a more superficial position, thus gradually establishing the six-layer formation of the mature cortex in an "inside-out" fashion (1, 13, 15). The distinct classes of PN are born in sequential and overlapping temporal waves where

the peak birth of deep layer V SCPN and upper layers II/III CPN occurs at E13.5 and E15.5 respectively (1, 16).

1.2.2. The mammalian neocortex is populated by distinct subtypes of PN, including CSMN and other SCPN.

The excitatory glutamatergic PN of the neocortex connect to diverse ipsilateral or contralateral cortical, subcortical or subcerebral targets (1, 17-21). Among these, CPN project their axons to targets within the cortex while CfuPN project their axons to targets away from the cortex (1, 17-21). CPN belong to a larger class of commissural PN that extend their axonal projections within the cortex to the opposite hemisphere via either the corpus callosum or anterior commissure (1, 17-21). CfuPN can be further divided into subcortical PN that connect to targets below the cortex like CThPN that project to the thalamus (Th), and SCPN that connect to targets below the brain (1, 17-21). SCPN include various subpopulations classified based on their final projection targets. Among others, these include the corticopontine PN which project to the pons, the corticotectal PN (CTPN) which project to the superior colliculus, and the CSMN which project to the spinal cord (SC) (1, 17-21). Diverse PN subtypes are born at different times from neural progenitors of the dorsal telencephalon and occupy distinct laminar positions in the neocortex. CfuPN are located in the deep cortical layers V/VI while CPN mainly reside in the superficial layers II/III, with smaller numbers in layer Va and VI (2, 13-15, 22-24).

1.2.3. The molecular pathways that control CSMN and other SCPN development are beginning to be understood.

As opposed to molecular signals that broadly control neuronal development in the cortex (25-32), the mechanisms that govern the development of individual classes of PN are only beginning to be elucidated for some populations (1, 5-9, 33-35). My P.I., Professor Paola Arlotta, together with Dr. Bradley J. Molyneaux, identified neuronal subtype-specific genes that label with different degrees of specificity SCPN/CSMN (5) during her postdoctoral work in Professor Jeffrey Macklis's laboratory. Among these genes, selected ones regulate specific aspects of CSMN development *in vivo* (5). In the Arlotta and Molyneaux's study, they compared the gene expression profile by microarray of purified CSMN to that of two other cortical PN populations, the CPN and the CTPN (5). Purification of these distinct PN populations enabled them not only to overcome the cellular heterogeneity that often confounds gene expression profiling within the central nervous system (CNS), but also to determine differential gene expression between the diverse populations without contamination by other cell types. Through this study, they identified genes that are expressed with various degrees of specificity in CSMN at early (e.g., *Ctip2* and *Clim1*), intermediate (e.g., *Crim1* and *Mu-crystallin*), late (e.g., *Encephalopsin* and *Cadherin 22*), or through all stages (e.g., *Fezf2* and *Cadherin 13*) of development (5). They also distinguished markers that were exclusively expressed in CSMN but not in CTPN (e.g., *Diap3* and *S100a10*), as well as genes that were selectively expressed in other PN subtypes but not in CSMN (e.g., *Lmo4*) (5, 36). A more recent study by Molyneaux and Arlotta *et al.* identified additional, novel genes that are preferentially expressed in CPN but not in SCPN (36).

1.2.4. *Fezf2* is a critical transcription factor that is necessary and partly sufficient for the specification and differentiation of SCPN/CSMN.

The screen, described above in section 1.2.4., enabled the identification of many

SCPN/CSMN-specific genes that had not previously been functionally characterized in the CNS. To verify that the screen revealed true SCPN/CSMN genes, the functional roles of *COUP-TF-interacting protein 2* (*Ctip2)* (5), *Forebrain Embryonic Zinc Finger 2* (*Fezf2*) (6) and *SRY-box 5* (*Sox5*) (33) in CSMN development were characterized.

Most importantly, *Fezf2*, which encodes a 455 amino acid transcription factor that contains six C2H2 zinc fingers and an engrailed homology repressor domain, was discovered to be necessary for the birth and early differentiation of SCPN/CSMN from cortical progenitors (6-9). *Fezf2*$^{-/-}$ mice display a complete absence of CSMN as well as other SCPN, and lacked the corticospinal tract as well as all subcerebral projections (6). Absence of SCPN/CSMN is accompanied by the specification of additional CPN (8). Gain-of-function analysis also showed that *Fezf2* overexpression in cortical progenitors fated to form the upper layer CPN "fate-switched" them to become neurons that not only express CfuPN-specific genes like *Ctip2*, *Sox5*, *Tle4* and *Tbr1*, but also extend axons subcortically (i.e., to the thalamus) and subcerebrally (i.e., to the cerebral peduncle) (6, 37) (refer to the Appendix/Chapter 6 for more details). Together, these loss and gain-of-function experiments indicate that *Fezf2* plays a central role in controlling various aspects of SCPN/CSMN-specification and differentiation. Understanding how *Fezf2* mediates its function via downstream effectors is crucial for enhancing our knowledge of SCPN development and differentiation.

1.2.5. *Fezf2* controls the expression of a cascade of genes that mark SCPN/CSMN during embryonic and postnatal stages of development.

Although the first screen by Arlotta and Molyneaux *et al.* provided important information on the combinatorial code of genes that define the CSMN subtype during development, CSMN

could not be purified based on their projection target nor could it be profiled earlier than E18.5, when their fate specification has most likely already occurred. Since *Fezf2* is critical for SCPN/CSMN early differentiation (i.e., *Fezf2*$^{-/-}$ mice do not have SCPN as early as E14.5, one day after peak SCPN birth *in vivo*) (6-9), and overexpression of *Fezf2* is sufficient to fate-switch neural progenitors as well as early postmitotic CPN to acquire a deep layer CfuPN identity, it is likely that *Fezf2* acutely regulates genes acting early during SCPN/CSMN differentiation. In addition, *Fezf2*, expressed throughout all stages of development, is potentially crucial to maintain SCPN/CSMN identity by initiating a cascade of gene expression that ultimately leads to induction of genes acting at late stages of SCPN/CSMN development. Therefore, to identify genes crucial for early CSMN fate specification as well as to expand the pool of genes expressed at late stages of CSMN development, Dr. Simona Lodato and Alyssa Meleski in our laboratory have recently completed a new microarray screen to identify molecular pathways that act downstream of *Fezf2* (Lodato *et al.*, unpublished). They overexpressed *Fezf2* in E14.5 cortical progenitors (i.e., destined to generate upper layer CPN) via *in utero* ultrasound-guided microinjection and electroporation of a *Fezf2*^{GFP} vector (Lodato *et al.*, unpublished). This initiates precise molecular changes that direct SCPN/CSMN differentiation. The same procedure was repeated with an empty control *Ctl*^{GFP} vector (Lodato *et al.*, unpublished). *Fezf2*$^{+}$/GFP^{+} and control GFP^{+} cells were isolated at 24 hours and 48 hours after electroporation and purified by FACS for subsequent expression profiling by microarray analysis (Lodato *et al.*, unpublished). Using this approach, they successfully identified a new repertoire of promising candidate genes that were differentially up or downregulated by *Fezf2*. *In situ* hybridization (ISH) on the developing neocortex for a selected set of *Fezf2*-triggered genes verifies their restricted expression in the developing SCPN/CSMN (Lodato *et al.*, unpublished). Significantly, this

screen revealed not only some of the earliest SCPN/CSMN-specific markers, which may play critical roles during early SCPN/CSMN fate specification, but also notably SCPN/CSMN-specific markers that may be important during later, more mature stages of differentiation (Lodato *et al.*, unpublished). Particularly, I am interested in identifying molecular controls that govern the survival of SCPN. Understanding how distinct subtypes regulate and maintain their survival will shed light on disease mechanisms that leads to subtype-specific degeneration and inform the development of potential therapeutic strategies. Thus, I have identified *Ppargc1α* to be an ideal candidate to study neuronal survival in the neocortex because it has been shown to be a key regulator in energy metabolism and has been implicated in neuronal survival upon acute cellular stress.

1.3. *Ppargc1α* function.

1.3.1. *Ppargc1α* is a transcriptional co-activator.

Numerous intricate biological programs are governed at the level of genetic regulation by DNA-binding, sequence-specific transcription factors. While most studies investigating gene transcription are centered on the amount or activity of transcription factors as a key mode of genetic control, there is an increasing focus on transcriptional co-activators as important, if not primary, players of transcriptional regulation (38).

Transcriptional co-activators are increasingly found to be crucial determinants of genetic control because they are often tissue-specific, sensitive to extracellular cues, capable of binding to various transcription factors, and can be principal targets of signal transduction pathways as well as hormone signaling (39). Notably, the *Peroxisome Proliferative-Activated Receptor Gamma, Co-activator 1* (*PGC-1*) family of co-activators has developed into exemplars of transcriptional co-activators as they emerge to be versatile multifunctional components that act as "molecular switches" to integrate environmental cues with internal signaling mechanisms to control cellular and systemic metabolism (38, 40). They are also sequence conserved in many chordate species such as amphibians, birds, rodents and primates (38, 40), with the drosophila *PGC-1* homolog *Spargel* being recently identified (40, 41).

Ppargc1α or *PGC-1α* is the first member of the *PGC-1* family to be identified (38, 42) and it shares more sequence identity with homolog *PGC-1β* than with its other family member *PRC* (38, 43-45). It functions as a critical transcriptional co-activator with powerful transcriptional activity when activated by associating with DNA sequences, either through transcription factor docking or linkage with a heterologous DNA binding domain (46, 47). It can also interact with distinct nuclear hormone receptors like *Peroxisome Proliferative-Activated*

Receptor Gamma (*PPARγ*) (38, 42, 42, 48-50) and *Thyroid Hormone Receptor Beta* (*TRβ*) (38, 42, 51-53), as well as *Nuclear Respiratory Factors* like *NRF-1* and *NRF-2* (38, 54, 55).

Ppargc1α encodes for a 797 amino acid protein that contains (i) a potent activation domain at its N terminus which interacts with components of the histone acetyltransferase (HAT) complex consisting of CBP/p300 and SRC-1 (46), (ii) a repression domain that contains several p38 MAPK phosphorylation sites (56), (iii) LXXLL motifs present in the activation and repression domains which bind to the ligand binding domains of nuclear receptors (42, 57), (iv) RNA processing motifs which consists of a arginine/serine-rich RS domain and a RNA binding domain which have been shown to interact with the C-terminal domain of RNA polymerase II via the Thyroid Hormone Receptor-Associated Proteins (TRAP) / Vitamin D Receptor Interacting Protein (DRIP) / Mediator complex (42, 58). Therefore, *Ppargc1α* enhances transcriptional activity by (i) mediating chromatin remodeling via bound HAT-containing proteins (46), (ii) recruiting the mediator complex and RNA polymerase to facilitate transcription (58), and (iii) displacing repressor proteins such as histone deacetylase and small heterodimer partner (59, 60). In all, *Ppargc1α* is a key transcriptional co-activator whose function is well characterized in tissue with high metabolic demand like brown fat and skeletal muscle, but remains relatively unknown in the brain and CNS, particularly in SCPN/CSMN.

1.3.2. *Ppargc1α* is important for energy metabolism in several tissues.

1.3.2.A. *Ppargc1α* is crucial for adaptive thermogenesis in brown adipose tissue.

Ppargc1α was first discovered to be a molecular switch that can turn on significant regulators of adaptive thermogenesis in brown adipose tissue (BAT) (42, 61). BAT functions to

dissipate energy primarily in the form of heat, while white adipose tissue functions to store energy (40). Adaptive thermogenesis dispels heat by inducing fuel intake, increasing mitochondrial fatty acid oxidation and enhancing heat production via the expression of *Uncoupling Protein-1* (*UCP1*), which dissipates the mitochondrial proton gradient and uncouples oxidative phosphorylation from ATP production (38, 40, 42). Upon exposure to cold, *Ppargc1α* mRNA expression in BAT is quickly and highly stimulated and "kick starts" adaptive thermogenesis (38, 40, 42). Loss-of-function analysis showed that *Ppargc1α* null mice are remarkably sensitive to cold exposure due to defective thermogenesis (62, 63). Gain-of-function analysis demonstrated that *Ppargc1α* is sufficient to specify brown adipocytes from white preadipocytes by stimulating *UCP1* expression in mouse cells (42), and more recently in human cells (64). Thus, *Ppargc1α* is a cold-inducible regulator crucial for adaptive thermogenesis in BAT.

1.3.2.B. *Ppargc1α* is critical for mitochondrial biogenesis and fat metabolism in skeletal muscle.

Ppargc1α is an exercise-inducible co-activator important for mitochondrial biogenesis (51, 54, 61) as well as fatty acid metabolism in skeletal muscle (40, 65). For mitochondrial biogenesis, *Ppargc1α* induces the expression of and coactivates transcription factors *NRF-1* and *NRF-2*, which in turn stimulates the expression of many nuclear-encoded mitochondrial genes, notably mitochondrial transcription factor A (*Tfam*) (38, 54, 61). *Tfam* is a key mitochondrial transcriptional activator essential for the replication and transcription of mitochondrial DNA (66, 67). Regarding fat metabolism, *Ppargc1α* promotes the transcription of enzymes critical for fat metabolism such as *Fatty Acid Translocase* (*FAT*) or *CD36*, *Carnitine Palmitoyltransferase 1* (*CPT 1*) and *Medium-chain acyl-Coenzyme A Dehydrogenase* (*MCAD*) (40, 65). Loss-of-

function analysis of *Ppargc1α* null and muscle-specific conditional null mice showed that these mice are intolerant of exercise and are particularly sensitive to contraction-induced fatigue (40, 62). The studies also demonstrated that these null mice have reduced amounts of mitochondrial respiratory chain proteins and ATP synthase (40, 62). Remarkably, gain-of-function analysis revealed that transgenic expression of *Ppargc1α* in white glycolytic fast-twitch skeletal muscle can "fate-switch" them to display genetic and physiological features characteristic of red oxidative slow-twitch skeletal muscle, such as the expression of contractile proteins like *Troponin I,* and greater resistance to electrically stimulated fatigue (38, 68). Hence, *Ppargc1α* plays a critical role in mitochondrial biogenesis and fat metabolism in skeletal muscle.

1.3.2.C. *Ppargc1α* is essential for oxidative metabolism in the heart.

Ppargc1α is a key regulator for mitochondrial biogenesis as well as fatty acid β-oxidation, and acts as a molecular switch to transform cardiac muscle from a glycolytic state to an oxidative phosphorylated state (38, 40, 69). Loss-of-function analysis demonstrated that *Ppargc1α* null mice display lower cardiac reserves after electrical or chemical stimulation, decreased treadmill-running capacity and reduced cardiac functions such as atypical heart rate and defective left ventricular function after exercise (38, 40, 62, 70). These null mice also showed early symptoms of cardiac failure by expressing cardiac genes reminiscent of an early embryonic stage and stimulating the production of circulated atrial natriuretic peptide which is used as an indicator of cardiac dysfunction (38, 40, 70). Gain-of-function analysis revealed that *Ppargc1α* overexpression *in vivo* and in cultured neonatal cardiomyocytes *in vitro* can induce mitochondrial biogenesis and gene expression (38, 40, 69, 71). Therefore, *Ppargc1α* is essential for oxidative mitochondrial metabolism in the heart.

1.3.3. *Ppargc1α* function in the CNS remains relatively unknown.

Despite its well-studied function in many tissues and its involvement in neurodegenerative diseases, the cell-autonomous role of *Ppargc1α* in the neocortex is relatively unknown, especially its function in the differentiation of SCPN, including CSMN.

For neurodegenerative diseases, three studies have implicated *Ppargc1α* in repressing the neurodegeneration of striatal neurons in a mouse model of HD by suppressing reactive oxygen species (ROS) and protecting against mitochondrial dysfunction, thereby enhancing neuronal survival against oxidative insults (72-74). In these studies, it was revealed that ectopic expression of *Ppargc1α* in the striatum of transgenic HD mice protects them against atrophy and leads to an increase in mean neuronal volume (73). In the context of Parkinson's disease (PD), previous work has shown that when exposed to the neurotoxin MPTP, *Ppargc1α*$^{-/-}$ mice show greater dopaminergic cell death, similar to what is observed in mice with PD (72). In this case, enhanced cell death is caused by excessive oxidative damage to the dopaminergic neurons present in the substantia nigra, as evident by an increase in nitrosylated proteins – a marker for ROS-induced cell damage (72). The association of *Ppargc1α* with PD is also supported by a genome-wide expression study showing that mitochondrial genes responsive to *Ppargc1α* are underexpressed in patients with PD (75), as well as another recent study showing that PARIS, a parkin interacting molecule that contributes to neurodegeneration in PD, transcriptionally represses *Ppargc1α* (76). In addition, there is preliminary work linking *Ppargc1α* to ALS (77-79), multiple sclerosis (80), Alzheimer's disease (81), bipolar disorder and schizophrenia (82). Interestingly, it has been suggested that *Ppargc1α* enhances neuronal recovery from hypoxia (83) and protects neurons against reperfusion injury, ischemia as well as stroke (84-87). Although these studies support a role for *Ppargc1α* in controlling neuronal survival, possibly by regulating mitochondria

function and biogenesis, it is important to note that they were performed in the context of acute cellular stress caused by either the administration of toxic substances or by ongoing neurodegeneration with selective cell loss. Therefore, it remains unknown whether cell-intrinsic loss of *Ppargc1α*, either in the absence of acute cellular stress or in combination with chronic stress caused by aging, can induce cell death. This question motivated me to investigate whether *Ppargc1α* in SCPN is important for neuronal survival, as described in Chapter 2.

In addition, gross examination of the *Ppargc1α* null brain revealed spongiform-like lesions in the striatum (63). Since SCPN project through the internal capsule in the striatum, I was prompted to study whether *Ppargc1α* in SCPN contributes to the generation of these lesions, as detailed in Chapter 2.

In the process of elucidating *Ppargc1α's* function in SCPN with regard to neuronal survival and lesion development, I discovered a novel function for *Ppargc1α* in SCPN. In Chapter 3, I investigated whether SCPN-specific *Ppargc1α* is involved in the regulation of neocortical myelination, a process exclusively governed by oligodendrocytes. This is the first study implicating *Ppargc1α* to be important for neuron-to-glia interactions, a role that has not previously been described. Interestingly, a recent report has also suggested that the spongiform lesions reflect a myelination deficit in the striatum of *Ppargc1α* null mutants (88).

In the context of nervous system development, early *in vitro* studies implicate *Ppargc1α* in the differentiation of neurons or Schwann cells (89-91), as well as the regulation of mitochondrial density in primary cortical neurons (92). Few *in vivo* studies point to a role in governing the expression of *Parvalbumin* in GABAergic interneurons (93, 94), the formation and maintenance of neuronal dendritic spines (95) but not in the maintenance of medium spiny neurons in the striatum (96). In the study by Cowell and her group focusing on *Parvalbumin* and

GABAergic dysfunction in *Ppargc1α* null mutants, they found that *Ppargc1α* is required for *Parvalbumin* expression throughout the cortex, hippocampus, striatum and cerebellum (97). However, analysis of other GABAergic markers such as *GAD67*, *GAD65*, *KV3.1*, *Calbindin*, *Calretinin*, *Cholecystokinin* and *Somatostatin* showed that these markers are unaffected in the *Ppargc1α* null mutants (97). Hence, in line with a prior study looking at the rat brain, *Ppargc1α* null mutants do not suffer from a loss of *Parvalbumin* expressing interneurons but from a loss of *Parvalbumin* expression (94, 97). Consistent with this result, electrophysiological tests showed that spontaneous synaptic inhibition was not altered in the *Ppargc1α* null mutants though evoked synaptic responses showed decreased paired-pulse depression and dramatic facilitation in response to repetitive stimulation at the gamma frequency (97). In addition, Lucas *et al.* showed that overexpression of *Ppargc1α* can induce the mRNA expression of *Parvalbumin* in cultured neuroblastoma cells (97). Therefore, *Ppargc1α* is required for *Parvalbumin* expression in the brain.

In spite of these initial studies, the cell-autonomous function of *Ppargc1α* in neocortical development, particularly in SCPN/CSMN differentiation, remains unknown. Hence, in Chapters 2 and 3, I chose to investigate the functional role of transcriptional co-activator *Ppargc1α* in the postnatal differentiation of SCPN, including CSMN, in relation to neuronal survival, spongiform lesion formation and neocortical myelination.

1.4. Neuronal survival

Neurons in the central nervous system can be induced to die by apoptosis (98, 99). Extrinsic apoptotic pathways operate through the stimulation of death receptors by extracellular ligands to induce downstream JNK (c-Jun-N-terminal kinase) pathways that activate effector caspases (99). They can also combine with intrinsic apoptotic pathways at the mitochondria (99). Intrinsic apoptotic pathways cause the mitochondria to release cytochrome c that results in the assembly of the apoptosome complex, which further stimulates effector caspases to kill the cell (99). Translocation of apoptotic factors like BH3 proteins to the mitochondrial membrane to cause the release of cytochrome c from the mitochondria highlights the key role played by this organelle (99).

Many neuronal survival factors promote survival by inhibiting apoptotic pathways at distinct sites of action: upstream of the mitochondria, at the mitochondria to prevent the release of pro-apoptotic factors, or downstream of the mitochondria (99). Upstream of the mitochondria, there are decoy proteins that prevent apoptosis by competing with pro-apoptotic ligands for binding with death receptors such as cFLIP/cFLAR (100, 101), or by sequestering the ligands like DCR3 (102). Downstream of the mitochondria, survival factors can either act as decoys or they can associate with and prevent cytochrome c from forming the apoptosome (103, 104). At the mitochondria, neuronal survival factors typically prevent the permeabilization of mitochondrial membranes and the release of apoptotic factors. Many well-known factors include the anti-apoptotic BCL2-like family members (105) and the uncoupling proteins from the UCP family that reduce reactive oxygen species (ROS) (106). Interestingly, *Ppargc1α* is known to be important for mitochondrial biogenesis in skeletal muscle (51, 54, 61) and has been shown to be able to induce UCP-1 expression in brown fat (42). Hence, *Ppargc1α* is purported to be

important for cellular survival, acting potentially by inhibiting apoptosis at the mitochondria to prevent the release of pro-apoptotic factors.

Previous studies have reported that *Ppargc1α*$^{-/-}$ mice develop striking lesions predominantly in the striatum that are reminiscent of those in HD mice (63). Spongiform-like lesions are found in a variety of diseases that range from prion diseases like transmissible spongiform encephalopathies (107), white matter disorders such as leukodystrophies (108, 109) and multiple sclerosis (110), to neurodegenerative diseases like HD (111). Lesions are typically characterized based on commonly used histological stainings such as hematoxylin and eosin, as well as their location of occurance. The inability to define lesions with specific markers that are yet to be identified limits current research into lesion characterization and generation across various disorders. Hence, it remains unknown how lesions are formed and whether they differ or are similar across distinct diseases. More importantly, it remains unknown how genetic factors causes lesions and whether different molecular signals can converge into a common pathway that is shared across the different disorders.

In Chapter 2, I elucidate whether *Ppargc1α* is cell-intrinsically necessary in SCPN to govern neuronal survival *in vivo*, either in the native cellular context without acute external stress or neurodegeneration, or in the context of chronic stress caused by aging. Initial studies in the context of neurodegenerative diseases and acute cellular stress have implicated *Ppargc1α* in neuronal survival. Yet, it is unclear if the developmental function of *Ppargc1α* in the nervous system is to maintain cell survival. Focusing on the neocortex, I found that *Ppargc1α* is not required for neuronal survival, especially in the native cellular context where there is no acute external stress or concurrent neurodegeneration. These findings motivated another study to investigate whether *Ppargc1α* is important for neuronal survival in the context of chronic stress

caused by aging. Remarkably, examination of 18-month-old *Ppargc1α* null and conditional null mutants in the dorsal telencephalon revealed similar results where there are neither gross cortical, neuronal or PN subtype-specific anomalies, nor enhanced cell death. Thus, *Ppargc1α* is not cell-intrinsically required in SCPN to control neuronal survival, either in the native cellular context without external stress or neurodegeneration or in the context of chronic stress caused by aging. These results show that *Ppargc1α* is not important for SCPN birth, migration, laminar positioning nor survival. They further augment my new data in Chapter 3 by showing that the hypomyelination defects are not caused by neuronal loss.

In addition, in Chapter 2, I also study whether *Ppargc1α* is cell-autonomously required in SCPN to govern the development of spongiform-like lesions in the striatum. This was motivated by the fact that SCPN/CSMN project through the internal capsule of the striatum where these lesions are localized in *Ppargc1α* null mutants. Understanding the contribution of *Ppargc1α* in SCPN to these lesions will allow us not only to identify the cellular origins of these lesions, but, more importantly, to understand if these lesions affect the SCPN axonal efferents. First, I determine the expression profile of *Ppargc1α* and study the exact localization and temporal profile of these lesions. I find that *Ppargc1α* is highly expressed in SCPN predominantly during postnatal ages. I also elucidate that these lesions are closely associated with, or exactly localized to, the internal capsule through which SCPN project. By generating conditional null mutants for *Ppargc1α* in the dorsal telencephalon, I discover that conditional loss of *Ppargc1α* in the dorsal forebrain do not cause lesion formation, even in 18-month-old mutants. These data indicate that *Ppargc1α* in SCPN is not required for lesion formation. They further suggest that other neuronal regions may be responsible for the lesions and, more importantly, that SCPN axonal efferents are normal and not affected by these lesions. These data further support my novel findings in

Chapter 3 by showing that the hypomyelination defects are not caused by abnormal SCPN axonal projections.

1.5. Myelination by oligodendrocytes in the central nervous system

1.5.1. Myelin

The myelin sheath is an important development in the vertebrate nervous system during evolution (112, 113). By providing neurons with electrical insulation, it greatly increases the conduction velocity of action potentials and hence allows for efficient saltatory propagation of nerve impulses over long distances (112, 113). It is generated by oligodendrocytes in the central nervous system (CNS) or by Schwann cells in the peripheral nervous system (PNS), and is made by consecutive wrapping and subsequent compaction of stacked glial plasma membrane bilayers over the neuronal axon (112, 113). Essentially, myelin is a lipid-rich membrane that is replete with glycosphingolipids as well as cholesterol, and contains a myriad of proteins including the two major CNS myelin proteins – myelin basic proteins (MBP) and proteolipid proteins (PLP/DM20) (112, 113).

1.5.2. Oligodendrocyte origins in the dorsal telencephalon

During embryonic development, oligodendrocyte precursors are produced by cells that reside in the ventricular zone that lies adjacent to the ventricles in both the spinal cord and in the brain (114-116). In the telencephalon, oligodendrocyte precursors first originate from ventral regions (114, 115, 117). As early as E11.5 to E12.5, oligodendrocyte progenitors from the most ventrally located medial ganglionic eminence (MGE) and anterior entopeduncular area (AEP) begin to be produced and they migrate in a ventral to dorsal fashion to occupy both the ventral and dorsal telencephalon (115, 117-119). At around E16.5, these progenitors are joined by a second group of progenitors from the lateral and/or caudal ganglionic eminence (LGE and CGE respectively) (115, 117). In contrast, oligodendrocyte progenitors from dorsal regions within the

cortex only start to be produced postnatally after birth (115, 117). These precursors will generate committed oligodendrocyte progenitors that will proliferate and migrate laterally and dorsally over long distances to generate white matter over all parts of the telencephalon (112, 116). In the cerebral cortex, the MGE and/or AEP derived *Nkx2.1* positive oligodendrocyte population is the first to arrive at the neocortex as early as E16.5 and they populate the entire cortex by E18.5 (115, 117). At the same time around E18.5, the second population of ventrally derived oligodendrocytes precursors - the *Gsh2* positive population from the LGE - arrives at the cortex (115, 117). Hence by E18.5, all of the oligodendrocyte populations in the neocortex are ventral in origin (115, 117). After E18.5 and by birth, the third wave of dorsally derived *Emx1* positive oligodendrocyte populates the cortex (115, 117). This population migrates and stays within the dorsal forebrain and do not migrate to ventral regions (115, 117). Hence, depending on the developmental age, distinct populations of oligodendrocyte precursors from both dorsal and ventral regions inhabit the cerebral cortex.

During postnatal development, oligodendrocyte precursors are located in the subventricular zone near the tips of the lateral ventricles (115, 116, 120-122). This postnatal germinal zone, which is derived primarily from the LGE and the lateral cortex, remains active and continues to generate oligodendrocytes postnatally and through adulthood (115-117). Hence, the ventral-most MGE- and AEP-derived *Nkx2.1* positive oligodendrocyte precursors do not contribute to the postnatal subventricular zone and thus do not contribute to resident oligodendrocyte populations in the postnatal brain (115-117). This is further supported by prior work showing that at P10, the earliest population of ventrally derived *Nkx2.1* positive oligodendrocytes is eliminated from the cortex as well as from all other parts of the brain (117). Hence, the cortex is predominantly occupied by *Gsh2* and *Emx1* positive oligodendrocyte

progenitors as well as differentiated oligodendrocytes from P10 to adulthood (117). This study has also shown that targeted ablation of any one of the three abovementioned populations by diphtheria toxin results in functional compensation by the remaining populations where mutant mice display not only have a normal complement of myelin and oligodendrocytes but also normal behavior (117). Therefore, these distinct populations of oligodendrocyte progenitors are functionally redundant and have been proposed to compete for space in the developing brain.

1.5.3. Cell-intrinsic control of oligodendrocyte development and myelination

In the CNS, the formation of the myelin sheath by oligodendrocytes is temporally and spatially regulated and is critically dependent on a multitude of cell-autonomous as well as non-cell-autonomous factors (112).

Cell-intrinsic factors that control oligodendrocyte development include factors that affect transcriptional regulation. Some well-studied transcription factors that are expressed throughout oligodendrocyte development include the basic helix – loop – helix transcription factors *Olig1* and *Olig2* (118, 123-128), homeodomain transcription factor *Nkx2.2* (129, 130) and HMG transcription regulator *Sox10* (131, 132). These factors are expressed in oligodendrocyte progenitors as well as postmitotic differentiated oligodendrocytes and thus may play different roles at distinct stages of oligodendrocyte development that is likely dependent on other regulators that are differentially expressed. Some transcription factors that are predominantly expressed in oligodendrocyte progenitors like *Id2*, *Id4*, *Hes5* and *Sox6* have been shown to be active inhibitors of oligodendrocyte differentiation (114). Other determinants that are mainly expressed in differentiated oligodendrocyte include *MRF* that has been shown to be important to induce expression of myelin genes (133).

Besides transcriptional regulation, oligodendrocyte development is also controlled by posttranscriptional changes mediated by microRNAs. It has been shown that conditional loss of *Dicer* in oligodendrocyte lineage results in dysmyelination where selective loss of *Dicer* in mature oligodendrocytes causes dysfunction in lipid homeostasis (134-136). In addition, microRNA profiling has also revealed important microRNAs like *mir-219* (134) and *mir-338* (135) that have been shown to be important to inhibit oligodendrocyte differentiation by targeting progenitor genes like *PDGFRα*, *Hes5* and *Sox6*.

Epigenetic regulation via chromatin remodeling mediated by histone deacytalases (HDAC) have also been shown to be important for oligodendrocyte differentiation. Loss of function analyses with conditional null mutants for *HDAC1* and *HDAC2* revealed a loss of oligodendrocyte progenitors as well as differentiated oligodendrocytes, suggesting that HDAC are important for various stages of oligodendrocyte development (137). HDAC can promote differentiation of oligodendrocytes by inhibiting genes that maintain oligodendrocyte precursors in an undifferentiated state. For instance, HDAC can interact with transcription factor *YY1* to inhibit the expression of *Id4* (138).

In all, cell-intrinsic determinants can control oligodendrocyte birth, specification and differentiation at various levels, ranging from transcriptional and posttranscriptional control to epigenetic regulation.

1.5.4. Cell-extrinsic control of oligodendrocyte development and myelination

Besides cell-intrinsic determinants that affect oligodendrocyte birth, specification and differentiation, cell extrinsic determinants that include hormones like thyroid hormone, growth and trophic factors such as *fibroblast growth factor 2* (*FGF-2*) and *insulin-like growth factor 1*

(*IGF-1*) are also crucial in affecting oligodendrocyte development and subsequent myelin biogenesis (112, 113, 139).

Notably, the increasing importance of neuron-derived factors for myelination highlights the fact that reciprocal neuron and glia communication is imperative for oligodendrocyte development as well as proper myelination. This is supported by increasing evidence showing that neurons can regulate oligodendrocyte development by affecting their proliferation, differentiation and survival so as to ensure the right ratio of oligodendrocytes to axonal surface for myelination (113, 139), and the fact that myelination of neuronal axons must occur at the right time during development and not before the neurons are equipped to be myelinated (113, 140). Conversely, oligodendrocytes need to communicate with neurons to organize protein complexes at the nodes of Ranvier (113, 141-144) and have been shown to affect axonal cytoskeleton and transport (113, 145, 146). Thus, complementary interactions between neurons and oligodendrocytes are important for oligodendrocyte development and myelination.

Many studies have shown that neuron-derived molecules, whether secreted or not, are involved at various stages of oligodendrocyte development from proliferation to differentiation. Some known secreted signals include *platelet-derived growth factor subunit A* (*PDGF-A*), *neurotrophin 3* (*NT-3*), *ciliary neurotrophic factor* (*CNTF*), *FGF-2* and *IGF-1* (113, 147-149). *PDGF-A* is a soluble factor released by both neurons and astrocytes. While loss-of-function experiments have demonstrated that it controls the proliferation and survival of oligodendrocyte progenitors (113, 150-152), gain-of-function analyses have shown that *PDGF-A* induction leads to an increase in the number of oligodendrocytes (153). Besides secreted factors, non-secreted molecules that can act as cell surface receptors such as *Jagged 1* (154) and *contactin* (155) are also implicated in neuron glia signaling. *Jagged 1* is a cell surface ligand located on neuronal

axons that can interact with the *Notch 1* receptor found on oligodendrocytes, thus activating Notch signaling in oligodendrocytes to inhibit their differentiation (154). The decrease in *Jagged 1* expression in neurons with age coincides with the onset and promotion of myelination (113, 154). Therefore, *Jagged 1* has been proposed to be a way neurons regulate the timing of oligodendrocyte differentiation to affect myelination.

In addition to affecting oligodendrocyte development, other studies have shown that neuron-derived signals can affect myelination itself. For instance, electrical activity of neurons has been shown to be necessary to trigger myelination (156). It has been suggested that electrical activity in axons after target innervation not only leads to the secretion of promyelinating molecules like adenosine (157), but also induces changes in axonal protein expression (158) such as decreasing the amount of polysialated adhesion molecule *NCAM* on the cell membrane to enable myelination (159).

In Chapter 3, I investigate whether *Ppargc1α* is cell-autonomously necessary in SCPN to establish a correct myelination pattern in the neocortex and whether it is sufficient to induce ectopic myelination. I discovered that neuron-specific *Ppargc1α* is necessary for proper neocortical myelination but not sufficient to induce ectopic myelination. Employing various genetic null and newly generated conditional null mutants for *Ppargc1α*, I demonstrate that global or conditional loss of *Ppargc1α* in either neurons or the dorsal forebrain causes hypomyelination across all cortical layers in the neocortex. Aging studies of these null and conditional null mutants at 18 months further revealed that these hypomyelination defects are not due to a delay in myelination because they persist with age. However, overexpression of *Ppargc1α* did not result in ectopic myelination. Initial results of research into the mechanistic action of *Ppargc1α* show that the loss of *Ppargc1α* leads to decreased neuronal metabolism,

suggesting that secreted metabolites can act as mediators for neuron-specific *Ppargc1α* to interact with oligodendrocytes to control myelination. This study is significant because it purports a novel function for *Ppargc1α* in SCPN by implicating it, for the first time, in neocortical myelination and broadly in neuron-to-glia interactions. It is especially interesting because it suggests that a transcriptional co-activator restricted to neurons can control a process like myelination that is exclusively executed by another cell type–the oligodendrocytes.

1.6. Neuron-to-glia metabolism

1.6.1. Neuron-to-astrocyte metabolic interactions

Neurons can interact with glial cells via secreted metabolites, such as glutamate and glutamine for astrocytes as well as N-acetyl-aspartate (NAA) for oligodendrocytes (160). The metabolic interactions between neurons and astrocytes have been extensively studied over the past few decades with particular focus on the glutamate-glutamine-GABA shuttle (161). Excitatory glutamatergic neurons release neurotransmitter glutamate in the synapses. Excess glutamate is taken up predominantly by astrocytes via specific high-affinity glutamate transporters or by pre-synaptic reuptake (162, 163). This reabsorption of glutamate is important to prevent neuronal excitotoxicity. Within the astrocytes, glutamine synthetase, an enzyme that is found exclusively in astrocytes but not in neurons, convert glutamate to glutamine (164, 165). The resultant glutamine is then transferred back to neurons where it is converted back to glutamate, thus closing the glutamate-glutamine cycle (160). It has also been shown that glutamine released by astrocytes can also be converted to GABA via glutamate in inhibitory neurons (166, 167). Therefore, the metabolic interactions between neurons and astrocytes have been extended to be the glutamate-glutamine-GABA cycle.

1.6.2. Neuron-to-oligodendrocyte metabolic interactions

The metabolic interactions between neurons and oligodendrocytes have not been as well-studied as that between neurons and astrocytes. However, two recent studies that revealed a connection between glycolytic metabolism in oligodendrocytes and neuronal axonal integrity renewed interest in the field (168, 169). These studies have suggested that lactate can metabolically support neuronal axons and can be transported from oligodendrocytes to axons via

monocarboxylate transporter 1 (MCT1), which is exclusively expressed in oligodendrocytes (168, 169).

Another metabolic pathway of interest that characterizes neuron-to-oligodendrocyte interactions involves the enigmatic molecule NAA. NAA is synthesized from acetyl CoA and aspartate (170-177). However, the aspartate needed for NAA production can only be synthesized *de novo* in astrocytes, where it is then transported as glutamine to neurons (170-177). After which, a recently identified enzyme NAT8L that is exclusively expressed in the mitochondria of neurons is responsible for the synthesis of NAA (178). The resultant NAA molecule is then released from neurons and taken up by oligodendrocytes, where it is broken down to release acetate and aspartate by aspartoacylase, an ezyme that is selectively expressed in oligodendrocytes (170-177). It has been suggested that the resultant acetyl groups released within oligodendrocytes after NAA breakdown are used as building blocks for myelin to generate the insulating sheath that wraps around axons (170-177). The compartamentalization of NAA production to neurons has been contested by studies showing that cultured mature oligodendrocytes *in vitro* can produce NAA, suggesting that a parallel mechanism may exist *in vivo* (179). Solving the exclusive compartmentalization of NAA is crucial in understanding the astrocytes-neuron-oligodendrocyte metabolic interactions and but more importantly, in our interpretation of clinical MRS data that relies on using NAA as a marker for neuronal health and viability.

1.6.3. mTOR pathway and cellular metabolism

The mechanistic target of rapamycin (mTOR) signaling pathway is a fundamentally important pathway that integrates extracellular signals to intracellular pathways to control

cellular growth, size and homeostasis (180). It is first identified as a target of macrolide rapamycin in *Streptomyces Hygroscopicus* bacteria and became known to be an antiproliferative agent (180). mTOR is an serine/threonine protein kinase that is part of the phosphoinositide3-kinase (PI3K)-related family (180). It assembles with several proteins to form two distinct complexes, namely mTOR complex 1 (mTORC1) and 2 (mTORC2) (180).

mTORC1 is acutely sensitive to rapamycin and is better studied than mTORC2 (180). The mTORC1 pathway can sense intracellular as well as extracellular signals like stress, oxygen, energy, growth factors and amino acids (180). It can then integrate these signals to provoke a cellular response by promoting crucial processes such as protein synthesis, lipogenesis, and energy metabolism while inhibiting autophagy and lysosome biogenesis (180). A major upstream regulator of mTORC1 includes heterodimer tuberous sclerosis 1 and 2 (TSC1/2) that acts as a GTPase-activating protein for the Ras homolog enriched in brain (Rheb) GTPase. GTP-bound Rheb interacts directly with mTORC1 and greatly stimulates the kinase activity of mTORC1, thus enabling it to phosphorylate downstream effectors. Hence, TSC1/2 negatively regulates mTORC1 by converting Rheb from its active GTP bound form to its inactive GDP-bound form (181, 182). TSC1/2 integrates many of the signals that converge onto the mTORC1 complex (180). For instance, growth factors like insulin and insulin-like growth factor (IGF1) that induces the PI3K and Ras pathways can lead to the activation of downstream kinases such as protein kinase B (Akt/PKB) (183-185), extracellular-signal-regulated kinase 1/2 (ERK1/2) (186) and ribosomal S6 kinase (RSK1) (187). These effector kinases can directly phosphorylate TSC1/2 and inactivate it, thus stimulating the mTORC1 complex. A similar mechanism is also used by proinflammatory cytokines, like tumor necrosis factor (TNFα), to activate the mTORC1 complex (188). In addition, canonical Wnt signaling pathway also stimulates the mTORC1 complex by

inhibiting glycogen synthase kinase 3β (GSK-3β), which normally phosphorylates and activates TSC2 (189). Besides its upstream regulators, mTORC1 complex can regulate the activity of important downstream translational regulators such as S6 kinase 1 (S6K1) and eukaryotic translation initiation factor 4E (elF4E)-binding protein (4E-BP1) (190). Activated S6K1 increases mRNA synthesis, translational initiation as well as translational elongation (180, 190). Stimulated 4E-BP1 binds to the elF4F complex and aids in cap-dependent translation (180, 190).

mTORC2 is insensitive to acute rapamycin treatment but is sensitive to chronic rapamycin treatment in selected cell types (180). It is also not as well-studied as the mTORC1 pathway (180). The mTORC2 pathway can sense extracellular signals like growth factors and can integrate these signals to provoke a cellular response by promoting cytoskeletal organization, cellular survival and cellular metabolism (180). Upstream regulators of mTORC2 include PI3K of which its mechanism is currently unclear and may include the binding of ribosomes to mTORC2 in a PI3K-dependent manner (191). Downstream effectors of mTORC2 include predominantly members of the AGC subfamily of kinases such as Akt (192), serum- and glucocorticoid-induced protein kinase 1 (SGK-1) (193) and protein kinase C-α (PKC- α) (194, 195). Activated Akt can control several cellular pathways like metabolism, survival, apoptosis, growth and proliferation (180). Stimulated SGK-1 can regulate processes like cellular growth and transport of ions (180). Activated PKC- α can control cellular shape via changes to the actin cytoskeleton (194, 195).

While it is known that mTOR pathways can control cell growth, size and survival by regulating energy metabolism, it remains unclear how it controls mitochondrial oxidative metabolism. Interestingly, it has been shown that mTOR controls mitochondrial oxidative function through a YY1-PPARGC1A transcriptional complex (196). This links *Ppargc1α* to the

mTOR signaling pathway and cellular metabolism, and presents an important basis to understand the molecular mechanisms underlying *Ppargc1α* action in the neocortex and particularly in SCPN postnatal differentiation. The background information presented here will inform my global discussion in Chapter 4 where I conclude with a hypothetical model on potential ways *Ppargc1α* mediates its effects on myelination.

In Chapter 4, I conclude with a discussion on the implications of my findings on enhancing our knowledge of neuronal survival, spongiform lesion development, and more importantly, neocortical myelination in which I include a hypothetical model on potential ways *Ppargc1α* mediates its function to affect myelination by integrating previous work and my new data. I also discuss how these results enable us to better delineate the role of *Ppargc1α* in governing various aspects of postnatal SCPN differentiation. Lastly, I discuss the role of *Ppargc1α* as a metabolic switch and its implication in cell differentiation and cell fate. I hope the work presented in this dissertation will motivate future research into the function of *Ppargc1α* in the brain, especially in SCPN of the neocortex. Future work is necessary to delve into the role played by *Ppargc1α* in neocortical myelination and to probe how *Ppargc1α* mediates its function in neuron-to-glia communications.

Chapter 2:

Ppargc1α in the dorsal forebrain is not necessary to control neuronal survival and does not contribute to spongiform-like lesions in the internal capsule.

Author contribution: I designed all the experiments and interpreted all the data, with the input of Professor Paola Arlotta. I performed all *in situ* hybridizations and the majority of the colocalization analyses to determine the expression profile of *Ppargc1α* in the brain. I performed all the Nissl histological staining and did pilot immunohistochemistry analysis for neurons and distinct PN subtypes on both *Ppargc1α* null mutants and the newly generated conditional null mutants for *Ppargc1α* in the dorsal telencephalon. I also executed preliminary cell death analysis by immunostaining for caspase 3 on the *Ppargc1α* null and conditional null mutants. Travis Hallett ascertained the results by performing additional immunohistochemical analysis for neurons, PN subclasses and caspase 3 on the *Ppargc1α* null and conditional null mutants. He also performed all the Neurosilver histological staining. I established the exact localization of the spongiform lesions to the internal capsule in the striatum and determined the time course of their appearance in *Ppargc1α* null mice. I performed similar localization analyses of these lesions in neuron-specific *Ppargc1α* conditional null mice and confirmed the results of prior studies. I generated two new and distinct conditional null mice models for *Ppargc1α* – one in the dorsal telencephalon and the other in the thalamus – and performed similar spongiform lesion localization and time course analysis on these mice. Edward Stronge and Travis Hallett performed the colocalization of *Ppargc1α* to Parvalbumin-expressing interneurons.

Publication: These data will be published separately or in conjunction with Chapter 3.

2.1. Abstract.

Ppargc1α is implicated to be a survival factor for neurons and is linked to Huntington's disease (HD) as well as Parkinson's disease (PD). Yet, in these prior studies, *Ppargc1α* function was elucidated in a cellular context of acute stress or even concurrent neurodegeneration. Hence, it remains unknown whether the developmental function of *Ppargc1α* is to govern neuronal survival.

Focusing on the neocortex, I report that *Ppargc1α* alone is cell-intrinsically not sufficient to affect neuronal survival. Examination of *Ppargc1α* null and newly generated conditional null mutants in the dorsal forebrain demonstrated that global and conditional loss of *Ppargc1α* do not lead to any gross cortical or neuronal abnormalities, where distinct PN populations are born, specified and positioned normally in the neocortex. Cell death analysis also showed that there is no enhanced cell death in these mutants. Therefore, *Ppargc1α* is not cell-autonomously required for neuronal survival in the neocortex, especially in the native cellular state where there is no acute external stress or neurodegeneration.

These findings motivated another study to investigate whether *Ppargc1α* is important for neuronal survival in the context of accumulated chronic stress caused by aging. Remarkably, examination of 18-month-old *Ppargc1α* null and conditional null mutants revealed similar results: there are neither gross cortical, neuronal or PN subtype-specific anomalies nor enhanced cell death in these mutants. Thus, aging together with the loss of *Ppargc1α*, do not cause neuronal death. In all, my results refine our current understanding of *Ppargc1α*'s role in the neocortex with regard to neuronal survival. *Ppargc1α* alone is not necessary to maintain survival and may be important only in the context of acute cellular stress.

Previous studies have also shown that global loss of *Ppargc1α* leads to spongiform-like lesions in the striatum and suggests that these lesions resemble degenerative lesions observed in mice models of Huntington's disease (HD). Yet, it is unclear where these lesions are exactly localized, when they develop and whether they persist with age or recover with time. Most importantly, it is unknown what neuronal subclass in the brain contributes to these lesions. Understanding the cellular origins of these lesions will provide new insights into common disease mechanisms behind distinct disorders that share similar characteristic lesions.

Here, I describe in detail that global loss of *Ppargc1α* causes spongiform-like lesions to develop by P28 and persist with age through 18 months. These lesions are localized within the axonal bundles of the internal capsule (IC) through which descending fibers of subcerebral projection neurons (SCPN) and ascending axons of thalamocortical projection neurons (TCPN) extend. Interestingly, I find that *Ppargc1α* is preferentially expressed in SCPN, including corticospinal motor neurons (CSMN), as well as in selected nuclei of the thalamus during postnatal development. In order to determine whether cell-autonomous loss of *Ppargc1α* in SCPN or TCPN causes these lesions, I generated two new conditional null mutant lines that ablated *Ppargc1α* specifically from one of these two neuronal populations and determined if similar lesions develop. Surprisingly, cell-intrinsic loss of *Ppargc1α* in SCPN or TCPN does not contribute to spongiform-like lesions in the IC. These data suggests that formation of these lesions may involve a more complex mechanism that either includes the simultaneous loss of *Ppargc1α* in multiple neuronal regions, or a hitherto unexamined neuronal subclass. It is also possible that systemic components contribute to the development of these lesions.

2.2. Introduction.

Neurons in the central nervous system can be induced to die by apoptosis (98, 99). Extrinsic apoptotic pathways operate through the stimulation of death receptors by extracellular ligands to induce downstream JNK (c-Jun-N-terminal kinase) pathways that activate effector caspases (99). They can also combine with intrinsic apoptotic pathways at the mitochondria (99). Intrinsic apoptotic pathways cause the mitochondria to release cytochrome c that results in the assembly of the apoptosome complex which further stimulates effector caspases to kill the cell (99). Translocation of apoptotic factors like BH3 proteins to the mitochondrial membrane to cause the release of cytochrome c from the mitochondria highlights the key role played by this organelle (99).

Many neuronal survival factors promote survival by inhibiting apoptotic pathways at distinct sites of action: upstream of the mitochondria, at the mitochondria to prevent the release of pro-apoptotic factors, or downstream of the mitochondria (99). Upstream of the mitochondria, there are decoy proteins that prevent apoptosis by competing with pro-apoptotic ligands for binding with death receptors such as cFLIP/cFLAR (100, 101), or by sequestering the ligands like DCR3 (102). Downstream of the mitochondria, survival factors can either act as decoys or they can associate with and prevent cytochrome c from forming the apoptosome (103, 104). At the mitochondria, neuronal survival factors typically prevent the permeabilization of mitochondrial membranes and the release of apoptotic factors. Many well-known factors include the anti-apoptotic BCL2-like family members (105) and the uncoupling proteins from the UCP family that reduce reactive oxygen species (ROS) (106).

Interestingly, *Ppargc1α* is known to be important for mitochondrial biogenesis in skeletal muscle (51, 54, 61) and can induce UCP-1 expression in brown fat (42). Hence, *Ppargc1α* is purported to be important for cell survival.

In the context of neurodegenerative diseases, previous studies have involved *Ppargc1α* in repressing the neurodegeneration of striatal neurons in a mouse model of HD by suppressing ROS and protecting against mitochondrial dysfunction, thereby enhancing neuronal survival against oxidative insults (72-74). In the context of PD, prior work has shown that when exposed to the neurotoxin MPTP, *Ppargc1α* null mice show greater dopaminergic cell death, similar to what is observed in mice with PD (72). In this case, enhanced cell death was caused by excessive oxidative damage to the dopaminergic neurons present in the substantia nigra, as evident by an increase in nitrosylated proteins–a marker for ROS-induced cell damage (72). The association of *Ppargc1α* with PD is also supported by a genome-wide expression study showing that mitochondrial genes responsive to *Ppargc1α* are underexpressed in patients with PD (75), as well as another recent study showing that PARIS–a parkin interacting molecule that contributes to neurodegeneration in PD–transcriptionally represses *Ppargc1α* (76). In addition, there is some preliminary work linking *Ppargc1α* to ALS (77-79), multiple sclerosis (80), Alzheimer's disease (81), bipolar disorder and schizophrenia (82). However, notably in all these studies, the contribution of *Ppargc1α* to neuronal survival is achieved only in the context of acute cellular stress or ongoing neurodegeneration. It remains unknown if *Ppargc1α* is sufficient to govern neuronal survival in a native cellular context. Indeed, it is imperative to elucidate whether *Ppargc1α* itself is critical for neuronal survival. Doing so will not only augment our knowledge of disease mechanisms behind neuronal death, but also will instruct the development of potential therapeutic solutions to enhance neuronal survival.

Here, I hypothesize that *Ppargc1α* plays a cell-autonomous role in the dorsal forebrain to control their survival. To test this hypothesis, I examined *Ppargc1α* null mutant mice and newly generated conditional null mutant mice for *Ppargc1α* in the dorsal telencephalon, employing a number of neuron and PN subtype-selective markers to allow precise delineation of the development of distinct subpopulations of cortical neurons. Surprisingly, I found that in the absence of *Ppargc1α*, there are no gross cortical or neuronal abnormalities where distinct PN populations are born, specified and positioned normally in the neocortex. Moreover, cell death analysis by immunostaining and histological methods further demonstrated that there is no enhanced cell death caused by global or conditional loss of *Ppargc1α* in the dorsal forebrain. Hence, *Ppargc1α* is not cell-intrinsically required to regulate neuronal survival in the neocortex, particularly where there is no acute cellular stress.

These findings prompted me to explore whether *Ppargc1α* is important for neuronal survival in the event of chronic cellular stress caused by aging. I hypothesize that *Ppargc1α* plays a cell-autonomous role in SCPN to control neuronal survival in the context of aging. I tested this hypothesis by examining 18-month-old *Ppargc1α* null and conditional null mutant mice with similar methodologies. Interestingly, I discovered similar results in these aged mice: in the absence of *Ppargc1α*, there are no gross cortical or neuronal abnormalities and distinct PN populations are maintained normally in the neocortex. Moreover, there is no increased cell death caused by global or conditional loss of *Ppargc1α* in the dorsal forebrain, even in these 18-month-old mutant mice. Therefore, I conclude that *Ppargc1α* is not cell-intrinsically required to govern neuronal survival in the neocortex, even in the context of aging.

Previous studies have also shown that *Ppargc1α*$^{-/-}$ mice display not only behavioral abnormalities in terms of hyperactivity, hindlimb clasping and motor impairment indicative of

neuronal anomalies, but also, strikingly, develop lesions predominantly in the striatum that are reminiscent of those in HD mice (63). Yet, it remains unknown where these lesions are exactly localized in the striatum, when they develop and whether they persist with age or recover with time. Most importantly, it is unclear from which neuronal subclass do these lesions originate.

Here, I also examined the lesions in the striatum of *Ppargc1α*$^{-/-}$ mice across various ages using brightfield as well as immunohistological methodologies, and for the first time, describe in detail that these lesions are localized within the axonal bundles of the IC along the anteroposterior axis, develop by P28 and persist with time through 18 months of age. In order to determine the cell population responsible for these lesions, I elucidated the developmental time course, areal distribution and cell type specificity of *Ppargc1α* expression in the brain. Focusing on the cortex and the thalamus, I found that it is selectively expressed in SCPN of deep layer V in the neocortex and in certain TCPN that reside in the ventroposterior region of the thalamus. Since SCPN and TCPN extend axonal projections through the IC where spongiform lesions are localized in the mutant, I hypothesize that *Ppargc1α* plays a cell-intrinsic function in SCPN or TCPN in preventing the formation of these lesions in the IC. To test this hypothesis, I generated two distinct conditional null mutants, one in the dorsal forebrain and the other in the thalamus. I investigated the formation of these lesions, if any, in these mutants across various ages employing similar brightfield as well as immunohistological methods. Surprisingly, I found that cell-autonomous conditional loss of *Ppargc1α* in the neocortex or thalamus does not cause spongiform-like lesions, even in mutants at 18 months of age. Therefore, I conclude that *Ppargc1α* is not required in SCPN or TCPN to cause spongiform lesions in the IC. My data further suggest that the development of these lesions may implicate a more complicated mechanism that either involves the concurrent loss of *Ppargc1α* in multiple neuronal regions, or

a thus far unexamined neuronal subtype, or even the contribution of systemic components to the development of these lesions.

2.3. Results.

2.3.1. Selection of *Ppargc1α* as an interesting candidate to study neuronal survival.

I took advantage of the availability of this new microarray database, as described in section 1.2.5., to search for novel *Fezf2*-regulated genetic controllers of important aspects of SCPN/CSMN postnatal differentiation, particularly in neuronal survival. The screen revealed 732 statistically significant genes that were either upregulated or repressed by *Fezf2* at various stages of development. Of these genes, I first focused on 30 prime candidates that were highly upregulated by *Fezf2* within 24 and/or 48 hrs following *Fezf2* overexpression. From these, I further selected 24 novel genes with unknown function in SCPN/CSMN development and performed a thorough literature search on each one of them to determine if any could be implicated in specific aspects of SCPN/CSMN development. Subsequently, I narrowed down this list to 4 novel candidate genes, which included 2 transcription factors, 1 transcriptional coactivator, and 1 axon guidance molecule. Eventually, I decided to focus my analysis on *Ppargc1α* because of my interest in studying potential molecular signals that govern SCPN-specific survival. I chose *Ppargc1α* primarily because of (i) available studies implicating *Ppargc1α* in neuronal survival and in suppressing striatal neurodegeneration in Huntington's disease (72-74), and secondarily, due to (ii) the specific upregulation of this gene upon *Fezf2* overexpression and its restricted expression by microarray in SCPN/CSMN and not CPN (5), as well as (iii) prior work describing its fundamental role in regulating complex biological programs in a tissue-specific manner, which includes mitochondrial biogenesis, adaptive thermogenesis in brown adipose tissue, and fiber-type switching in skeletal muscles, among many others (38, 39, 61, 197, 198). I have been very fortunate to have established a collaboration with Dr. Bruce Spiegelman (Dana Farber Cancer Institute) who has graciously shared with us

Ppargc1α null mutants (*Ppargc1α*$^{-/-}$), floxed conditional mutants (*Ppargc1α*$^{fl/fl}$) and relevant reagents such as *Ppargc1α* antibodies for immunohistochemistry (IHC). Thus, I identified *Ppargc1α* as a very interesting gene candidate that potentially contributes to SCPN/CSMN-selective survival or other crucial aspects of SCPN/CSMN differentiation and function at late stages of maturation, a previously unexplored topic.

2.3.2. *Ppargc1α* is expressed in SCPN of layer V during postnatal development.

2.3.2.A. Temporal and spatial analysis.

To determine the temporal and spatial expression profile of *Ppargc1α* in the brain, I performed *in situ* hybridization (ISH) for *Ppargc1α* on wild type C57BL/6 coronal cortical sections at various embryonic ages from E13.5 to E18.5 and postnatal ages from P0 to P28. In the neocortex, I discovered that *Ppargc1α* is preferentially expressed in layer V at lower levels during P0 (Figure 2.1.D.) and at high levels progressively increasing throughout postnatal development from P3 to P28 (Figures 2.1.E to 2.1.H., data not shown for P21), but is not expressed at embryonic ages from E13.5 to E18.5 (Figures 2.1.A. to 2.1.C.). I also found that *Ppargc1α* is predominantly absent from other neocortical layers (Figures 2.1.D. to 2.1.H.). In addition, it is expressed in smaller cells scattered across the neocortex (Figures 2.1.D. to 2.1.H.), which I have confirmed to be Parvalbumin expressing cortical interneurons, as described in sections 2.3.1.B. and 2.3.4.A., and further supported by prior studies done in the rat cortex, and more recently in the murine cortex (94, 97). This temporal profile of *Ppargc1α* expression in layer V predominantly at postnatal ages is in agreement with the previously published microarray data on differential gene expression between major PN subtypes in the neocortex (5), as described in section 2.3.1.B., as well as in pilot studies characterizing *Ppargc1α* expression in

Figure 2.1. *Ppargc1α* is expressed in deep layer V predominantly during postnatal ages.

(A – C) ISH analysis showed that *Ppargc1α* is largely absent in the cortical plate during embryonic ages from E13.5 to E15.5 and is only expressed from E18.5. The faint expression seen in the progenitor zone is weak and undefined and does not seem cellular upon high magnification (data not shown).

(D – H) *Ppargc1α* is weakly expressed in deep cortical layer V at P0, and progressively increases its expression in layer V with time. It is predominantly expressed during postnatal ages from P3 to P28 (data not shown for P21). Ctx, cortex; LGE, lateral ganglionic eminence; CGE, caudal ganglionic eminence; MGE, medial ganglionic eminence; LGP, lateral globus pallidus; Str, striatum. Scale bars, 100 μm (A – H).

Figure 2.1. (Continued)

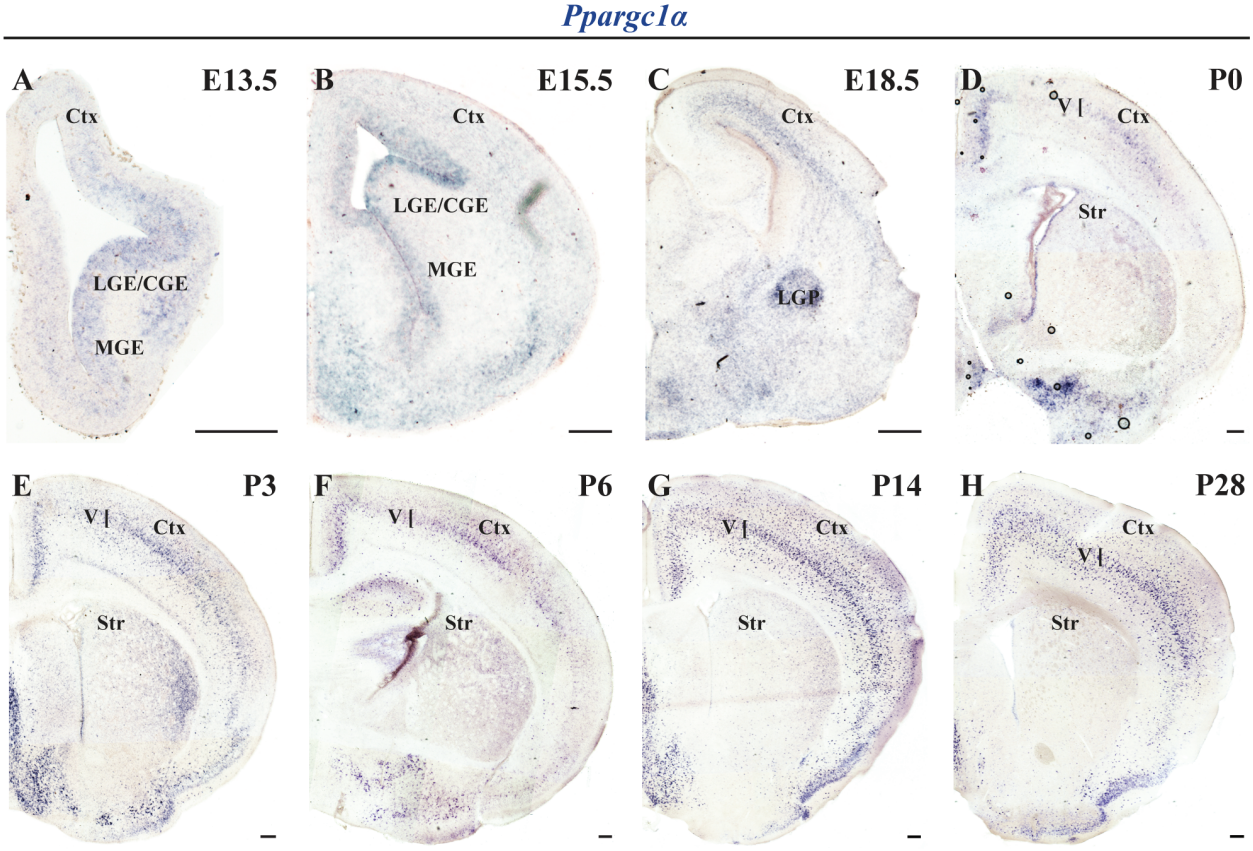

the adult murine brain (199).

Anteroposterior and mediolateral expression analysis of *Ppargc1α* in the neocortex revealed that it is expressed in layer V along these axes without evident arealization (Figures 2.2.A. to 2.2.E.). To confirm this, I performed ISH for *Ppargc1α* on wild type C57BL/6 sagittal cortical sections at P14. Similarly, I found that *Ppargc1α* is consistently expressed in layer V along the rostrocaudal axis (data not shown). Hence, *Ppargc1α* expression in layer V is not spatially arealized along the anteroposterior and mediolateral axes. This temporally and spatially distinct expression profile indicates that *Ppargc1α* is specifically and consistently expressed throughout layer V where SCPN reside in the neocortex, and is absent in other cortical layers. It also demonstrates that *Ppargc1α* is important at later stages of development during postnatal ages. Thus, these data suggest that *Ppargc1α* is important for the postnatal differentiation of SCPN, including CSMN.

Besides its expression in the neocortex, spatial analysis further revealed that *Ppargc1α* is expressed at high levels in the piriform cortex, hippocampus, as well as the diagonal band of Broca (Figures 2.2.A. to 2.2.E.). It is also highly expressed in certain regions of the basal ganglia such as the globus pallidus (lateral and medial), ventral pallidum, substantia nigra and the subthalamic nuclei (Figures 2.2.A. to 2.2.E., data not shown for some regions). In addition, it is expressed at high levels in certain thalamic nuclei (i.e., anterodorsal thalamic nucleus, ventral posterolateral thalamic nucleus, ventral posteromedial thalamic nucleus and lateral habenular nucleus), as well as in distinct regions of the subthalamus including the reticular thalamic nucleus (Figures 2.2.A. to 2.2.E., data not shown for some regions). Besides its strong expression in these areas, I also detected that *Ppargc1α* is expressed at low levels in regions like the striatum, amygdala and the hypothalamus (Figures 2.2.A. to 2.2.E.., data not shown for some

Figure 2.2. *Ppargc1α* is consistently expressed in deep layer V without evident arealization. (A – E) ISH analysis demonstrated that *Ppargc1α* is expressed along the anteroposterior and mediolateral axes without evident arealization. Further analysis on P14 sagittal cortical sections further ascertained these results (data not shown). Ctx, cortex; Str, striatum; Pir, piriform cortex; DB, diagonal band of Broca; Hip, hippocampus; Rt, reticular thalamic nuclei; LGP, lateral globus pallidus; VP, ventroposterior thalamic nuclei (including ventral posterolateral and ventral posteromedial thalamic nuclei). Scale bars, 100 μm (A – E).

Figure 2.2. (Continued)

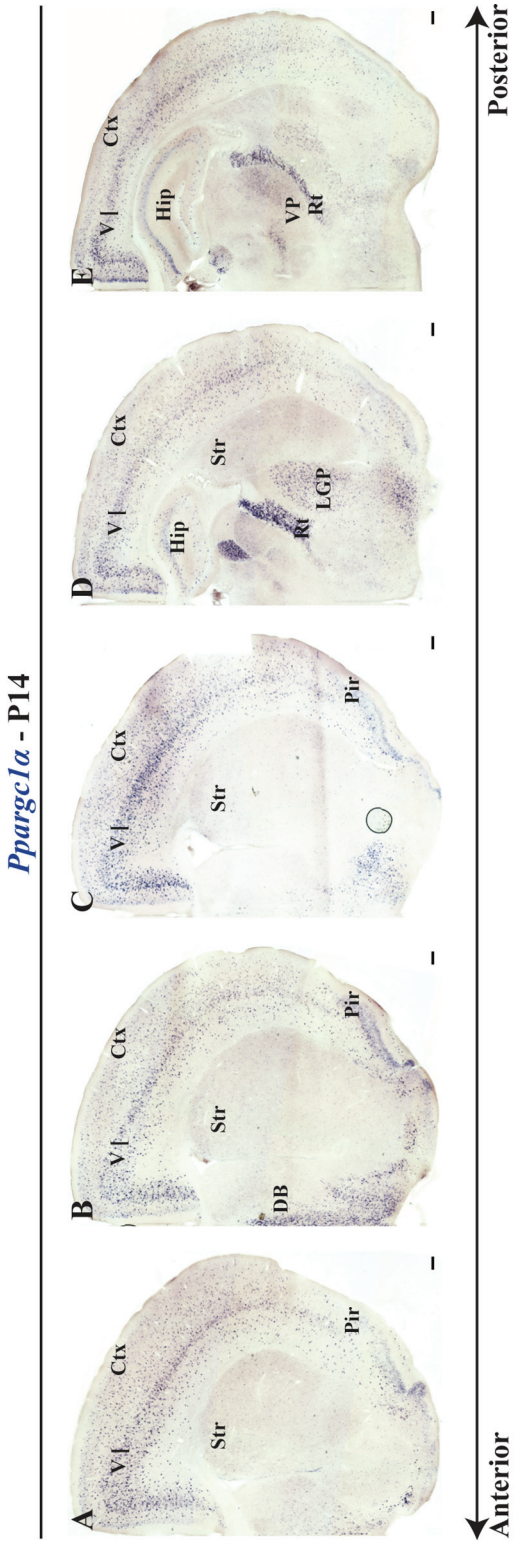

regions). Temporal analysis from P3 to P28 showed that *Ppargc1α* is expressed in these areas of the brain consistently throughout postnatal development (in at least 3 distinct postnatal ages) (Table 2.1.). Results of the temporal and spatial analysis of *Ppargc1α* expression in the brain from P3 to P28 is summarized in Table 2.1.. This is the first expression profile of *Ppargc1α* in the murine brain across multiple postnatal ages and is in line with work done in the adult (199).

Together, these data demonstrate that in the neocortex, *Ppargc1α* is preferentially expressed at high levels in layer V where SCPN are located, and is lacking in other cortical layers. They also indicate that *Ppargc1α* expression in layer V is not spatially arealized along the anteroposterior and mediolateral axes and that it is selectively expressed at later postnatal stages of development. Therefore, *Ppargc1α* is potentially a novel critical factor for the postnatal differentiation of SCPN, including CSMN.

2.3.2.B. Cell type specific analysis.

To elucidate the neuronal subtype-specific expression of *Ppargc1α* in the neocortex, I looked at the microarray expression profile done on purified CSMN, corticotectal projection neurons (CTPN) and callosal projection neurons (CPN) by Arlotta and Molyneaux, *et al.* (data available at NCBI Gene Expression Omnibus accession number GSE2039/GDS1076) (5) . These microarray data indicated that *Ppargc1α* is expressed in CSMN and CTPN, two closely related subtypes of SCPN, but not in CPN (Figure 2.3.A.). They also showed that *Ppargc1α* expression in CSMN is negligible at E18.5 and progressively increases from P3 to P14, suggesting a novel role for *Ppargc1α* at postnatal stages of SCPN/CSMN differentiation (Figure 2.3.A.).

To verify the previously published microarray data and to determine whether *Ppargc1α* expression in layer V is restricted to SCPN, I performed an ISH for *Ppargc1α* combined with an immunostaining for CTIP2–a marker that is expressed at high levels in SCPN but not CPN in

Table 2.1. Temporal and spatial expression profile of *Ppargc1α* in the brain during postnatal development.

This table summarizes where and when *Ppargc1α* is expressed in the brain during postnatal ages. A check (✓) indicates that *Ppargc1α* is detected at the stated region and time while a cross (X) shows that *Ppargc1α* is not detected at the stated region and time. ND signifies that *Ppargc1α* expression was not determined at the stated region and time.

Table 2.1. (Continued)

		P3	P6	P14	P21	P28
Cerebral Cortex	Layer V - with small scattered cells spread around all cortical layers - from cingulate to auditory (no apparent arealization)	✓	✓	✓	✓	✓
	PIR- piriform cortex	✓	✓	✓	✓	✓
Diagonal Band of Broca	MS - medial septal nucleus	✓	✓	✓	✓	✓
	LSI - lateral septal nucleus - weaker signal than MS	✓	✓	✓	✓	ND
	VDB - nucleus of the vertical limb of the diagonal band	✓	✓	✓	✓	✓
	HDB - nucleus of the horizontal limb of the diagonal band	✓	✓	✓	✓	✓
Hippocampus	Hip- Hippocampus - from CA1 to CA3, spread from Py (pyramidal cell layer) to Or (Oriens layer)	✓	✓	✓	✓	✓
Thalamus	AD - anterodorsal thalamic nucleus	✓	✓	✓	ND	✓
	IAD - interanterodorsal thalamic nucleus	✓	✓	✓	ND	ND
	MD - mediodorsal thalamic nucleus	✓	✓	✓	✓	ND
	CM - central medial thalamic nueclus (weak)	✓	✓	✓	✓	✓
	PF - parafascicular thalamic nucleus	✓	✓	✓	ND	ND
	OPC and PC - oval paracentral thalamic nucleus	✓	✓	✓	✓	✓
	VLGMC - ventral lateral geniculate nucleus, magnocellular part	✓	✓	✓	✓	✓
	VLGPC- ventral lateral geniculate nucleus, parvicellular part	✓	✓	✓	✓	✓
	DLG - dorsal lateral geniculate nucleus (weak)	ND	ND	✓	ND	✓
	LPLR - lateral posterior thalamic nucleus, laterorostral part (weak @ P21)	✓	✓	ND	✓	ND
	LPMR - lateral posterior thalamic nucleus, mediorostral part (weak @ P21)	✓	✓	ND	✓	ND
	LDVL- laterodorsal thalamic nucleus, ventrolateral part - some parts (weak signal - scattered cells)	X	✓	✓?	✓	ND
	LDDM - laterodorsal thalamic nucleus, dorsomedial part	X	✓	ND	✓	ND
	VPL - ventral posterolateral thalamic nucleus	✓	✓	✓	✓	✓
	VPM - ventral posteromedial thalamic nucleus	✓	✓	✓	✓	✓
	Parts of Po - posterior thalamic nuclear group	✓	✓	✓?	✓?	✓
	LHb - lateral habenular nucleus	✓	✓	✓	✓	✓

Table 2.1. (Continued)

		P3	P6	P14	P21	P28
Subthalamus	Rt - reticular thalamic nucleus	✓	✓	✓	✓	✓
	ZI - zona incerta (weak)	✓	✓	✓	✓	✓
	STh - subthalamic nuclei	✓	✓	ND	✓	✓
Basal Ganglia	CPu- Striatum- arealized to the most lateral edges (P3-P6); few scattered cells (P14)	✓	✓	✓	ND	ND
	LGP - lateral globus pallidus	✓	✓	✓	✓	✓
	MGP- medial globus pallidus	X	✓	✓	ND	ND
	VP- ventral pallidum	✓	✓	✓	✓	✓
	Substantia nigra	ND	ND	✓	ND	ND
	STh - subthalamic nuclei	✓	✓	ND	✓	✓
Amygdala	PLCo - posterolateral cortical amygdaloid nucleus	✓	✓	ND	ND	ND
	PMCo - posteromedial cortical amygdaloid nucleus	✓	✓	ND	ND	ND
	MePV - medial amygdaloid nucleus, posterovental part	✓	✓	ND	✓?	ND
	MePD? -- medial amygdaloid nucleus, posterodorsal part	✓	✓	ND	✓?	ND
	BLP - basolateral amygdaloid nucleus, posterior part	✓	✓	ND	✓	✓
	BLA - basolateral amygdaloid nucleus, anterior part	✓	✓	✓	✓	✓
	BMP - basolateral amygdaloid nucleus, posterior part	✓	✓	ND	✓	ND
Hypothalamus	LPO - lateral preoptic area	✓	✓	✓	✓	ND
	MCPO - magnocellular preoptic nucleus	✓	✓	✓	✓	✓
	DM - dorsomedial hypothalamic nucleus	✓	ND	ND	✓?	ND
	LH- lateral hypothalamic area	X	✓	ND	✓	ND

= strong signal
= weaker signal

Figure 2.3. *Ppargc1α* is expressed in layer V SCPN and Parvalbumin-expressing interneurons but not in CThPN, majority of CPN and glial cells of the neocortex.

(A) Published microarray analysis revealed that *Ppargc1α* is preferentially expressed in SCPN such as CSMN and CTPN but not in CPN. *Ppargc1α* expression in CSMN also progressively increases with age from E18 to P14 – a result consistent with my new findings as described in section 2.3.1. and shown in Figure 2.1.. This figure is adapted from (5).

(B) *Ppargc1α* is selectively expressed in majority of CTIP2-positive SCPN of deep layer V (arrows). Single positive cells for *Ppargc1α* and CTIP2 are also detected (arrowheads).

(C) *Ppargc1α* is not expressed in CTIP2-positive CThPN of deep layer VI.

(D) *Ppargc1α* is not expressed in several SATB2-positive CPN of deep layer V (arrowheads). Some double positive cells for *Ppargc1α* and SATB2 are detected in deep layer V (arrows). In contrast, *Ppargc1α* is not expressed in SATB2-positive CPN of other cortical layers (data not shown).

(E) *Ppargc1α* is not expressed in CUX1positive CPN of cortical layers II – IV (data shown for layer IV).

(F) *Ppargc1α* is selectively expressed in Parvalbumin (PV)-positive cortical interneurons (arrows, data shown for deep layer V). Single positive cells for *Ppargc1α* are also detected (arrowheads).

(G) *Ppargc1α* is not expressed in OLIG2-positive oligodendrocyte progenitors as well as myelinating oligodendrocytes across all cortical layers (data shown for deep layer V).

(H) *Ppargc1α* is not expressed in APC-positive mature myelinating oligodendrocytes that are located mainly in the deep cortical layers V/VI (data shown for deep layer V).

(I) *Ppargc1α* is not expressed in S100β-positive astrocytes across all cortical layers (data shown for deep layer V).

Figure 2.3. (Continued)

(J – L) In agreement with the results in G and H, *Ppargc1α* is not expressed in major white matter tracts like the corpus callosum and anterior commissure where oligodendrocytes are found in large numbers. Scale bars, 100 μm (J), 50 μm (B – I and K – L).

Figure 2.3. (Continued)

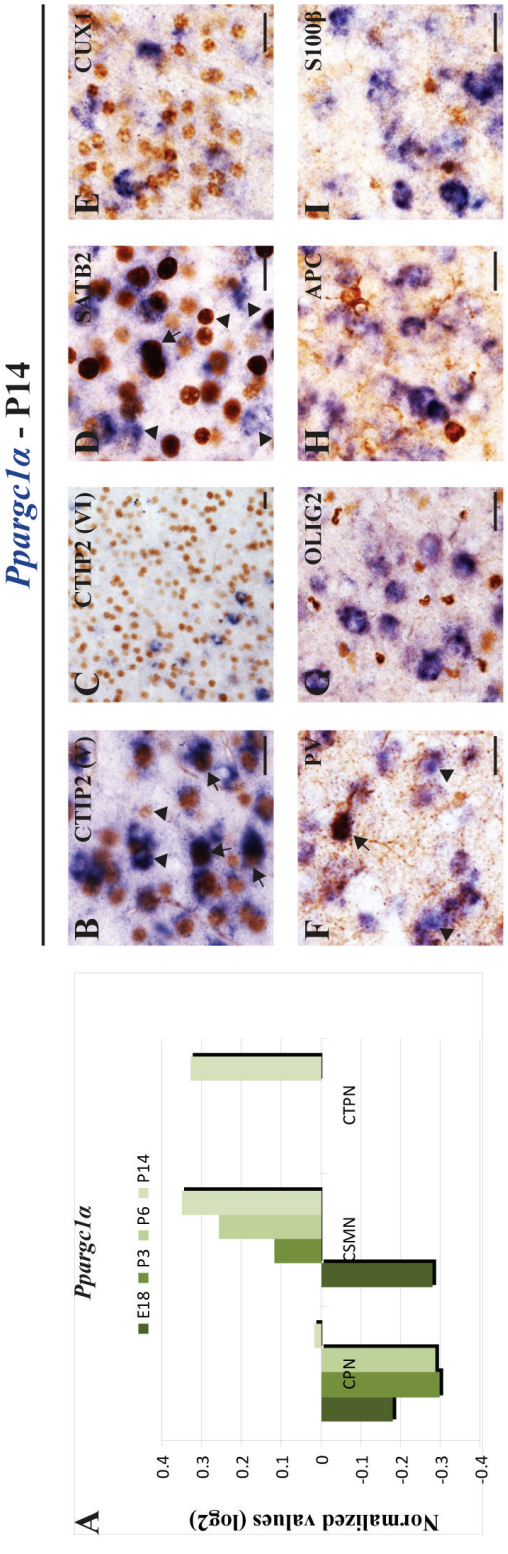

Figure 2.3. (Continued)

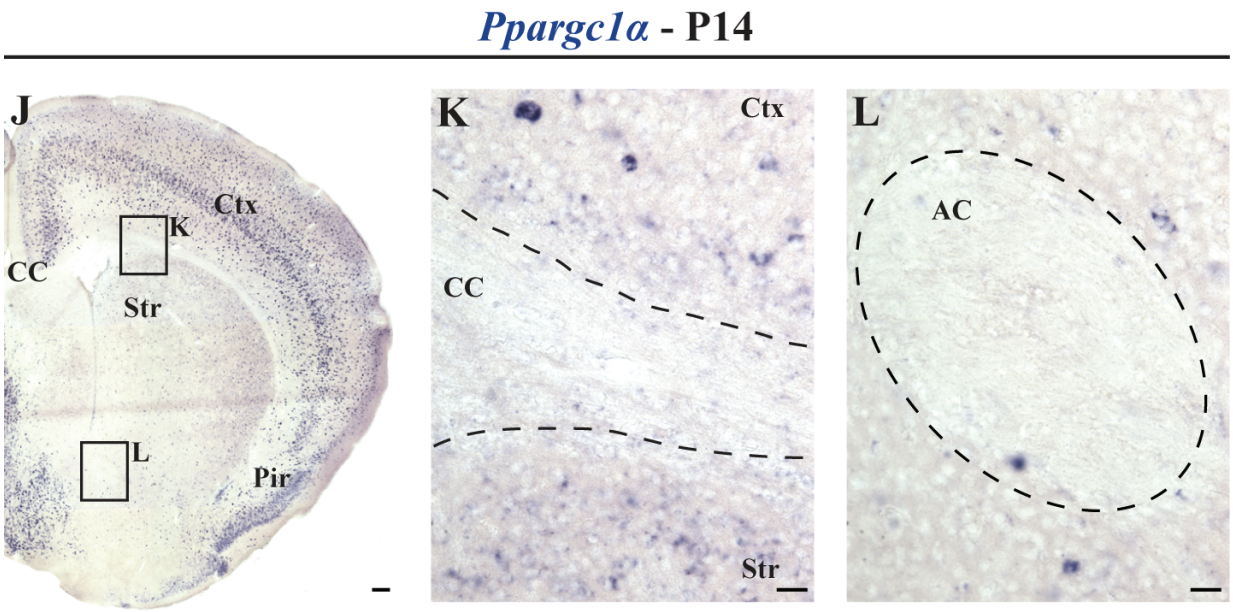

layer V and at lower levels in layer VI CThPN (5)–on P14 wild type C57BL/6 coronal cortical sections. I found that several of the CTIP2 expressing cells in layer V expressed *Ppargc1α*, indicating that *Ppargc1α* is expressed in SCPN (Figure 2.3.B., arrows). Interestingly, cells that were single positive for either CTIP2 or *Ppargc1α* were also detected (Figure 2.3.B. arrowheads). The presence of single positive cells for CTIP2 suggests that *Ppargc1α* labels a subset of SCPN. Consistent with prior studies done in the rat and mouse cortex (94, 97), the single positive cells for *Ppargc1α* are possibly Parvalbumin expressing cortical interneurons, a result confirmed by data described below, in Figure 2.3.F. as well as in section 2.3.4.A.. In addition, colocalization analysis of *Ppargc1α* and CTIP2 positive CThPN of layer VI revealed that CTIP2 expressing cells of layer VI do not express *Ppargc1α*, showing that *Ppargc1α* is not expressed in layer VI CThPN (Figure 2.3.C.). Together, these prior data and my new results demonstrate that *Ppargc1α* is specifically expressed in SCPN, including CSMN, of deep layer V but is absent from CThPN of deep layer VI postnatally.

To ascertain the prior microarray data and to elucidate that *Ppargc1α* is not expressed in CPN, I did an ISH for *Ppargc1α* combined with an immunostaining for CUX1—a marker that is expressed in CPN of upper layers II-V but not in deep layers V-VI (1, 200)—as well as SATB2—a marker that is expressed in CPN across all cortical layers from II to VI but not in layer V SCPN (34, 35)—on P14 wild type C57BL/6 coronal cortical sections. I found that most, if not all, of the CUX1 positive cells of upper layers II-IV do not express *Ppargc1α*, indicating that *Ppargc1α* is not expressed in CPN of cortical upper layers II-IV (Figure 2.3.E.). Colocalization analysis of *Ppargc1α* and SATB2 positive CPN of deep layer V revealed that several SATB2 expressing cells of layer V do not express *Ppargc1α*, showing that *Ppargc1α* is not expressed in many of layer V CPN (Figure 2.3.D., arrowheads). However, cells that are

double positive for *Ppargc1α* and SATB2 were also detected in layer V (Figure 2.3.D., arrows). This suggests that either there is a small subset of layer V CPN that express *Ppargc1α*, or that *Ppargc1α* is expressed in a subgroup of layer V CTIP2 positive SCPN that continue to express SATB2. It is known that at early stages of development, early postmitotic neurons that will give rise to distinct SCPN and CPN subtypes in layer V often share similar molecular markers that will eventually parcelate and become localized to different subclasses with time (1, 201, 202). In fact, immature postmitotic neurons that will give rise to SCPN are double positive for CTIP2 and SATB2 (201). Further analysis of SATB2 positive cells in deep layer VI demonstrated that SATB2 positive cells of layer VI do not express *Ppargc1α*, indicating that *Ppargc1α* is not expressed in deep layer VI CPN (data not shown). Consistent with the previously published microarray data, my new results show that *Ppargc1α* is not expressed in CPN of upper layers II – IV and deep layer VI, and in some CPN of deep layer V. Thus, with regard to major PN classes of the neocortex, *Ppargc1α* is expressed preferentially in SCPN of layer V but not in CPN and CThPN of the neocortex.

To study whether *Ppargc1α* is expressed in Parvalbumin expressing cortical interneurons, I performed an ISH for *Ppargc1α* combined with an immunostaining for PARVALBUMIN, a marker that is expressed in a subset of cortical interneurons (203, 204), on P14 wild type C57BL/6 coronal cortical sections. I found that PARVALBUMIN expressing cortical interneurons across cortical layers II-VI expressed *Ppargc1α*, indicating that *Ppargc1α* is expressed in Parvalbumin expressing cortical interneurons (Figure 2.3.F., arrows). This is consistent with prior work done in the rat and more recently mouse cortex (94, 97). However, I also detected cells that are single positive for *Ppargc1α* throughout cortical layers II-VI (Figure 2.3.F., arrowheads). Single positive cells for *Ppargc1α* in layer V are likely to be SCPN as

described above and shown in Figure 2.3.B., while similar cells in other layers are potentially representative of alternative subsets of cortical interneurons.

To investigate whether *Ppargc1α* is expressed in glial cells, I did an ISH for *Ppargc1α* combined with an immunostaining for (i) OLIG2, a marker that is expressed in oligodendrocyte progenitors as well as mature myelinating oligodendrocytes (205), (ii) APC, a marker that is expressed only in mature myelinating oligodendrocytes (206, 207), and (iii) S100β, a marker that is exclusively expressed in astrocytes (208), on P14 wild type C57BL/6 coronal cortical sections. I discovered that OLIG2 expressing oligodendrocyte progenitors and myelinating oligodendrocytes as well as APC expressing mature oligodendrocytes do not express *Ppargc1α*, indicating that *Ppargc1α* is not expressed in oligodendrocyte progenitors as well as mature oligodendrocytes of the neocortex (Figure 2.3.G. and 2.3.H.). Furthermore, in line with the above result, I did not find *Ppargc1α* expression in white matter tracts like the corpus callosum and anterior commissure where oligodendrocytes are found in large numbers (Figure 2.3.J. to 2.3.L.). In addition, I found that S100β expressing astrocytes do not express *Ppargc1α*, showing that *Ppargc1α* is not expressed in astrocytes (Figure 2.3.I.). Therefore, my new results demonstrate that *Ppargc1α* is not expressed in glial cells of the neocortex, specifically in oligodendrocytes and astrocytes. These further support the above result that the smaller scattered cells expressing *Ppargc1α* in the neocortex are likely to be cortical interneurons that have migrated from the ventral parts of the brain, in concordance with the result in 2.3.4.A..

A microarray analysis done by Ben Barres and his group showed that *Ppargc1α* is absent in the myelinating oligodendrocytes (209). This is in agreement with my colocalization analysis of *Ppargc1α* expression in the cortex with APC, a marker for mature myelinating oligodendrocytes (206, 207), as shown in Figure 2.3.H.. However, their analysis showed that

there is weak expression of *Ppargc1α* in oligodendrocytes and oligodendrocyte progenitors (209). This is in contrast with my data showing that *Ppargc1α* is not expressed in OLIG2 positive oligodendrocyte progenitors as well as differentiated postmitotic oligodendrocytes in the neocortex. This can be due to a couple of factors. First, the microarray analysis was done on cultured oligodendrocytes *in vitro* and there can be differences in gene expression between cultured oligodendrocytes and *bona fide* oligodendrocytes found *in vivo*. This could also explain the discrepancy with another report suggesting that *Ppargc1α* is expressed in cultured oligodendrocytes and can regulate the expression of myelin basic protein (MBP) *in vitro* (88). Secondly, it is possible that *Ppargc1α* is expressed in oligodendrocyte progenitors weakly early on during development. My temporal expression profile shows that *Ppargc1α* is weakly expressed in the ventricular zone of the ventral telencephalon at E13.5 and E15.5, where MGE-, LGE, and CGE-derived oligodendrocyte progenitors are born before migrating to the dorsal telencephalon (117). Hence, in this case, the embryonic profile of *Ppargc1α* expression is in agreement with that of the published dataset. Note that this weak expression of *Ppargc1α* in oligodendrocyte progenitors does not contradict our conclusion that neuron-specific *Ppargc1α* is important for the establishment of proper myelination of the neocortex. This is because prior work has shown that even in the event where a single oligodendrocyte population is ablated, there is functional compensation by remaining oligodendrocyte populations that will result in a normal complement of myelination and oligodendrocytes (117). Furthermore, the MGE-derived oligodendrocyte population is eliminated from the neocortex shortly after birth and does not play a part in the myelination of the postnatal neocortex (117). Hence, it is unlikely that *Ppargc1α* in oligodendrocyte progenitors play a significant role in causing the hypomyelination phenotype as observed in the adult cortex, a novel phenotype that is further described in Chapter 3.

In conclusion, *Ppargc1α* is consistently expressed in SCPN throughout layer V without arealization predominantly during postnatal development from P3 to P28. It is neither expressed in the CThPN of layer VI, nor in the majority of CPN across all cortical layers. However, it is expressed in Parvalbumin expressing cortical interneurons and likely other subsets of interneurons. *Ppargc1α* is not expressed in glial cells such as oligodendrocytes and astrocytes.

2.3.3. PN are born, specified and positioned normally in *Ppargc1α*$^{-/-}$ and *Emx1-Cre; Ppargc1α*$^{fl/fl}$ mice.

Although prior studies have implicated *Ppargc1α* in neuronal survival in the context of acute cellular stress and neurodegeneration (72-74), it remains unknown if *Ppargc1α* is cell-intrinsically important by itself to control neuronal survival. Here, I hypothesize that *Ppargc1α* is cell-autonomously required in neurons, or in SCPN of the neocortex, to govern survival.

If this hypothesis is true, I expect that global and conditional loss of *Ppargc1α* in the dorsal telencephalon will cause neuronal loss. To test this hypothesis and to determine whether global and conditional loss of *Ppargc1α* leads to gross cortical abnormalities–particularly layer V defects–in terms of cell numbers, cell size and morphology, I performed Nissl staining on P28 and 2-month-old *Ppargc1α*$^{-/-}$, 2-month-old *Emx1-Cre; Ppargc1α*$^{fl/fl}$ and their respective matched littermate wild type and *Ppargc1α*$^{fl/fl}$ control coronal cortical sections (n = 3 per genotype at all ages). I compared the gross formation of the six distinct cortical layers, the morphology and the size of cells residing in each layer–especially those of layer V–in *Ppargc1α*$^{-/-}$ and *Emx1-Cre; Ppargc1α*$^{fl/fl}$ mutants to that of their respective control mice. I did not detect any obvious, significant difference between *Ppargc1α*$^{-/-}$, *Emx1-Cre; Ppargc1α*$^{fl/fl}$ and their respective controls at the ages tested (Figures 2.4.A. to 2.4.F., data not shown for 2-month-old *Ppargc1α*$^{-/-}$ and

Figure 2.4. PN are born, specified and positioned normally in *Ppargc1α*$^{-/-}$ and *Emx1-Cre; Ppargc1α*$^{fl/fl}$ mice.

(A – F) Nissl staining revealed that the six cortical layers are grossly normal in P28 *Ppargc1α*$^{-/-}$ and wild type mice. High magnification analysis detected distinct large somas of SCPN/CSMN (arrows) in cortical layer V of both *Ppargc1α*$^{-/-}$ and wild type mice at P28. (B – C and E – F) Boxed areas in (A) and (D) respectively.

(G – H and Q – R) IHC stain for NeuN, a neuron-specific marker, showed that neurons across the six cortical layers appear normal and comparable between 2 month old *Ppargc1α*$^{-/-}$ (G – H), *Emx1-Cre; Ppargc1α*$^{fl/fl}$ (Q – R) and their respective controls.

(I – J and S – T) IHC for CTIP2 that labels layer V SCPN/CSMN and layer VI CThPN showed that layer V SCPN and layer VI CThPN are born and can migrate normally to their destined layers in *Ppargc1α*$^{-/-}$ (I – J), *Emx1-Cre; Ppargc1α*$^{fl/fl}$ (S – T) and their respective controls.

(K – L and U – V) IHC stain for SATB2, which marked all CPN across layers II to VI, revealed that CPN are born and can be positioned normally in their destined layers in 2 month old *Ppargc1α*$^{-/-}$ (K –L), *Emx1-Cre; Ppargc1α*$^{fl/fl}$ (U – V) and their respective controls.

(M – N and W – X) In line with results shown in K – L and U – V, IHC for CUX1 that labels upper layer CPN, indicated that CPN are born and can migrate normally to their destined layers in *Ppargc1α*$^{-/-}$ (M – N), *Emx1-Cre; Ppargc1α*$^{fl/fl}$ (W – X) and their respective controls.

(O – P) In agreement with results shown in I – J and S – T, ISH for *Fezf2*, which marked all SCPN/CSMN in deep layer V at high levels and CThPN in deep layer VI at lower levels, showed that SCPN and CThPN are born and can migrate normally to their destined layers in P28 *Ppargc1α*$^{-/-}$ and wild type mice. Roman numerals indicate the distinct cortical layers. Scale bars, 100 μm (A and D, G – X), 10 μm (B – C and E – F).

Figure 2.4. (Continued)

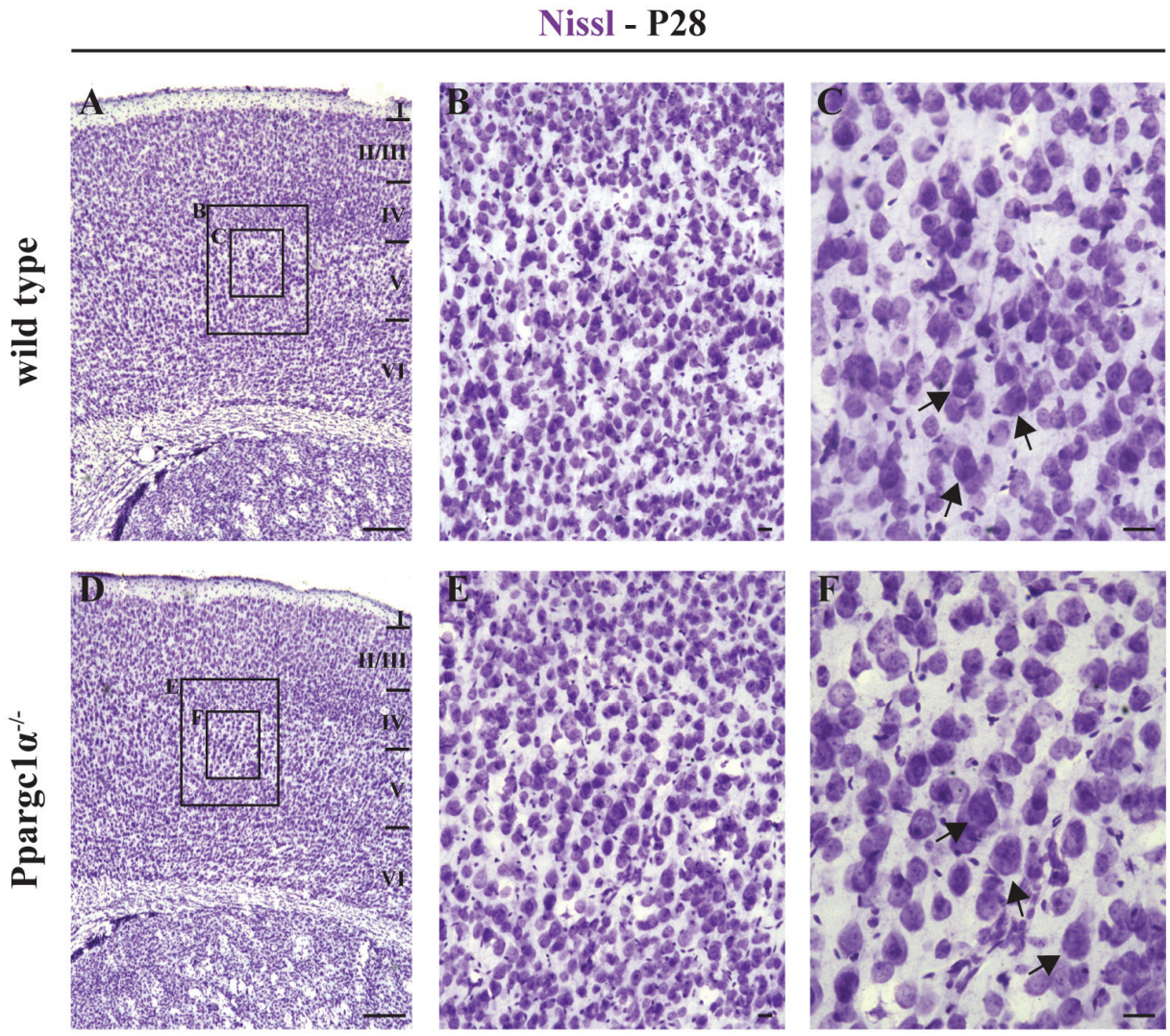

Figure 2.4. (Continued)

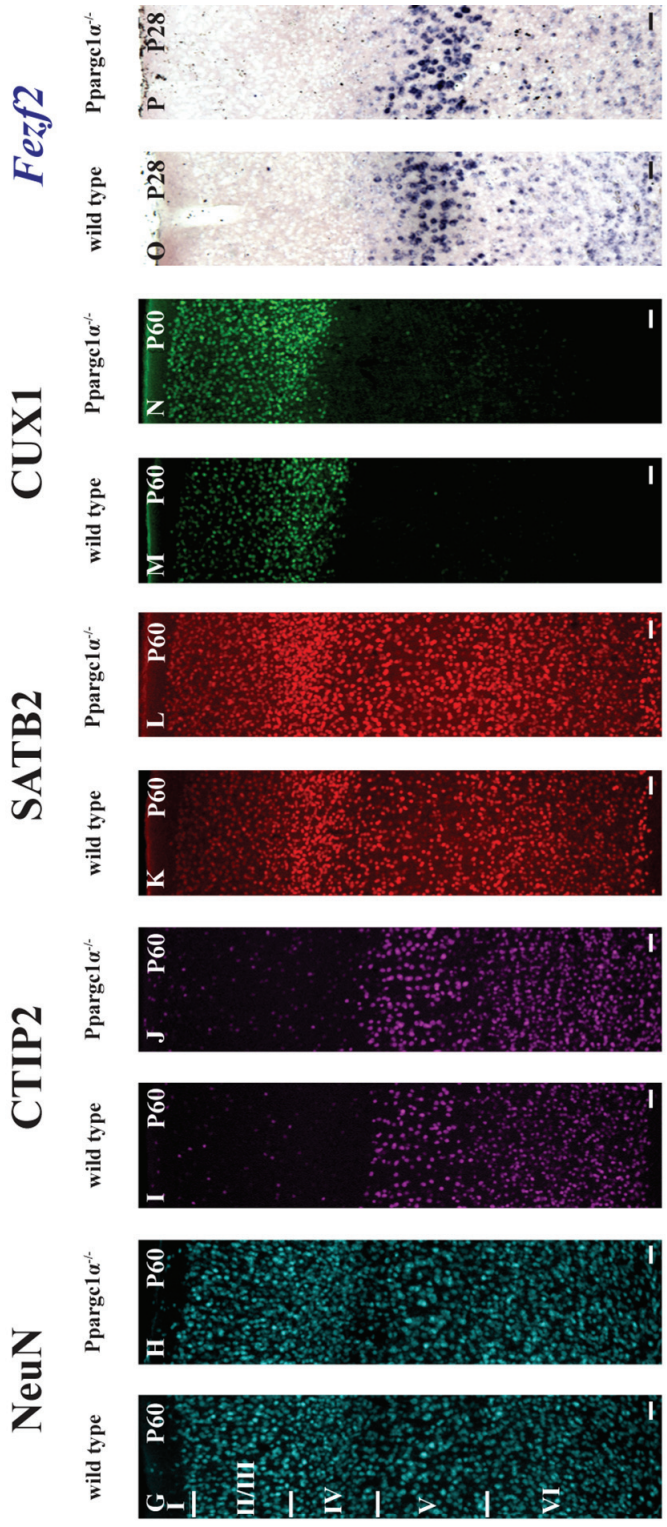

Figure 2.4. (Continued)

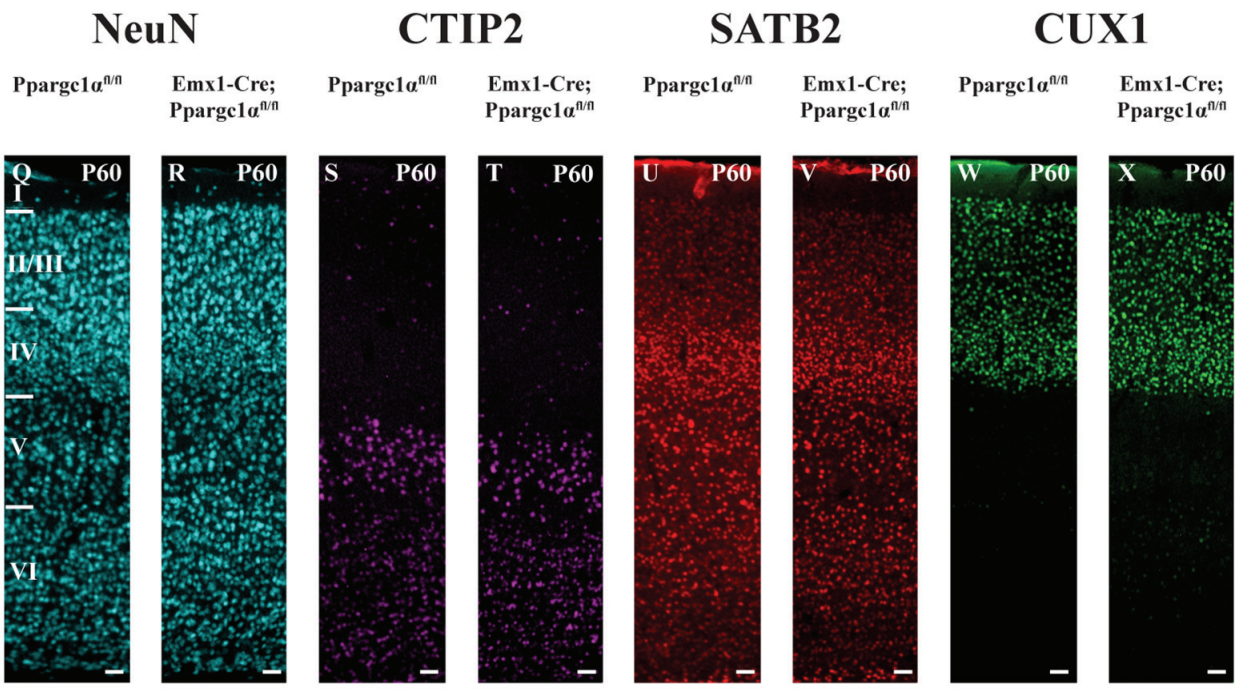

Emx1-Cre; Ppargc1α$^{fl/fl}$ mice). Particularly, distinct large somas of SCPN/CSMN (arrows) in layer V were found in *Ppargc1α*$^{-/-}$, *Emx1-Cre; Ppargc1α*$^{fl/fl}$ and their respective control mice at the ages tested (Figures 2.4.C. and 2.4.F., data not shown for 2-month-old *Ppargc1α*$^{-/-}$ and *Emx1-Cre; Ppargc1α*$^{fl/fl}$ mice). This observation suggests that SCPN/CSMN are born, fate specified, and are able to reach their destined layer in *Ppargc1α*$^{-/-}$ and *Emx1-Cre; Ppargc1α*$^{fl/fl}$ mice. These data also indicate that global and conditional loss of *Ppargc1α* do not cause gross cortical anomalies by allowing cortical cells to be born and migrate normally to form the six distinct cortical layers. This implies that *Ppargc1α* is not cell-intrinsically necessary to maintain cell survival in the neocortex.

To investigate if the global and conditional loss of *Ppargc1α* leads to gross neuronal aberrations, I executed an immunohistochemistry (IHC) stain for NeuN–a marker selective to neurons (210) –on adult *Ppargc1α*$^{-/-}$, *Emx1-Cre; Ppargc1α*$^{fl/fl}$ and their respective matched littermate wild type and *Ppargc1α*$^{fl/fl}$ control coronal cortical sections at 2 months of age (n = 3 per genotype). Similarly, I did not detect any obvious, significant difference between the NeuN positive neurons located in all six different cortical layers between *Ppargc1α*$^{-/-}$ (Figures 2.4.G. and 2.4.H.), *Emx1-Cre; Ppargc1α*$^{fl/fl}$ (Figures 2.4.Q. and 2.4.R.) and their respective matched control mice. In agreement with my above findings, this result shows that neurons are born and can migrate normally to form the six distinct cortical layers in both *Ppargc1α*$^{-/-}$ and *Emx1-Cre; Ppargc1α*$^{fl/fl}$ mice. Hence, these data indicate that global and conditional loss of *Ppargc1α* does not cause gross neuronal loss, suggesting that *Ppargc1α* is not cell-intrinsically required for neuronal survival in the neocortex.

To study whether the global and conditional loss of *Ppargc1α* leads to loss of SCPN or other major PN subclasses, I stained for markers specific for different PN subclasses on P14, P28

and 2-month-old *Ppargc1α*$^{-/-}$, 2-month-old *Emx1-Cre; Ppargc1α*$^{fl/fl}$ and their respective matched littermate wild type and *Ppargc1α*$^{fl/fl}$ control cortical sections (n = 1 per genotype for P14, n = 2 per genotype for P28, n = 3 per genotype for 2 month-old-animals). Markers included CUX1 for CPN in upper layers II/III-IV (1, 200), SATB2 for CPN in upper layers II/III-IV and deep layers V/VI (34, 35), and CTIP2 for SCPN/CSMN in layer V (stained at high levels) and corticothalamic PN (CThPN) in layer VI (stained at low levels) (5). I did not detect any obvious difference in the overall distribution of these distinct neuronal subtypes between *Ppargc1α*$^{-/-}$ (Figures 2.4.I. to 2.4.N.), *Emx1-Cre; Ppargc1α*$^{fl/fl}$ (Figures 2.4.S. to 2.4.X.) and their respective matched control mice (data not shown for P14 and P28 animals). Moreover, I performed *in situ* hybridization (ISH) for *Fezf2*–which labels all SCPN/CSMN in deep layer V at high levels and CThPN in deep layer VI at lower levels (6)–on P28 *Ppargc1α*$^{-/-}$ and matched littermate wild type coronal cortical sections (n = 1 per genotype). Likewise, I found that the distribution of layer V and VI PN is comparable between *Ppargc1α*$^{-/-}$ and wild type control mice (Figures 2.4.O. and 2.4.P.).

To ascertain these results, I quantified the number of CTIP2, CUX1 and SATB2 positive PN located at a range of depths covering all cortical layers of 2-month-old adult *Ppargc1α*$^{-/-}$, *Emx1-Cre; Ppargc1α*$^{fl/fl}$ and their respective matched littermate wild type and *Ppargc1α*$^{fl/fl}$ control mice over the motor, somatosensory and visual areas. Afterwhich, I performed comparative and statistical analyses with a two-tailed student's T test on the total numbers of these distinct cell types over the three areas. I did not find any significant difference in the total numbers of CTIP2 (average total number of CTIP2 positive PN: motor area, wild type, 637 ± 78; *Ppargc1α*$^{-/-}$, 637 ± 41; p = 9.96 x 10^{-1}; *Ppargc1α*$^{fl/fl}$, 724 ± 169; *Emx1-Cre; Ppargc1α*$^{fl/fl}$, 725 ± 152; p = 9.93 x 10^{-1}, somatosensory area, wild type, 464 ± 121; *Ppargc1α*$^{-/-}$, 497 ± 157; p = 6.90

x 10^{-1}; *Ppargc1α*$^{fl/fl}$, 547 ± 57; *Emx1-Cre; Ppargc1α*$^{fl/fl}$, 529 ± 38; p = 5.50 x 10^{-1}, visual area, wild type, 319 ± 7; *Ppargc1α*$^{-/-}$, 315 ± 55; p = 8.83 x 10^{-1}; *Ppargc1α*$^{fl/fl}$, 340 ± 50; *Emx1-Cre; Ppargc1α*$^{fl/fl}$, 329 ± 44; p = 7.22 x 10^{-1}), SATB2 (average total number of SATB2 positive PN: motor area, wild type, 1076 ± 181; *Ppargc1α*$^{-/-}$, 887 ± 133; p = 9.58 x 10^{-2}; *Ppargc1α*$^{fl/fl}$, 1020 ± 215; *Emx1-Cre; Ppargc1α*$^{fl/fl}$, 912 ± 108; p = 3.04 x 10^{-1}, somatosensory area, wild type, 951 ± 214; *Ppargc1α*$^{-/-}$, 838 ± 276; p = 4.47 x 10^{-1}; *Ppargc1α*$^{fl/fl}$, 895 ± 49; *Emx1-Cre; Ppargc1α*$^{fl/fl}$, 886 ± 104; p = 8.45 x 10^{-1}, visual area, wild type, 582 ± 127; *Ppargc1α*$^{-/-}$, 542 ± 191; p = 7.74 x 10^{-1}; *Ppargc1α*$^{fl/fl}$, 655 ± 115; *Emx1-Cre; Ppargc1α*$^{fl/fl}$, 548 ± 52; p = 1.02 x 10^{-1}), and CUX1 positive PN (average total number of CUX1 positive PN: motor area, wild type, 448 ± 77; *Ppargc1α*$^{-/-}$, 422 ± 21; p = 6.13 x 10^{-1}; *Ppargc1α*$^{fl/fl}$, 521 ± 126; *Emx1-Cre; Ppargc1α*$^{fl/fl}$, 448 ± 71; p = 2.42 x 10^{-1}, somatosensory area, wild type, 487 ± 49; *Ppargc1α*$^{-/-}$, 439 ± 27; p = 1.02 x 10^{-1}; *Ppargc1α*$^{fl/fl}$, 460 ± 52; *Emx1-Cre; Ppargc1α*$^{fl/fl}$, 422 ± 71; p = 3.56 x 10^{-1}, visual area, wild type, 314 ± 70; *Ppargc1α*$^{-/-}$, 317 ± 99; p = 9.71 x 10^{-1}; *Ppargc1α*$^{fl/fl}$, 387 ± 67; *Emx1-Cre; Ppargc1α*$^{fl/fl}$, 376 ± 23; p = 7.57 x 10^{-1}) (n = 2 to 3 sections per area per animal, n = 3 animals per genotype) (Figure 2.5.A. to 2.5.C.). The statistical analysis is summarized in Table 2.2.. These results support the above qualitative finding and demonstrate that there is no significant difference in the total numbers of distinct PN populations in the *Ppargc1α* null and conditional null mutants, as compared to their respective age-matched littermate controls.

Together, these data indicate that the global and conditional loss of *Ppargc1α* in the dorsal forebrain do not affect the birth, specification, migration and laminar positioning of cells within the neocortex, including the major PN subclasses and in particular the SCPN/CSMN. This is in concordance with my expression profile data, as described in section 2.3.2., showing that

Figure 2.5. Quantification of distinct PN populations in adult *Ppargc1α*$^{-/-}$ and *Emx1-Cre; Ppargc1α*$^{fl/fl}$ mice.

(A – C) Quantification and statistical analysis with two tailed student's T test on the total numbers of these different CTIP2, SATB2 and CUX1 positive PN populations over the motor, somatosensory and visual areas did not detect any statistically significant difference between 2-month-old adult *Ppargc1α*$^{-/-}$, *Emx1-Cre; Ppargc1α*$^{fl/fl}$ and their respective matched littermate wild type and *Ppargc1α*$^{fl/fl}$ control mice. WT refer to wild type mice while KO refer to *Ppargc1α*$^{-/-}$ mutant mice. cWT refer to *Ppargc1α*$^{fl/fl}$ mutant control mice while cKO refer to *Emx1-Cre; Ppargc1α*$^{fl/fl}$ mutant mice.

Figure 2.5. (Continued)

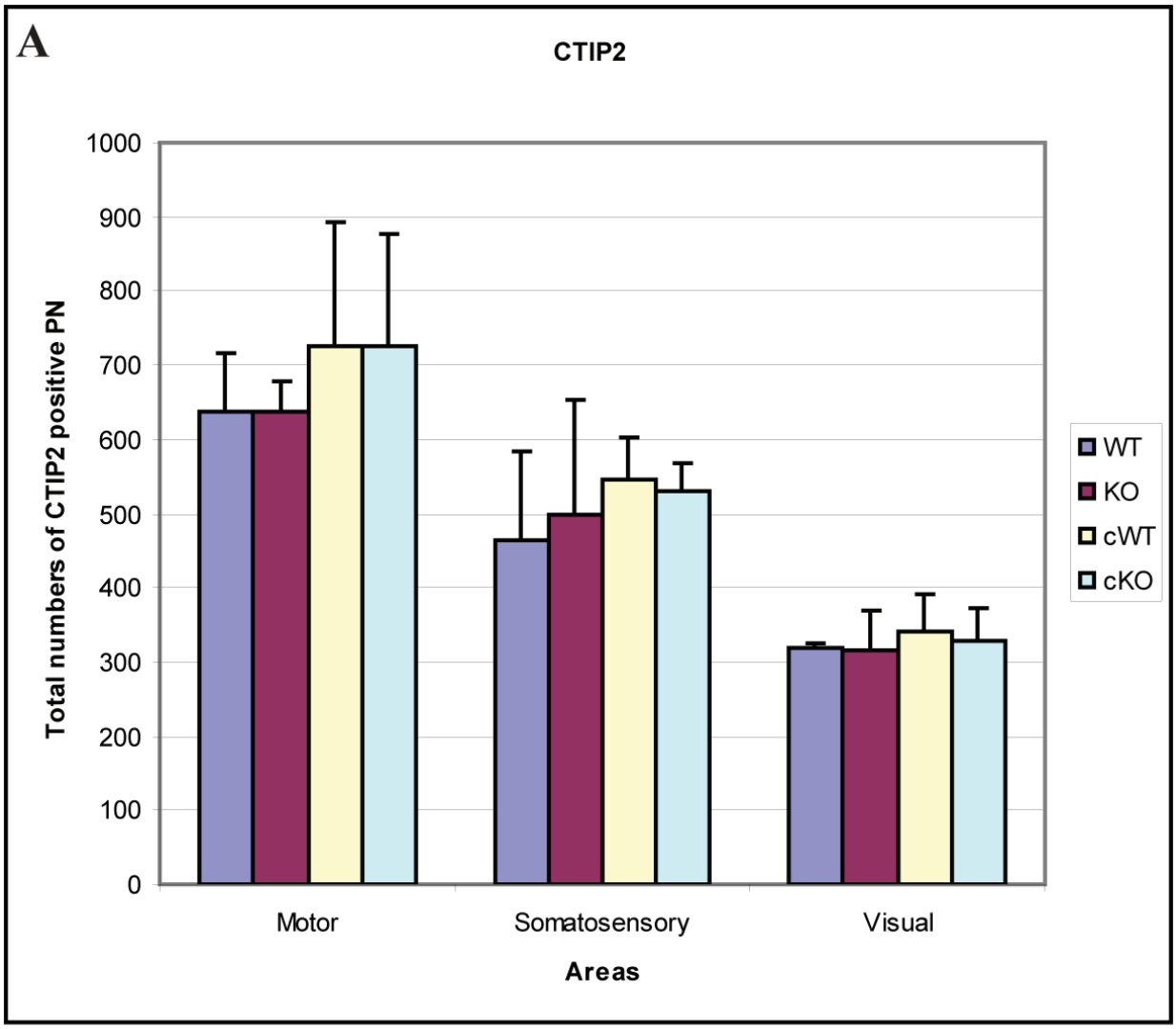

Figure 2.5. (Continued)

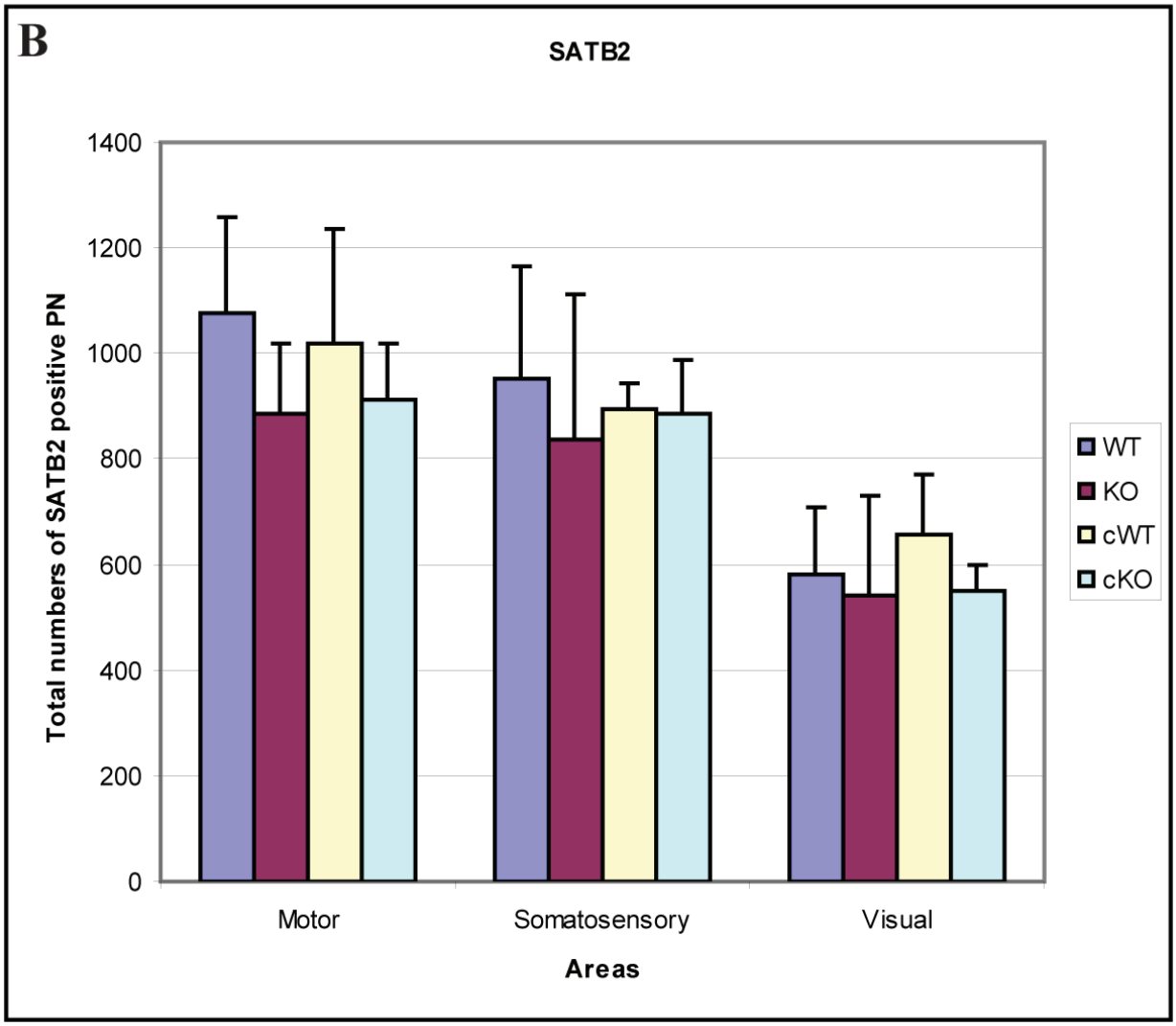

Figure 2.5. (Continued)

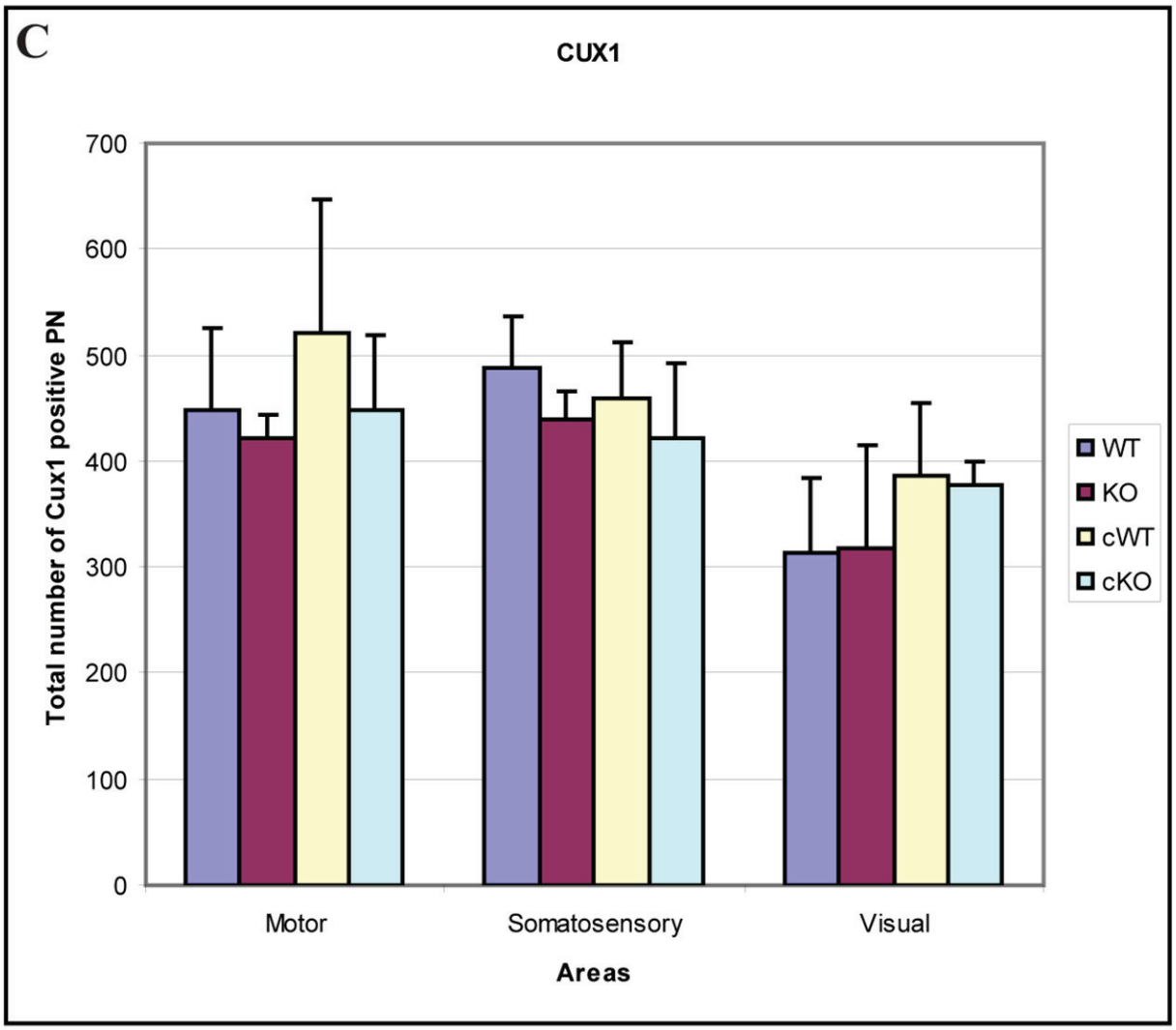

Table 2.2. Statistical analysis of the total numbers of distinct PN populations in adult *Ppargc1α*$^{-/-}$ and *Emx1-Cre; Ppargc1α*$^{fl/fl}$ mice.

This table summarizes the p values obtained after statistical analysis with two tailed student's T test on the total numbers of distinct CTIP2, SATB2 and CUX1 positive PN over the motor, somatosensory and visual areas. No significant values $p \leq 0.05$ were obtained. Hence, there is no statistically significant difference in these populations between *Ppargc1α*$^{-/-}$, *Emx1-Cre; Ppargc1α*$^{fl/fl}$ and their respective matched littermate wild type and *Ppargc1α*$^{fl/fl}$ control mice.

Table 2.2. (Continued)

WT and KO	P values (two tailed student's T test)		
	Motor	Somatosensory	Visual
CTIP2	0.996	0.690	0.883
SATB2	0.0958	0.447	0.774
CUX1	0.613	0.102	0.971
cWT and cKO	P values (two tailed student's T test)		
	Motor	Somatosensory	Visual
CTIP2	0.993	0.550	0.722
SATB2	0.304	0.845	0.102
CUX1	0.242	0.356	0.757

Ppargc1α is largely expressed postnatally, after the fate specification and migration of most cortical PN have already occurred.

In conclusion, these data indicate that global and conditional cell-intrinsic loss of *Ppargc1α* do not cause the obvious neuronal loss that is expected if *Ppargc1α* is cell-autonomously important for survival in neurons. Therefore, they demonstrate that *Ppargc1α* is cell-intrinsically not necessary for neuronal survival in the neocortex, and suggest that its involvement in neuronal survival is context dependent.

2.3.4. No enhanced cell death observed in *Ppargc1α*$^{-/-}$ and *Emx1-Cre; Ppargc1α*$^{fl/fl}$ mice.

My hypothesis is that *Ppargc1α* is cell-autonomously important for neuronal and/or SCPN-selective survival, even in the absence of environmental triggers. If this hypothesis is true, I predict that the global and conditional loss of *Ppargc1α* in the dorsal telencephalon will lead to enhanced cell death. To test this, I performed a IHC stain for caspase 3 that identifies apoptotic cells (211), and a histological Neurosilver stain that detects degenerating cells and axons (212), on adult *Ppargc1α*$^{-/-}$, *Emx1-Cre; Ppargc1α*$^{fl/fl}$ and their respective matched littermate wild type and *Ppargc1α*$^{fl/fl}$ control coronal cortical sections at 2 months of age (n = 3 per genotype). I performed the same stains on P7 C57Bl/6 wild type and Neurosilver control coronal sections that acted as positive controls. While I found caspase 3 positive cells and silver stained cells on the positive controls, I did not observe any obvious or significant difference in the number of caspase 3-positive cells or silver-stained cells or axons between *Ppargc1α*$^{-/-}$, *Emx1-Cre; Ppargc1α*$^{fl/fl}$ and their respective control mice (Figures 2.6.A. to 2.6.E., data not shown for caspase 3). This indicates that there is no enhanced cell death in both *Ppargc1α*$^{-/-}$ and *Emx1-Cre;*

Figure 2.6. No enhanced cell death observed in *Ppargc1α*$^{-/-}$ and *Emx1-Cre; Ppargc1α*$^{fl/fl}$ mice. (A – E) Neurosilver staining did not detect any dark silver stained cells that are dying in the neocortices of 2 month old adult (A) wild type, (B) *Ppargc1α*$^{-/-}$, (C) *Ppargc1α*$^{fl/fl}$ and (D) *Emx1-Cre; Ppargc1α*$^{fl/fl}$ mice. Degenerating dark silver stained cells (arrows) were found in the accompanying adult rat positive control. Similar results were obtained with immunostaining for caspase 3 (data not shown). Scale bars, 100 μm (A – E).

Figure 2.6. (Continued)

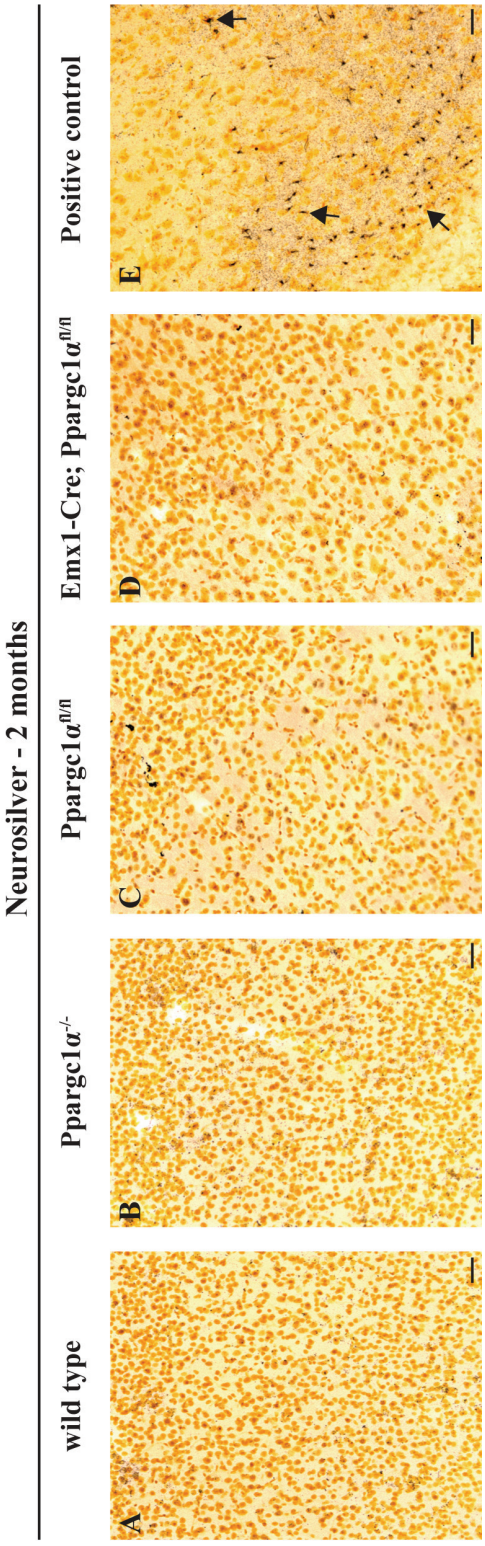

Ppargc1α$^{fl/fl}$ mice, as compared to their respective control mice. Thus, these data reveal that global and conditional cell-intrinsic loss of *Ppargc1α* do not cause enhanced cell death in the neocortex, demonstrating that *Ppargc1α* is not cell-intrinsically required for neuronal survival in the neocortex. This conclusion is further supported by my outcomes in section 2.3.3., showing that distinct PN subtypes are born, specified and positioned normally in the neocortex. In all, these studies, as described in sections 2.3.3. and 2.3.4., demonstrate that the developmental function of *Ppargc1α* in the neocortex is not to maintain neuronal survival in the neocortex.

Yet, it is important to note that these findings do not contradict previous work that implicated *Ppargc1α* in neuronal survival. In prior studies, the involvement of *Ppargc1α* in neuronal survival is achieved either in the circumstance where toxic substances–like kainic acid or MPTP–were administered to induce cell death (72), or in the situation where *Ppargc1α* null mice were crossbred to mice models of neurodegeneration such as the HD knock in mouse models with CAG repeats (73). This, together with my results, suggest that *Ppargc1α* is important for survival in the event of acute cellular stress or an unbalanced non-homeostatic cellular state, where the lack of *Ppargc1α* increases the cells' susceptibility to die. In contrast, the cell-autonomous loss of *Ppargc1α* alone in the context of a balanced cellular homeostatic state or during normal development does not cause cell death, showing that *Ppargc1α* is not required to govern neuron and/or SCPN-specific survival. These data are significant in refining our current understanding of the developmental role of *Ppargc1α* in the brain by clarifying that its involvement in survival is context dependent in the event of acute cellular stress or neurodegeneration.

2.3.5. PN are maintained normally in aged 18 month old *Ppargc1α*$^{-/-}$ and *Emx1-Cre; Ppargc1α*$^{fl/fl}$ mice.

Together with prior work (72-74), my findings, as described in sections 2.3.3. and 2.3.4., demonstrate that the developmental function of *Ppargc1α* is not required for neuronal survival in the neocortex, except in the context of cellular stress. These results motivated me to explore whether *Ppargc1α* is important for neuronal survival in the neocortex, in the context of aging. Aging is an intricate balance between damage and repair, presents as a complex progression in the accrual of molecular damage that affects normal cellular function, and is intricately associated with cellular stress response mechanisms that includes mitochondrial oxidative stress pathways (213-215). Since aging presents as an accumulated chronic stress state, I hypothesize that *Ppargc1α* plays a cell-autonomous role in SCPN to control neuronal survival in the context of aging, where aging is a robust contributory factor that, when combined with the loss of *Ppargc1α*, can cause enhanced cell death. This is the first study that investigates the role of *Ppargc1α* and its contribution to neuronal survival in the neocortex in terms of aging. The study is significant as it will illuminate our understanding of whether *Ppargc1α* plays a different role in survival with time or age. If *Ppargc1α* proves to be only crucial for neuronal survival in aged but not young animals, this result will provide insights into *Ppargc1α's* role in neural deterioration since many neurodegenerative diseases are late-onset and are linked to mitochondrial dysfunction (216, 217).

If this hypothesis is true, I expect that the loss of *Ppargc1α* combined with aging, will cause neuronal and/or neocortical-specific loss due to increased cell death. To test this hypothesis and to investigate whether the global and conditional loss of *Ppargc1α* in aged mice leads to gross cortical abnormalities—particularly layer V defects—in terms of cell numbers, cell

size and morphology, I bred *Ppargc1α*$^{-/-}$, *Emx1-Cre; Ppargc1α*$^{fl/fl}$ and their respective matched littermate wild type and *Ppargc1α*$^{fl/fl}$ control mice for 18 months, and performed Nissl staining on coronal cortical sections from these aged mice (n = 5 *Ppargc1α*$^{-/-}$, n = 4 *Emx1-Cre; Ppargc1α*$^{fl/fl}$, n = 2 wild type and n = 4 *Ppargc1α*$^{fl/fl}$). I compared the gross formation of the six distinct cortical layers, the morphology and the size of cells residing in each layer—especially those of layer V in *Ppargc1α*$^{-/-}$ and *Emx1-Cre; Ppargc1α*$^{fl/fl}$ mutant mice—to that of their respective controls. I did not find any obvious, significant difference between aged *Ppargc1α*$^{-/-}$, *Emx1-Cre; Ppargc1α*$^{fl/fl}$ and their respective control mice (data not shown). Particularly, distinct large somas of SCPN/CSMN in layer V were detected in both aged *Ppargc1α*$^{-/-}$, *Emx1-Cre; Ppargc1α*$^{fl/fl}$ and their respective control mice at 18 months of age (data not shown), showing that the SCPN/CSMN are maintained normally in aged *Ppargc1α*$^{-/-}$ and *Emx1-Cre; Ppargc1α*$^{fl/fl}$ mutant mice. These data also indicate that global and conditional loss of *Ppargc1α* do not cause gross cortical anomalies by maintaining cortical cells in the six distinct cortical layers, thereby suggesting that *Ppargc1α* is not cell-intrinsically necessary to maintain cell survival in the neocortex, even in the event of aging.

To study whether the global and conditional loss of *Ppargc1α* in the neocortices of aged mice cause gross neuronal aberrations, I executed an IHC stain for NeuN—a marker for all subtypes of neurons (210) —on aged 18-month-old *Ppargc1α*$^{-/-}$, *Emx1-Cre; Ppargc1α*$^{fl/fl}$ and their respective matched littermate wild type and *Ppargc1α*$^{fl/fl}$ control cortical sections (n = 5 *Ppargc1α*$^{-/-}$, n = 4 *Emx1-Cre; Ppargc1α*$^{fl/fl}$, n = 2 wild type and n = 4 *Ppargc1α*$^{fl/fl}$). Similarly, I did not detect any obvious, significant difference between the NeuN positive neurons located in all six different cortical layers between aged *Ppargc1α*$^{-/-}$ (Figures 2.7.A. and 2.7.B.), *Emx1-Cre; Ppargc1α*$^{fl/fl}$ (Figures 2.7.I. and 2.7.J.), and their respective control mice. Agreeing with my

Figure 2.7. PN are maintained normally in aged 18 month old *Ppargc1α*$^{-/-}$ and *Emx1-Cre; Ppargc1α*$^{fl/fl}$ mice.

(A – B and I – J) IHC stain for NeuN, a neuron-specific marker, showed that neurons across the six cortical layers appear normal and comparable between aged 18 month old *Ppargc1α*$^{-/-}$ (A – B), *Emx1-Cre; Ppargc1α*$^{fl/fl}$ (I – J) and their respective controls.

(C – D and K – L) IHC stain for SATB2, which marked all CPN across layers II to VI, revealed that CPN are maintained normally in their destined layers in aged 18 month old *Ppargc1α*$^{-/-}$ (C – D), *Emx1-Cre; Ppargc1α*$^{fl/fl}$ (K – L) and their respective controls.

(E – F and M – N) In agreement with results shown in C – D and K – L, immunostaining for CUX1, that labeled CPN in upper layers II/III-IV, indicated that CPN are maintained normally in their destined layers in aged 18 month old *Ppargc1α*$^{-/-}$ (E – F), *Emx1-Cre; Ppargc1α*$^{fl/fl}$ (M – N) and their respective controls.

(G – H and O – P) ISH for *Fezf2*, which marked all SCPN/CSMN in deep layer V at high levels and CThPN in deep layer VI at lower levels, showed that SCPN and CThPN are maintained normally in their destined layers in aged 18 month old *Ppargc1α*$^{-/-}$ (G – H), *Emx1-Cre; Ppargc1α*$^{fl/fl}$ (O – P) and their respective controls. Roman numerals indicate the distinct cortical layers. Scale bars, 100 μm (A – P).

Figure 2.7. (Continued)

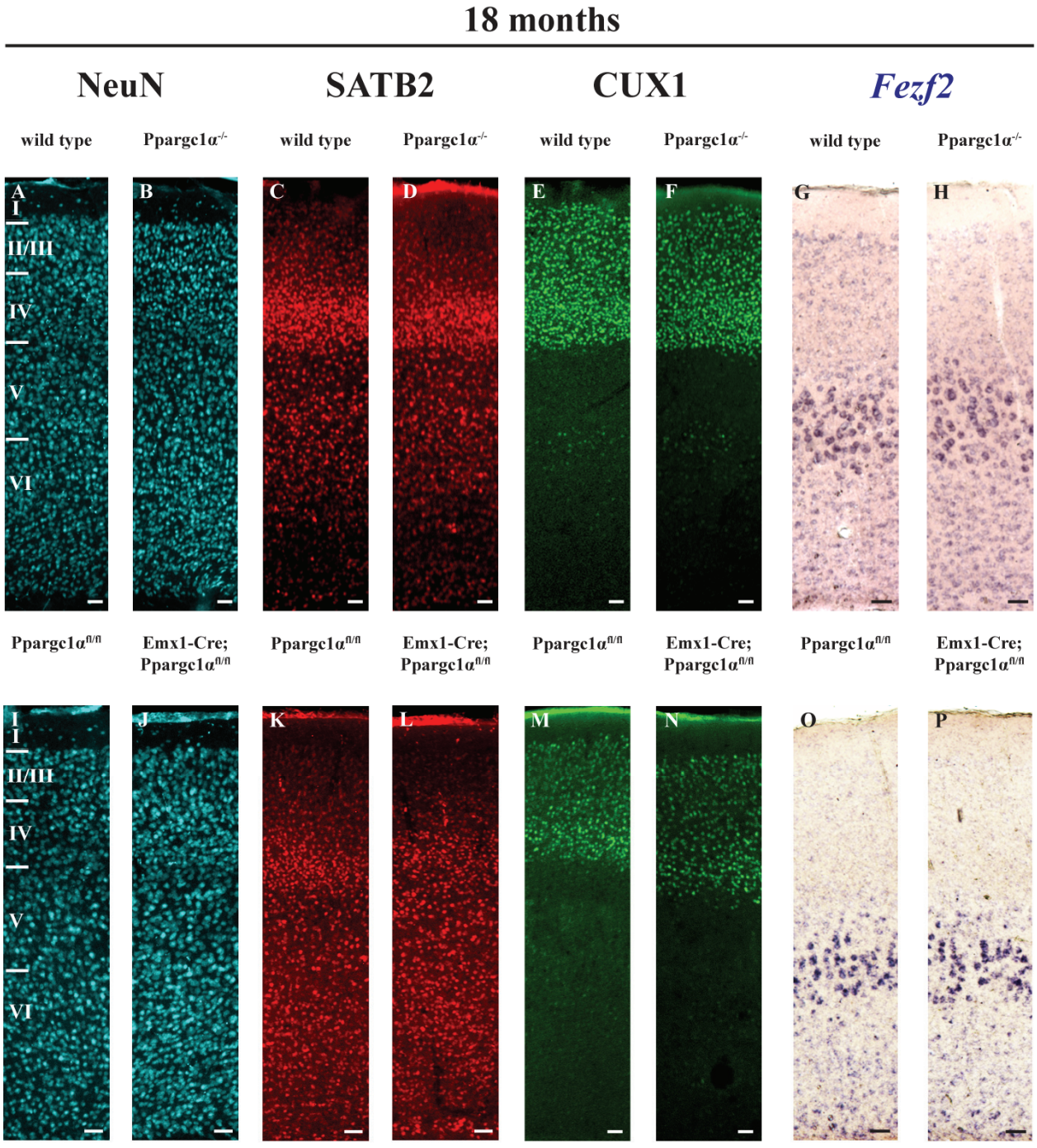

above findings, this shows that neurons are maintained normally in aged *Ppargc1α*$^{-/-}$ and *Emx1-Cre; Ppargc1α*$^{fl/fl}$ mice. Hence, these data indicate that global and conditional loss of *Ppargc1α* combined with aging, do not cause gross significant neuronal loss in the neocortex, implying that *Ppargc1α* is cell-autonomously not required for neuronal survival in the neocortex, even in the event of aging caused by cellular stress.

To determine whether the global and conditional loss of *Ppargc1α* in aged mice leads to abnormalities in different PN populations, I stained for markers specific to various subclasses on aged 18-month-old *Ppargc1α*$^{-/-}$, *Emx1-Cre; Ppargc1α*$^{fl/fl}$ and their respective matched littermate wild type and *Ppargc1α*$^{fl/fl}$ control cortical sections (n = 5 *Ppargc1α*$^{-/-}$, n = 4 *Emx1-Cre; Ppargc1α*$^{fl/fl}$, n = 2 wild type and n = 4 *Ppargc1α*$^{fl/fl}$). Markers included CUX1 for CPN in upper layers II/III-IV (1, 200), SATB2 for CPN in upper layers II/III-IV and deep layers V/VI (34, 35). I did not find any significant difference in the overall distribution of CUX1 positive and SATB2 positive CPN across all cortical layers between aged *Ppargc1α*$^{-/-}$ (Figures 2.7.C. to 2.7.F.), *Emx1-Cre; Ppargc1α*$^{fl/fl}$ (Figures 2.7.K. to 2.7.N.), and their respective control mice. Moreover, I performed ISH for *Fezf2*, which labels all SCPN/CSMN in deep layer V at high levels and CThPN in deep layer VI at lower levels (6), on aged 18 month old *Ppargc1α*$^{-/-}$, *Emx1-Cre; Ppargc1α*$^{fl/fl}$ and their respective littermate control coronal cortical sections (n = 4 *Ppargc1α*$^{-/-}$, n = 4 *Emx1-Cre; Ppargc1α*$^{fl/fl}$, n = 1 wild type, and n = 4 *Ppargc1α*$^{fl/fl}$ mice). Similarly, I discovered that the distribution of layer V and VI corticofugal PN is comparable between aged *Ppargc1α*$^{-/-}$ (Figures 2.7.G. and 2.7.H.), *Emx1-Cre; Ppargc1α*$^{fl/fl}$ (Figures 2.7.O. and 2.7.P.) and their respective control mice. Thus, these data show that the PN subpopulations of upper layers II/III-IV and deep layer V/VI are maintained normally in aged 18-month-old *Ppargc1α*$^{-/-}$ and *Emx1-Cre; Ppargc1α*$^{fl/fl}$ mice. Together, these data demonstrate that global and conditional cell-

intrinsic loss of *Ppargc1α* in the neocortex, in combination with cellular stress caused by aging, do not cause obvious neuronal loss. They also show that global and conditional loss of *Ppargc1α*, in conjunction with aging, do not affect the maintenance of cortical cells—particularly distinct PN classes such as SCPN/CSMN—within the neocortex in terms of their laminar positioning and numbers. Thus, these data suggest that *Ppargc1α* is not cell-intrinsically required for neuronal survival in the neocortex, even in the context of aging.

2.3.6. No enhanced cell death observed in aged 18 month old *Ppargc1α*$^{-/-}$ and *Emx1-Cre; Ppargc1α*$^{fl/fl}$ mice.

My hypothesis is that *Ppargc1α* is cell-autonomously important for neuronal and/or SCPN-selective survival in the neocortex, in the presence of cellular stress caused by aging. If this hypothesis is true, I predict that the global loss of *Ppargc1α* will lead to increased cell death. To test this, I performed an IHC stain for caspase 3 that identifies apoptotic cells (211) and a histological Neurosilver stain that detects degenerating cells and axons (212) on aged 18-month-old *Ppargc1α*$^{-/-}$, *Emx1-Cre; Ppargc1α*$^{fl/fl}$ and their respective matched littermate wild type and *Ppargc1α*$^{fl/fl}$ control cortical sections (n = 5 *Ppargc1α*$^{-/-}$, n = 4 *Emx1-Cre; Ppargc1α*$^{fl/fl}$, n = 2 wild type and n = 4 *Ppargc1α*$^{fl/fl}$), as well as on P7 C57Bl/6 wild type and Neurosilver control coronal sections that acted as positive controls. Surprisingly, I did not detect any obvious or significant difference in the number of caspase 3-positive cells or silver-stained cells between aged 18-month-old *Ppargc1α*$^{-/-}$, *Emx1-Cre; Ppargc1α*$^{fl/fl}$ and their respective control mice (Figures 2.8.A. to 2.8.E., data not shown for caspase 3). These data indicate that there is no enhanced cell death in aged 18-month-old *Ppargc1α*$^{-/-}$ and *Emx1-Cre; Ppargc1α*$^{fl/fl}$ mice, as compared to their respective control mice. Therefore, global and conditional loss of *Ppargc1α* in

Figure 2.8. No enhanced cell death observed in aged 18 month old *Ppargc1α*$^{-/-}$ and *Emx1-Cre; Ppargc1α*$^{fl/fl}$ mice.

(A – E) Neurosilver staining did not detect any dying dark silver stained cells in the neocortices of aged 18 month old adult (A) wild type, (B) *Ppargc1α*$^{-/-}$, (C) *Ppargc1α*$^{fl/fl}$ and (D) *Emx1-Cre; Ppargc1α*$^{fl/fl}$ mice. Degenerating dark silver stained cells (arrows) were found in the accompanying adult rat positive control. Similar results were obtained with immunostaining for caspase 3 (data not shown). Scale bars, 100 μm (A – E).

Figure 2.8. (Continued)

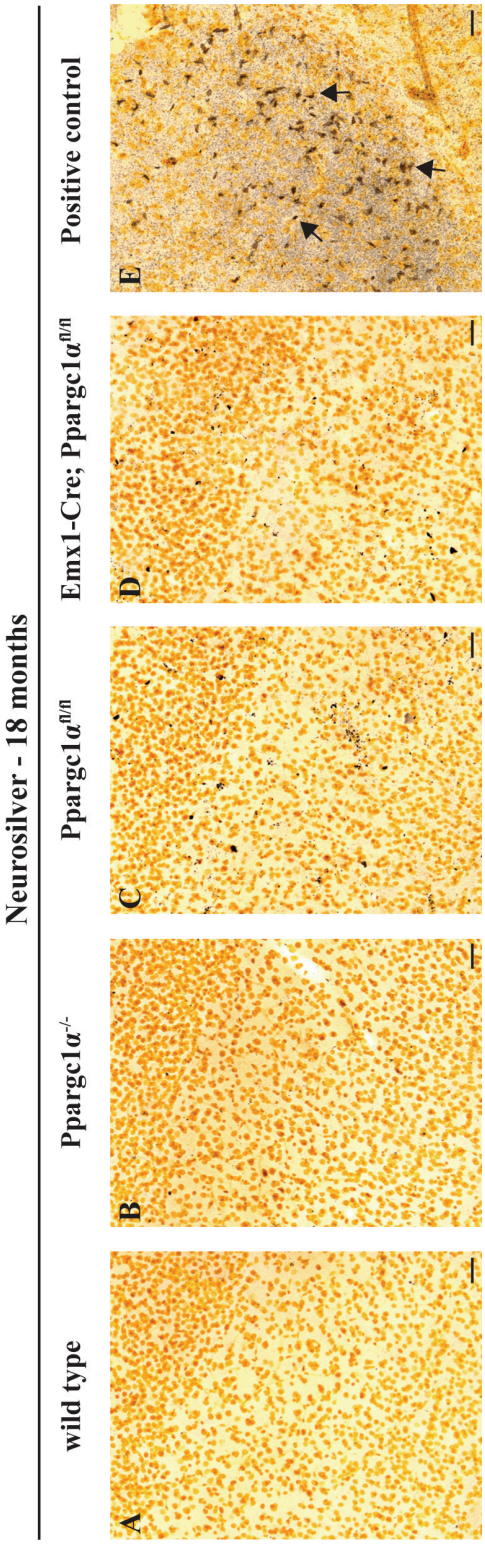

SCPN, in conjunction with a state of cellular stress caused by aging, do not cause enhanced cell death. This indicates that *Ppargc1α* is cell-autonomously not necessary for cell survival in the neocortex, even in response to cellular aging. This conclusion is further supported by my findings in section 2.3.5., which show that distinct PN subpopulations are maintained normally in the neocortex with no observable neuronal loss. Together, these studies as shown in sections 2.3.5. and 2.3.6., demonstrate for the first time that the developmental function of *Ppargc1α* is not to govern neuronal survival in the neocortex, even in the context of cellular aging as a stress factor. These outcomes seek to refine our current comprehension of *Ppargc1α's* function in neural development of the dorsal telencephalon, specifically its role in neuronal survival, or conversely, neural degeneration.

2.3.7. Loss-of-function analysis: spongiform-like lesions are localized to axonal bundles of the IC and persist with age in *Ppargc1α*$^{-/-}$ mice, even to 18 months of age.

Previous reports have briefly described that *Ppargc1α*$^{-/-}$ mice develop spongiform lesions in the striatum and deep cortical layer V/VI (62, 63). To determine the exact localization of these lesions and the time course of their appearance, I examined brightfield images of *Ppargc1α*$^{-/-}$ and matched wild type littermate coronal cortical sections in PBS at various stages of postnatal development, namely P14, P28, 2 months, 3 months, 6 months and 18 months of age (n = 3 per genotype for all ages except n = 2 wild type and n = 5 *Ppargc1α*$^{-/-}$ mice at 18 months of age). While spongiform lesions in the mutant striatum were not found at P14, I detected distinct lesions in the striatum of *Ppargc1α*$^{-/-}$ mice at P28, 2 months, 3 months, 6 months, and 18 months, as compared to the wild type controls (data not shown). Fiber bundles of the IC of *Ppargc1α*$^{-/-}$ mice also appeared to be smaller in diameter and partially defasciculated (Figures 2.9.E and

Figure 2.9. Brightfield analysis showed that lesions are closely associated with or localized within the IC along the anteroposterior axis in *Ppargc1α*$^{-/-}$ mice.

(A – F) Brightfield analysis in phosphate buffer saline (PBS) showed that lesions developed in close association with or within the anterior part of the IC (red arrows) of P28 *Ppargc1α*$^{-/-}$ mice (D – F), as compared to wild type controls (A – C). (B – C and E – F) Boxed areas in (A) and (D) respectively.

(G – L) Similarly, brightfield analysis in PBS showed that lesions developed in close association with or within the posterior part of the IC (red arrows) of P28 *Ppargc1α*$^{-/-}$ mice (J – L), as compared to wild type controls (G – I). (H – I and K – L) Boxed areas in (G) and (J) respectively. Scale bars, 100 μm (A – B, D – E, G – H and J – K), 10 μm (C, F, I and L).

Figure 2.9. (Continued)

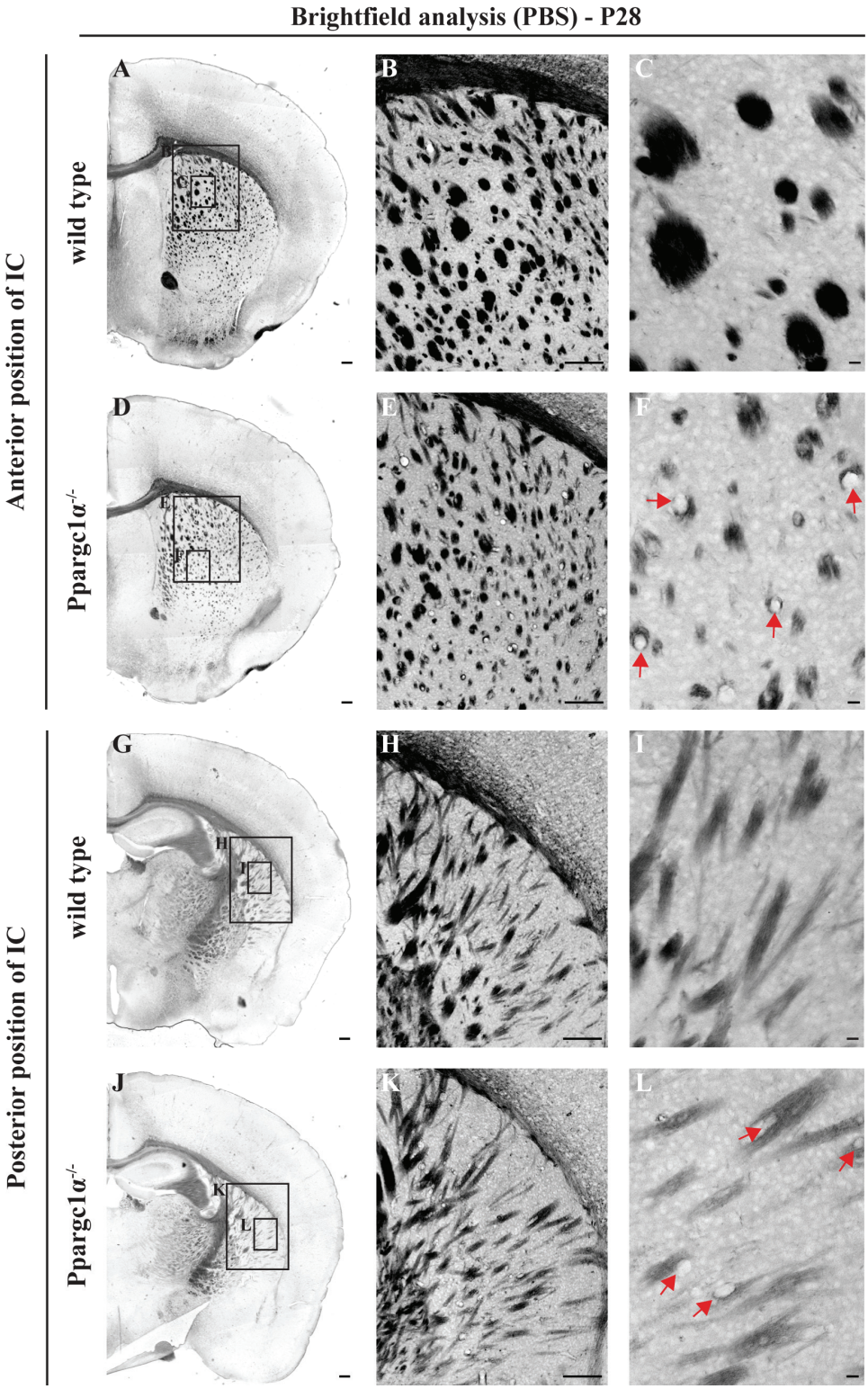

2.9.F.). Strikingly, high magnification analysis of the striatum revealed that these lesions (red arrows) are in close association with, or are exactly localized within, the fiber tracts of the IC—the pathways taken by SCPN/CSMN efferent axons among others (20, 21) (Figure 2.9.F.). Anteroposterior analysis demonstrated that these lesions (red arrows) are found at both anterior (Figure 2.9.F.) and posterior positions in the IC (Figure 2.9.L.). Mediolateral and dorsoventral analysis did not detect any evident arealization of these lesions within the IC (Figures 2.9.E. and 2.9.K.). These data also indicate that these lesions develop by P28 and persist with age into adulthood and even old age. Comparative analysis between the various ages also showed that the severity of these lesions is maintained from P28 to 6 months of age but appeared to decrease by 18 months of age when lesions are fewer, smaller and are located at more anterior positions of the IC (data not shown). Hence, temporal and spatial analysis showed that these spongiform-like lesions develop within the axonal bundles of the IC along the rostrocaudal axis, are not arealized along the mediolateral and dorsoventral axes, are absent at P14 but are formed by P28 and persist throughout adulthood and old age.

To better delineate the position of the lesions, I defined the limits of the fiber bundles of the IC by staining for Myelin Basic Protein (MBP)—a protein found within the myelin sheath that surrounds the axonal fibers (112)—on *Ppargc1α*$^{-/-}$ and matched wild type littermate coronal cortical sections at P14, P28, 2 months, 3 months, 6 months and 18 months of age (n = 3 per genotype for all ages except n = 2 wild type and n = 5 *Ppargc1α*$^{-/-}$ mice at 18 months of age). Confirming my initial finding, I detected that the lesions (red arrows) in *Ppargc1α*$^{-/-}$ mice are closely associated with, or are even within, the IC at both anterior (Figures 2.10.E. and 2.10.F.) and posterior positions (Figures 2.10.K. and 2.10.L.). I also found that they are not spatially arealized along the mediolateral and dorsoventral axes (data not shown). I further ascertained

Figure 2.10. Immunostaining showed that lesions are closely associated with or localized within axonal bundles of the IC along the anteroposterior axis in *Ppargc1α*$^{-/-}$ mice.

(A – F) Immunohistochemistry analysis for Myelin Basic Protein showed that lesions developed in close association with or within the anterior part of the IC (red arrows) of P28 *Ppargc1α*$^{-/-}$ mice (D – F), as compared to wild type controls (A – C). (B – C and E – F) Boxed areas in (A) and (D) respectively.

(G – L) Similarly, immunostaining for myelin basic protein showed that lesions developed in close association with or within the posterior part of the IC (red arrows) of P28 *Ppargc1α*$^{-/-}$ mice (J – L), as compared to wild type controls (G – I). (H – I and K – L) Boxed areas in (G) and (J) respectively.

(M – N) Immunohistochemistry for Neurofilament, a neuronal marker, further ascertained that the spongiform-like lesions are closely associated with or localized within axonal fibers of the IC (red arrows). Scale bars, 100 μm (A, D, G and J), 10 μm (B – C, E – F, H – I, K – L and M – N).

Figure 2.10. (Continued)

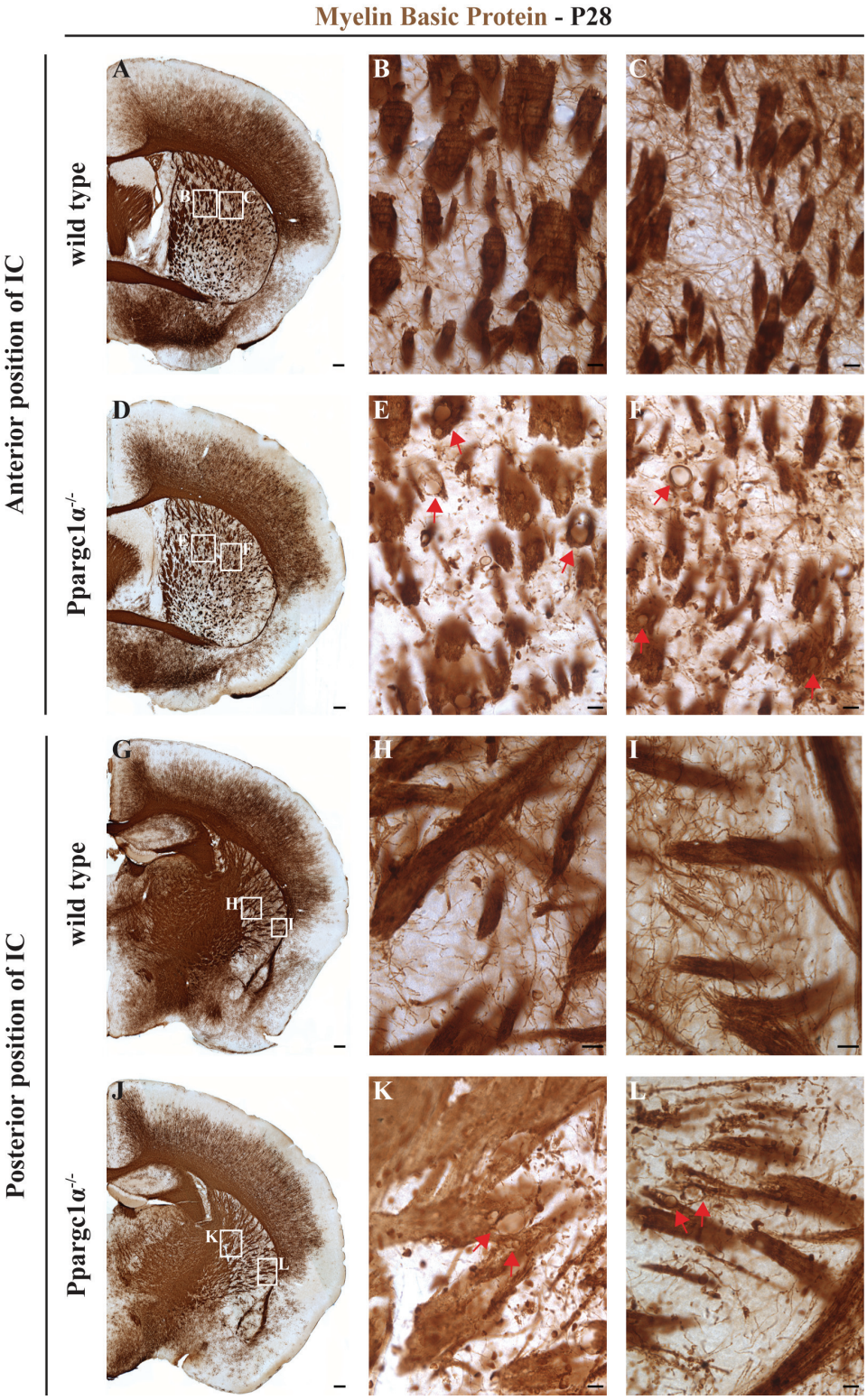

Figure 2.10. (Continued)

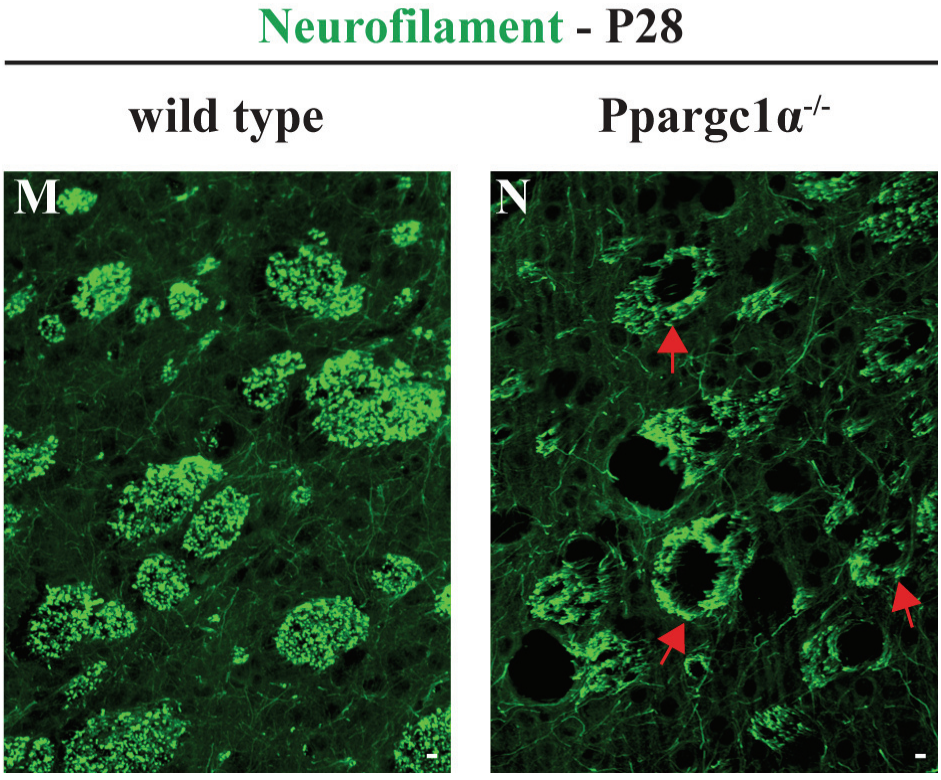

that these lesions in the IC are not present at P14 but develop by P28 and are maintained throughout adulthood and old age at 18 months (Figures 2.10.C. and 2.10.D.). Similar comparative analysis between various ages also verified my finding that the severity of these lesions is maintained from P28 to 6 months of age (Figures 2.11.C. and 2.11.D.) but appeared to decrease by 18 months of age when lesions are fewer, smaller and are located at more anterior positions of the IC (data not shown).

To further validate that these lesions are associated with the axonal bundles of the IC, I delineated the axonal bundles of the IC by staining for another marker NEUROFILAMENT, a protein that is found within axonal fibers (218), on *Ppargc1α*$^{-/-}$ and matched wild type littermate cortical sections at P28 (n = 3 per genotype). Confirming my results, I found that the lesions are in close association with, or are exactly localized within, the fiber tracts of the IC (red arrows) at both anterior (Figure 2.10.N.) and posterior regions (data not shown). I also discovered that these lesions are NEUROFILAMENT negative (red arrows), indicating that they are devoid of axon fibers (Figure 2.10.N.).

Expanding on published observations (62, 63), my new data is the first long-term descriptive study illustrating the exact location and developmental time course of these spongiform-like lesions in the striatum due to the global loss of *Ppargc1α*. They revealed that these lesions in the caudate putamen are closely associated with, or are exactly localized within, axonal bundles of the IC along the rostrocaudal axis, without evident arealization along the mediolateral and dorsoventral axes. My data also demonstrated that these lesions are not formed at P14 but develop by P28 and persist throughout adulthood and even old age. Since global loss of *Ppargc1α* causes lesions to develop within the IC, I conclude that *Ppargc1α* is cell-autonomously necessary to prevent the formation of these spongiform-like lesions.

Figure 2.11. Spongiform-like lesions in *Ppargc1α*$^{-/-}$ mice develop by P28 and persist with age through adulthood and even old age of 18 months.

(A – D) Spongiform-like lesions are not found at P14 (data not shown) but are formed at P28 (red arrows), 2 months (data not shown), 3 months (data not shown), 6 months (red arrows) and even to the old age of 18 months (data not shown) in *Ppargc1α*$^{-/-}$ mice (C – D), as compared to wild type controls (A – B). High magnification of a representative lesion is shown in C' and D' at P28 and 6 months respectively. Scale bars, 50 μm (A – D), 10 μm (C' and D').

Figure 2.11. (Continued)

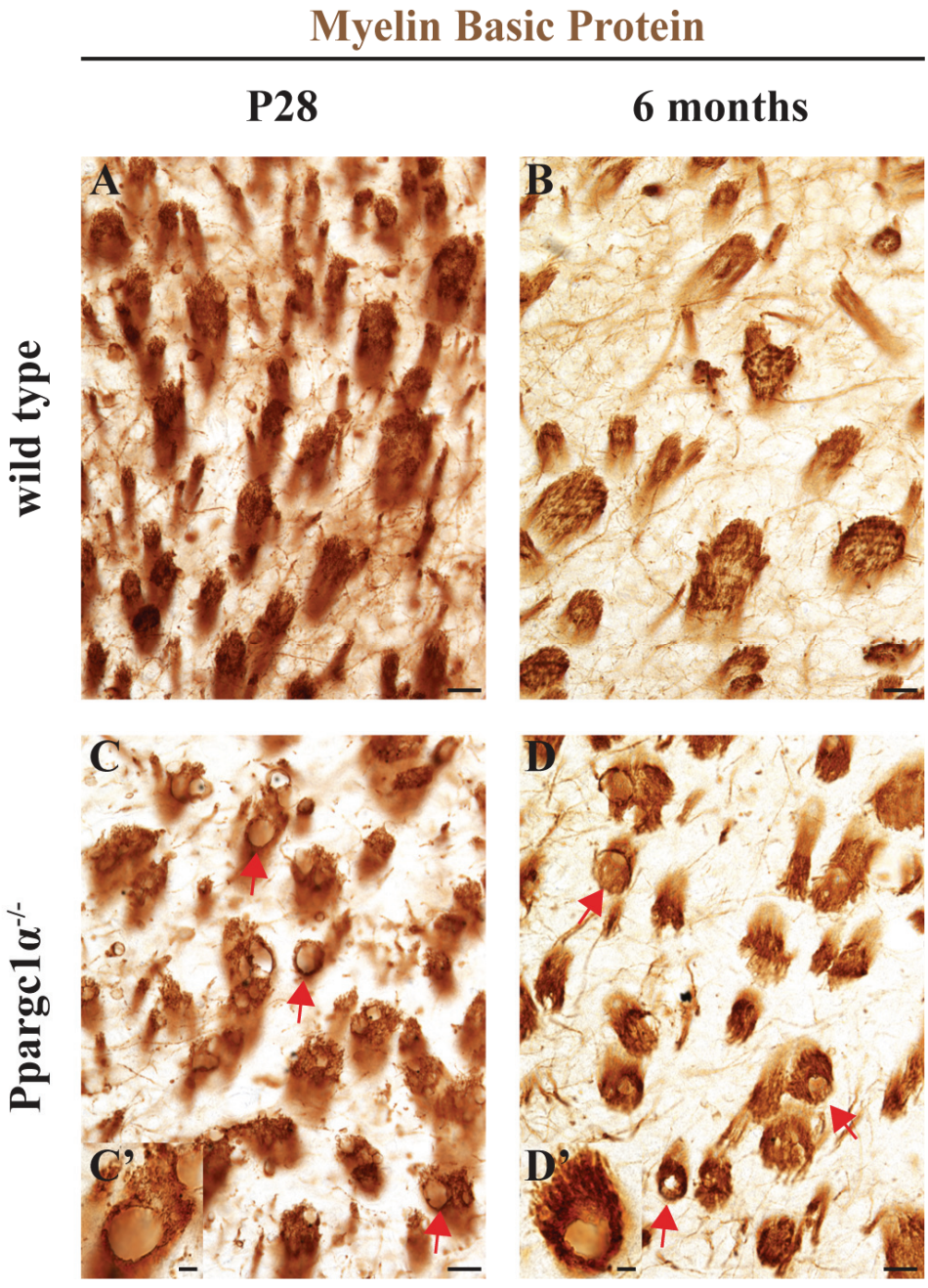

2.3.8. Loss-of-function analysis: smaller and much fewer spongiform-like lesions develop in the IC of adult *CamkIIα-Cre; Ppargc1α*$^{fl/fl}$ mice.

A recent report by Ma *et al.* showed that neuronal loss of *Ppargc1α* causes the formation of spongiform-like lesions in the striatum, albeit the lesions are smaller and fewer in numbers (219). This supports a role for *Ppargc1α* in neurons, indicating that it is required in neurons to control the development of these lesions. To ascertain their finding, I performed brightfield and MBP immunostaining analysis on 4-month-old *CamkIIα-Cre; Ppargc1α*$^{fl/fl}$ and matched *Ppargc1α*$^{fl/fl}$ littermate control cortical sections (n = 3 animals per genotype) (a gift from Professor Jiandie D. Lin, University of Michigan). I confirmed their finding and detected lesions in the IC in *CamkIIα-Cre; Ppargc1α*$^{fl/fl}$ mice, as compared to matched *Ppargc1α*$^{fl/fl}$ littermate controls (Figure 2.12.B.). Notably, these lesions are significantly less severe as compared to the *Ppargc1α*$^{-/-}$ mutants; the lesions are much smaller in size or diameter and much fewer in numbers (Figures 2.12.B., 2.10.E, 2.10.F., 2.11.C. and 2.11.D.). Anteroposterior, mediolateral and dorsoventral analysis did not unveil any evident arealization (data not shown). In all, these data show that neuronal loss of *Ppargc1α* causes the formation of smaller and fewer spongiform lesions localized to the IC in the striatum with no apparent spatial arealization, indicating that neuron-specific *Ppargc1α* is partly responsible for the formation of these IC localized lesions. Thus, *Ppargc1α* is cell-intrinsically required in neurons to govern the development of these lesions, making it clinically relevant to identify the neuronal subclass from which these lesions originate in order to identify potential degenerative cell types. These data also suggest that a non-neuronal, possibly systemic component or a more complex multifactorial mechanism may be involved in the formation of these lesions.

Figure 2.12. Smaller and much fewer spongiform-like lesions develop in the IC of adult *CamkIIα-Cre; Ppargc1α$^{fl/fl}$* mice.

(A – B) Immunohistochemistry analysis for Myelin Basic Protein showed that lesions developed in 4 month old adult *CamkIIα-Cre; Ppargc1α$^{fl/fl}$* mice (red arrows), as compared to *Ppargc1α$^{fl/fl}$* controls. These lesions are smaller and much fewer in numbers as compared to that observed in *Ppargc1α$^{-/-}$* mutants. They are also not spatially arealized along the anteroposterior, mediolateral and dorsoventral axes (data not shown). Similar results were obtained with brightfield analysis (data not shown). Scale bars, 100 μm (A – D).

Figure 2.12. (Continued)

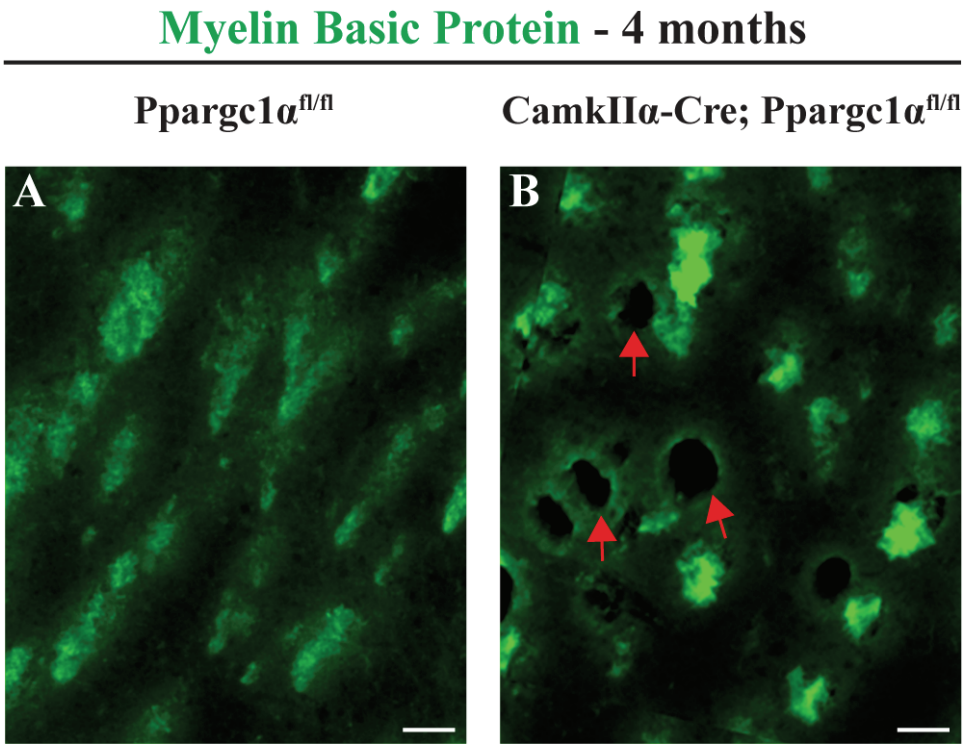

2.3.9. Loss-of-function analysis: spongiform-like lesions do not develop in the IC of *Emx1-Cre; Ppargc1α$^{fl/fl}$* mice, even in aged 18 month old mutants.

Since *Ppargc1α* is expressed specifically in SCPN that project their descending axons through the IC (20, 21) where the spongiform-like lesions are localized, I hypothesize that *Ppargc1α* plays a cell-autonomous role in SCPN to regulate the development of these lesions. To test this hypothesis, I generated conditional null mutants for *Ppargc1α* in the dorsal forebrain and employed similar brightfield and immunohistological methodologies, as described above in sections 2.3.7. and 2.3.8. to characterize the lesion formation, if any, in these mutants.

2.3.9.A. Generation of *Emx1-Cre; Ppargc1α$^{fl/fl}$* mice.

Since my prior results in section 2.3.2. showed that *Ppargc1α* is highly expressed in layer V SCPN that extend descending axonal projections through the IC to reach subcerebral targets (20, 21), and given that *Ppargc1α* is expressed in cortical and subcortical structures, I crossed a loxP-flanked (floxed) *Ppargc1α* line (63) with an *Emx1-Cre* line (220) to generate *Emx1-Cre;Ppargc1α$^{fl/fl}$* mutants that are conditionally null for *Ppargc1α* in the dorsal telencephalon to study if cell-autonomous conditional loss of *Ppargc1α* in the neocortex causes these IC localized lesions. I verified the ablation of *Ppargc1α* in the dorsal telencephalon by using combined ISH for *Ppargc1α* against the deletion region from exon 3 to 5 and immunohistochemistry (IHC) for CTIP2, a marker of SCPN. I found that *Ppargc1α* is not expressed in layer V CTIP2 positive SCPN in *Emx1-Cre; Ppargc1α$^{fl/fl}$* mutants (Figure 2.13.F.), as compared to control *Ppargc1α$^{fl/fl}$* mice (Figure 2.13.C.), indicating that there is loss of *Ppargc1α* in SCPN in *Emx1-Cre; Ppargc1α$^{fl/fl}$* mutants. In agreement with the fact that *Emx1* is not expressed in the ventral telencephalon, *Ppargc1α* expression remains unchanged in smaller scattered cells across the neocortex of *Emx1-Cre; Ppargc1α$^{fl/fl}$* mutants (Figure 2.13.E.), likely representing Parvalbumin

Figure 2.13. *Emx1-Cre* efficiently excises *Ppargc1a* in neocortical projection neurons.

(A and D) ISH for *Ppargc1α* against the deletion region from exon 3 to 5 showed that *Ppargc1α* is expressed in deep cortical layer V (red arrows) and ventral structures like the lateral globus pallidus and reticular thalamic nuclei in 2 month old control *Ppargc1α*$^{fl/fl}$ mice. In contrast, *Ppargc1α* is absent in deep cortical layer V while its expression is retained in ventral structures like the lateral globus pallidus and reticular thalamic nuclei in 2 month old *Emx1-Cre;* *Ppargc1α*$^{fl/fl}$ conditional null mutants.

(B and E) High magnification analysis of boxed area in (A) and (D) respectively.

(C and F) Combined ISH for *Ppargc1α* (exon 2 – 5) and CTIP2, a marker for layer V SCPN, revealed that *Ppargc1α* is expressed in CTIP2-positive SCPN in control *Ppargc1α*$^{fl/fl}$ mice but not in *Emx1-Cre; Ppargc1α*$^{fl/fl}$ conditional null mutants. Ctx, cortex; Str, striatum; Hip, hippocampus; Rt, reticular thalamic nuclei; LGP, lateral globus pallidus. Scale bars, 100 μm (A – B and D – E) and 10 μm (C and F).

Figure 2.13. (Continued)

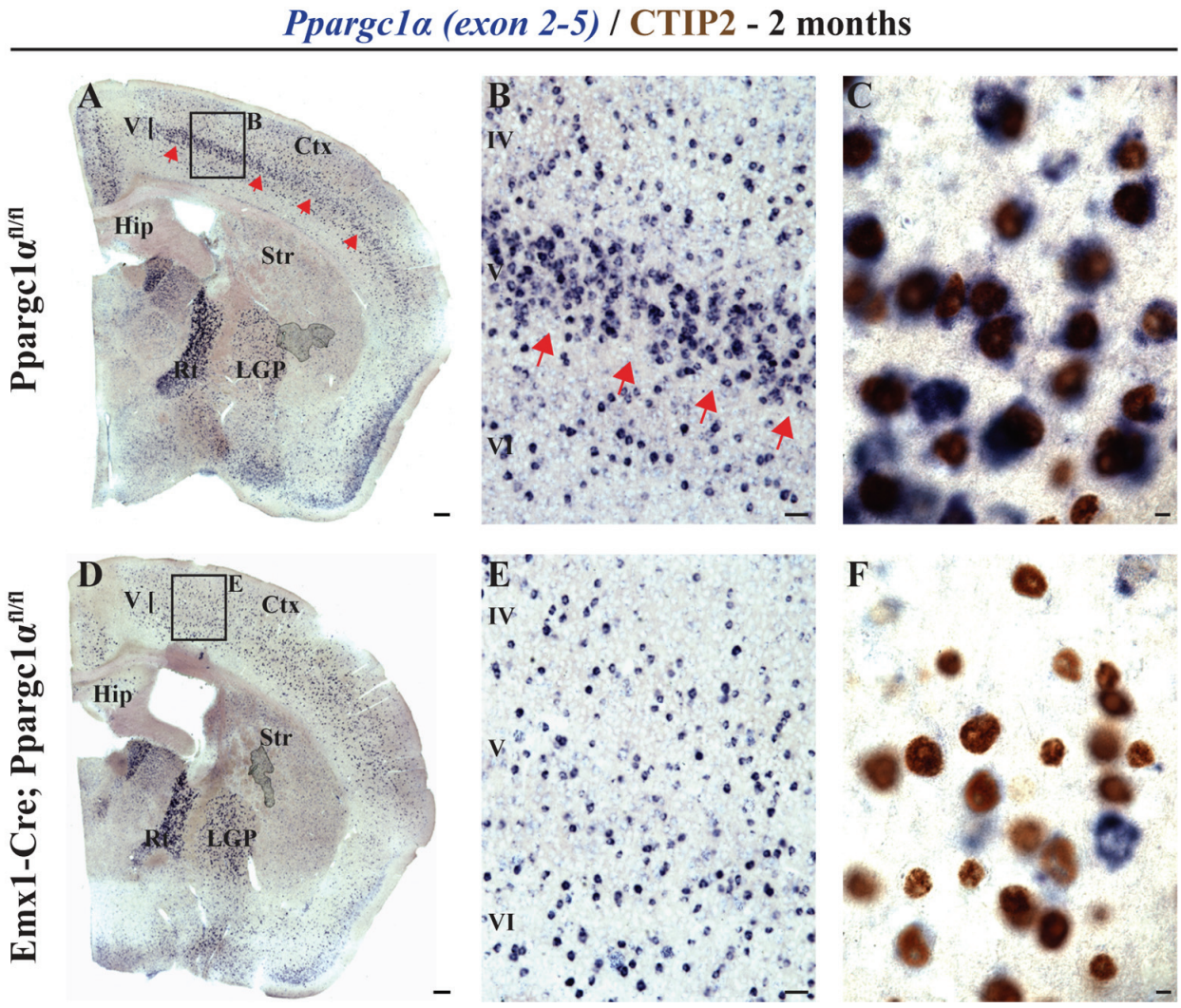

expressing GABAergic or other cortical interneurons that have migrated from the ventral forebrain to the cortex during embryonic development (94, 97). Its expression is also retained in ventral brain structures, such as the lateral globus pallidus and reticular thalamic nuclei, of *Emx1-Cre; Ppargc1α*$^{fl/fl}$ and *Ppargc1α*$^{fl/fl}$ mice (Figures 2.13.A. and 2.13.D.). Therefore, the generation of *Emx1-Cre; Ppargc1α*$^{fl/fl}$ mice provide me with the best possible model with current techniques to look at the specific loss of *Ppargc1α* in the neocortex and enable me to investigate whether *Ppargc1α* is cell-intrinsically required in SCPN to control the formation of spongiform lesions in the IC through which descending axonal projections of SCPN extend.

2.3.9.B. Temporal and spatial analysis of spongiform lesions in *Emx1-Cre; Ppargc1α*$^{fl/fl}$ *mice* from P28 to 18 months of age.

To test my hypothesis by elucidating whether cell-autonomous loss of *Ppargc1α* in SCPN causes these lesions and to determine the time course of these lesions, if any, in the striatum, I repeated similar brightfield and MBP immunostaining analysis on P28, 2 month, 3 month, 6 month and 18 month old *Emx1-Cre; Ppargc1α*$^{fl/fl}$ and matched *Ppargc1α*$^{fl/fl}$ littermate control cortical sections (n = 3 animals per genotype for all ages). Interestingly, I did not find clear IC localized lesions in the *Emx1-Cre; Ppargc1α*$^{fl/fl}$ mice at all ages investigated (Figures 2.14.A. to 2.14.H., data not shown for 2-month-old mutants). However, I did detect occasional small vacuolar lesions (yellow arrows) in the IC of a subset of the conditional mutants examined (Figures 2.14.E. and 2.14.F.) (n = 2 for P28 and n = 1 for 3-month-old *Emx1-Cre; Ppargc1α*$^{fl/fl}$ mutants). Comparative temporal analysis across all ages revealed that these lesions are not formed, even in 18-month-old mutants, indicating that these lesions are not delayed in their formation. In all, these data demonstrate that the formation of spongiform lesions in the IC is largely not dependent on the specific ablation of *Ppargc1α* in the dorsal forebrain, and show that

Figure 2.14. Spongiform-like lesions do not develop in the IC of *Emx1-Cre; Ppargc1α$^{fl/fl}$* mice, even in 18 month old mutants.

(A – H) Immunostaining against myelin basic protein demonstrated that lesions do not develop within the axonal bundles of the IC of *Emx1-Cre; Ppargc1α$^{fl/fl}$* conditional null mutants, as compared to control *Ppargc1α$^{fl/fl}$* mice at P28 (A and E), 2 months (data not shown), 3 months (B and F), 6 months (C and G) and 18 months of age (D and H). Occasional small vacuolar lesions (yellow arrows) in the IC of a subset of the conditional mutants examined were detected (n = 2 for P28 and n = 1 for 3 month old *Emx1-Cre; Ppargc1α$^{fl/fl}$* mutants). Similar results were obtained with brightfield analysis (data not shown). Scale bars, 50 μm (A – H).

Figure 2.14. (Continued)

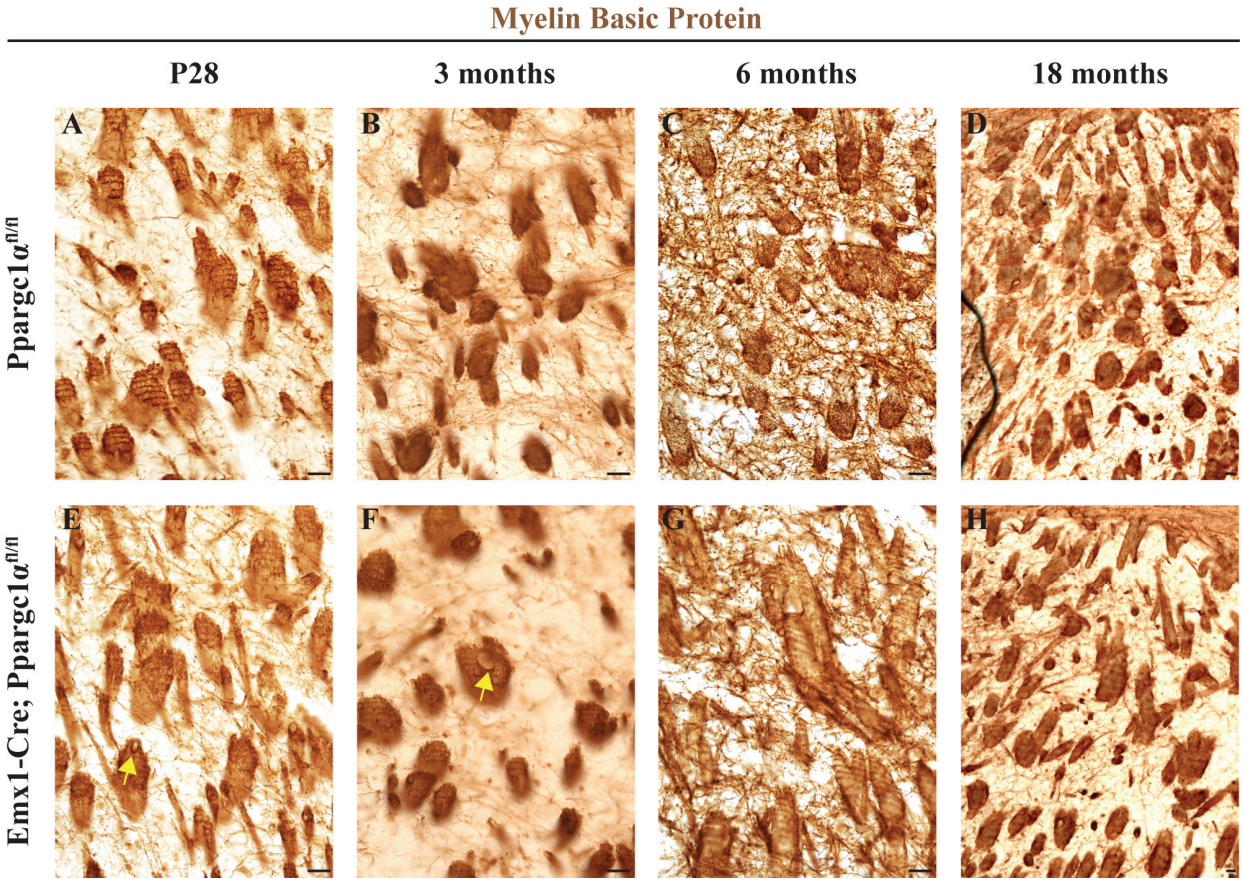

the lesions observed in the IC of the *Ppargc1α* null mutants do not affect descending corticofugal projections. Hence, I conclude that *Ppargc1α* is not cell-autonomously necessary in SCPN to regulate the development of these lesions.

2.3.10. Loss-of-function analysis: spongiform-like lesions do not develop in the IC of adult *Gbx2-CreER; Ppargc1α$^{fl/fl}$* mice.

Besides its expression in SCPN, given that *Ppargc1α* is also expressed in certain TCPN populations that project their ascending axons through the IC (20, 21) where the spongiform-like lesions are localized, I hypothesize that *Ppargc1α* plays a cell-intrinsic role in TCPN to govern lesion formation. To test this hypothesis, I generated conditional null mutants for *Ppargc1α* in the thalamus and used similar brightfield and immunohistological methods, as described above in sections 2.3.7. to 2.3.9. to characterize lesion formation, if any, in these mutants.

2.3.10.A. Generation of *Gbx2-CreER; Ppargc1α$^{fl/fl}$* mice.

Since TCPN extend ascending axonal projections through the IC to reach cortical targets (20, 21), I crossed a loxP-flanked (floxed) *Ppargc1α* line (63) with an *Gbx2-CreER* line (221) to generate *Gbx2-CreER; Ppargc1α$^{fl/fl}$* mutants that are conditionally null for *Ppargc1α* in the thalamus to investigate whether cell-autonomous loss of *Ppargc1α* in TCPN causes these IC localized lesions. The generation of *Gbx2-CreER; Ppargc1α$^{fl/fl}$* mice provide me with an exemplary model to look at the selective loss of *Ppargc1α* in the thalamus and allow me to investigate whether *Ppargc1α* is cell-intrinsically required in TCPN to control lesions development in the IC where ascending axonal projections of TCPN extend through.

2.3.9.B. Temporal and spatial analysis of spongiform lesions in *Gbx2-CreER; Ppargc1α$^{fl/fl}$* mice from P28 to 2 months of age.

To test my hypothesis by determining whether cell-autonomous loss of *Ppargc1α* in TCPN causes these lesions and to determine the time course of these lesions, if any, in the striatum, I repeated similar brightfield and MBP immunostaining analysis on P28 and 2-month-old *Gbx2-CreER; Ppargc1α*$^{fl/fl}$ and matched *Ppargc1α*$^{fl/fl}$ littermate control cortical sections (n = 2 animals per genotype at P28, n = 1 *Ppargc1α*$^{fl/fl}$ and n = 3 *Gbx2-CreER; Ppargc1α*$^{fl/fl}$ at 2 months of age). Surprisingly, I did not detect clear IC localized lesions in the striatum of *Gbx2-CreER; Ppargc1α*$^{fl/fl}$ and *Ppargc1α*$^{fl/fl}$ mice at these ages (Figures 2.15.A. and 2.15.B.). These data suggest that the formation of spongiform lesions in the IC is largely not dependent on the specific ablation of *Ppargc1α* in the thalamus, and further imply that the lesions observed in the IC of the *Ppargc1α* null mutants do not affect ascending afferent projections.

To confirm that the absence of spongiform lesions in the internal capsule of adult *Gbx2-CreER; Ppargc1α*$^{fl/fl}$ mice occurred despite the loss of *Ppargc1α* in the thalamus, I performed ISH for *Ppargc1α* against the deletion region of exon 3 to 5 in all of the *Gbx2-CreER; Ppargc1α*$^{fl/fl}$ and matched *Ppargc1α*$^{fl/fl}$ littermate mutants under investigation. For a subset of mutants, the ISH procedure did not work (2 animals per genotype at P28, n = 1 *Ppargc1α*$^{fl/fl}$ and n = 3 *Gbx2-CreER; Ppargc1α*$^{fl/fl}$ at 2 months of age) (data not shown). Hence, it remains inconclusive whether the formation of spongiform lesions in the IC is dependent or not on the specific ablation of *Ppargc1α* in the thalamus. For another subset of mutants, I detected *Ppargc1α* expression in the thalamus in both *Gbx2-CreER; Ppargc1α*$^{fl/fl}$ and matched *Ppargc1α*$^{fl/fl}$ littermate mice (n = 1 animal per genotype at P28 and 2 months of age) (Figure 2.16.A. and 2.16.B., data not shown for P28). Thus, for these mutants, the lack of spongiform lesion formation may be attributed to the incomplete ablation of *Ppargc1α* in the thalamus. To conclude definitively, in the future, these data would need to be further verified with analysis of

Figure 2.15. Spongiform-like lesions do not develop in the IC of adult *Gbx2-CreER; Ppargc1α$^{fl/fl}$* mice.

(A – B) Immunostaining against myelin basic protein demonstrated that lesions do not develop within the axonal bundles of the IC of *Gbx2-CreER; Ppargc1α$^{fl/fl}$* conditional null mutants, as compared to control *Ppargc1α$^{fl/fl}$* mice, at P28 (data not shown) and 2 months. Similar results were obtained with brightfield analysis (data not shown). Scale bars, 50 μm (A – B).

Figure 2.15. (Continued)

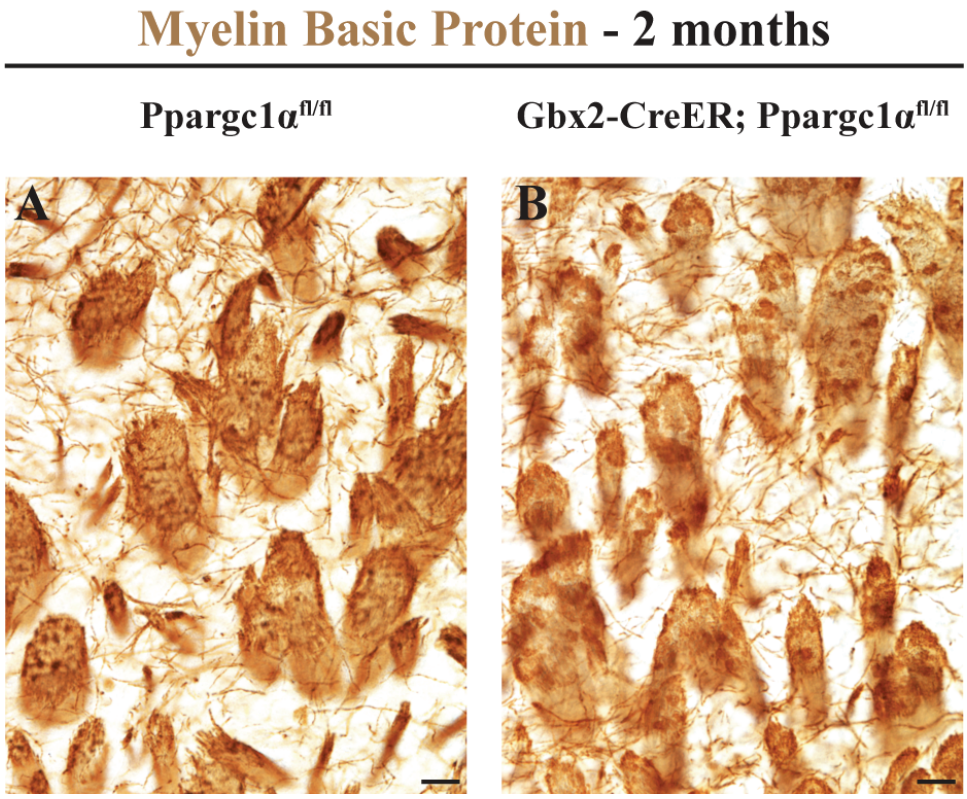

Figure 2.16. *Ppargc1α* expression in *Gbx2-CreER; Ppargc1α*$^{fl/fl}$ mutants.

(A – B) For a subset of mutants, I detected *Ppargc1α* expression in the thalamus in both *Gbx2-CreER; Ppargc1α*$^{fl/fl}$ and matched *Ppargc1α*$^{fl/fl}$ littermate mice (n = 1 animal per genotype at P28 and 2 months of age) (data not shown for P28). Thus, for these mutants, the lack of spongiform lesion formation is attributed to the incomplete ablation of *Ppargc1α* in the thalamus. For another subset of mutants, multiple ISH analyses failed where the procedure did not work (i.e. control wild type sections did not show any *Ppargc1α* expression in the cortex despite of repeated ISH attempts) (2 animals per genotype at P28, n = 1 *Ppargc1α*$^{fl/fl}$ and n = 3 *Gbx2-CreER; Ppargc1α*$^{fl/fl}$ at 2 months of age) (data not shown). Hence, it remains inconclusive whether the formation of spongiform lesions in the IC is dependent or not on the specific ablation of *Ppargc1α* in the thalamus for these mutants. Scale bars, 100 μm (A – B).

Figure 2.16. (Continued)

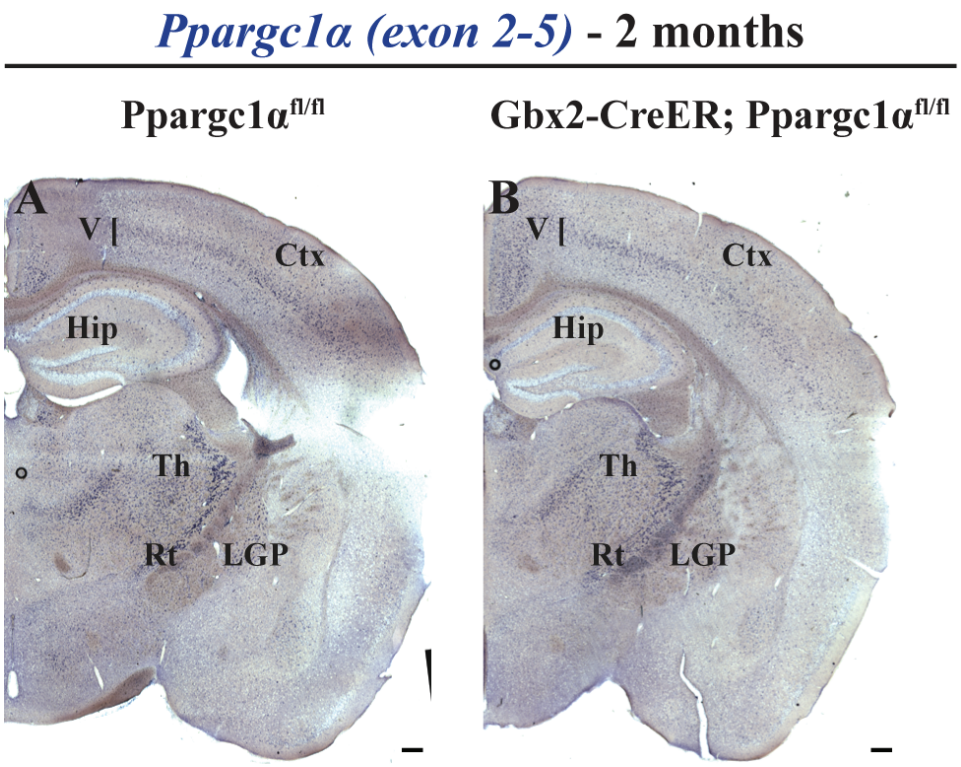

additional mutants with clear ISH profiles demonstrating *Ppargc1α* ablation in the thalamus.

2.3.11. MBP-positive vacuoles develop in neocortices of *Ppargc1α*$^{-/-}$ and *Emx1-Cre; Ppargc1α*$^{fl/fl}$ mice.

Besides the generation of spongiform-like lesions in the striatum, I also found a hitherto undescribed phenomomen of MBP positive circular vacuoles of various sizes in the neocortices of *Ppargc1α*$^{-/-}$ and *Emx1-Cre; Ppargc1α*$^{fl/fl}$ mice.

IHC for MBP—a protein found within the myelin sheath that surrounds the axonal fibers (112)—on *Ppargc1α*$^{-/-}$ and matched wild type littermate coronal cortical sections at P14, P28, 2 months, 3 months, 6 months and 18 months of age revealed the presence of MBP positive vacuoles in the *Ppargc1α*$^{-/-}$ cortex (n = 3 per genotype for all ages except n = 2 wild type and n = 5 *Ppargc1α*$^{-/-}$ mice at 18 months of age). While I did not find vacuoles at P14 (data not shown), I found them (red arrows) in *Ppargc1α*$^{-/-}$ but not in wild type mice at P28, 2 months, 3 months and 6 months (Figure 2.17.A. – B. and 2.17.E. – F., data not shown for 2 and 3 months). High magnification analysis of these vacuoles revealed circular ring structures of various sizes that are positive for MBP (Figure 2.17.B'. and 2.17.F'.). Interestingly, I observed that the number of vacuoles seemed to decrease with age as *Ppargc1α*$^{-/-}$ mice had more vacuoles at P28 than at 6 months (Figure 2.17.B. and 2.17.F.). This observation is also supported by my analysis of 18-month-old mutants where I did not find any MBP positive vacuoles in their necortices (data not shown). This suggests that the vacuolar phenotype "recovers" with age.

To determine whether the formation of MBP positive vacuoles is due to the cell-autonomous loss-of-function of *Ppargc1α* in the dorsal forebrain, I repeated the analysis on P28, 2 month, 3 month, 6 month and 18-month-old *Emx1-Cre; Ppargc1α*$^{fl/fl}$ and matched *Ppargc1α*$^{fl/fl}$

Figure 2.17. MBP-positive vacuoles develop in the neocortices of *Ppargc1α*$^{-/-}$ and *Emx1-Cre; Ppargc1α*$^{fl/fl}$ mice.

(A – D) Immunostaining for MBP on P28 *Ppargc1α*$^{-/-}$ (B) and *Emx1-Cre; Ppargc1α*$^{fl/fl}$ (D) cortical sections revealed the formation of MBP-positive vacuoles (red arrows) that are absent in wild type (A) and *Ppargc1α*$^{fl/fl}$ (C) controls. (B', D', F' and H') High magnification images of MBP-positive vacuoles in B, D, F and H respectively.

(E – H) IHC for MBP on 6-month-old *Ppargc1α*$^{-/-}$ (F) and *Emx1-Cre; Ppargc1α*$^{fl/fl}$ (H) cortical sections revealed the presence of vacuoles (red arrows) but in fewer numbers, as compared to that at P28. Scale bars, 50 μm (A – H), 10 μm (B', D', F' and H').

Figure 2.17. (Continued)

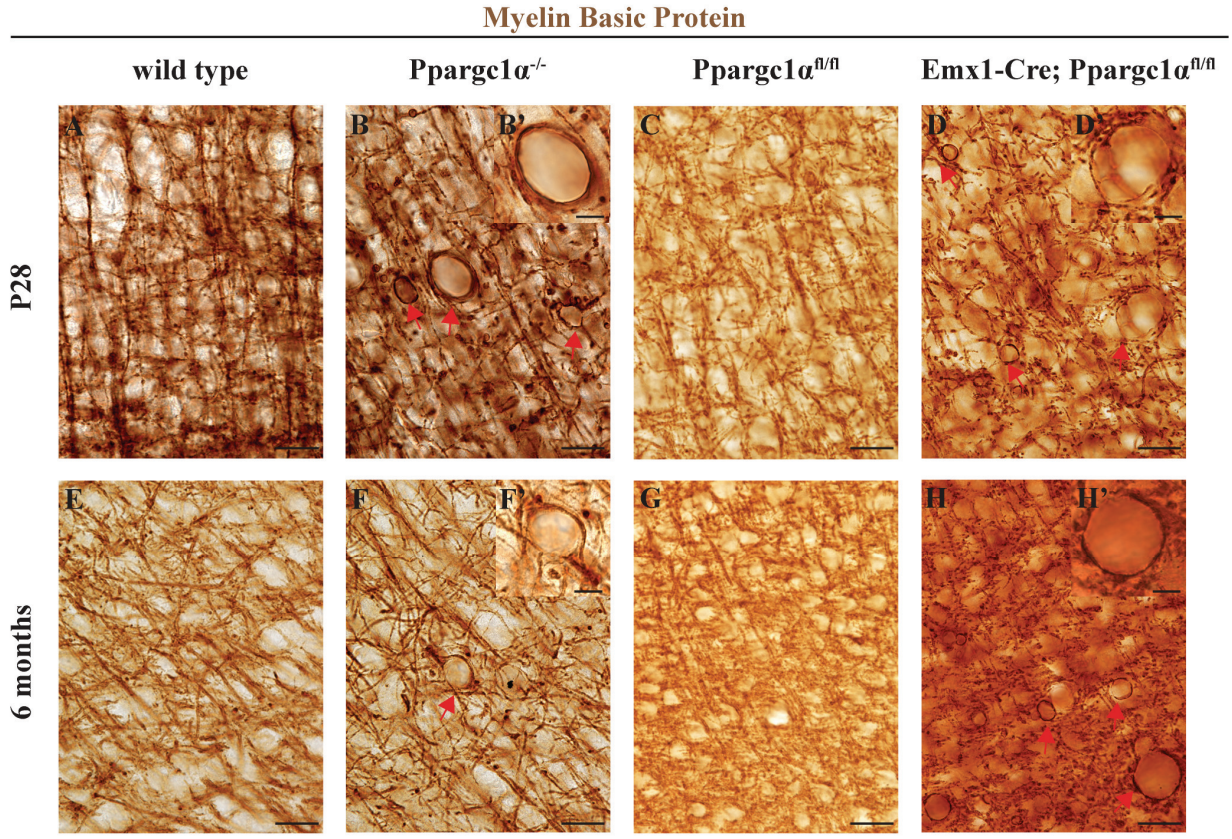

littermate cortical sections (n = 3 animals per genotype). I found similar vacuoles in *Emx1-Cre; Ppargc1α$^{fl/fl}$* mice but not in *Ppargc1α$^{fl/fl}$* controls at all ages up to 6 months of age but not at 18 months of age (Figure 2.17.C. – D. and 2.17.G. – H., data not shown for 2-month-old and 3-month-old mutants). High magnification analysis of these vacuoles also revealed circular ring structures of various sizes that are positive for MBP (Figure 2.17.D'. and 2.17.H'.). Similarly to *Ppargc1α$^{-/-}$* mice, I also found that the number of vacuoles in *Emx1-Cre; Ppargc1α$^{fl/fl}$* mice decrease with age (Figure 2.17.D. and 2.17.H.). In all, these data indicate that the formation of vacuoles in the cortex is at least in part caused by the cell-autonomous loss-of-function of *Ppargc1α* in the dorsal telencephalon.

These MBP positive vacuoles differ from the spongiform-like lesions found in the striatum because (i) they "recover" with age with peak formation at P28 and 2 months before decreasing at 3 to 6 months and eventually disappear at 18 months while the spongiform-like lesions persist with age from P28 to 18 months, and (ii) they are only revealed with MBP staining while the lesions can be observed with both brightfield as well as immunostaining for MBP. Hence, I conclude that these MBP positive vacuoles are a distinct phenotype from the spongiform-like lesions found in the internal capsule. I also conclude that *Ppargc1α* in the dorsal telencephalon is necessary to generate these MBP positive vacuoles but not IC-localized lesions.

2.3.12. MBP-positive vacuoles are distributed throughout the neocortex.

To determine whether the distribution of the vacuoles corresponds to particular cortical layers and possibly affects preferentially selected neuronal populations of the cortex, I imaged matched sections of 2-month-old *Emx1-Cre; Ppargc1α$^{fl/fl}$* and matched *Ppargc1α$^{fl/fl}$* littermate controls (n = 3 per genotype, 2 hemispheres per area, for each mouse) and superimposed a red

dot in place of every vacuole that I observed in their cortices. I found that the vacuoles are distributed throughout the cortex along the anterior-posterior axis, with less vacuoles detectable in the upper layers II/III (Figure 2.18.A. – B., 2.18.D. – E. and 2.18.G. – H.). For quantification, I superimposed on matched sections boxes of defined width (in three areas) that span the thickness of the cortex at matched locations on each section and divided each box into ten equally-sized bins, with bin 1 located nearer to the pia and bin 10 nearer to the corpus callosum. Fold differences were determined by dividing the number of vacuoles found in each bin within a given area of *Emx1-Cre; Ppargc1α*$^{fl/fl}$ mice over that found in the littermate control *Ppargc1α*$^{fl/fl}$ mice (Figure 2.18.C., 2.18.F. and 2.18.I.). The statistical analysis is summarized in Table 2.3.. Preliminary analysis confirmed my initial finding that the vacuoles are distributed throughout layers IV-VI of the cortex, across all areas (Figure 2.18.C., 2.18.F. and 2.18.I.). However, it is unclear whether the absence of vacuoles in upper layers II/III (bin 2) is due to their genuine absence or the fact that very few axons stain for MBP in these layers, compromising detection. It is also possible that I may detect more vacuoles in the deep layers because MBP staining is limited in the upper layers and this limition may relate to the hypomyelination defect as described in Chapter 3.

2.3.13. Preliminary electron microscopy analysis reveals limitations in identifying MBP-positive vacuoles without a definitive marker.

To better define and understand the nature of these MBP-positive vacuoles in the neocortex, I performed electron microscopy to visualize these vacuoles at a high resolution. Under the electron microscope, myelin is easily identified without the need to immunostain for any proteins associated with the myelin sheath. Pilot analysis on P28 *Ppargc1α*$^{-/-}$ and wild type

Figure 2.18. MBP-ppositive vacuoles are distributed throughout the neocortex.

(A – I) Immunostaining for MBP on 2 month old *Ppargc1α*$^{fl/fl}$ (A, D, G) and *Emx1-Cre; Ppargc1α*$^{fl/fl}$ (B, E, H) cortical sections showed that the vacuoles (red dots) are distributed throughout the cortex. (C, F, I) Vacuoles were quantified in 2 month old *Ppargc1α*$^{fl/fl}$ and *Emx1-Cre; Ppargc1α*$^{fl/fl}$ mice. Fold differences were determined by dividing the number of vacuoles found in each bin within a given area of *Emx1-Cre; Ppargc1α*$^{fl/fl}$ mice over that found in the *Ppargc1α*$^{fl/fl}$ controls. Bin 1 is located nearer to the pia while bin 10 is located nearer to the corpus callosum (CC). Primary motor, somatosensory and visual areas were quantified. * $p<0.05$, ** $p<0.01$, two tailed student's T test. Scale bars, 100 μm (A – H).

Figure 2.18. (Continued)

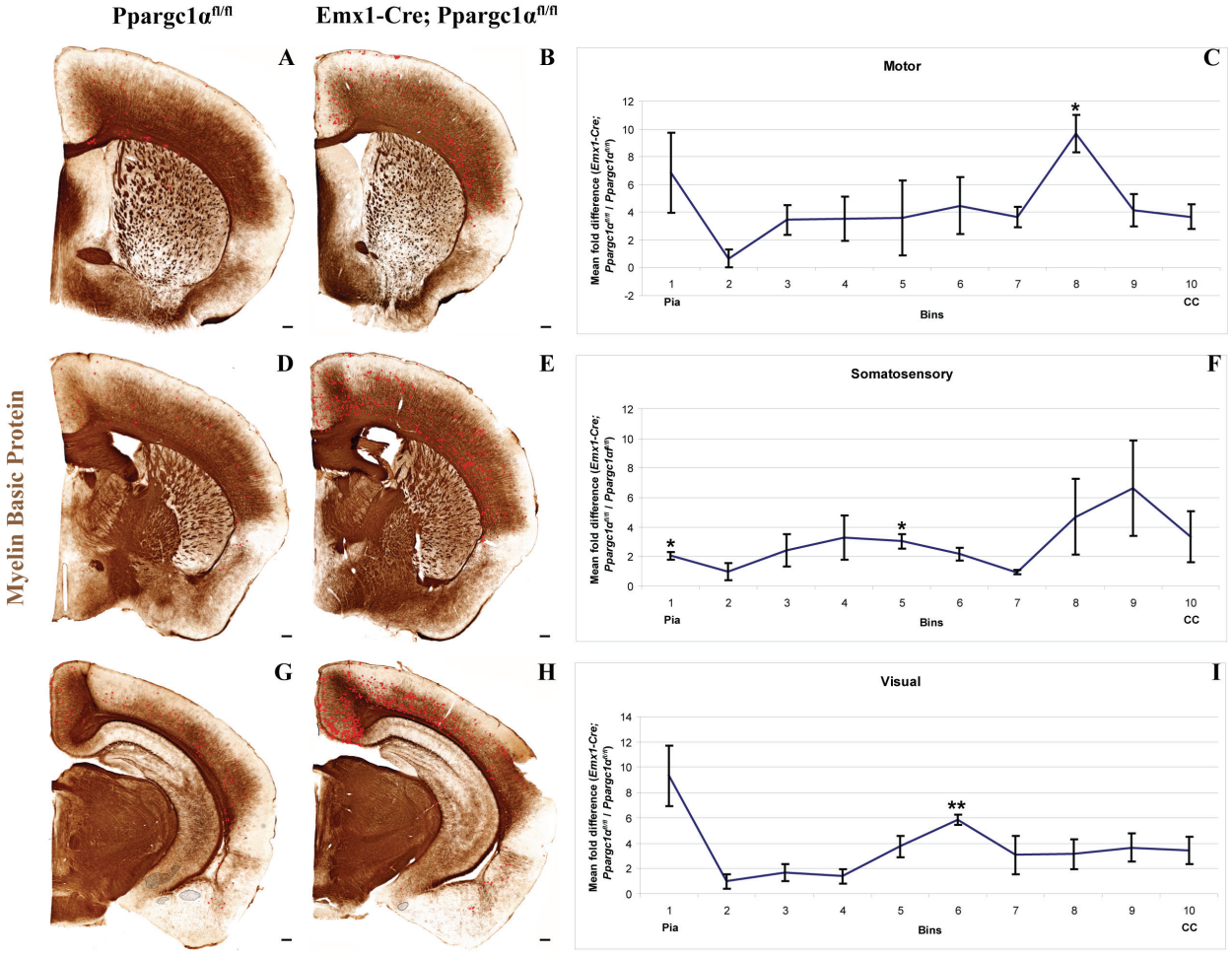

Table 2.3. Statistical analysis of the fold difference of MBP positive vacuoles between adult *Emx1-Cre; Ppargc1α$^{fl/fl}$* and *Ppargc1α$^{fl/fl}$* mutants.

This table summarizes the p values obtained after statistical analysis with two tailed student's T test on the fold difference between the number of MBP positive vacuoles spread throughout all the cortical layers divided into ten bins from pia to corpus callosum (CC) in 2-month-old *Ppargc1α$^{fl/fl}$* and *Emx1-Cre; Ppargc1α$^{fl/fl}$* mice. Numbers in red represent significant values ≤ 0.05.

Table 2.3. (Continued)

	P values (two tailed student's T test)		
	Motor	Somatosensory	Visual
Pia 1	0.181	0.0488	0.0741
2	0.423	1.00	0.667
3	0.155	0.318	0.423
4	0.249	0.270	0.562
5	0.441	0.0522	0.0832
6	0.235	0.109	0.00600
7	0.0669	0.776	0.300
8	0.0229	0.290	0.210
9	0.113	0.223	0.141
CC 10	0.0742	0.312	0.150

littermate control mice revealed the difficulties in identifying these MBP-positive vacuoles or circular structures as cross sections of axons in the neocortex also present themselves as circular rings of myelin (n = 1 animal per genotype) (Figure 2.19.A.). Without immunostaining for a specific marker that defines these vacuoles, I cannot distinguish with confidence whether a circular ring of myelin belongs to an abnormal vacuole or to a normal axon.

I have tried to define these vacuoles with markers like prohibitin that have been reported to identify neuroaxonal spheroids found in the brain. However, this marker did not identify these vacuoles of interest. Hence, the nature of these vacuoles remains elusive and further analyses will be limited by the lack of specific markers.

Figure 2.19. Preliminary electron microscopy analysis reveals limitations in identifying MBP-positive vacuoles without a definitive marker.

(A – D) Under the electron microscope, myelin is easily identified as dark circular rings (red arrows) without the need to immunostain for any proteins associated with the myelin sheath. Pilot analysis on P28 *Ppargc1α*$^{-/-}$ mutant revealed the difficulties in identifying these MBP-positive vacuoles or circular structures as cross sections of axons in the neocortex also present themselves as circular rings of myelin. Scale bars, 2 μm (A – B and D), 10 μm (C).

Figure 2.19. (Continued)

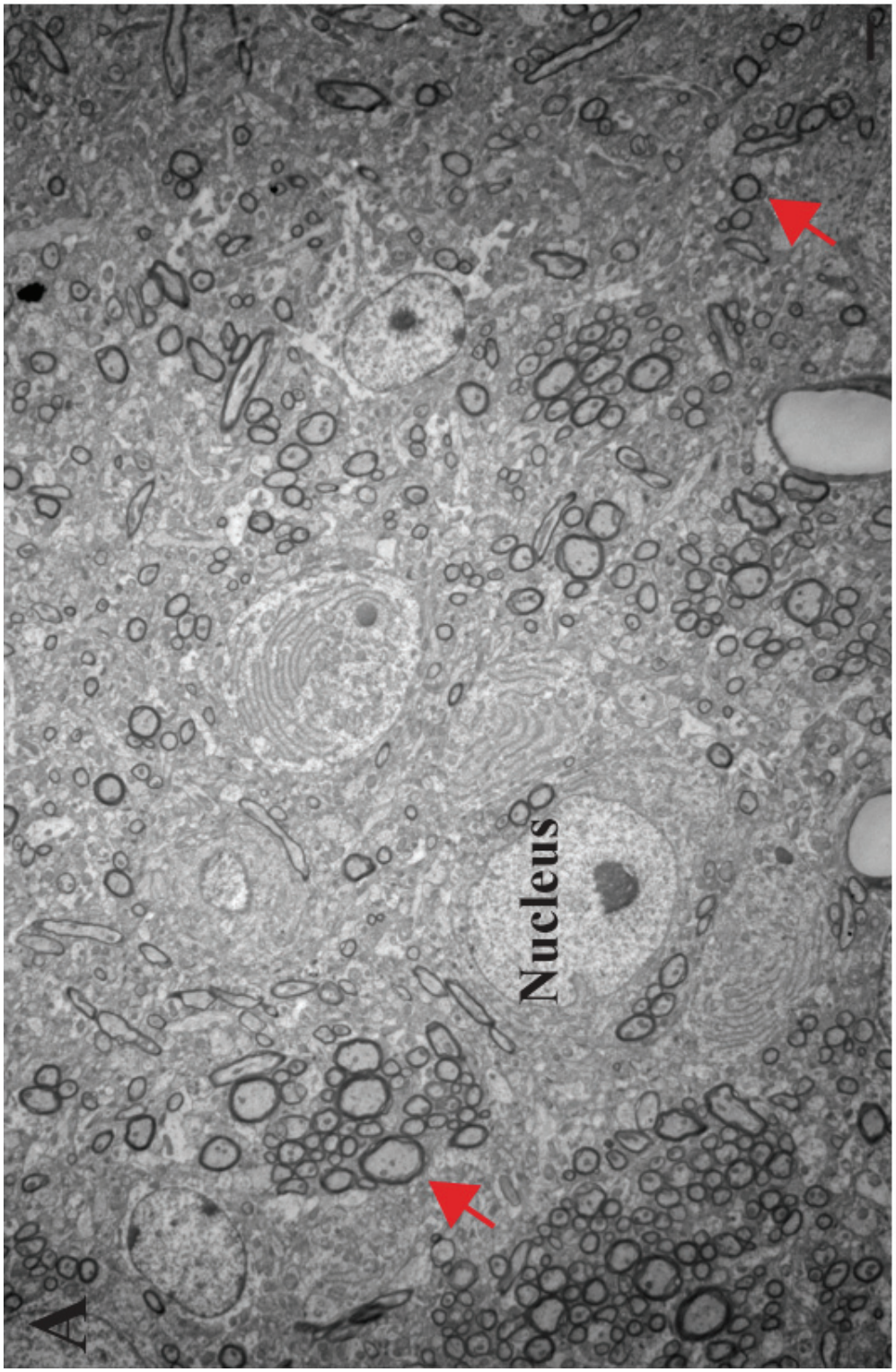

Figure 2.19. (Continued)

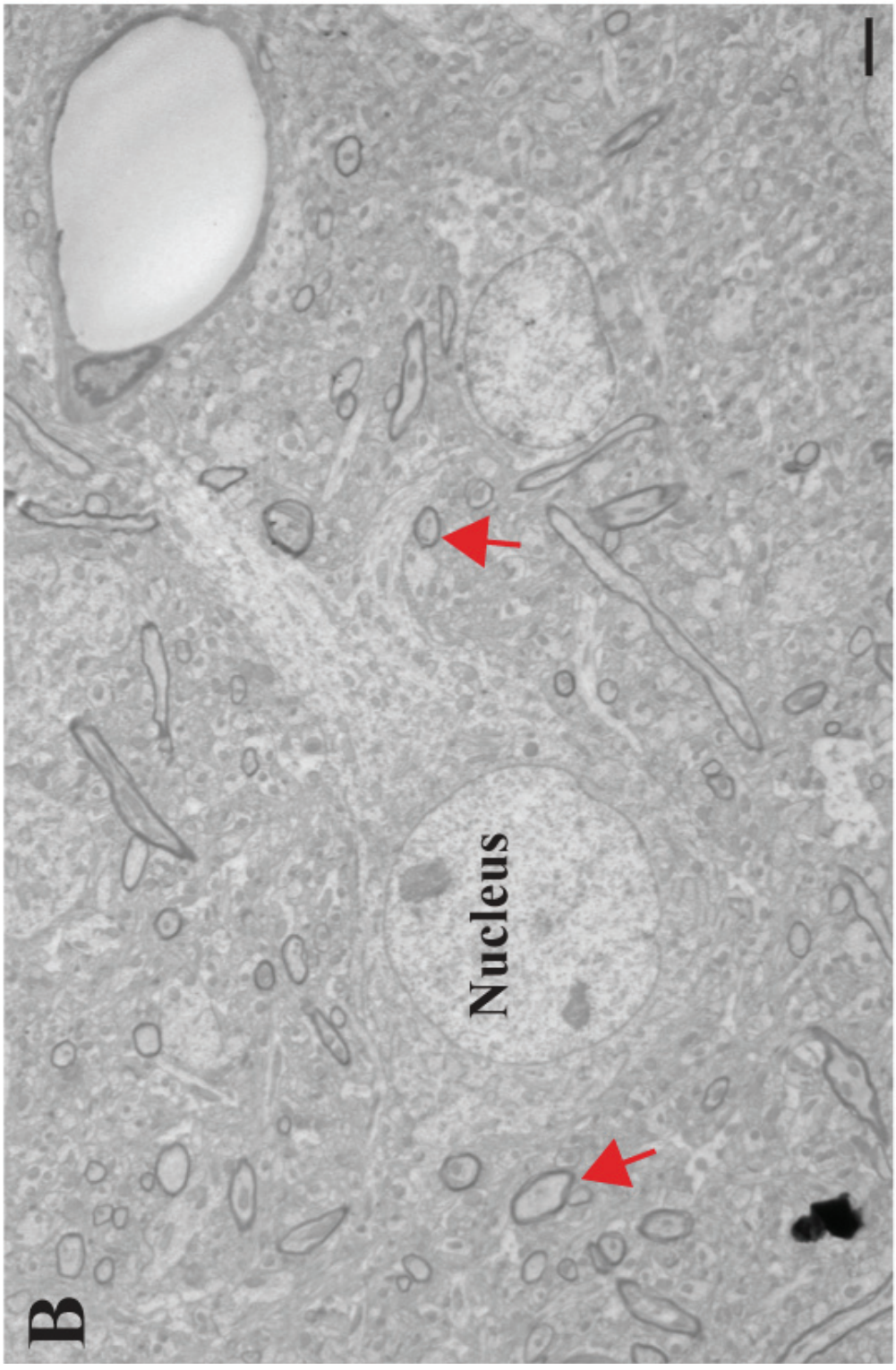

Figure 2.19. (Continued)

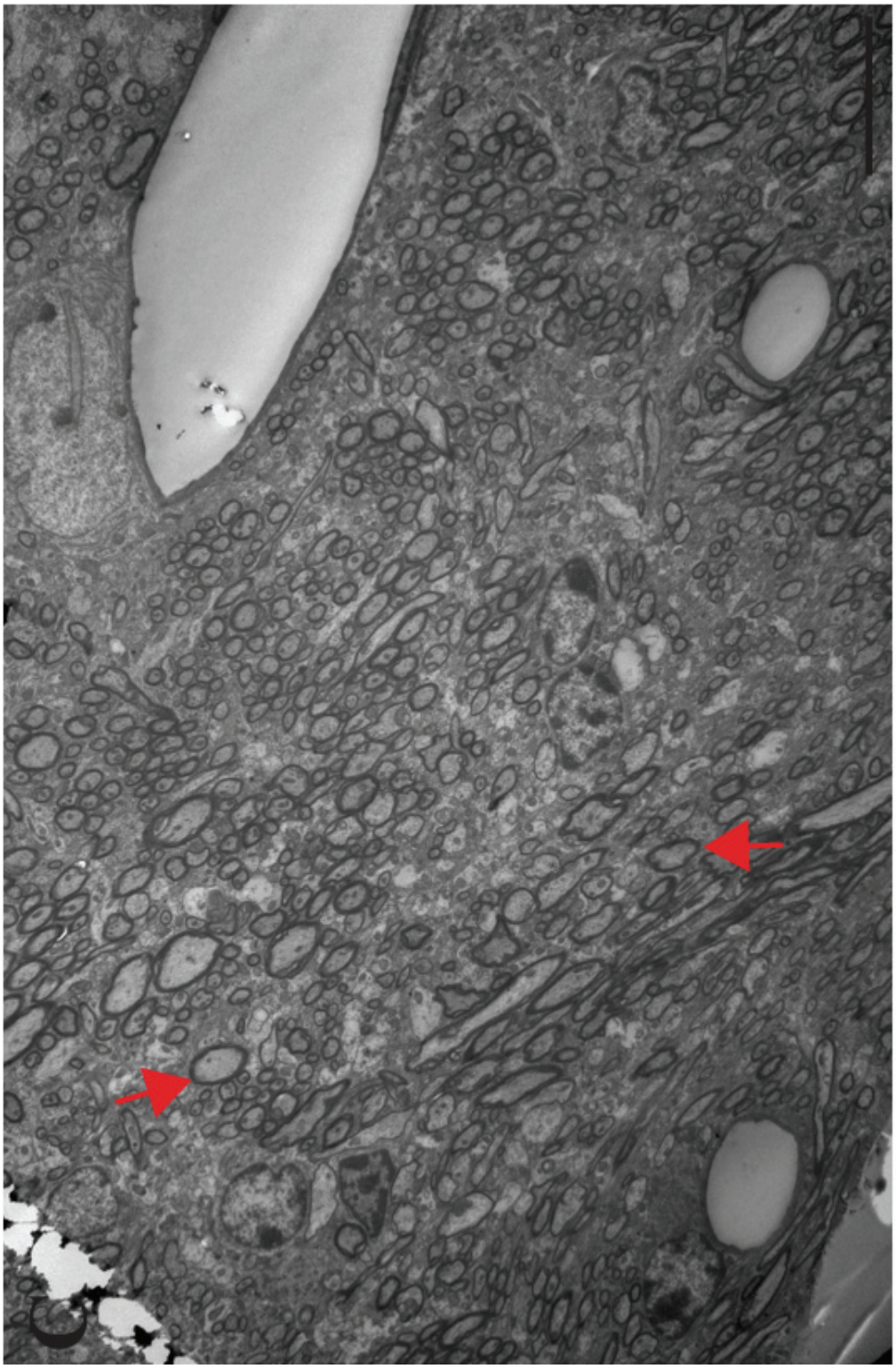

Figure 2.19. (Continued)

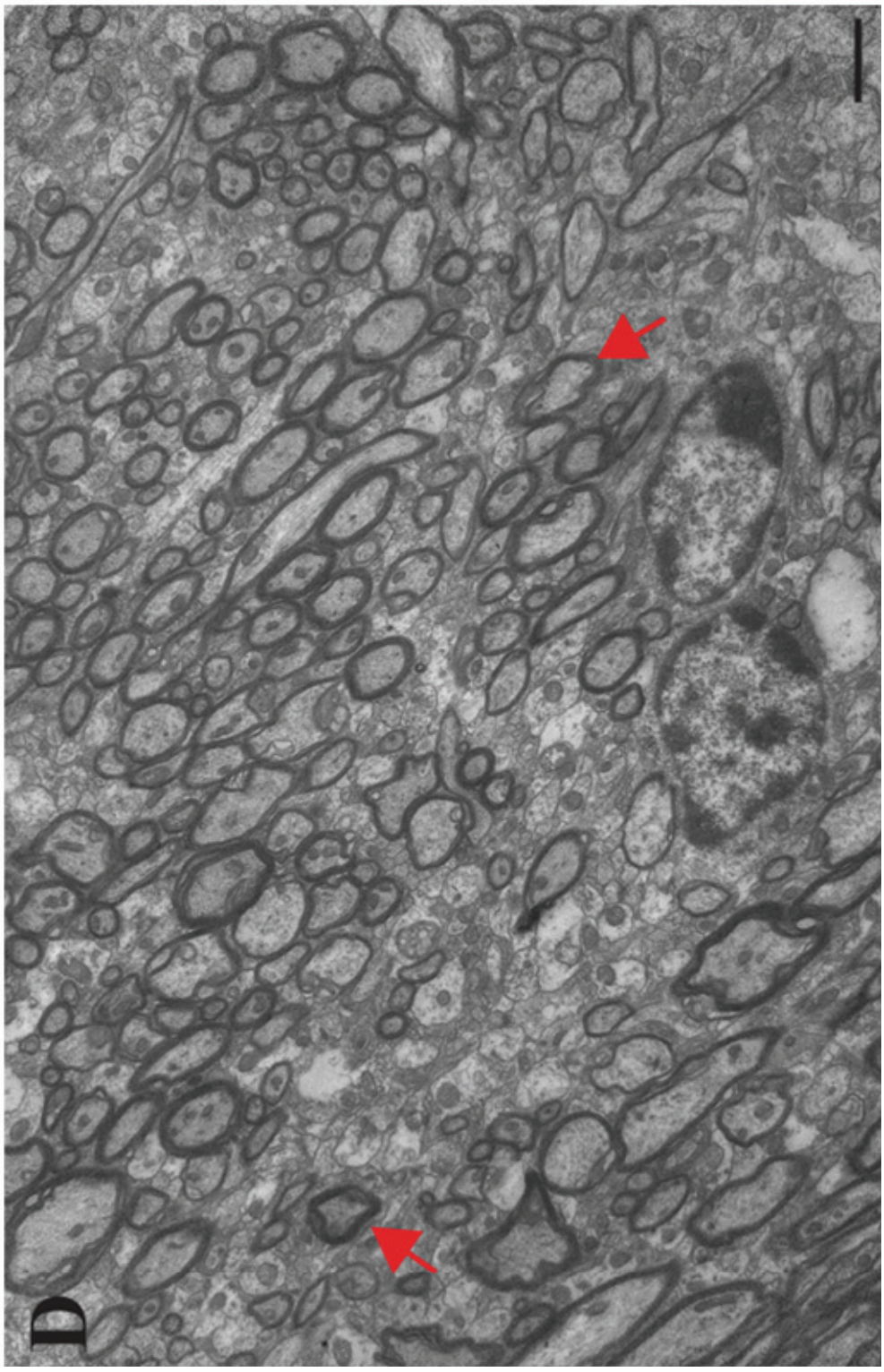

2.4. Discussion.

Previous studies have involved *Ppargc1α* in neuronal survival, purporting that its functional role—by suppressing ROS and protecting against mitochondrial dysfunction—promotes neuronal survival against oxidative insults (72-74). However, these studies were conducted in one of two circumstances: where toxic substances like kainic acid or neurotoxin MPTP were administered to induce cell death (72), or where *Ppargc1α* null mice were crossbred to mice models of neurodegeneration such as the HD knock in mouse models with CAG repeats (73). Most importantly, in all of these studies, the contribution of *Ppargc1α* to neuronal survival is achieved only in the context of acute cellular stress or concurrent neurodegeneration. Hence, it remains unknown whether the developmental function of *Ppargc1α* is to regulate neuronal survival.

Focusing on the neocortex, I presented a study that investigates the developmental role of *Ppargc1α* in neuronal survival. I employed genetic null and newly generated conditional null mutant mice for *Ppargc1α* in the neocortex to study whether *Ppargc1α* is cell-autonomously necessary for neuronal and/or SCPN-selective survival in the neocortex. Surprisingly, loss-of-function analysis showed that in the absence of *Ppargc1α* alone, there are no gross cortical or neuronal abnormalities where distinct PN subtypes are born, specified and positioned normally in the neocortex. In addition, cell death analysis further revealed that there is no increased cell death caused by global or conditional loss of *Ppargc1α* in the dorsal forebrain. Hence, my findings demonstrate that *Ppargc1α* is not cell-autonomously required to control neuronal survival where there is no concurrent acute cellular stress or neuronal degeneration.

These results also motivated me to elucidate whether *Ppargc1α* is cell-intrinsically required for neuronal survival in response to aging as a cellular stress factor. This study is

significant because it will allow us to better distinguish *Ppargc1α's* role in the neocortex in relation to neuronal survival and to determine whether that differs with time or age. To address this, I present the first long-term aging study of 18-month-old *Ppargc1α* null and newly generated conditional null mutant mice for *Ppargc1α* in the dorsal forebrain. Interestingly, I discovered similar results in these aged mice where in the absence of *Ppargc1α*, there are no gross cortical or neuronal abnormalities and the main PN subtypes are maintained normally in the neocortex. Furthermore, there is no enhanced cell death caused by global or conditional loss of *Ppargc1α* in the dorsal forebrain, even in these 18-month-old mutant mice. Thus, I conclude that *Ppargc1α* is not cell-autonomously necessary to regulate neuronal survival in the neocortex, even in the context of cellular stress triggered by aging.

Building on prior studies (62, 63), I also report that transcriptional co-activator *Ppargc1α* is required to prevent the generation of spongiform-like lesions in the striatum. I depicted the first long-term study describing the exact location, arealization and developmental time course of these striatal lesions. My results demonstrated that global ablation of *Ppargc1α* causes lesions to be generated either in close association with, or localized within axonal bundles of the IC, where SCPN and TCPN among other neuronal subtypes project through. These lesions are not spatially arealized along the anteroposterior, mediolateral and dorsoventral axes. They are also not formed at P14 but develop by P28 and persist throughout adulthood and even into old age of 18 months.

Besides their position and temporal development, it is important to comprehend the cellular origins of these lesions. This will allow us not only to understand possible degenerative regions, but more crucially, to elucidate if these lesions affect SCPN axonal extensions that project through the IC. To determine this, I first studied the temporal, spatial and cell type specific expression profile of *Ppargc1α* in the brain. My results showed that *Ppargc1α* is

preferentially expressed in layer V SCPN and in certain TCPN populations primarily during postnatal ages. They also demonstrated that *Ppargc1α* is absent in other major PN subtypes such as CThPN of deep layer VI and the majority of CPN across all cortical layers as well as in glial cells.

Since *Ppargc1α* is preferentially expressed in SCPN and certain thalamic nuclei that project through the IC where the spongiform lesions are localized, I investigated whether *Ppargc1α* plays a cell-intrinsic function in SCPN or TCPN to govern the formation of spongiform-like lesions in the IC, by generating novel conditional null mutants for *Ppargc1α* in the dorsal telencephalon and thalamus respectively. Strikingly, I found that conditional loss of *Ppargc1α* in the neocortex or thalamus does not cause these lesions in the IC, even in 18-month-old mutants. This indicates that these lesions are not delayed in their formation and they are never formed throughout the lifespan of these mutants. Therefore, as illustrated in Figure 2.20., I conclude that *Ppargc1α* is cell-autonomously not necessary in SCPN or TCPN to cause spongiform lesions in the IC.

It is possible that striatal neurons may contribute to lesion formation in the IC. However, a recent report by Cowell and her group suggests that striatal neurons are predominantly unaffected in the *Ppargc1α* null mutant (96). They explored the transcriptional profile of general striatal projection markers (e.g. *Gad1*, *Calb1*, *Opm*), striatal direct pathway markers (e.g. *Pdyn*, *Tac1*, *Drd1a*), striatal indirect pathway markers (e.g. *Penk1* and *Drd2*) and striatal interneuron markers (e.g. *Parvalbumin*, *Calb2*, *NPY*, *Chat* and *Nos1*) in the *Ppargc1α* null mutant (96). Besides the known decrease in Parvalbumin expression, they found that majority of the striatal markers remained unchanged in the *Ppargc1α* null mutant, except for unexpected increases in gene expression of general striatal PN markers like *Calb1* and *Opm*, direct pathway markers such

Figure 2.20. Spongiform lesion formation across multiple mutant models for *Ppargc1α* in the brain.

(A – E) Representative images of the IC delineated by myelin basic protein staining across wild type (A), *Ppargc1α*$^{-/-}$ (B), *Ppargc1α*$^{fl/fl}$ (C), *Emx1-Cre; Ppargc1α*$^{fl/fl}$ (D), *Gbx2-CreER; Ppargc1α*$^{fl/fl}$ (E). Conditional null mutants do not develop the IC localized lesions (red arrows) that are observed in the null mutant for *Ppargc1α*. Schematics above the images show where *Ppargc1α* is expressed (white areas) and where it is ablated (yellow areas). Ctx, cortex; Str, striatum; CC, corpus callosum; Hip, hippocampus; Th, thalamus. Scale bars, 50 μm (A – E).

Figure 2.20. (Continued)

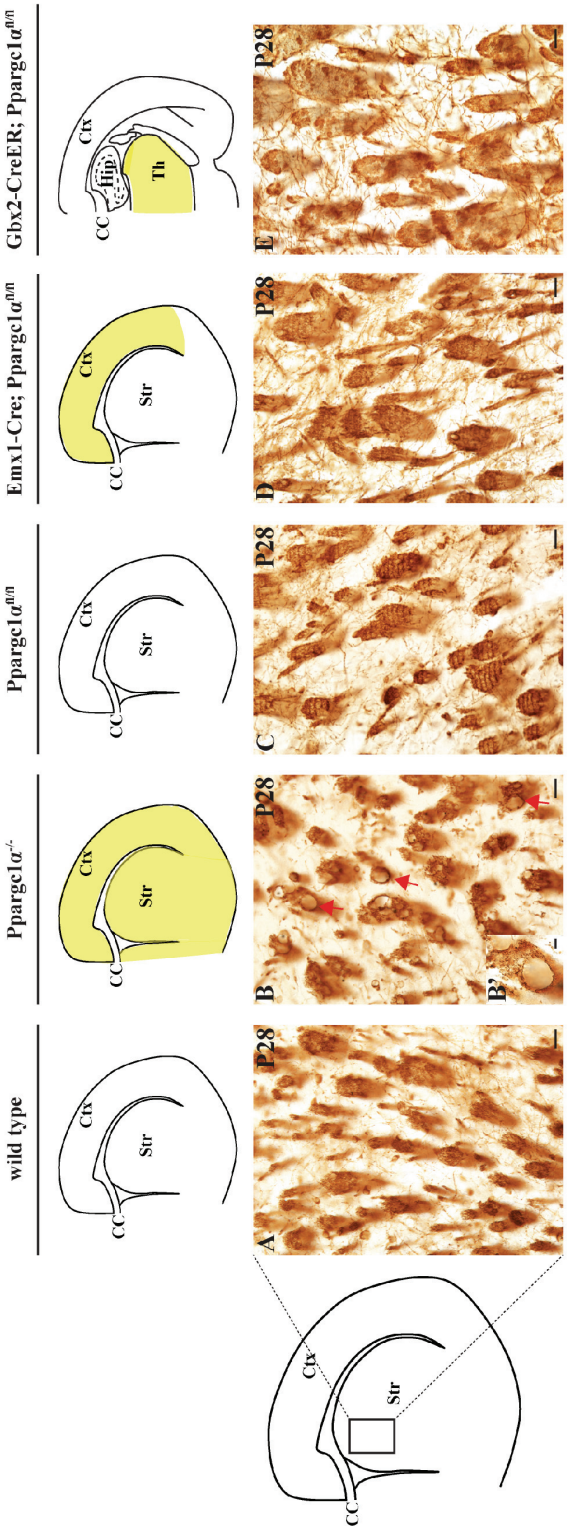

as *Pdyn* and *Tac1*, indirect pathway markers like *Penk1* and *Drd2*, as well as interneuron marker such as NPY (96). The expression profile of the abovementioned markers in the *Ppargc1α* null mutant are in stark contrast with that of the R6/2 Huntington's disease mice model where there is concurrent degeneration of striatal neurons. In the R6/2 mice, there are significant decreases in the gene expression of general striatal PN marker like *Gad1*, striatal direct pathway marker such as *Pdyn*, striatal indirect pathway markers like *Penk1* and *Drd2*, as well as many interneuron markers such as *Calb2*, *NPY*, *Chat* and *Nos1*(96). These prior results suggest that the striatal neurons are relatively normal in the *Ppargc1α* null mutant and that *Ppargc1α* do not regulate survival without any acute cellular stress. This further supports my results in the neocortex that *Ppargc1α* is not required for neuronal survival in the native cellular state without acute cellular stress or in the context of chronic stress caused by aging.

My findings show that *Ppargc1α* is cell-intrinsically not required to govern neuronal survival during normal development, either in the lack of acute external environmental stress triggers or in the context of cellular stress caused by aging. Together with previous work (72-74), my data purport that *Ppargc1α* is implicated in neuronal survival, but only in the context of an unbalanced non-homeostatic cellular state caused by acute cellular stress or neurodegeneration. In this case, the absence of *Ppargc1α* may increase the cells' susceptibility to die, potentially by interfering with the ROS defense system and mitochondrial function, or by thus far unexplored mechanisms. It also suggests that the increased cell death observed in previous work is caused by possible additive or more complex effects of already innate cell toxicity or death.

For future work, it will be interesting to determine other novel downstream effectors responsible for *Ppargc1α* role in neuronal survival in the event of acute cellular stress and neurodegeneration. Although mitochondrial genes involved in the ROS defense system have

been involved in prior work (72-74), it remains to be determined whether other currently unidentified genes are also implicated, and if so, how *Ppargc1α* controls the expression of these genes and the molecular pathways that enable them to be crucial for cell survival.

Prior work shows that neuron-specific loss of *Ppargc1α* causes smaller and fewer spongiform-like lesions in the striatum (219). I ascertained these results in section 2.3.3. and described in further detail the localization and arealization of these lesions in the neuron-specific conditional null mutants for *Ppargc1α*. These data show that selective loss of *Ppargc1α* in neurons is only partly accountable for the development of IC localized lesions. This shows that while *Ppargc1α* in neurons is necessary to control lesion development, it does so only to a certain extent. My above findings show that *Ppargc1α* alone, in either SCPN or TCPN, is not required to control lesion development. Thus, these data in totality suggest that lesion generation requires either the concurrent absence of *Ppargc1α* in SCPN and TCPN, or the specific loss of *Ppargc1α* in a thus far unexamined region like the substantia nigra where *Ppargc1α* is highly expressed, or in the striatum where *Ppargc1α* is weakly expressed up to P7. I have tested the possibility that these lesions may necessitate concurrent loss of *Ppargc1α* in SCPN and TCPN by generating double conditional null mutants for *Ppargc1α.* Unfortunately, breeding these animals has been difficult; four breeding cycles with foster dams over the past eight months did not yield any animals with the genotype of interest. Hence, it remains unknown if lesion formation is caused by the singular loss of *Ppargc1α* in a defined neuronal region or by the additive deficit of *Ppargc1α* in multiple neuronal regions.

Since my data and others have demonstrated that neuron-selective absence of *Ppargc1α* leads to smaller and fewer lesions (219) as compared to that of the null mutant, there is a non neuronal, potentially systemic or a more complex multifactorial mechanism responsible for these

lesions. A recent study has shown that *Ppargc1α* expression in muscles can stimulate the production of FNDC5, a precursor that is cleaved and secreted as irisin—a newly identified hormone or myokine that can stimulate a broad program of brown adipose tissue development (222). Irisin secretion is stimulated by exercise and can lead to improvements in obesity and glucose homeostasis (222). However, its function in brain development remains unexplored and it remains to be seen whether irisin is involved in the development of spongiform lesions in the IC. It will be interesting to determine whether a systemic or secreted component like irisin, or a hitherto unidentified molecule leading to a multiplex pathway, is responsible for lesion formation.

Chapter 3:

Neuron-specific *Ppargc1α* is required to control myelination in the neocortex.

Author contribution: I designed all the experiments and interpreted all the data, with the input of Professor Paola Arlotta. I performed all *in situ* hybridizations and majority of the colocalization analyses to determine the expression profile of *Ppargc1α* in the brain (Chapter 2). I also ascertained that *Ppargc1α* expression in SCPN requires *Fezf2*. Through immuno-staining, I studied the neocortical myelination patterns of *Ppargc1α* null mutants, neuron-specific null mutants, as well as newly generated conditional null mutants in the dorsal telencephalon and in the thalamus. Together with Travis Hallett, I executed histological and immunohistochemistry analyses to demonstrate that projection neurons are normal and that there is no enhanced cell death in these mutants (Chapter 3). In addition, I established the method to determine metabolic levels in the *Ppargc1α* conditional null mutants with Kelly Chatman from the Small Molecule Mass Spectrometry Facility at Harvard University and advice from Dr. Giulio Srubek Tomassy. Travis Hallett characterized the different oligodendrocyte populations in the *Ppargc1α* conditional null mutants while Dr. Simona Lodato performed the *in utero* electroporation experiment. I thank Dr. Giulio Srubek Tomassy for his advice in this project.

Publication: These data will be published either in conjunction with Chapter 2 and/or Chapter 3.

3.1. Abstract.

Myelin is a compacted multilayer lipid membrane that sheaths axons and provides neurons with electrical insulation in order to increase the conduction velocity and efficient propagation of action potentials. The generation of myelin, undertaken by oligodendrocytes in the central nervous system, is dependent on a multitude of intrinsic as well as extrinsic factors, among which the reciprocal interactions between neurons and oligodendrocytes is an essential contributor.

Here, I report for the first time that *Ppargc1α*, a cell-autonomous transcriptional co-activator in subcerebral projection neurons (SCPN), is necessary for proper myelination of the neocortex, a process governed by oligodendrocytes. Employing various genetic null and newly generated conditional null mutants for *Ppargc1α*, I demonstrate that global or conditional loss of *Ppargc1α* in neurons or in the neocortex causes hypomyelination across all cortical layers. Aging studies of these null and conditional null mutants at 18 months further reveal that these hypomyelination defects are not due to a delay in myelination because they persist with age. Moreover, the hypomyelination phenotypes are not caused by gross cortical abnormalities, loss of projection neuron subtypes or enhanced cell death. However, overexpression of *Ppargc1α* did not result in ectopic myelination. Initial results of research into the mechanistic action of *Ppargc1α* show that the loss of *Ppargc1α* leads to decreased neuronal metabolism, suggesting that secreted metabolites can act as mediators for neuron-specific *Ppargc1α* to interact with oligodendrocytes to control myelination. Hence, these data indicate that neuron-specific *Ppargc1α* is required for the proper establishment of neocortical myelination, and suggest a novel function for *Ppargc1α* in neuron-to-glia communication to regulate myelination.

3.2. Introduction.

The myelin sheath provides neurons with electrical insulation. It greatly enhances the conduction speed of action potentials and thus enables efficient saltatory propagation of nerve impulses over long distances (112, 113). It is produced by Schwann cells in the peripheral nervous system (PNS) or by oligodendrocytes in the central nervous system (CNS). It consists of consecutive wrapping and subsequent compaction of stacked glial plasma membrane bilayers over the neuronal axon (112, 113). In essence, myelin is a lipid-rich membrane that is filled with glycosphingolipids and cholesterol. It also has a myriad of proteins such as the myelin basic proteins (MBP) and proteolipid proteins (PLP/DM20) (112, 113).

In the CNS, the generation of the myelin sheath by oligodendrocytes is temporally and spatially controlled. It also crucially depends on a number of cell-intrinsic as well as non-cell-intrinsic factors (112). Cell-autonomous factors include basic helix – loop – helix transcription factor *Olig2* (125, 128, 223, 224) and HMG transcription regulator *Sox10* (131, 132) that affect oligodendrocyte birth, specification and differentiation. Non-cell-autonomous factors include hormones like thyroid hormone, growth and trophic factors such as fibroblast growth factor 2 (FGF-2) and insulin-like growth factor 1 (IGF-1) (112, 113, 139). Interestingly, there is an increasing appreciation in the field that neuron-derived factors are important for myelination. Notably, reciprocal neuron and glia communication is important for oligodendrocyte development as well as proper myelination. This is supported by studies demonstrating that neurons can govern oligodendrocyte development by influencing their proliferation, differentiation and survival in order to make certain the appropriate ratio of oligodendrocytes to axonal surface for myelination (113, 139). Moreover, neuronal axons must be myelinated at the correct time during development and not before the neurons are equipped to be myelinated (113,

140). On the other hand, oligodendrocytes have to interact with neurons to arrange protein complexes at the nodes of Ranvier (113, 141-144) and have been demonstrated to affect axonal cytoskeleton and transport (113, 145, 146). Hence, complementary interactions between neurons and oligodendrocytes are crucial for oligodendrocyte development and myelination.

Neuron-derived molecules, whether secreted or not, are implicated at different stages of oligodendrocyte development from proliferation to differentiation. Some known secreted signals include platelet-derived growth factor subunit A (PDGF-A), neurotrophin 3 (NT-3), ciliary neurotrophic factor (CNTF), FGF-2 and IGF-1 (113, 147-149). PDGF-A is a soluble molecule released by both neurons and astrocytes. Loss-of-function experiments have shown that it regulates the proliferation and survival of oligodendrocyte progenitors (113, 150-152). Gain-of-function analyses have demonstrated that PDGF-A overexpression leads to an increase in the number of oligodendrocytes (153). Besides secreted factors, non-secreted molecules that can act as cell surface receptors such as Jagged 1 (154) and contactin (155) are also involved in neuron-to-glia signaling. Jagged 1 is a cell surface ligand on neuronal axons that can interact with the Notch 1 receptor on oligodendrocytes. Hence, Notch signaling is stimulated in oligodendrocytes to inhibit their differentiation (154). Jagged 1 expression also decreases with age, which parallels with the onset of myelination (113, 154). Thus, neurons can regulate the timing of oligodendrocyte differentiation to affect myelination via molecules like Jagged 1.

Besides oligodendrocyte development, neuron-derived signals can also influence myelination itself. Studies have shown that neuronal electrical activity is required to induce myelination (156). Axonal electrical activity after target innervation may lead to the secretion of promyelinating molecules like adenosine (157), and may induce changes in axonal protein

expression (158). For instance, polysialated adhesion molecule NCAM on the cell membrane may be decreased to enable myelination (159).

Although this prior work has enriched our current knowledge about the non-cell-autonomous neuron-derived factors that affect oligodendrocyte development as well as myelination, many molecular pathways and their communication affecting neuron-to-glia communication remains unknown. Here, I present data showing that transcriptional co-activator *Ppargc1α* plays a novel role in neurons to affect myelination in the neocortex. I discovered that *Ppargc1α* is exclusively expressed in SCPN but is excluded from oligodendrocyte progenitors as well as mature oligodendrocytes of the neocortex. Yet, genetic null and newly generated conditional null mutants for *Ppargc1α* in neurons or in the dorsal telencephalon demonstrate that global, neuron- and neocortical-specific loss of *Ppargc1α* cause hypomyelination across all cortical layers. Aging studies of these null and conditional null mutants at 18 months further reveal that these hypomyelination defects are not due to a delay in myelination because they persist with age. Furthermore, the hypomyelination abnormalities are not due to gross cortical anomalies, or loss of PN, or even enhanced cell death. However, gain-of-function analyses show that overexpression of *Ppargc1α* did not induce ectopic myelination. Hence, neuron-specific *Ppargc1α* is cell-autonomously required for proper neocortical myelination.

Initial results into the mechanistic action of *Ppargc1α* reveal that the conditional loss of *Ppargc1α* in the dorsal forebrain leads to decreased neuronal metabolism, suggesting that secreted metabolites might act as mediators for neuron-specific *Ppargc1α* to interact with oligodendrocytes to control myelination. In all, this study is the first report describing that *Ppargc1α* acting in neurons of the neocortex can affect myelination.

3.3. Results.

3.3.1. *Ppargc1α* expression in SCPN of layer V requires *Fezf2*.

Since prior work has shown that *Fezf2* is a critical transcription factor that is necessary and partly sufficient for the specification and differentiation of SCPN (6-9, 37), and that *Ppargc1α* is expressed in SCPN during postnatal development after the early expression of *Fezf2*, as shown in Chapter 2 and described in section 2.3.2.A. and 2.3.2.B., I hypothesize that *Ppargc1α* expression in layer V SCPN requires *Fezf2*. To test this hypothesis, I mined a new microarray dataset established by Simona Lodato and Alyssa Meleski, of our laboratory, in which they identified molecular pathways that act downstream of *Fezf2* (Lodato *et al.*, unpublished). Microarray analysis showed that *Ppargc1α* mRNA expression is significantly upregulated upon *Fezf2* overexpression, with greater induction at 24 hours (fold = 2.5, $p = 1.17 \times 10^{-6}$) than at 48 hours (fold = 1.9, $p = 1.54 \times 10^{-3}$) (Figure 3.1.A.) (Lodato *et al.*, unpublished). This indicates that *Ppargc1α* mRNA is ectopically induced upon *Fezf2* overexpression.

To determine whether *Fezf2* is necessary for *Ppargc1α* expression in SCPN, I performed an ISH for *Ppargc1α* on P28 tissue from *Fezf2*$^{-/-}$ and matched wild type littermates (n = 3 animals per genotype). Strikingly, the expression of *Ppargc1α* in SCPN is completely lost in *Fezf2*$^{-/-}$ mice, as compared to wild type controls (red arrows) (Figure 3.1.B. to 3.1.E.). In contrast, small, scattered cells expressing *Ppargc1α*, likely representing Parvalbumin-expressing interneurons, remain in the neocortex of *Fezf2*$^{-/-}$ mice, similar to what is observed in wild type controls (Figure 3.1.B. to 3.1.E.) (94, 97). This effect is specific because the expression of *Ppargc1α* in other areas of the brain such as the reticular thalamic nuclei is comparable between *Fezf2*$^{-/-}$ and wild type mice (data not shown). Thus, these data indicate that *Fezf2* is required either directly or indirectly for *Ppargc1α* expression in SCPN.

Figure 3.1. *Ppargc1α* expression in SCPN of layer V requires *Fezf2*.

(A) Microarray analysis by Simona Lodato anad Alyssa Melaski revealed that *Ppargc1α* mRNA expression is significantly upregulated upon *Fezf2* overexpression, with greater induction at 24 hrs (fold = 2.5, $p = 1.17 \times 10^{-6}$) than at 48 hrs (fold = 1.9, $p = 1.54 \times 10^{-3}$). ** represents p value ≤ 0.01, * represents p value ≤ 0.05. This figure is adapted from Lodato *et al.*, unpublished.

(B – E) ISH for *Ppargc1α* showed that *Ppargc1α* is expressed in SCPN of layer V (red arrows) of P28 wild type (B – C) but not in *Fezf2*$^{-/-}$ mice (D – E). In contrast, small scattered cells expressing *Ppargc1α*, which likely represent Parvalbumin-expressing interneurons, remain in the neocortex of wild type and *Fezf2*$^{-/-}$ mice. (C and E) Boxed areas in (B) and (D) respectively. Ctx, cortex; Str, striatum; AC, anterior commissure. Roman numerals indicate the distinct cortical layers. Scale bars, 100 μm (B and D), 10 μm (C and E).

Figure 3.1. (Continued)

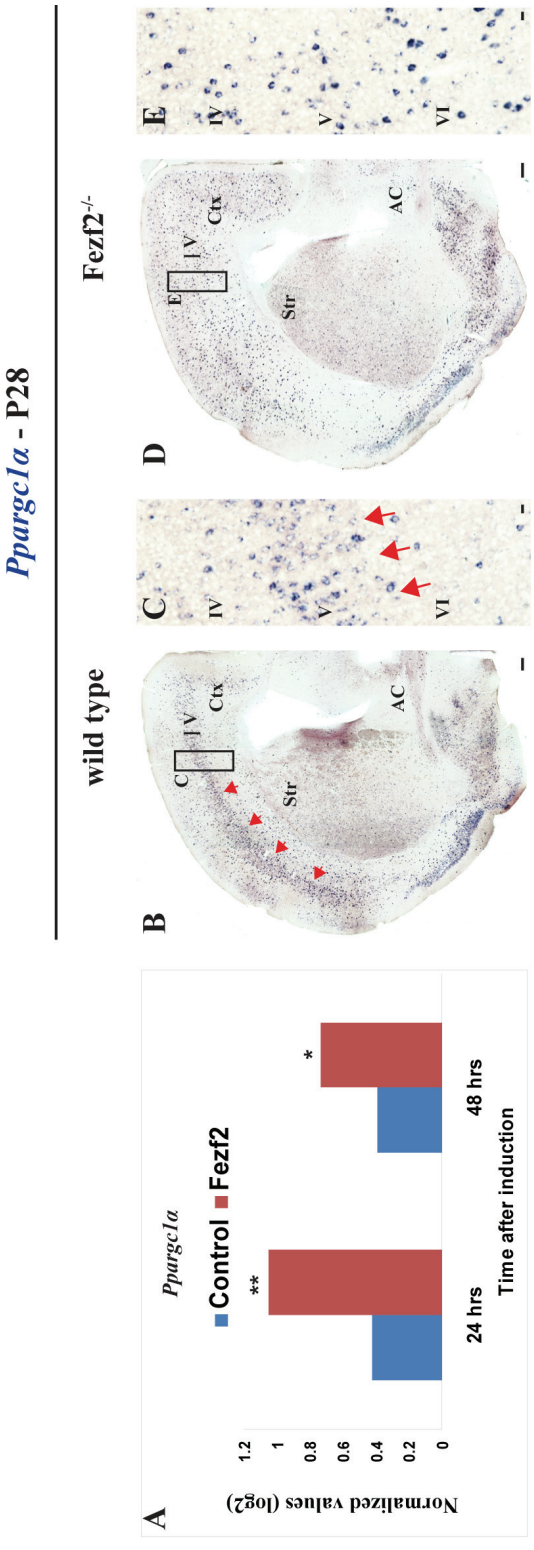

Together with the preferential expression of *Ppargc1α* in SCPN, as shown in section 2.3.2., the data suggest that *Ppargc1α* is a novel downstream target of *Fezf2*, potentially controlling key aspects of SCPN/CSMN development downstream of this critical transcription factor, from postnatal stages to adulthood.

3.3.2. *Ppargc1α*$^{-/-}$ mice are hypomyelinated across all cortical layers.

In the process of analyzing the axonal connectivity of *Ppargc1α*$^{-/-}$ mice by observing *Ppargc1α*$^{-/-}$ cortical sections in PBS and stained by MBP, as described in Chapter 2, I have always observed a seemingly hypomyelinated neocortex in *Ppargc1α*$^{-/-}$ mice. To confirm my observations and better determine whether the global loss of *Ppargc1α* causes myelination abnormalities in the neocortex, and if so, how these anomalies develop with time, I examined brightfield images of *Ppargc1α*$^{-/-}$ and matched wild type littermate coronal cortical sections in phosphate buffer saline (PBS) at various stages of development, namely P14, P28, 2 months, 3 months and 6 months of age (n = 3 per genotype for all ages). I found that the neocortices of *Ppargc1α*$^{-/-}$ mice are hypomyelinated in the deep layers (red arrows) as well as the corpus callosum (data not shown), as compared to their wild type counterparts (Figure 3.2.A. and 3.2.B.). Time course analysis revealed that this hypomyelination aberration is apparent at P14 and becomes more severe with time, persisting through adulthood of 6 months (Figure 3.2.A and 3.2.B., data shown for 6 months of age but not for earlier ages). Anteroposterior analysis showed that the neocortices of *Ppargc1α*$^{-/-}$ mutants are hypomyelinated throughout the rostrocaudal axis, with a more severe phenotype observed caudally (data not shown). Therefore, these data showed that global loss of *Ppargc1α* results in hypomyelination defects of the neocortex, supporting my hypothesis that *Ppargc1α* is necessary for proper myelination of the neocortex.

Figure 3.2. *Ppargc1α*$^{-/-}$ mice are hypomyelinated across all cortical layers.

(A – B) Brightfield analysis in PBS revealed that the neocortices of 6 month old *Ppargc1α*$^{-/-}$ mutant mice are hypomyelinated in the deep layers (red arrows) as well as in the corpus callosum (data not shown), as compared to their wild type controls. Time course analysis also showed that this hypomyelination aberration is apparent at P14 and become more severe with time, persisting through adulthood of 6 months of age (data shown for 6 months of age but not for earlier ages). Anteroposterior analysis also demonstrated that the neocortex is hypomyelinated throughout the rostrocaudal axis, with a more severe phenotype observed caudally (data not shown).
(C – F) Immunohistochemistry analysis for Myelin Basic Protein, a protein found within the myelin sheath that surrounds the axonal fibers, confirmed the results obtained by brightfield analysis, as shown in A and B. Interestingly, the upper layers of *Ppargc1α*$^{-/-}$ mutant mice are also hypomyelinated (red arrows), particularly layer I fibers, as compared to wild type mice. (D and F) Boxed areas in (C) and (E) respectively. Scale bars, 100 μm (A – L).

Figure 3.2. (Continued)

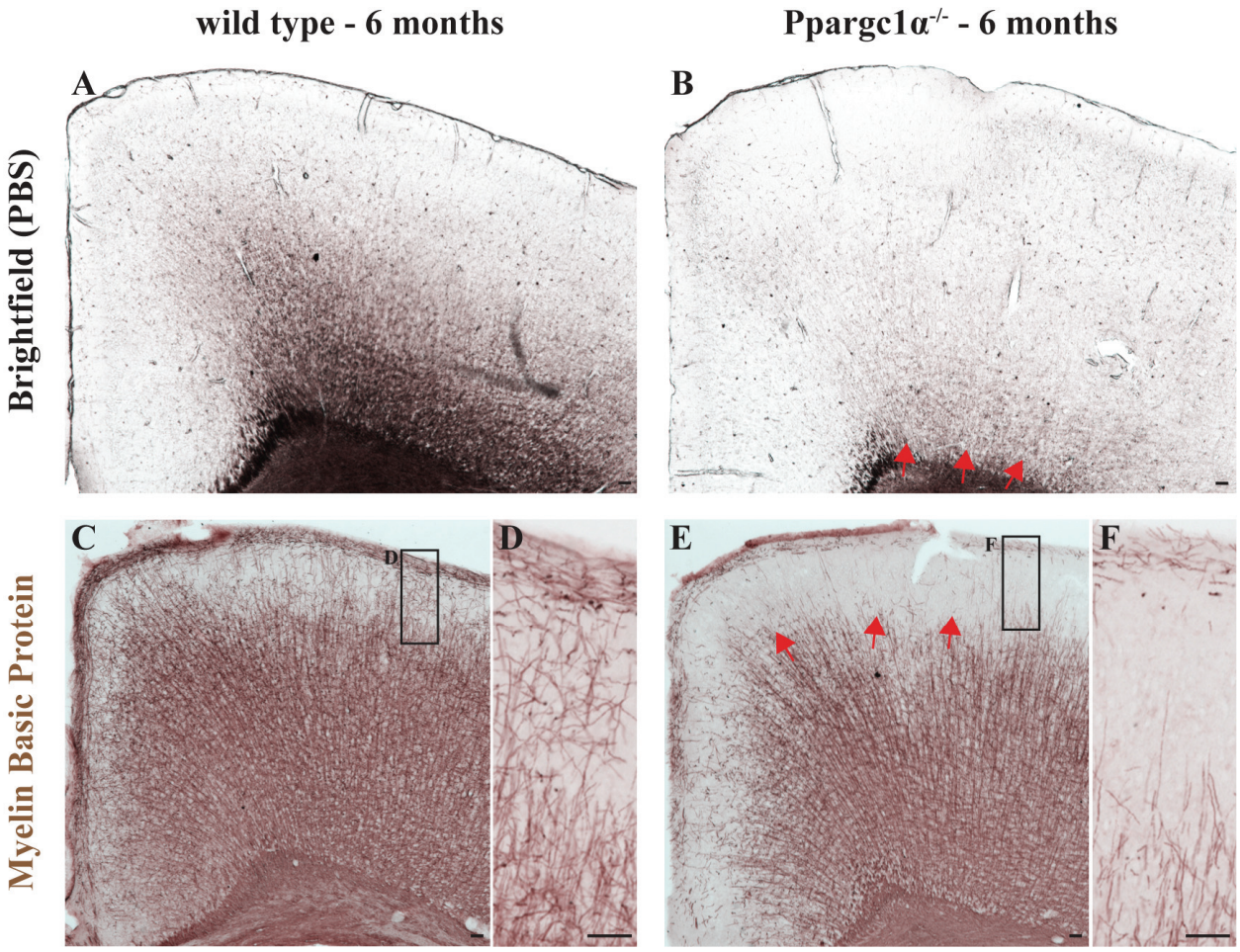

To ascertain my results obtained by brightfield analysis, I defined the myelinated fibers of the neocortex by staining for Myelin Basic Protein (MBP)—a protein found within the myelin sheath that surrounds the axonal fibers (112)—on *Ppargc1α*$^{-/-}$ and matched wild type littermate coronal cortical sections at P14, P28, 2 months, 3 months and 6 months of age (n = 3 per genotype for all ages). Confirming my initial finding, I found that the neocortices of *Ppargc1α*$^{-/-}$ mutant mice are hypomyelinated in the deep layers as well as the corpus callosum (data not shown), as compared to their wild type counterparts (Figure 3.2.C. and 3.2.E.). Surprisingly, I discovered that the upper layers are also hypomyelinated (red arrows), particularly layer I fibers, in the neocortex of *Ppargc1α*$^{-/-}$ mutant mice, as compared to wild type mice (Figure 3.2.C. to 3.2.F.). Time course analysis also verified that this hypomyelination abnormality is apparent at P14 and become more severe with time, persisting through 6 months of age (data shown for 6 months of age but not for earlier ages). Anteroposterior analysis further affirmed that the neocortex is hypomyelinated throughout the rostrocaudal axis, with a more severe phenotype observed caudally (data not shown). Hence, these data demonstrate that global loss of *Ppargc1α* results in hypomyelination anomalies of the neocortex across all cortical layers, supporting my hypothesis that *Ppargc1α* is necessary for establishing the correct neocortical myelination pattern.

To ensure that the hypomyelination aberrations are not due to a delay in myelination, I performed brightfield analysis as well as immunostaining for MBP on aged *Ppargc1α*$^{-/-}$ and matched wild type littermate coronal cortical sections at 18 months of age (n = 5 *Ppargc1α*$^{-/-}$, n = 2 wild type mice). I found that 18-month-old *Ppargc1α*$^{-/-}$ mutant mice continue to be hypomyelinated in the neocortex, if not more severely hypomyelinated when compared to younger mice (data not shown). These data showed that the hypomyelination defect observed is not caused by a delay in myelination, thus indicating that the hypomyelination is persistent with

age, does not recover with time and develop as early as P14. Therefore, *Ppargc1α* is necessary for proper myelination of the neocortex.

In all, my data revealed that global loss of *Ppargc1α* results in hypomyelination of both the upper and deep layers of the neocortex. These results demonstrate that *Ppargc1α* is necessary for establishing the correct myelination pattern of the neocortex.

Interestingly, as described in section 2.3.2.B., *Ppargc1α* is expressed in SCPN and in subsets of cortical interneurons but not in the majority of CPN and notably not in oligodendrocytes. Yet, global loss of *Ppargc1α* results in hypomyelination not only of the layers where SCPN reside in deep layer V, but also of the upper layers where CPN that do not express *Ppargc1α* are located. Furthermore, *Ppargc1α* is not expressed in oligodendrocytes but loss of *Ppargc1α* results in an abnormality of myelination, a process exclusively controlled by oligodendrocytes. Hence, my results suggest that *Ppargc1α* plays a novel role in SCPN that is important for the maintenance of myelination by oligodendrocytes.

3.3.3. *CamKIIα-Cre; Ppargc1α*$^{fl/fl}$ mice are hypomyelinated across all cortical layers.

To investigate whether the hypomyelination anomaly seen in *Ppargc1α*$^{-/-}$ mice is due to the specific loss of *Ppargc1α* in neurons, I examined the myelination pattern of *CamKIIα-Cre; Ppargc1α*$^{fl/fl}$ mice (gift from Professor Jiandie Lin, University of Michigan) by brightfield analysis on adult 4-month-old *CamKIIα-Cre; Ppargc1α*$^{fl/fl}$ and matched *Ppargc1α*$^{fl/fl}$ littermate coronal cortical sections in PBS (n = 3 per genotype). I found a similar hypomyelination aberration in *CamKIIα-Cre; Ppargc1α*$^{fl/fl}$ mice where their neocortices are hypomyelinated in the deep layers as well as in the corpus callosum, as compared to the *Ppargc1α*$^{fl/fl}$ controls (data not shown). Anteroposterior analysis also detected that the hypomyelination defect is more severe at

posterior regions of the neocortex, as compared to more anterior regions (data not shown). Thus, my data demonstrate that neuronal selective loss of *Ppargc1α* results in a hypomyelinated neocortex, indicating that *Ppargc1α* in neurons is necessary for proper myelination of the neocortex.

To ascertain my results obtained with brightfield analysis, I delineated the myelinated fibers of the neocortex by immunostaining for MBP on adult 4-month-old *CamKIIα-Cre; Ppargc1α$^{fl/fl}$* and matched *Ppargc1α$^{fl/fl}$* littermate coronal cortical sections (n = 3 per genotype). Confirming my initial finding, I discovered that the neocortices of *CamKIIα-Cre; Ppargc1α$^{fl/fl}$* mice are hypomyelinated in the deep layers as well as in the corpus callosum, as compared to their *Ppargc1α$^{fl/fl}$* counterparts (data not shown). Surprisingly, further analysis revealed that the upper layers are also hypomyelinated (red arrows), particularly layer I fibers, in the neocortex of *CamKIIα-Cre; Ppargc1α$^{fl/fl}$* mice, as compared to *Ppargc1α$^{fl/fl}$* controls (Figure 3.3.A. and 3.3.B.). Anteroposterior analysis further verified that the neocortex is hypomyelinated throughout the rostrocaudal axis, with a more severe phenotype observed caudally (data not shown). Therefore, these new data demonstrate that neuronal loss of *Ppargc1α* results in hypomyelination abnormalities of the neocortex across all cortical layers, indicating that *Ppargc1α* in neurons is necessary for establishing the correct neocortical myelination pattern.

3.3.4. *Emx1-Cre; Ppargc1α$^{fl/fl}$* mice are hypomyelinated across all cortical layers.

To study if the hypomyelination anomaly seen in *Ppargc1α$^{-/-}$* mice is due to specific loss of *Ppargc1α* in the dorsal forebrain, and if so, how these aberrations develop with time, I examined the myelination pattern of *Emx1-Cre; Ppargc1α$^{fl/fl}$* mice by brightfield analysis of *Emx1-Cre; Ppargc1α$^{fl/fl}$* and matched *Ppargc1α$^{fl/fl}$* littermate coronal cortical sections in PBS at

Figure 3.3. *CamKIIα-Cre; Ppargc1α*$^{fl/fl}$ mice are hypomyelinated across all cortical layers. (A – B) Immunostaining for Myelin Basic Protein showed that *CamKIIα-Cre; Ppargc1α*$^{fl/fl}$ mutant mice are hypomyelinated in the deep (data not shown) and upper layers (red arrows), particularly in layer I fibers, of the neocortex, as compared to *Ppargc1α*$^{fl/fl}$ controls. Anteroposterior analysis also demonstrated that the neocortex is hypomyelinated throughout the rostrocaudal axis, with a more severe phenotype observed caudally (data not shown). Dotted lines indicate the boundary of the pia. Scale bars, 100 μm (A – B).

Figure 3.3. (Continued)

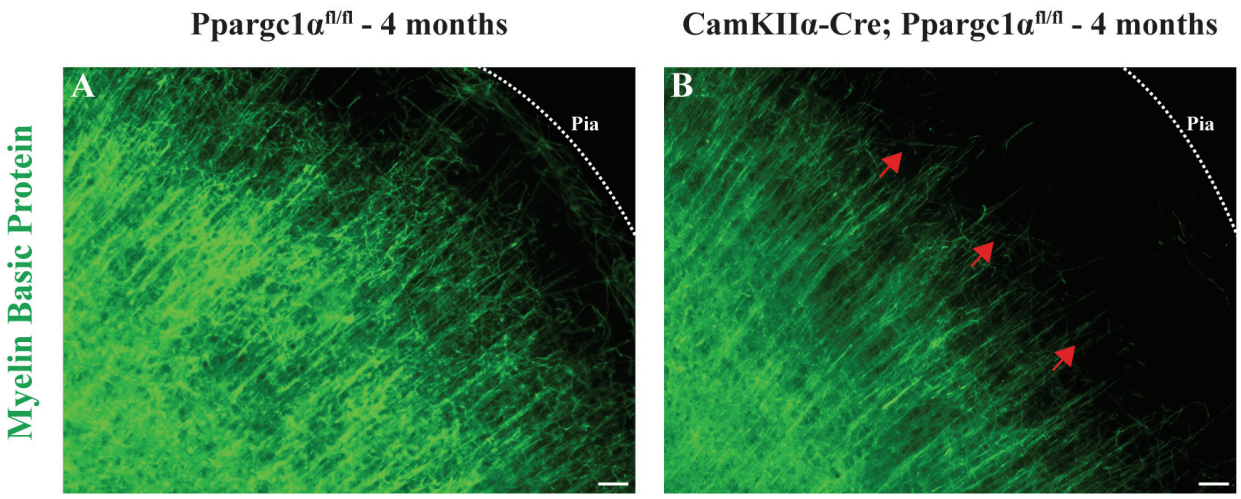

various stages of development, namely P14, P28, 2 months, 3 months and 6 months of age (n = 3 per genotype for all ages). Strikingly, I discovered that the neocortices of *Emx1-Cre; Ppargc1α*$^{fl/fl}$ mice are hypomyelinated in the deep layers (red arrows) as well as in the corpus callosum (data not shown), as compared to their *Ppargc1α*$^{fl/fl}$ counterparts (Figure 3.4.A. and 3.4.B.). Time course analysis also revealed that this hypomyelination defect is apparent at P14 and becomes more severe with time, persisting through adulthood of 6 months of age (Figure 3.4.A and 3.4.B., data shown for 6 months of age but not for earlier ages). Anteroposterior analysis further detected that the neocortices of *Emx1-Cre; Ppargc1α*$^{fl/fl}$ mutant mice are hypomyelinated throughout the rostrocaudal axis, with a more severe phenotype observed caudally (data not shown). Hence, these new data are in agreement with the results obtained with *Ppargc1α*$^{-/-}$ mice, as shown in section 3.3.2.. They demonstrate that preferential loss of *Ppargc1α* in the dorsal telencephalon results in hypomyelination abnormalities of the neocortex, thus supporting my hypothesis that neuron-specific *Ppargc1α* is necessary for establishing the proper myelination pattern of the neocortex.

To ascertain my findings with brightfield analysis, I defined the myelinated fibers of the neocortex by staining MBP on *Emx1-Cre; Ppargc1α*$^{fl/fl}$ and matched *Ppargc1α*$^{fl/fl}$ littermate coronal cortical sections at P14, P28, 2 months, 3 months and 6 months of age (n = 3 per genotype for all ages). Confirming my initial finding, I found that the neocortices of *Emx1-Cre; Ppargc1α*$^{fl/fl}$ mice are hypomyelinated in the deep layers as well as in the corpus callosum, as compared to their *Ppargc1α*$^{fl/fl}$ controls (Figure 3.4.C. and 3.4.E.). Surprisingly, I discovered that the upper layers are also hypomyelinated (red arrows), particularly layer I fibers, in the neocortex of *Emx1-Cre; Ppargc1α*$^{fl/fl}$ mutant mice, as compared to *Ppargc1α*$^{fl/fl}$ mice (Figure 3.4.C. to 3.4.F.). Time course analysis also verified that this hypomyelination defect is apparent at P14

Figure 3.4. *Emx1-Cre; Ppargc1α*$^{fl/fl}$ mice, even aged 18 month old mutants, are hypomyelinated across all cortical layers.

(A – B) Brightfield analysis in PBS revealed that the neocortices of 6 month old *Emx1-Cre; Ppargc1α*$^{fl/fl}$ mutant mice are hypomyelinated in the deep layers (red arrows) as well as in the corpus callosum (data not shown), as compared to their *Ppargc1α*$^{fl/fl}$ controls. Time course analysis also showed that this hypomyelination aberration is apparent at P14 and become more severe with time, persisting through adulthood of 6 months of age (data shown for 6 months of age but not for earlier ages). Anteroposterior analysis demonstrated that the neocortex is hypomyelinated throughout the rostrocaudal axis, with a more severe phenotype observed caudally (data not shown).

(C – F) Immunohistochemistry analysis for Myelin Basic Protein – a protein found within the myelin sheath that surrounds the axonal fibers, confirmed the results obtained by brightfield analysis, as shown in A and B. Interestingly, the upper layers of *Emx1-Cre; Ppargc1α*$^{fl/fl}$ mutant mice are also hypomyelinated (red arrows), particularly the layer I fibers, as compared to *Ppargc1α*$^{fl/fl}$ mice. (D and F) Boxed areas in (C) and (E) respectively.

(G – L) Brightfield analysis in PBS (G – H) and immunostaining for Myelin Basic Protein (I – L) revealed similar if not more severe hypomyelination (red arrows) of the deep and upper layers of aged 18 month old *Emx1-Cre; Ppargc1α*$^{fl/fl}$ mutant mice, as compared to *Ppargc1α*$^{fl/fl}$ controls. These results indicate that the hypomyelination defect observed is not caused by a delay in myelination, and that the hypomyelination is persistent with age, does not recover with time and develop as early as P14. (J and L) Boxed areas in (I) and (K) respectively. Scale bars, 100 μm (A – L).

Figure 3.4. (Continued)

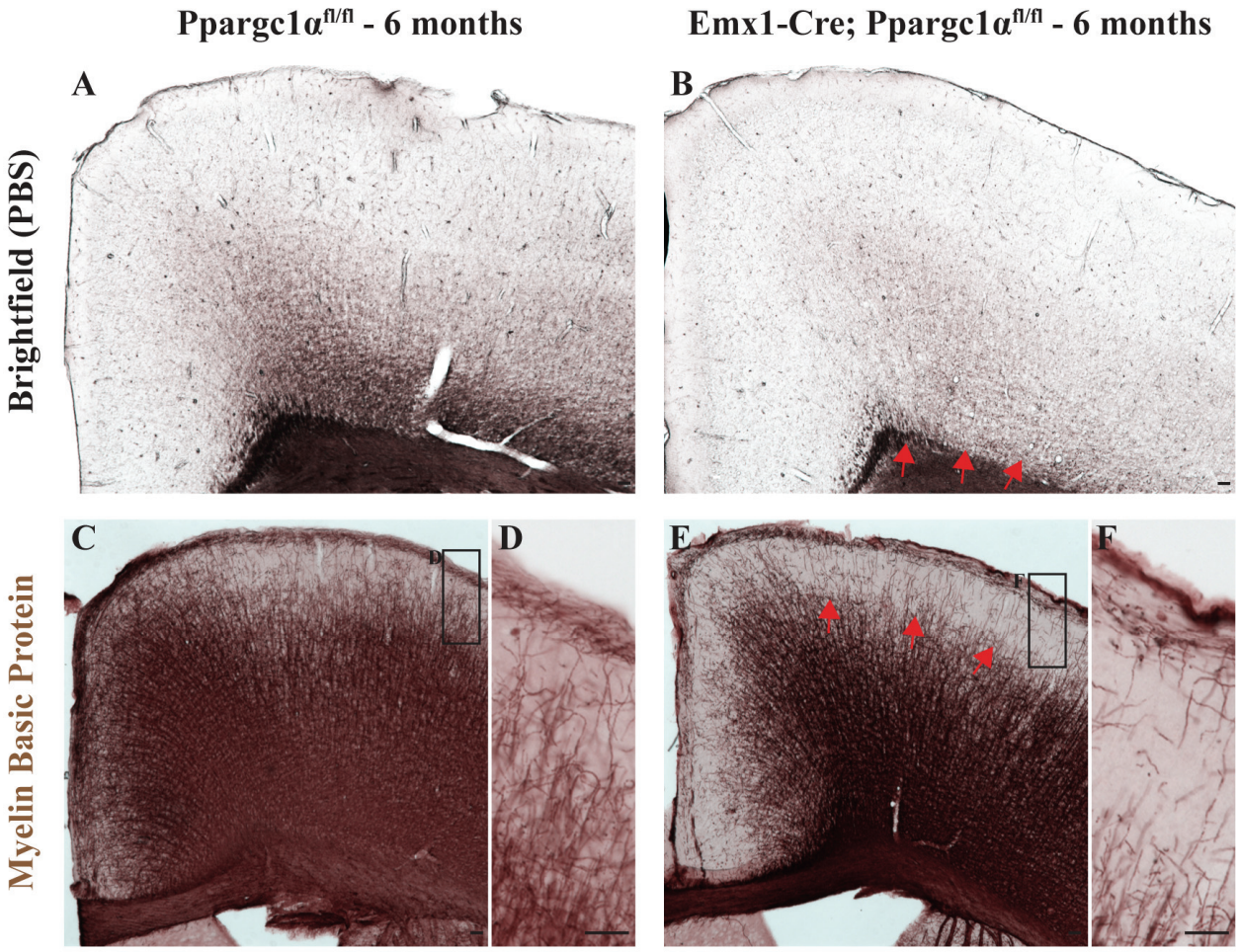

Figure 3.4. (Continued)

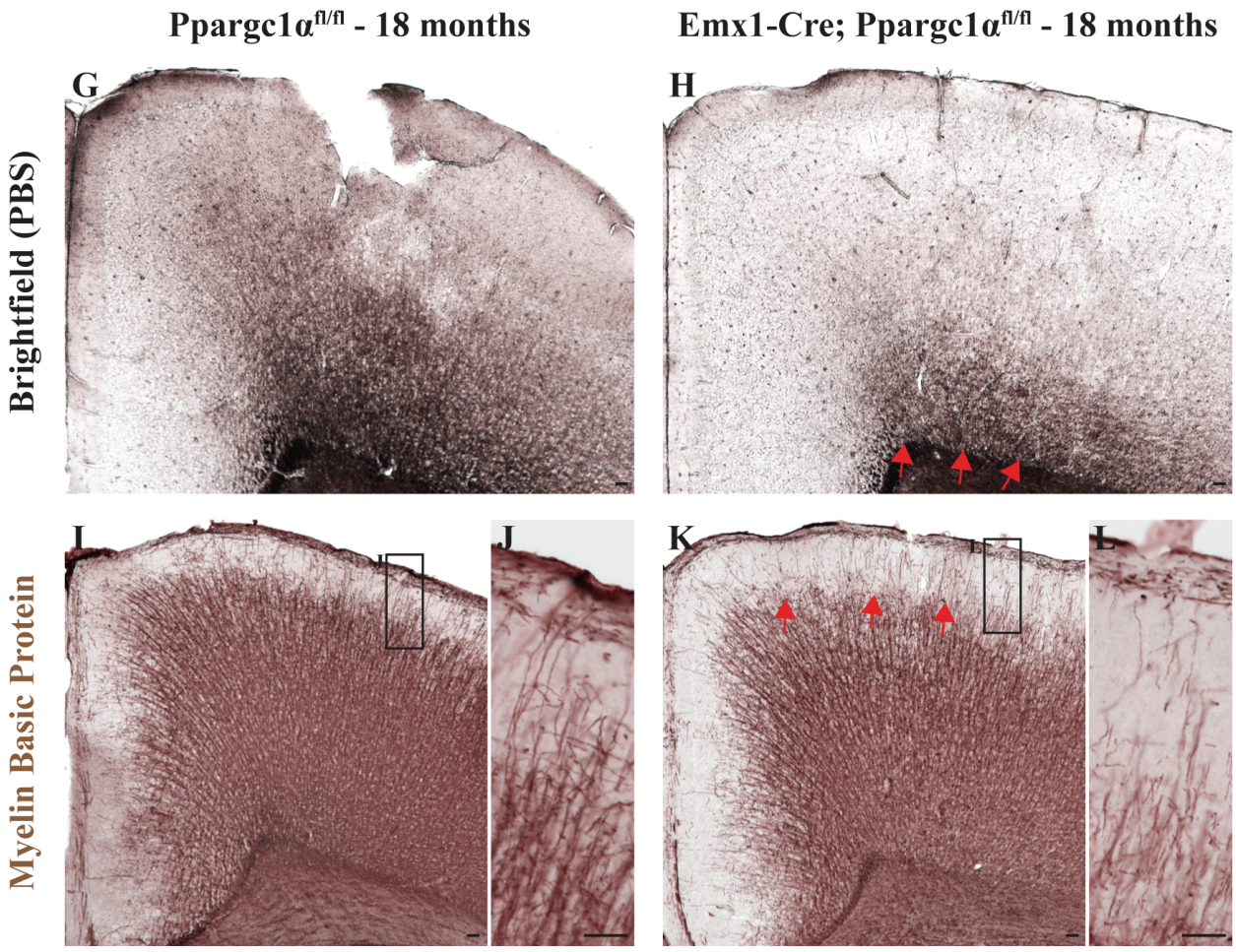

and become more severe with time, persisting throughout adulthood of 6 months of age (data not shown). Anteroposterior analysis further determined that the neocortex is hypomyelinated throughout the rostrocaudal axis, with a more severe phenotype observed caudally (data not shown). Therefore, these data demonstrate that specific loss of *Ppargc1α* in the dorsal forebrain results in hypomyelination anomalies of the neocortex across all cortical layers, indicating that neuron-specific *Ppargc1α* is necessary for correct neocortical myelination.

To ensure that the hypomyelination aberrations are not due to a delay in myelination, I performed brightfield analysis as well as immunostaining for MBP on aged *Emx1-Cre;* *Ppargc1α*$^{fl/fl}$ and matched *Ppargc1α*$^{fl/fl}$ littermate coronal cortical sections at 18 months of age (n = 4 per genotype). I discovered that 18-month-old *Ppargc1α*$^{fl/fl}$ mice continue to be hypomyelinated in the neocortex, if not more severely hypomyelinated when compared to younger mice (Figure 3.4.G. to 3.4.L.). These data reveal that the hypomyelination abnormalities observed are not caused by a delay in myelination, and indicate that the defects are persistent with age and do not recover with time and develop as early as P14. Thus, neuron-specific *Ppargc1α* is necessary for establishing proper myelination patterns of the neocortex.

In all, my new findings show that neuron-specific loss of *Ppargc1α* causes hypomyelination of the neocortex across all cortical layers. They further demonstrate that *Ppargc1α* is cell-autonomously required by SCPN for establishing the correct neocortical myelination pattern. These results are novel because the function of *Ppargc1α* in the neocortex has not been elucidated thus far and notably neuron-specific expression of *Ppargc1α* affects an oligodendrocyte-executed process of myelination in the neocortex. Furthermore, this is the first report purporting that *Ppargc1α* plays a role in neuron glia interactions to affect neocortical myelination.

3.3.5. *Gbx2-CreER; Ppargc1α$^{fl/fl}$* mice are <u>not</u> hypomyelinated across all cortical layers.

To investigate whether selective loss of *Ppargc1α* in TCPN can affect the myelination of their afferent axons in the neocortex as they project to cortical layers I and IV through the deep cortical layers V/VI (20, 21), I examined the myelination pattern of *Gbx2-CreER; Ppargc1α$^{fl/fl}$* mice by brightfield analysis of *Gbx2-CreER; Ppargc1α$^{fl/fl}$* and matched *Ppargc1α$^{fl/fl}$* littermate coronal cortical sections in PBS at P28 and 2 months of age (n = 2 animals per genotype at P28, n = 1 *Ppargc1α$^{fl/fl}$* and n = 3 *Gbx2-CreER; Ppargc1α$^{fl/fl}$* at 2 months of age). Surprisingly, I found that the neocortices of *Gbx2-CreER; Ppargc1α$^{fl/fl}$* mice are myelinated normally in the deep layers as well as in the corpus callosum, similar to their *Ppargc1α$^{fl/fl}$* controls (data not shown). Time course analysis revealed that the myelination patterns of *Gbx2-CreER; Ppargc1α$^{fl/fl}$* mice are normal at P28 and 2 months of age, comparable to their *Ppargc1α$^{fl/fl}$* controls (data not shown). Anteroposterior analysis further determined that the neocortices of *Gbx2-CreER; Ppargc1α$^{fl/fl}$* mice display a normal myelination pattern throughout the rostrocaudal axis (data not shown). Hence, these data demonstrate that specific loss of *Ppargc1α* in the thalamus does not affect the myelination pattern of their axons as they innervate the neocortex, indicating that *Ppargc1α* in TCPN is not required for establishing proper myelination patterns of the neocortex. These results also support the conclusion in section 3.3.4. that *Ppargc1α* in neurons is necessary to establish a correct neocortical myelination pattern.

To ascertain my findings with brightfield analysis, I delineated the myelinated fibers of the neocortex by staining MBP on *Gbx2-CreER; Ppargc1α$^{fl/fl}$* and matched *Ppargc1α$^{fl/fl}$* littermate coronal cortical sections at P28 and 2 months of age (n = 2 animals per genotype at P28, n = 1 *Ppargc1α$^{fl/fl}$* and n = 3 *Gbx2-CreER; Ppargc1α$^{fl/fl}$* at 2 months of age). Confirming my

initial finding, I found that the neocortices of *Gbx2-CreER; Ppargc1α*$^{fl/fl}$ mice are myelinated normally in the deep layers as well as in the corpus callosum, similar to their *Ppargc1α*$^{fl/fl}$ counterparts (data not shown.). Moreover, I discovered that the upper layers are also myelinated normally, even in layer I fibers, in the neocortex of *Gbx2-CreER; Ppargc1α*$^{fl/fl}$ mice (Figure 3.5.A. and 3.5.B.). Time course analysis revealed that the myelination patterns of *Gbx2-CreER; Ppargc1α*$^{fl/fl}$ mice are normal at P28 and 2 months of age, comparable to that of the *Ppargc1α*$^{fl/fl}$ controls (data not shown). Anteroposterior analysis also showed that the neocortices of *Gbx2-CreER; Ppargc1α*$^{fl/fl}$ mice display a normal myelination pattern throughout the rostrocaudal axis (data not shown). Therefore, these data demonstrate that selective loss of *Ppargc1α* in the thalamus does not affect the myelination pattern of their axons as they innervate the neocortex, indicating that *Ppargc1α* in TCPN is not required for establishing the proper myelination pattern of the neocortex. These results further support the conclusion in section 3.3.4. that *Ppargc1α* in neurons of the neocortex is necessary to establish a correct myelination pattern.

In all, these new findings revealed not only that specific loss of *Ppargc1α* in the thalamus does not affect the myelination pattern of their axons as they innervate the neocortex, but also that it does not cause the hypomyelination defects of the neocortex as observed in the different null and conditional null mutants for *Ppargc1α* as described hitherto. These novel data further support my results in section 3.3.5., showing that the hypomyelination aberration seen in the neocortex is caused specifically by the loss of *Ppargc1α* in neocortical neurons. Thus, my loss-of-function analysis with distinct genetic null and conditional null mice models for *Ppargc1α* indicates that *Ppargc1α* is cell-autonomously required in SCPN to establish a proper myelination pattern in the neocortex.

Figure 3.5. *Gbx2-CreER; Ppargc1α*$^{fl/fl}$ mice are <u>not</u> hypomyelinated across all cortical layers. (A – B) Immunostaining for Myelin Basic Protein showed that 2 month old adult *Gbx2-CreER; Ppargc1α*$^{fl/fl}$ mutant mice are myelinated normally in the deep (data not shown) and upper layers, particularly in the layer I fibers, of the neocortex as compared to *Ppargc1α*$^{fl/fl}$ controls. Time course and anteroposterior analysis further demonstrated that the neocortex is myelinated normally throughout the rostrocaudal axis from P28 and 2 months of age (data not shown). Scale bars, 100 μm (A – B).

Figure 3.5. (Continued)

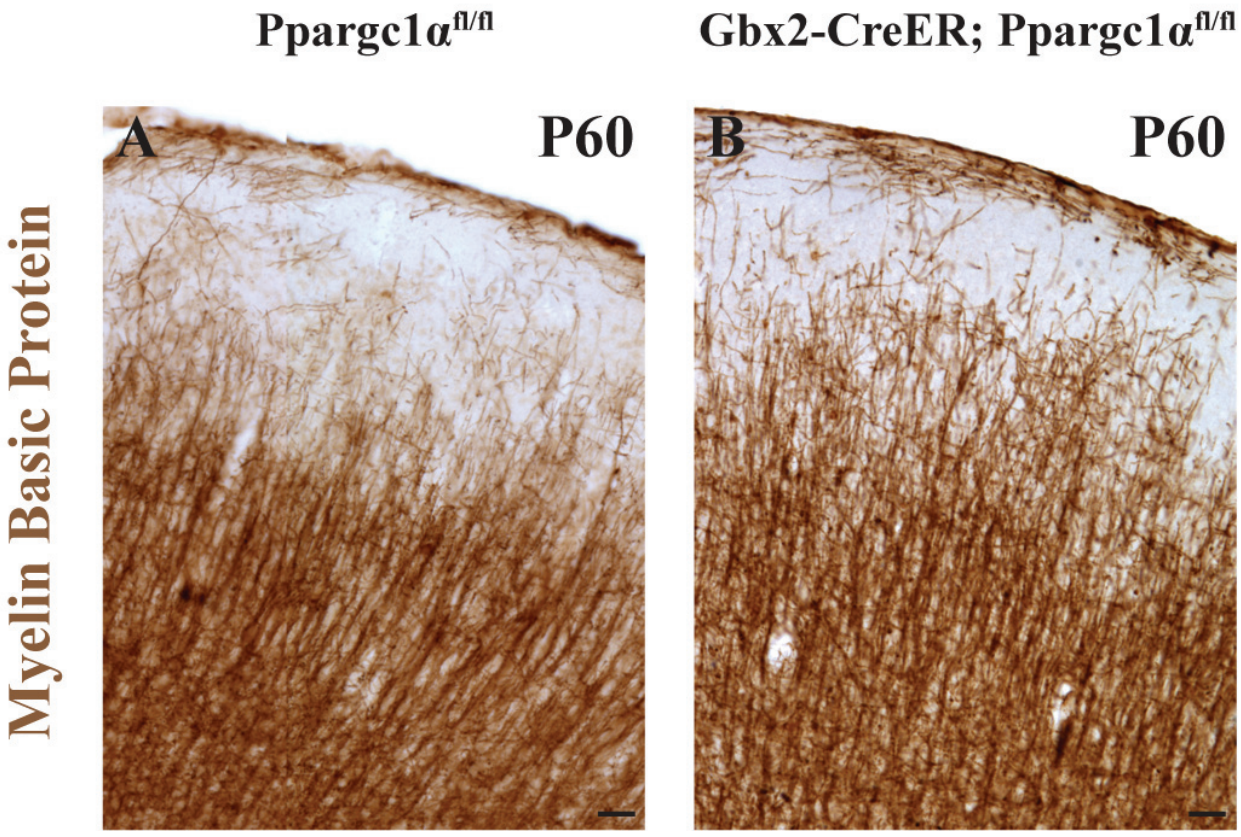

As shown in Chapter 2, global or selective loss of *Ppargc1α* in the dorsal forebrain does not result in gross cortical abnormalities or observable losses of major PN classes such as SCPN, CThPN and CPN (Figure 2.4., Figure 2.5. and Table 2.2.). Moreover, global or exclusive loss of *Ppargc1α* in the dorsal telencephalon does not result in enhanced cell death (Figure 2.6.). Similar results were obtained in aged 18-month-old *Ppargc1α* null and conditional null mutants (Figure 2.7. and 2.8.). Hence, these data indicate that the hypomyelination defects in the deep and upper cortical layers across the distinct null and conditional null mutants for *Ppargc1α*, as described in sections 3.3.2. to 3.3.4., are not due to a loss of neurons or increase in cell death.

3.3.6. Characterization of oligodendrocytes in *Emx1-Cre; Ppargc1α$^{fl/fl}$* mice.

Since global or conditional loss of *Ppargc1α* either in neurons or the dorsal forebrain causes hypomyelination in the neocortex across all cortical layers, I hypothesize that the hypomyelination is due either to loss, abnormal migration, or anomalous maturation of oligodendrocytes. To test this hypothesis, together with Travis Hallet, an undergraduate student in the laboratory, I characterized distinct oligodendrocyte progenitors and mature myelinating oligodendrocytes by immunostaining for (i) OLIG2, a marker that is expressed in oligodendrocyte progenitors as well as mature myelinating oligodendrocytes (205), (ii) PDGFRα, a marker that is expressed exclusively in oligodendrocyte progenitors (112, 225-227), and (iii) APC, a marker that is expressed only in mature myelinating oligodendrocytes (206, 207), on 2-month-old adult *Emx1-Cre; Ppargc1α$^{fl/fl}$* and matched *Ppargc1α$^{fl/fl}$* littermate coronal cortical sections (n = 3 animals per genotype). I did not find any qualitative difference in these various oligodendrocyte classes between *Emx1-Cre; Ppargc1α$^{fl/fl}$* and matched *Ppargc1α$^{fl/fl}$* controls (Figure 3.6.A. to 3.6.F.). These data show that oligodendrocyte progenitors as well as mature

Figure 3.6. Characterization of oligodendrocytes in *Emx1-Cre; Ppargc1α$^{fl/fl}$* mice.

(A – F) Immunostaining for OLIG2 (A – B), a marker that is expressed in oligodendrocyte progenitors as well as mature myelinating oligodendrocytes, (ii) PDGFRα (C – D), a marker that is expressed exclusively in oligodendrocyte progenitors, and (iii) APC (E – F), a marker that is expressed only in mature myelinating oligodendrocytes, revealed no observable difference in these distinct oligodendrocyte populations between 2 month old adult *Emx1-Cre; Ppargc1α$^{fl/fl}$* and matched *Ppargc1α$^{fl/fl}$* mutant mice. CC, corpus callosum. Roman numerals indicate the distinct cortical layers. Scale bars, 100 μm (A – F).

(G) Quantification and statistical analysis with two tailed student's T test on the total numbers of these different OLIG2, PDGFRα and APC positive oligodendrocyte populations did not detect any statistically significant difference between 2 month old adult *Emx1-Cre; Ppargc1α$^{fl/fl}$* and matched *Ppargc1α$^{fl/fl}$* mutant mice. cKO refer to *Emx1-Cre; Ppargc1α$^{fl/fl}$* mutant mice while cWT refer to *Ppargc1α$^{fl/fl}$* mutant controls.

(H – J) Quantification and statistical analysis with two tailed student's T test on the distribution of OLIG2 (H), PDGFRα (I) and APC (J) positive oligodendrocyte populations showed that there is no significant difference between *Emx1-Cre; Ppargc1α$^{fl/fl}$* and matched *Ppargc1α$^{fl/fl}$* mutant mice with respect to OLIG2 and PDGFRα positive populations. However, there seems to be a change in the spread of APC positive oligodendrocytes, where there is an increase in the numbers in the upper layers in *Emx1-Cre; Ppargc1α$^{fl/fl}$* mutants, as compared to *Ppargc1α$^{fl/fl}$* controls. ** represents p value ≤ 0.01, * represents p value ≤ 0.05.

Figure 3.6. (Continued)

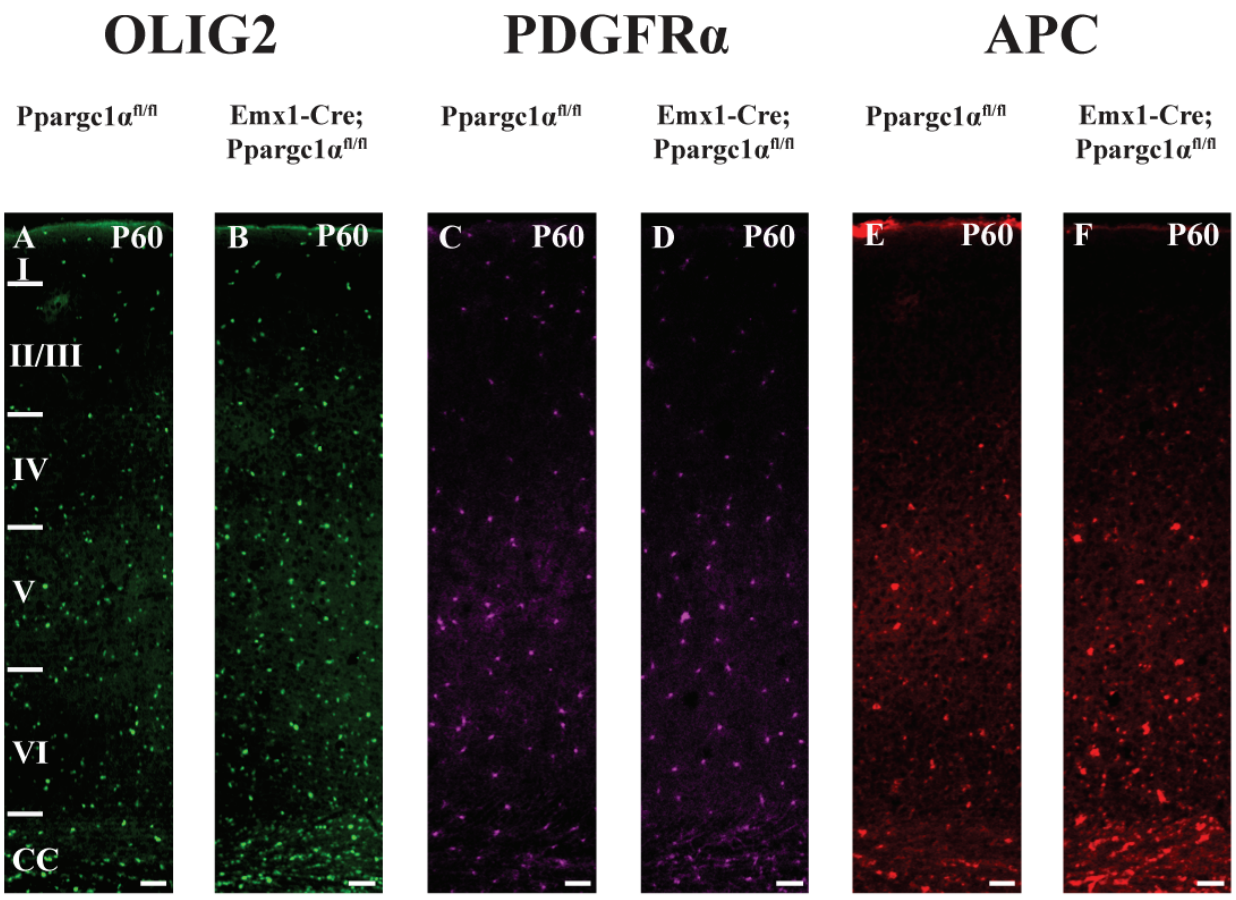

Figure 3.6. (Continued)

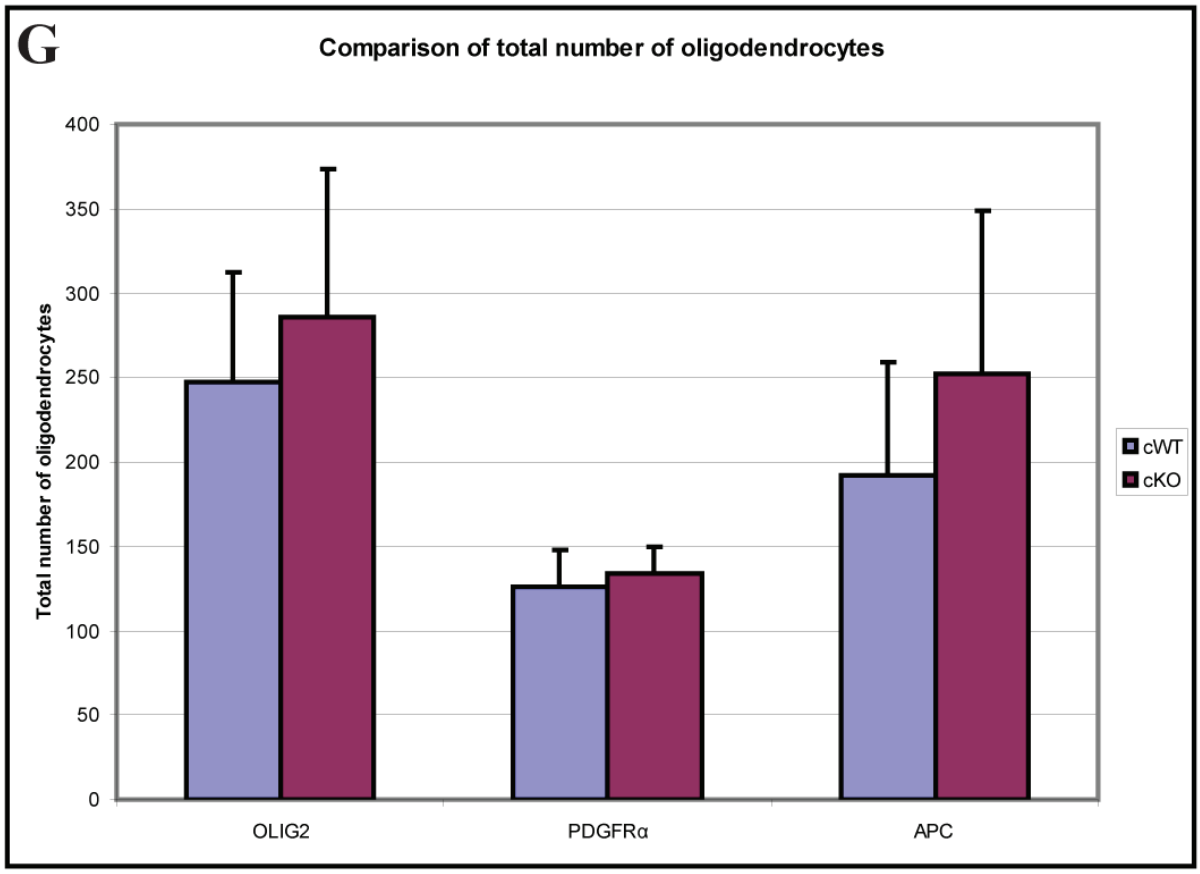

Figure 3.6. (Continued)

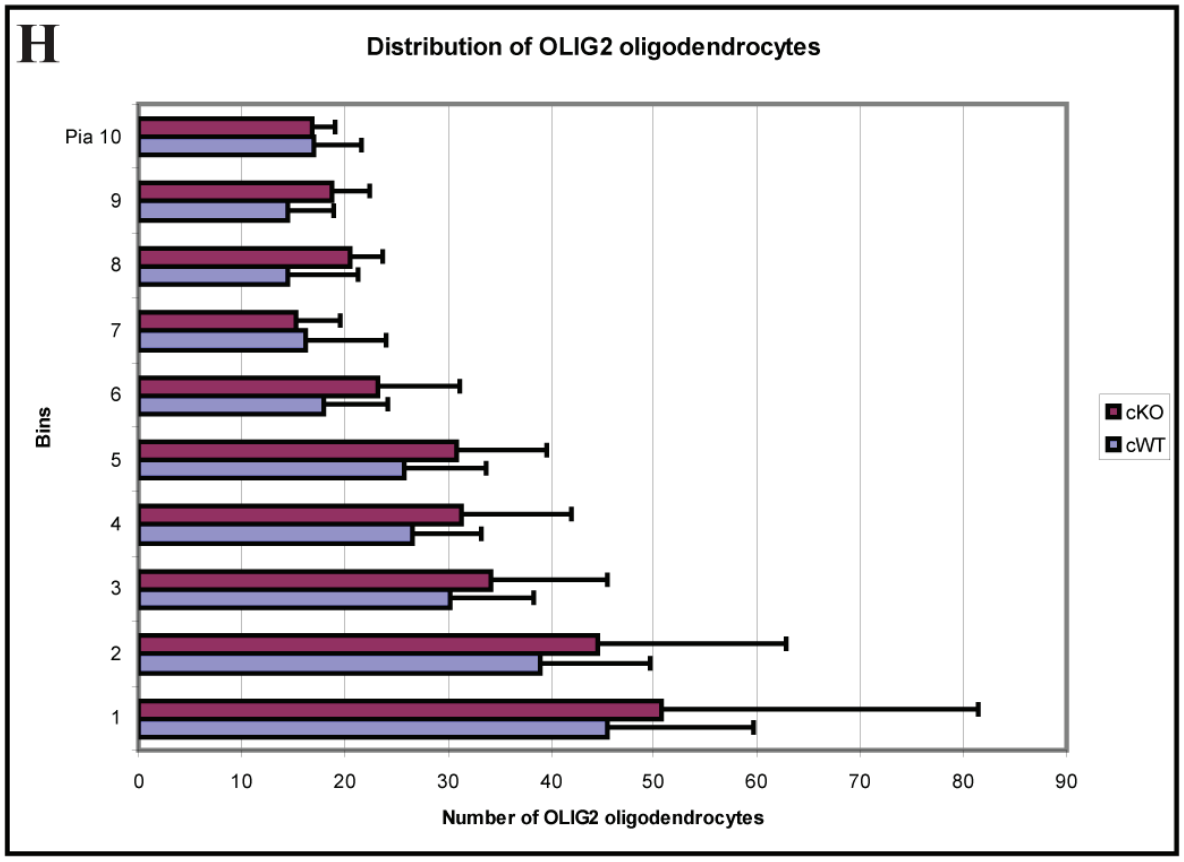

Figure 3.6. (Continued)

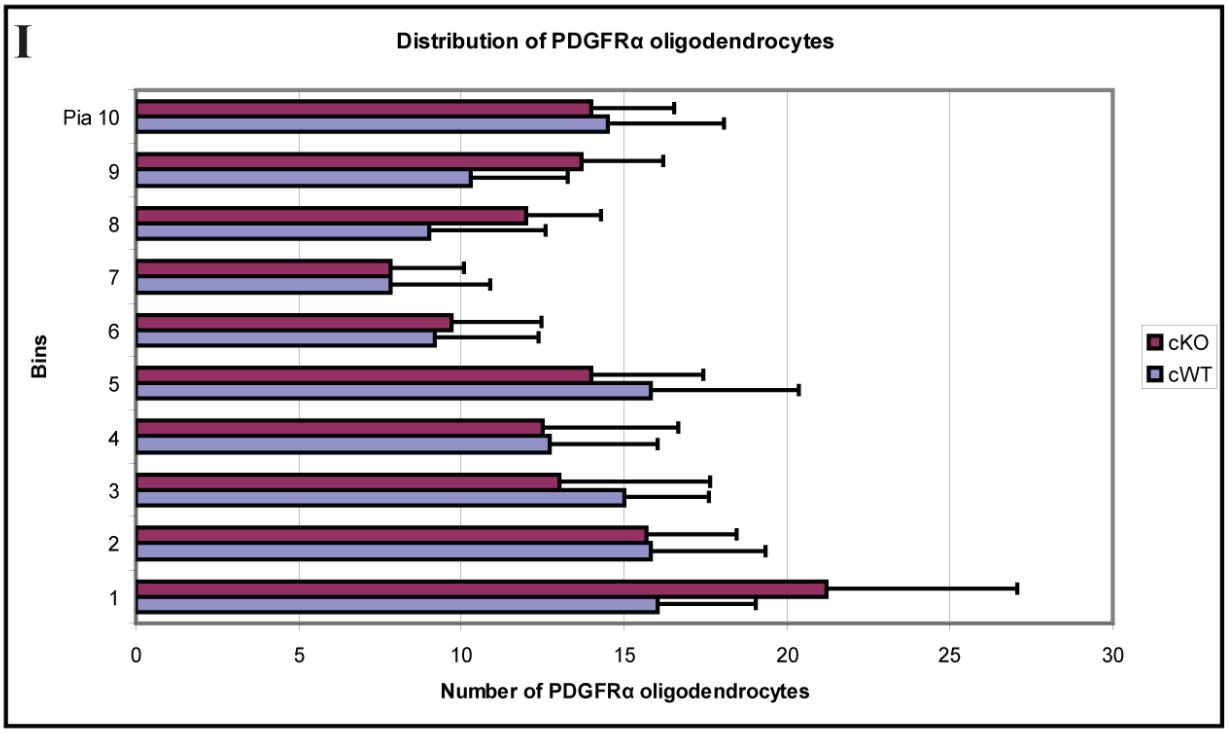

Figure 3.6. (Continued)

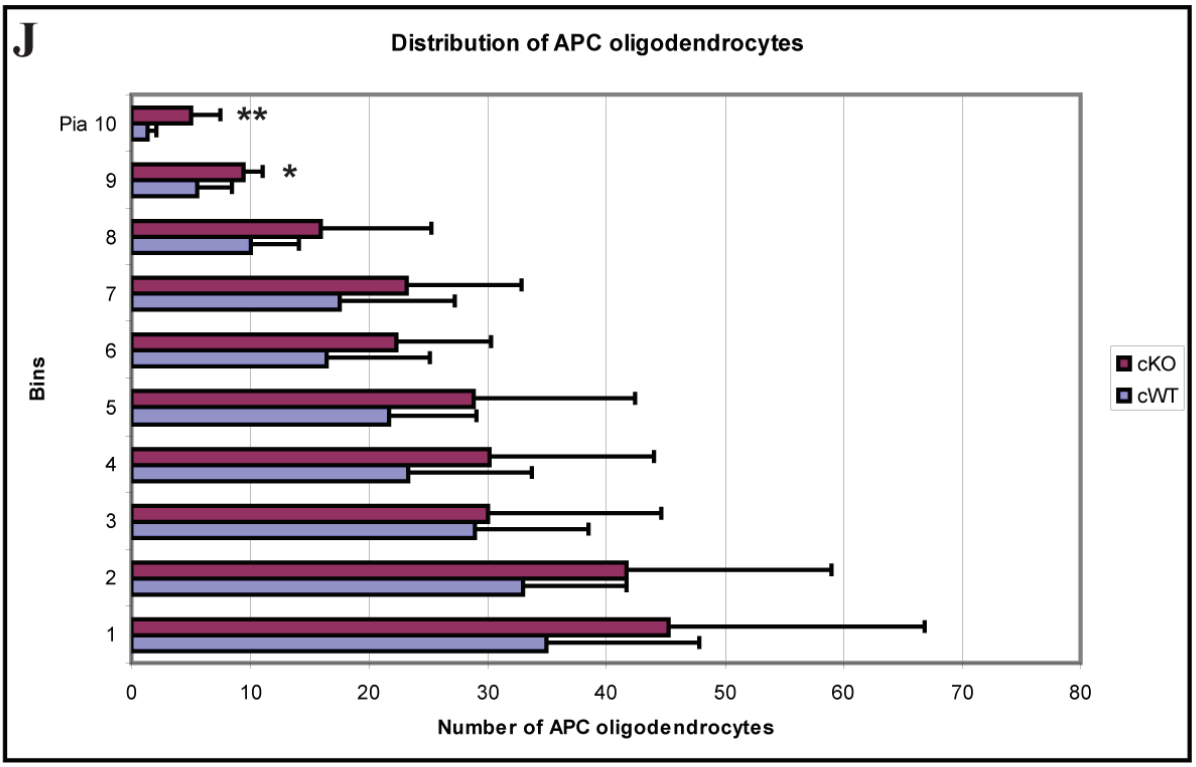

myelinating oligodendrocytes are born, specified and can migrate despite a specific loss of *Ppargc1α* in the neocortex. They suggest that *Ppargc1α* in the neocortex is not required for the birth, specification and migration of oligodendrocyte progenitors as well as mature myelinating oligodendrocytes. This is further supported by the results shown in Chapter 2 where *Ppargc1α* is not expressed in OLIG2 positive oligodendrocyte progenitors and oligodendrocytes as well as APC positive myelinating oligodendrocytes. It is also in concordance with data from Chapter 2 and section 2.3.4. where no enhanced cell death was detected in the neocortices of 2-month-old *Emx1-Cre; Ppargc1α*$^{fl/fl}$ and matched *Ppargc1α*$^{fl/fl}$ mutant mice. Notably, as described in sections 3.3.2. to 3.3.4., the mutant *Emx1-Cre; Ppargc1α*$^{fl/fl}$ neocortex remains myelinated but less so than normal, hence it is not surprising that there is no overt loss of oligodendrocytes in these mutants.

To ascertain these results, we quantified the number of OLIG2, PDGFRα and APC positive oligodendrocytes located at a range of depths covering all cortical layers of 2-month-old adult *Emx1-Cre; Ppargc1α*$^{fl/fl}$ and matched *Ppargc1α*$^{fl/fl}$ mutant mice, and performed comparative and statistical analyses with a two-tailed student's T test on the total numbers as well as the distribution of these different oligodendrocyte populations across ten bins from pia to just above the corpus callosum. We did not find any significant difference in the total numbers of OLIG2 (average total number of OLIG2 positive oligodendrocytes: *Ppargc1α*$^{fl/fl}$, 247 ± 65; *Emx1-Cre; Ppargc1α*$^{fl/fl}$, 286 ± 88; $p = 4.01 \times 10^{-1}$), PDGFRα (average total number of PDGFRα positive oligodendrocytes: *Ppargc1α*$^{fl/fl}$, 126 ± 21; *Emx1-Cre; Ppargc1α*$^{fl/fl}$, 134 ± 16; $p = 5.13 \times 10^{-1}$) and APC positive oligodendrocytes (average total number of APC positive oligodendrocytes: *Ppargc1α*$^{fl/fl}$, 193 ± 67; *Emx1-Cre; Ppargc1α*$^{fl/fl}$, 252 ± 97; $p = 2.46 \times 10^{-1}$) (n = 2 sections per animal, n = 3 animals per genotype) (Figure 3.6.G.). These results support the

above qualitative finding and demonstrate that there is no significant difference in the total numbers of distinct oligodendrocyte progenitors as well as myelinating oligodendrocytes. Travis Hallett is currently confirming these quantifications by analyzing additional sections across more animals. Together, these data reveal that oligodendrocyte progenitors as well as mature myelinating oligodendrocytes are born, specified and can migrate despite a specific loss of *Ppargc1α* in the dorsal forebrain, indicating that *Ppargc1α* is not necessary for the birth, specification and migration of oligodendrocyte progenitors as well as mature myelinating oligodendrocytes. These results also suggest that the hypomyelination defects are due to inherent anomalies in the oligodendrocytes' ability to generate the myelin sheath, and not by a reduction in numbers of oligodendrocytes.

Interestingly, comparative and statistical analysis of the distribution of distinct oligodendrocyte populations across ten bins did not detect significant differences between *Emx1-Cre; Ppargc1α*$^{fl/fl}$ and matched *Ppargc1α*$^{fl/fl}$ mutant mice with respect to OLIG2 and PDGFRα positive populations (Figure 3.6.H. and 3.6.I.). These data demonstrate that conditional loss *Ppargc1α* in the dorsal forebrain does not affect the spread of OLIG2 and PDGFRα positive oligodendrocyte populations, indicating that *Ppargc1α* is not required for the distribution of OLIG2 positive oligodendrocytes and PDGFRα positive oligodendrocyte progenitors in the neocortex. In contrast, there seems to be significantly more APC positive mature myelinating oligodendrocytes in the *Emx1-Cre; Ppargc1α*$^{fl/fl}$ mutants, particularly in the upper layers, as compared to *Ppargc1α*$^{fl/fl}$ control mice (average number of APC positive oligodendrocytes in Bin 10 closest to pia: *Ppargc1α*$^{fl/fl}$, 1.33 ± 0.816; *Emx1-Cre; Ppargc1α*$^{fl/fl}$, 5 ± 2.53; $p = 7.02 \times 10^{-3}$; average number of APC positive oligodendrocytes in Bin 9: *Ppargc1α*$^{fl/fl}$, 5.5 ± 2.95; *Emx1-Cre; Ppargc1α*$^{fl/fl}$, 9.5 ± 1.52; $p = 1.44 \times 10^{-2}$) (Figure 3.6.J.). Results of the statistical analysis of the

distribution of distinct oligodendrocyte populations are presented in Table 3.1.. These data show that loss of *Ppargc1α* leads to a slight increase in the number of APC oligodendrocytes in the upper layers, indicating that there is a slight shift in the spread of these oligodendrocytes. This change in the distribution of APC positive myelinating oligodendrocytes may be due to a natural response mechanism to increase the number of APC positive oligodendrocytes to ameliorate and myelinate the cortex back to its normal levels, in response to a loss of *Ppargc1α* in the neocortex and subsequent hypomyelination. This functional compensation is supported by prior work showing that when one oligodendrocyte population is ablated by diphtheria toxin, there is a functional compensation by the remaining populations where mutant mice display not only have a normal complement of myelin and oligodendrocytes but also normal behavior (117). Hence, the remaining oligodendrocytes may be in the process of ameliorating the hypomyelination defect. Another possibility is that while there is a slight increase in the number of APC positive oligodendrocytes, they may be abnormal in generating the myelin sheath, thus accounting for the hypomyelination phenotype. Travis Hallett is currently confirming these quantifications by analyzing additional sections across more animals.

Functional compensation by oligodendrocytes may account for the changes in the distribution of oligodendrocyte populations but it may not account for the persistant hypomyelination. To this, it is likely that the hypomyelination phenotype, particularly in the upper layers, remains a neuronal defect that is persistant with age, regardless of continual compensation by oligodendrocytes. It is possible that the hypomyelination is a secondary outcome of a defect in local neuronal branching. Previous work has shown that mTOR controls mitochondrial oxidative function through a *YY1-Ppargc1α* transcriptional complex (196). More recently, it has been reported that *Ppargc1α* can control the expression of BDNF via FNDC5

Table 3.1. Statistical analysis of the distribution of distinct oligodendrocyte populations between adult *Emx1-Cre; Ppargc1α$^{fl/fl}$* and *Ppargc1α$^{fl/fl}$* mutants.

This table summarizes the p values obtained after statistical analysis with two tailed student's T test on the numbers of distinct oligodendrocyte populations spread throughout all the cortical layers divided into ten bins from pia to corpus callosum (CC). Numbers in red represent significant values ≤ 0.05.

Table 3.1. (Continued)

	P values (two tailed student's T test)		
	OLIG2	PDGFRα	APC
Pia 10	0.939	0.785	0.00702
9	0.0938	0.0607	0.0144
8	0.0784	0.114	0.178
7	0.822	1.00	0.338
6	0.236	0.779	0.255
5	0.315	0.447	0.286
4	0.371	0.940	0.359
3	0.499	0.380	0.891
2	0538	0.929	0.298
CC 1	0.716	0.0836	0.337

expression in the hippocampus or in primary cortical neurons (228). These pathways and molecules are all involved in the establishment of a proper dendritic pattern (229). First, the PI3K-mTOR kinase pathway is known to be important for regulating cell size and has been shown to be crucial to control dendritic size (229-231). Moreover, it can also govern dendritic complexity and branching pattern, in conjunction with the mitogen activated protein kinase (MAPK) kinase pathway (230). BDNF can stimulate both the PI3K-mTOR as well as MAPK pathways to induce primary dendritic formation (232). Notably, it has been recently shown that *Ppargc1α* is required for the formation and maintenance of neuronal dendritic spines (95). Since *Ppargc1α* is involved in dendritic arborization, it is possible that defective neuronal dendritic arborization from SCPN leads to abnormal synapses that detrimentally affects the axonal projections of ascending fibers to the cortex in the upper layers. These abnormal afferent axons may then lead to defective myelination in the upper layers of the neocortex via mechanisms as described in Chapter 4.

3.3.7. Gain-of-function analysis: *Ppargc1α* overexpression in cortical progenitors fated to be CPN did not induce ectopic myelination.

Loss-of-function analysis, as shown in sections 3.3.2. to 3.3.4., demonstrated that *Ppargc1α* is required in neurons to establish proper neocortical myelination. Gain-of-function analysis is important to determine if *Ppargc1α* is sufficient to induce myelination. To test whether overexpression of *Ppargc1α* in otherwise fated cortical progenitors can induce ectopic myelination, together with Dr. Simona Lodato, a postdoctoral fellow in the laboratory, I overexpressed *Ppargc1α* by ultrasound-guided *in utero* electroporation in E15.5 cortical progenitors that are fated to form upper layer CPN. *In vivo* electroporation enables me to

exercise control over the timing and location of misexpression in an otherwise wild type environment (233). I expressed *Ppargc1α* under the control of a constitutively active CMV enhancer / β actin promoter with an IRES-enhanced GFP element for easy identification of electroporated cells (*Ppargc1α*^{GFP}, Figure 3.7.A.). Dr. Simona Lodato electroporated this vector construct into the neocortical ventricular zone of developing E15.5 wild type embryos while I recovered the electroporated embryos at two developmental stages, namely P16 (n = 5 animals across 2 distinct experiments) and P21 (n = 7 across 2 different experiments). I identified the electroporated cells by immunostaining for GFP and examined the myelination pattern by immunostaining for MBP on coronal cortical sections of electroporated neocortices at P16 and P21. Electroporation with *Ppargc1α*^{GFP} at E15.5 results in the transfection of cells that give rise to CPN predominantly of upper layers II/III where *Ppargc1α* is normally not expressed. Harvesting of electroporated pups at P16 and P21 allows me to easily identify any ectopic myelination due to the induction of *Ppargc1α* because the upper layers II/III are not fully myelinated at these stages. Although I found many electroporated GFP positive cells in the upper layers II/III, I did not detect any ectopic MBP positive cells or fibers in the vicinity of the GFP positive cells or more broadly in the upper layers II/III, when compared to the unelectroporated contralateral control hemispheres (Figure 3.7.B. to 3.7.G.). Therefore, my data demonstrate that overexpression of *Ppargc1α* in upper layer CPN does not induce ectopic myelination in the neocortex, indicating that *Ppargc1α* is insufficient to induce ectopic myelination in the neocortex.

3.3.8. Decrease in neuronal metabolism in deep layers of *Emx1-Cre; Ppargc1α*$^{fl/fl}$ mice.

Since *Ppargc1α* is implicated to be important for energy metabolism in tissue with high

Figure 3.7. *Ppargc1α* overexpression in cortical progenitors fated to be CPN did not induce ectopic myelination.

(A) A schematic showing the *Ppargc1α*^{GFP} construct that was *in utero* electroporated at E15.5 into wild type cortical progenitors fated to be upper layer CPN. Electroporated pups were subsequently harvested at P16 and P21.

(B – G) Immunostaining for GFP and Myelin Basic Protein (MBP) revealed that while GFP positive cells that overexpress *Ppargc1α* can migrate and occupy their destined position in the upper layers, they do not induce obvious ectopic myelination at P16 (data not shown) and P21, as compared to the unelectroporated control contralateral hemisphere. Scale bars, 100 μm (B – G).

Figure 3.7. (Continued)

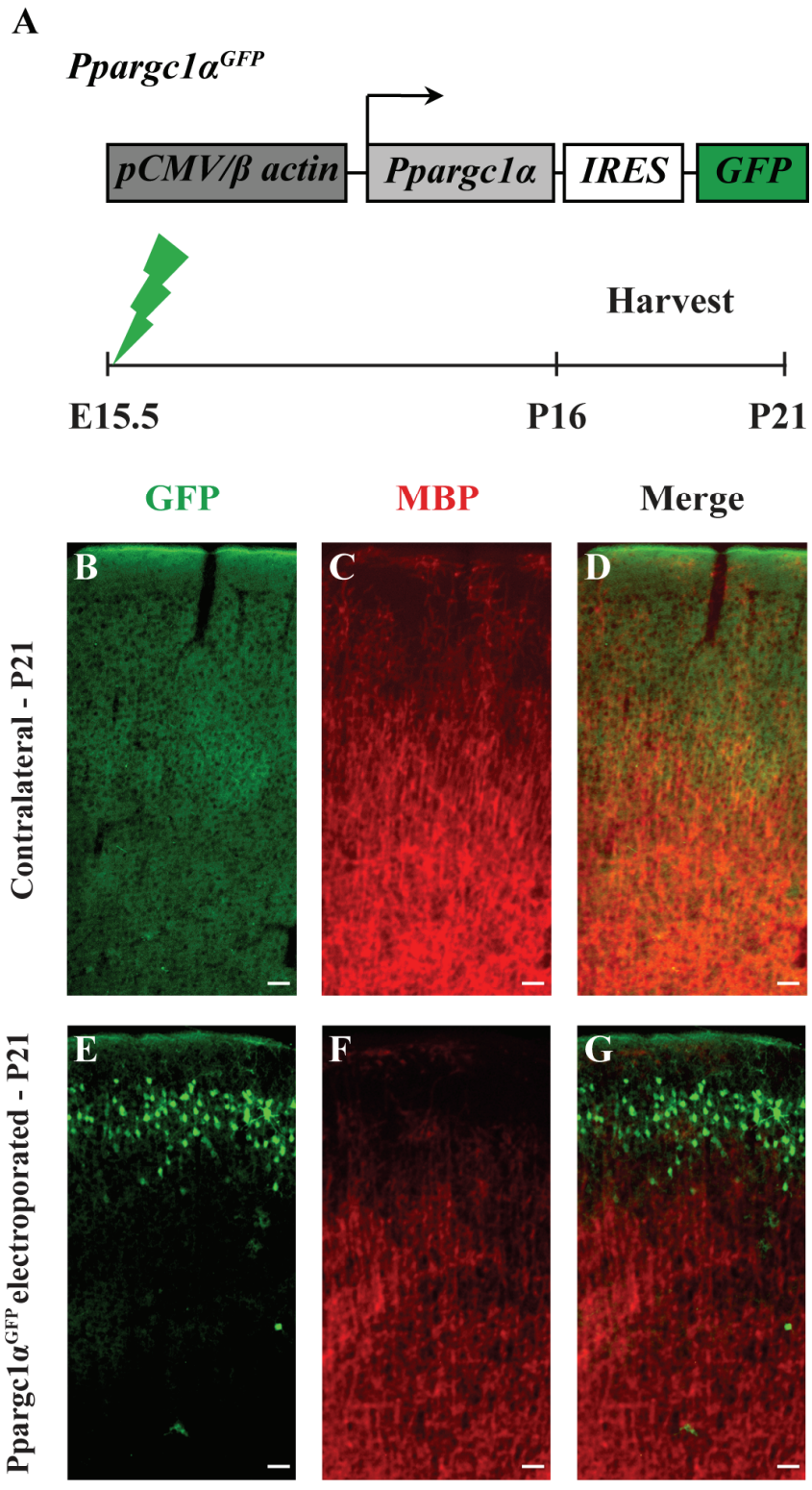

metabolic demand like brown adipose tissue (42, 61), skeletal muscle (51, 54, 61) and the heart (38, 40, 69), I hypothesize that *Ppargc1α* is important for metabolic control in SCPN of the neocortex. To test my hypothesis and determine if *Ppargc1α* is necessary for neuronal metabolism in the deep cortical layers, I extracted tissue with tissue punches from the deep cortical layers of *Emx1-Cre; Ppargc1α*$^{fl/fl}$ and matched *Ppargc1α*$^{fl/fl}$ littermate controls at P14 (n = 5 *Emx1-Cre; Ppargc1α*$^{fl/fl}$ and n = 3 *Ppargc1α*$^{fl/fl}$ animals over 2 distinct experiments) and 2 months of age (n = 7 *Emx1-Cre; Ppargc1α*$^{fl/fl}$ and n = 5 *Ppargc1α*$^{fl/fl}$ animals over 3 different experiments) (Figure 3.8.A.). I used high performance liquid chromatography followed by mass spectrometry (LC-MS) to determine N-acetylaspartate (NAA) and creatine concentrations, and determined the metabolic levels of these tissues using NAA over creatine (NAA/creatine) ratios as an indicator for neuronal metabolism.

NAA is a metabolite that is synthesized from acetyl CoA and aspartate by enzyme NAT8L that is found exclusively in the mitochondria and microsomes of neurons (170-177). It is one of the most concentrated molecules in the brain (170-177). Because of its exclusive production by neurons and its highly detectable levels by magnetic resonance spectroscopy (MRS) analysis, it is currently used as a clinical indicator for neuronal metabolism (234, 235). I found that NAA/creatine levels are significantly lower in *Emx1-Cre; Ppargc1α*$^{fl/fl}$ mice at P14 (71.2% ± 13.6% , decrease of 28.8% as compared to age-matched control, $p = 1.22 \times 10^{-2}$) and 2 months of age (86.8% ± 12.3%, decrease of 13.2% as compared to age-matched control, $p = 3.97 \times 10^{-2}$), as compared to that of *Ppargc1α*$^{fl/fl}$ controls. These data indicate that there is a decrease in neuronal metabolic levels in the deep layers of *Emx1-Cre; Ppargc1α*$^{fl/fl}$ mice, as compared to *Ppargc1α*$^{fl/fl}$ controls at P14 as well as 2 months of age. Thus, these data show that the specific loss of *Ppargc1α* in the dorsal forebrain, particularly in the deep layers, results in decreased

Figure 3.8. Decrease in neuronal metabolism in deep layers of *Emx1-Cre; Ppargc1α$^{fl/fl}$* mice.

(A) A representative image showing that tissue punches (arrows) were used to extract tissue from the deep cortical layers V/VI of mutant mice. Insert shows a close-up image of a tissue punch. Ctx, cortex; Hip, hippocampus.

(B) Neuronal metabolism analysis by LC-MS revealed that NAA/creatine levels, clinically relevant markers for neuronal metabolism, are significantly lower in *Emx1-Cre; Ppargc1α$^{fl/fl}$* mice at P14 (71.2% ± 13.6% , decrease of 28.8% as compared to age matched control, $p = 1.22 \times 10^{-2}$) and 2 months of age (86.8% ± 12.3%, decrease of 13.2% as compared to age matched control, $p = 3.97 \times 10^{-2}$), as compared to that of *Ppargc1α$^{fl/fl}$* controls. cKO refer to *Emx1-Cre; Ppargc1α$^{fl/fl}$* mutant mice while cWT refer to *Ppargc1α$^{fl/fl}$* mutant controls. Values plotted are calculated as percentage ratio of NAA/creatine values of cKO over that of cWT in the same controlled experiment. ** represents p value ≤ 0.01, * represents p value ≤ 0.05.

Figure 3.8. (Continued)

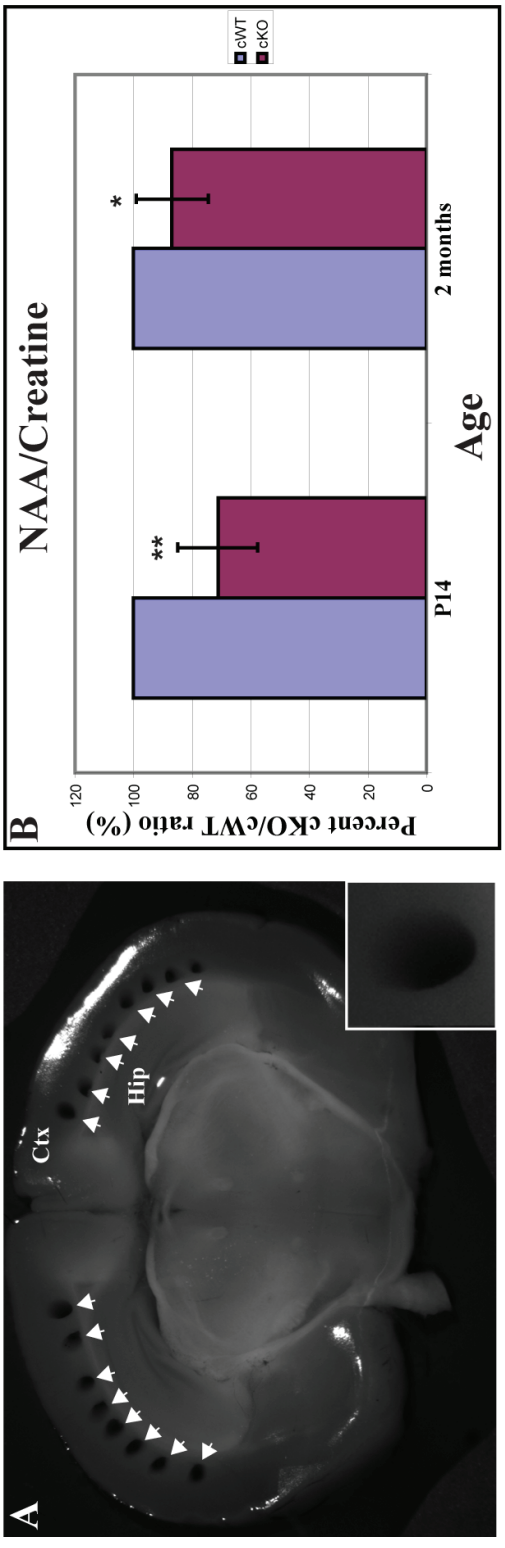

neuronal metabolism, demonstrating that *Ppargc1α* is required for normal neuronal metabolism in SCPN.

Interestingly, there is a smaller difference in the NAA/creatine levels found in 2 month-old mutants (~ 13.2%) as compared to P14 mutants (28.8%). This can be due to functional compensation with time in response to a decrease in NAA levels. The neuronal metabolic profile presents a correlation with the myelination phenotype though it does not prove a causative relationship. Since the metabolic profile appears to improve while the hypomyelination defect appears to be persistant, if not more severe with time, it is possible that neuronal metabolism may not responsible for the hypomyelination phenotype. However, it is also probable that neuronal metabolism plays a larger role in affecting myelination at earlier stages of postnatal development rather than during adulthood where another mechanism or factor becomes more important. In addition, it is also possible that *Ppargc1α* mediates its function via multiple pathways of which one of them implicates neuronal metabolism.

Together, these results suggest that *Ppargc1α*'s metabolic function in SCPN may be mechanistically important to regulate communication via yet unidentified secreted metabolites betwen SCPN and oligodendrocytes to affect neocortical myelination.

3.4. Discussion.

Here, I discovered that neuron-selective *Ppargc1α* plays a novel function in the neocortex to affect an oligodendrocyte-specific process of myelination; particularly it is cell-intrinsically required to establish a correct pattern of myelination in the neocortex.

Firstly, *Ppargc1α* is expressed primarily during postnatal ages, with increasing expression with age. This temporal expression corresponds with the onset of myelination during early postnatal ages. However, I found that *Ppargc1α* is selectively expressed in SCPN and in certain cortical interneuron subsets but not in CThPN and the majority of CPN in the neocortex. Most importantly, I showed that *Ppargc1α* is not expressed in glial cells of the neocortex; particularly it is excluded from oligodendrocyte progenitors as well as mature myelinating oligodendrocytes. This set of findings differs with a recent report purporting that *Ppargc1α* is expressed in cultured oligodendrocytes and can regulate the expression of myelin basic protein (MBP) *in vitro* (88). It is possible that cells cultured *in vitro* behave differently from cells *in vivo*. In all, my results show that *Ppargc1α* is a neuron-specific transcriptional co-activator that is not expressed in oligodendrocytes in the neocortex during postnatal development when neocortical myelination is induced.

Remarkably, examination of the neocortical myelination pattern of the *Ppargc1α* null mice revealed hypomyelination defects not only in the deep cortical layers V/VI, but also in the upper layers II-IV where *Ppargc1α* is not expressed. Further analysis of a conditional null mutant of *Ppargc1α* in neurons confirmed that the hypomyelination anomalies observed in the null mutant is caused by selective loss of *Ppargc1α* in neurons. This led me to investigate whether *Ppargc1α* plays a novel role in neocortical neurons to control neocortical myelination. I generated a conditional null mutant for *Ppargc1α* in the dorsal telencephalon, which provides the

best possible model to study the effects of *Ppargc1α* ablation in neocortex. Remarkably, brightfield and immunostaining analyses showed that conditional loss of *Ppargc1α* in the dorsal forebrain causes similar hypomyelination defects in the deep and upper layers, even in layer I fibers. On the contrary, examination of another newly generated conditional null mutant for *Ppargc1α* in the thalamus showed that ascending projections from TCPN are myelinated normally despite the loss of *Ppargc1α* in TCPN. These new data demonstrated that selective loss of *Ppargc1α* in the thalamus does not affect the myelination pattern of their axons as they innervate the neocortex, and most importantly that it does not cause the hypomyelination defects of the neocortex, as observed in the different null and conditional null mutants for *Ppargc1α* described so far. In all, my loss-of-function analyses with distinct genetic null and conditional null mice models for *Ppargc1α* indicate that neuron-specific *Ppargc1α* is cell-autonomously necessary to establish a proper myelination pattern in the neocortex. Together with the expression profile of *Ppargc1α*, these new findings present a conundrum where a neuron-specific gene in *Ppargc1α* is required to control an oligodendrocyte-specific process of myelination in the neocortex.

In addition to loss-of-function analysis, gain-of-function analysis is important to test whether *Ppargc1α* is sufficient to induce ectopic myelination. *In utero* electroporation experiments revealed that the induction of *Ppargc1α* in cortical progenitors destined to form upper layer CPN where *Ppargc1α* is normally not expressed failed to induce ectopic myelination. Therefore, *Ppargc1α*, though necessary, is not sufficient to induce myelination in the neocortex.

Since *Ppargc1α* is known to be a master regulator of energy metabolism in tissue with high metabolic demand such as brown adipose tissue (42, 61), skeletal muscle (51, 54, 61) and the heart (38, 40, 69), I investigated whether *Ppargc1α* is required for normal neuronal

metabolism. Initial experiments demonstrated a decrease in neuronal metabolism, or more specifically in NAA over creatine ratios, in the deep cortical layers of the conditional null mutant for *Ppargc1α* in the dorsal forebrain. These data revealed that *Ppargc1α* is necessary for normal neuronal metabolic function in the neocortex. They also purport that *Ppargc1α* may be able to directly or indirectly regulate the production of metabolites that are secreted and eventually taken up by oligodendrocytes to affect their formation of the myelin sheath.

My results demonstrate that *Ppargc1α* –a transcriptional co-activator–is important for neocortical myelination. This is the first involvement of a transcriptional co-activator in regulating neocortical myelination as well as in neuron-to-glia interactions. Current research on neuron-to-glia communication in oligodendrocyte function and myelin biogenesis is mainly focused on secreted factors or membrane-associated cell surface molecules (112, 113). Since *Ppargc1α* is a transcriptional co-activator, it has to partner DNA-docking transcription factors or nuclear receptors to mediate its function (46, 47). Therefore, it will be interesting for future work to investigate the DNA-binding partners of *Ppargc1α* and to identify and elucidate their downstream effectors to better understand the mechanism of *Ppargc1α* in controlling myelination.

Ppargc1α is known to be a master regulator of energy metabolism and mitochondrial biogenesis in tissue with high metabolic demand such as brown adipose tissue (42, 61), skeletal muscle (51, 54, 61) and the heart (38, 40, 69). My findings purport a similar role for *Ppargc1α* in SCPN as ablation of *Ppargc1α* in the deep layers of the neocortex leads to decreased neuronal metabolism. Moreover, previous studies have reported that *Ppargc1α* is able to regulate mitochondrial density and ATP levels in primary cortical neuron cultures (92). Therefore, it is possible that *Ppargc1α* regulates neuronal mitochondria. This is interesting because neuronal

mitochondria have been suggested to be important for myelination and can be a mechanistic link between *Ppargc1α* and myelination. Prior work has shown that mitochondrial size, activity and density, and even speed of axonal mitochondrial transport, increase as an adaptation to dysmyelination or demyelination in distinct mouse mutant models (236-238). This increase can be interpreted as an attempt to stimulate remyelination of demyelinated axons. Furthermore, similar axonal mitochondrial changes in response to demyelination and remyelination are well documented in mice models of multiple sclerosis (239-241). In fact, there is an increasing appreciation in the field that axonal mitochondria are important for regulating myelination. Besides *Ppargc1α*, another mitochondrial-related gene called *MRS2 magnesium homeostasis factor homolog* (*MRS2*) has also been involved in myelination (242, 243). Through encoding a mitochondrial magnesium channel, prior work has reported that a mutation in the *MRS2* gene causes demyelination in the rat (242, 243). It will be interesting to elucidate if *Ppargc1α* governs the expression of *MRS2* or other mitochondrial associated genes, and if so, how they interact with each other to regulate neocortical myelination.

Interestingly, a tripartite relationship between myelination, axonal mitochondria and electrical activity has been proposed (239, 240). Although axonal electrical activity after target innervation can regulate myelination (156), myelination and electrical activity can also in turn affect the placement and mobility of axonal mitochondria (244). Therefore, these studies purport that myelination, electrical activity and axonal mitochondria have a reciprocal three-way relationship. In light of this, it will be important to test if *Ppargc1α* plays a role in controlling neuronal electrical activity and if so, determine whether this is the mechanistic pathway for it to affect myelination. Alternatively, *Ppargc1α* may regulate the production of secreted metabolites,

or some currently unidentified cell surface molecules that will allow it to communicate with oligodendrocytes to govern myelination.

Chapter 4:

Discussion

4.1. Role of *Ppargc1α* in neuronal survival and its implications.

4.1.1. Implications of findings for neuronal survival and lesion formation.

My findings in Chapter 2 demonstrated that *Ppargc1α* is cell-autonomously not necessary to control neuronal survival during normal development either in the absence of acute external environmental stress triggers or in the context of cellular stress caused by aging. Taken together with previous work (72-74), my new data suggest that *Ppargc1α* is involved in neuronal survival, but only in the context of an unbalanced non-homeostatic cellular state caused by acute cellular stress or neurodegeneration. In this case, the loss of *Ppargc1α* may increase the cells' susceptibility to die, possibly by interfering with the ROS defense system and mitochondrial function or by hitherto unexplored mechanisms. It also suggests that the enhanced cell death observed in prior studies is due to potential additive or more complex effects of already inherent cell toxicity or death.

For future work, it will be interesting to determine the downstream effectors responsible for *Ppargc1α's* role in neuronal survival in the event of acute cellular stress and neurodegeneration. Although mitochondrial genes involved in the ROS defense system have been implicated in previous studies (72-74), it remains to be determined whether novel genes that have not yet been identified are also involved, and if so, how *Ppargc1α* regulates the expression of these genes and the molecular pathways that enables it to be important for cell survival.

Previously published reports show that neuron-specific loss of *Ppargc1α* causes smaller and fewer spongiform-like lesions in the striatum (219). I confirmed these results in section 2.3.3. and described in further detail the localization and arealization of these lesions in the neuron-selective conditional null mutants for *Ppargc1α*. These data demonstrate that preferential loss of

Ppargc1α in neurons is only partly responsible for the development of IC localized lesions. This indicates that though *Ppargc1α* in neurons is required to govern the formation of these lesions, it does so only to a certain extent. My above findings indicate that *Ppargc1α* alone, in either SCPN or TCPN, is not necessary to control lesion development. Thus, these data in totality suggest that lesion formation requires either the simultaneous loss of *Ppargc1α* in SCPN and TCPN, or the conditional loss of *Ppargc1α* in a hitherto unexamined region like the substantia nigra where *Ppargc1α* is highly expressed, or in the striatum where *Ppargc1α* is weakly expressed up to P7. I have tested the possibility that these lesions may necessitate simultaneous loss of *Ppargc1α* in SCPN and TCPN by generating double conditional null mutants for *Ppargc1α.* Unfortunately, breeding these animals has been difficult; four breeding cycles with foster dams over the past eight months did not yield any animals with the genotype of interest. Therefore, it remains to be explored whether lesion development is caused by the singular loss of *Ppargc1α* in a defined neuronal domain or by the additive deficit of *Ppargc1α* in multiple neuronal regions.

Since my data and others have shown that neuron-specific loss of *Ppargc1α* results in smaller and fewer lesions (219) as compared to that of the null mutant, there is a non neuronal, potentially systemic or a more complex multifactorial mechanism responsible for these lesions. It has been recently reported that *Ppargc1α* expression in muscles can induce the production of FNDC5, a precursor that is cleaved and secreted as irisin—a newly identified hormone or myokine that can induce a broad program of brown adipose tissue development (222). Irisin secretion is induced by exercise and can lead to ameliorations in obesity and glucose homeostasis (222). Yet, its role in brain development is unknown and it remains to be seen whether irisin is involved in the development of spongiform lesions in the IC. It will be interesting to determine

whether a systemic or secreted component like irisin, or a thus far unidentified molecule leading to a multiplex pathway, is responsible for lesion formation.

4.1.2. Implications of findings for SCPN differentiation.

While my results in Chapter 2 are important to fill gaps of knowledge in the field about the cell-intrinsic function of *Ppargc1α* in neuronal survival, these findings are also very important to inform us about its role in SCPN differentiation. My results in Chapter 2 demonstrated that distinct classes of PN, particularly SCPN, are born, can migrate normally to their appropriate laminar positions and are maintained throughout adulthood to old age. This is in concordance with my expression profile data, as described in section 2.3.1., showing that *Ppargc1α* is largely expressed postnatally, after the fate specification and migration of most cortical PN have already occurred. Furthermore, cell death analysis did not reveal any significant increase in cell death. Hence, these data show that *Ppargc1α* in SCPN do not affect the birth, migration, laminar position and even survival of SCPN. Nissl staining further shows that the absence of *Ppargc1α* in SCPN does not affect their characteristic large pyramidal morphology. Hence, my findings show that *Ppargc1α* in SCPN also does not control SCPN morphological characteristics. In fact, *Ppargc1α* in SCPN do not cause any gross neuronal abnormalities in the neocortex. These data are important because they provide insights into potential aspects of SCPN differentiation in which *Ppargc1α* may play a role.

Investigating the contribution of *Ppargc1α* in SCPN to the formation of IC-localized lesions is not only important to understand their elusive cellular origins, but more importantly, to determine if these lesions affect the axonal extensions of SCPN that project through the IC and connect to distant targets like the SC. If conditional loss of *Ppargc1α* in SCPN causes similar

lesions, it is likely that SCPN axonal efferents are affected and bear abnormalities that will warrant further investigation. However, my results in Chapter 2 demonstrated that the conditional loss of *Ppargc1α* in SCPN do not cause spongiform lesions in the IC. These suggest that *Ppargc1α* in SCPN have normal axonal efferents and imply that the lesions observed in *Ppargc1α* null mutants do not affect descending subcerebral projections. Moreover, high magnification analysis of conditional null mutants for *Ppargc1α* in SCPN showed that the axonal bundles of the IC in these mutants are normally shaped and tightly fasciculated with no overt signs of loss, defasciulation or other aberrations. Examination of the cerebral peduncle and the dorsal funiculus in the spinal cord of both null and conditional null mutants also did not reveal any evident anomalies, indicating that subcerebral projections can extend and find their distant targets in the absence of *Ppargc1α* in SCPN. Therefore, my findings show that the loss of *Ppargc1α* in SCPN does not cause significant axonal aberrations in projections through the IC, suggesting that *Ppargc1α* in SCPN does not play a cell-autonomous role in axonal extension, pathfinding through the IC and fasciculation.

These implications are also in agreement with my expression profile of *Ppargc1α* where it is expressed in SCPN predominantly during postnatal ages, after initial axonal growth and pathfinding of most SCPN has already occurred. SCPN begin their axonal growth as early as E13.5 (245). By E17.5, pioneering axons have already projected through the IC to reach the upper levels of the mouse brainstem (245). Hence, it is unlikely that *Ppargc1α*, a mainly postnatal gene, plays a role in initial axonal growth and pathfinding by SCPN, which is in agreement with my results in Chapter 2. However, it remains to be determined whether *Ppargc1α* plays a role in target innervation and refinement of axonal connectivity which normally takes place postnatally (245).

4.1.3. Implications of findings for neocortical myelination.

My results from Chapter 2 suggest that *Ppargc1α* does not play a role in the birth, migration, laminar position, survival of SCPN. In addition, they show that conditional loss of *Ppargc1α* in SCPN does not cause overt axonal abnormalities or lesions in the IC. In Chapter 3, I showed that that loss of *Ppargc1α* in SCPN causes hypomyelination, indicating that neuron-specific *Ppargc1α* is important for neocortical myelination. Many may argue that this hypomyelination defect is caused by loss of neurons and their axons. My results in Chapter 2 show otherwise where conditional loss of *Ppargc1α* in SCPN does not cause gross cortical abnormalities, PN loss or increased cell death. They also show that the hypomyelination defect is not due to loss of SCPN axons. Hence, these data support that the hypomyelination defect is not caused by neuronal or axonal loss. These results further show that the hypomyelination occurred in a seemingly normal neocortex and further validates that neuron-specific *Ppargc1α* plays a role in myelination.

4.2. Role of *Ppargc1α* in neocortical myelination and its implications.

4.2.1. Implications of findings for neocortical myelination.

My results in Chapter 3 showed that *Ppargc1α*–a transcriptional co-activator–is important for neocortical myelination. This is the first implication of a transcriptional co-activator in regulating neocortical myelination as well as in neuron-to-glia interactions. Current research on neuron-to-glia communication in oligodendrocyte function and myelin biogenesis is mainly focused on secreted factors or membrane-associated cell surface molecules (112, 113). Since *Ppargc1α* is a transcriptional co-activator, it must partner DNA-docking transcription factors or nuclear receptors to mediate its function (46, 47). Hence, it will be interesting to elucidate the DNA-binding partners of *Ppargc1α*, as well as to identify and study their downstream effectors to gain insights into the mechanism of *Ppargc1α* in regulating myelination. Here, as illustrated in Figure 4.1., I present a hypothetical model that summarizes potential pathways through which neuron-specific *Ppargc1α* can exert its control on neocortical myelination. These possible mechanisms are not mutally exclusive and may indeed present a multifactorial system via which *Ppargc1α* in neurons can regulate myelination in the neocortex.

1) *Ppargc1α* is known to be a master regulator of energy metabolism and mitochondrial biogenesis in tissue with high metabolic demand such as brown adipose tissue (42, 61), skeletal muscle (51, 54, 61) and the heart (38, 40, 69). My results in Chapter 3 support a similar role for *Ppargc1α* in SCPN as loss of *Ppargc1α* in the neocortex leads to decreased neuronal metabolism. Furthermore, prior work has shown that *Ppargc1α* can regulate mitochondrial density and ATP levels in primary cortical neuron cultures (92). Thus, it is likely that *Ppargc1α* regulates neuronal mitochondria. This is interesting because neuronal mitochondria have been implicated in myelination and can be a mechanistic link between *Ppargc1α* and myelination. Studies have

Figure 4.1. Model of potential pathways where neuronal *Ppargc1α* can control neocortical myelination.

Neuronal *Ppargc1α* can potentially regulate neocortical myelination by (i) controlling neuronal mitochondria or mitochondrial genes like MRS2 that eventually regulates the secretion of metabolites, or (ii) regulating electrical activity, which forms a tripartite relationship with myelination and axonal mitochondria, or (iii) governing the production of FNDC5, which controls the secretion of neurotrophin brain-derived neurotrophic factor BDNF which has been implicated in myelination of the PNS and CNS. These possible mechanisms are not mutally exclusive and may indeed present a multifactorial system via which *Ppargc1α* in neurons can regulate myelination in the neocortex.

Figure 4.1. (Continued)

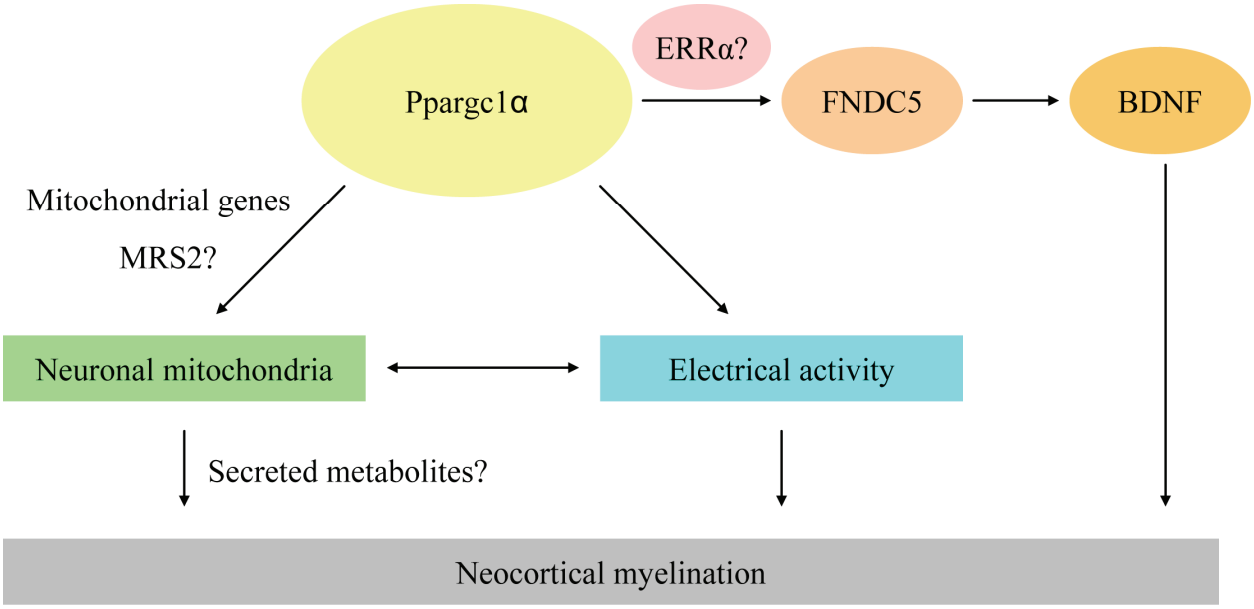

shown that mitochondrial size, activity and density, or even speed of axonal mitochondrial transport increase as an adaptation to dysmyelination or demyelination in distinct mouse mutant models (236-238). This increase can be interpreted as an attempt to induce remyelination of demyelinated axons. Moreover, similar axonal mitochondrial changes in response to demyelination and remyelination are well documented in mice models of multiple sclerosis (239-241). In fact, there is an increasing appreciation in the field that axonal mitochondria are important for regulating myelination. Besides *Ppargc1α*, another mitochondrial-related gene called *MRS2 magnesium homeostasis factor homolog* (*MRS2*) has also been implicated in myelination (242, 243). Through encoding a mitochondrial magnesium channel, previous studies have demonstrated that a mutation in the MRS2 gene causes demyelination in the rat (242, 243). It will be interesting to determine if *Ppargc1α* controls the expression of *MRS2* or other mitochondrial associated genes, and if so, how they interact with each other to control neocortical myelination.

2) Interestingly, a tripartite relationship between myelination, axonal mitochondria and electrical activity has been proposed (239, 240). While it has been shown that electrical activity in axons after target innervation can regulate myelination (156), it has also been reported that myelination and electrical activity can in turn affect the placement and mobility of axonal mitochondria (244). Thus, these studies suggest that myelination, electrical activity and axonal mitochondria have a reciprocal three-way relationship. In light of this, it will be important to test if *Ppargc1α* plays a role in regulating neuronal electrical activity and if so, determine whether this is the mechanistic pathway for it to affect myelination. Alternatively, *Ppargc1α* may control the production of secreted metabolites or some yet unidentified cell surface molecules that will enable it to communicate with oligodendrocytes to regulate myelination.

3) Notably, a recent report by the groups of Michael Greenberg and Bruce Spiegelman showed that exercise can induce the secretion of BDNF through a *Ppargc1α*/FNDC5 pathway (228). They showed that downregulating *Ppargc1α* expression in primary cortical neurons by lentiviral mediated shRNA knockdown resulted in a significant decrease of FNDC5 mRNA expression (228). This reduction is also observed in *Ppargc1α* null mutants (228). Moreover, overexpression of *Ppargc1α* in primary cortical neurons led to an induction of FNDC5 mRNA as well as protein levels (228). Hence, *Ppargc1α* is necessary and sufficient for FNDC5 expression in primary cortical culture (228). In this study, they also showed that ERRα is a key interacting transcription factor with *Ppargc1α* for regulating FNDC5 expression in primary cortical neurons (228). They further demonstrated that FNDC5 can regulate BDNF expression in a cell-autonomous fashion and that recombinant BDNF can decrease FNDC5 gene expression as part of a negative feedback loop (228). Therefore, *Ppargc1α* together with ERRα forms a pathway to regulate FNDC5 which in turns affects the expression and eventual secretion of BDNF.

This study is significant because BDNF, being a neurotrophic factor, has been implicated in the myelination of the PNS (246-249) as well as the CNS (250-253). BDNF has also been shown to be able to induce remyelination of injured axons (247-249, 254). Hence, it is highly possible that it may be one of the ways *Ppargc1α* in neurons of the cortex can control myelination.

4) Secreted molecules, whether metabolites or neurotrophic factors, can help in explaining how *Ppargc1α* can mediate its function throughout all cortical layers despite being expressed only in SCPN that reside in deep layer V of the neocortex. However, it is also possible that hypomyelination phenotype in the upper layers is only a secondary outcome of a defect in local neuronal branching. Previous work has shown that mTOR controls mitochondrial oxidative

function through a *YY1-Ppargc1α* transcriptional complex (196). More recently, it has been reported that *Ppargc1α* can control the expression in the hippocampus or in primary cortical neurons (228). These pathways and molecules are all involved in the establishment of a proper dendritic pattern (229). First, the PI3K-mTOR kinase pathway is known to be important for regulating cell size and has been shown to be crucial to control dendritic size (229-231). Moreover, it can also govern dendritic complexity and branching pattern, in conjunction with the mitogen activated protein kinase (MAPK) kinase pathway (230). BDNF can stimulate both the PI3K-mTOR as well as MAPK pathways to induce primary dendritic formation (232). Notably, it has been recently shown that *Ppargc1α* is required for the formation and maintenance of neuronal dendritic spines (95). Since *Ppargc1α* is involved in dendritic arborization, it is possible that defective neuronal dendritic arborization from SCPN leads to abnormal synapses that detrimentally affects the axonal projections of ascending fibers to the cortex in the upper layers. Abnormal afferent axons may then result in defective myelination in the upper layers of the neocortex via potential mechanisms as detailed above.

4.2.2. Implications of findings for SCPN differentiation.

While the results in Chapter 3 have important implications for *Ppargc1α* in neocortical myelination, they also present new questions that challenge our current understanding of SCPN development. As shown in Chapters 2 and 3, *Ppargc1α* in SCPN does not affect their birth, migration, laminar position, survival and axonal extension but instead affects their myelination pattern. These results call into question whether SCPN actively regulate their own myelination instead of taking a more passive role. It is also interesting to note that among major PN subclasses of the neocortex, only SCPN express *Ppargc1α* at high levels; CThPN and the

majority of CPN do not. Since SCPN project axons that are extremely long, particularly the CSMN that project all the way from the cortex to innervate the SC, it is extremely important to have efficient propagation of action potentials for signal transduction. Hence, SCPN may have a special requirement for proper myelination that other neuronal subtypes may not require. This brings into question whether neuronal subtypes broadly differ in their myelination patterns and whether molecular pathways controlling subtype identity include an active regulation of myelination. More importantly, it questions whether the myelination pattern of a neuron is part of its unique identity, just like morphological characteristics and electrophysiogical patterns. If so, this study may prompt others to look at the myelination pattern of distinct neuronal subtypes as another mode of classification.

4.3. Role of *Ppargc1α* as a metabolic switch and its implications in cell differentiation and cell fate.

There is increasing attention paid to the important role that metabolism plays in cellular differentiation. Many studies have shown that pluripotent stem cells are highly dependent on glycolysis which contrasts with differentiated cells that depend more on oxidative phosphorylation (255). Likewise, cancer stem cells have been shown to revert from a more differentiated oxidative state to a more rudimentary glycolytic state during malignant transformation (256, 257). Nuclear reprogramming of differentiated fibroblasts to induced pluripotent stem cells also shows a similar metabolic shift (255, 258-260). Collectively, these studies suggest that the metabolic state of a cell is important to mark stages of differentiation. Interestingly, *Ppargc1α* can induce a metabolic switch from glycolysis to oxidative phosphorylation in many tissues with high metabolic demand. For instance, in the heart, *Ppargc1α* expression is upregulated during early postnatal ages when the heart is switching from an embryonic glycolytic state to a more differentiated oxidative state (69). Hence, it will be interesting to determine whether *Ppargc1α* acts as a metabolic switch in SCPN differentiation during postnatal ages, similar to that in the heart, and if so, the consequences of failing to switch metabolically and its implications for SCPN differentiation.

Besides cellular differentiation, metabolic switches mediated by *Ppargc1α* can also specify cell fates in certain tissue like brown fat and muscle. For instance, *Ppargc1α* induction in white glycolytic fast-twitch skeletal muscle can "fate-switch" them to display genetic and physiological features characteristic of red oxidative slow-twitch skeletal muscle (38, 68). Likewise, overexpression of *Ppargc1α* in white fat can convert them to brown fat because of increased oxidative phosphorylation (42). These fate-switches occur because these cell types are

defined by their metabolic signature. Neuronal subtypes are defined traditionally by their morphology, axonal projections, electrophysiology and molecular identities. It will be interesting to determine if the metabolic status or the metabolome of a neuron is another characteristic that defines its identity and distinguishes it from other subclasses. In particular, it will be interesting to investigate if *Ppargc1α* is critical in defining the metabolic signature of SCPN.

In all, the work presented in this dissertation serves to fill knowledge gaps in the field about *Ppargc1α's* function in the brain with respect to spongiform lesion formation as well as neuronal survival. Most importantly, this work serves to provide new insights into the function of *Ppargc1α* in SCPN postnatal differentiation. Novel findings on *Ppargc1α's* role in controlling neocortical myelination and its implication in neuron-to-glia signaling serve as the beginning for many more studies. I hope with this dissertation that I have provided an original contribution to the field in enhancing our understanding of *Ppargc1α* function in SCPN, or more broadly in neocortical development.

Chapter 5:

Materials and Methods

5.1. Genetic mouse models.

5.1.1. Colony maintenance and genotyping.

Studies performed on all mouse lines were approved by the Harvard University Institutional Animal Care and Use Committee (IACUC) and the Massachusetts General Hospital IACUC, and were performed in accordance with institutional and federal guidelines. The day of vaginal plug was designated as embryonic day 0.5 (E0.5). The day of birth was designated as postnatal day 0 (P0). Mice were maintained on a standard rodent chow or breeder chow diet with 12-hour light and dark cycles.

Wild type C57BL/6 mice were either acquired from Charles River Laboratories in Wilmington, Massachusetts, USA, or bred in house. They were used for *in situ* hybridization analysis to determine the temporal and spatial expression profile of *Ppargc1α*.

Ppargc1α$^{-/-}$ mice were generated and generously given by Professor Bruce Spiegelman from the Department of Cell Biology, Harvard Medical School in Boston, Massachusetts, USA. They were also available from The Jackson Laboratory in Bar Harbor, Maine, USA (strain name: B6.129-*Ppargc1a*^{tm1Brsp}/J, stock number: 008597). *Ppargc1α*$^{fl/fl}$ conditional floxed mice were also generated by Professor Bruce Spiegelman and obtained from The Jackson Laboratory in Bar Harbor, Maine, USA (strain name: B6.129-*Ppargc1a*^{tm2Brsp}/J, stock number: 09666).

Snap frozen brains from 4 month old *CamkIIα-Cre; Ppargc1α*$^{fl/fl}$ mice were generated and generously given by Professor Jiandie D. Lin from the Life Sciences Institute and Department of Cell and Developmental Biology, University of Michigan Medical Center in Ann Arbor, Michigan, USA. *CamkIIα-Cre; Ppargc1α*$^{fl/fl}$ and *Ppargc1α*$^{fl/fl}$ littermate control mice were genotyped by a donor laboratory, in accordance to previously published protocols. Brains from

mutant mice were not fixed with any fixative before snap freezing with dry ice, and were subsequently stored at -80 ^{o}C.

Emx1-Cre mice were generated by Professor Kevin R. Jones from the Department of Molecular, Cellular, and Developmental Biology, University of Colorado in Boulder, Colorado, USA. They were generously given by Professor Jeffrey Macklis from the Harvard Stem Cell and Regenerative Biology, Harvard University in Cambridge, Massachusetts, USA.

Gbx2-CreER mice were generated and generously given by Professor James Y.H. Li from the Department of Genetics and Developmental Biology, University of Connecticut Health Center in Farmington, Connecticut, USA. 2 to 4 mg of tamoxifen (Catalog number: T5648-1G, Sigma-Aldrich, USA) freshly diluted in corn oil at 20 mg/mL (Catalog number: C8267, Sigma-Aldrich, USA) was administered to pregnant dams carrying *Gbx2-CreER; Ppargc1α*$^{fl/fl}$ and *Ppargc1α*$^{fl/fl}$ pups at E10.5 for collection at P28 and E12.5 for collection at 2 months of age.

DNA were extracted using the DNeasy Blood & Tissue Kit (Catalog number: 69506, Qiagen, USA) from toe clippings of all mice between P0 and P7. Genotyping were achieved by Polymerase Chain Reaction (PCR) analysis with GoTaq Green Master Mix (Catalog number: M7123, Promega, USA). The PCR primers and cycling parameters which were used are described in Table 5.1. and Table 5.2. respectively. PCR products were separated by gel electrophoresis on 1.5 % agarose gel, except for the conditional floxed allele for *Ppargc1α* (*Ppargc1α*$^{fl/fl}$ mice) where 2% agarose gel was used. They were then visualized with ethidium bromide solution (Catalog number: E1510, Sigma-Aldrich, USA) and Molecular Imager Gel Doc XR+ System with Image Lab Software (Catalog number: 170-8195, Bio-Rad, USA).

Table 5.1. PCR primers used for genotyping of genetic mice models.

This table summarizes the different primers used for PCR genotyping of the various genetic mice models used in this study, as described in section 2.5.1..

Table 5.1. (Continued)

Fezf2		
Wild type	Forward	5’ – GGG TTA ATG GGC GGT AAT TT – 3’
	Reverse	5’ – GCC ACA GTT GGT TTT GCA C – 3’
		Product size ~ 700 base pairs
Null	Forward	5’ – GGGTGTTGGGTCGTTTGTTCGGATCTGCTA - 3’
	Reverse	5’ – TCTGGGCGCTCACGGTGACAGGCTGGGATT – 3’
		Product size ~ 300 base pairs
Ppargc1α		
Wild type	Forward	5’ – CCA GTT TCT TCA TTG GTG TG – 3’
	Reverse	5’ – ACC TGT CTT TGC CTA TGA TTC – 3’
		Product size ~ 650 base pairs
Null	Forward	5’ – TCC AGT AGG CAG AGA TTT ATG AC – 3’
	Reverse	5’ – CCA ACT GTC TAT AAT TCC AGT TC – 3’
		Product size ~ 400 base pairs
Floxed	Forward	5’ – TCC AGT AGG CAG AGA TTT ATG AC – 3’
	Reverse	5’ – TGT CTG GTT TGA CAA TCT GCT AGG TC – 3’
		Product size ~ 400 base pairs or 360 base pairs (without floxed)

Table 5.1. (Continued)

Emx1-Cre		
Wild type	Forward	5’ – AAG GTG TGG TTC CAG AAT CG – 3’
	Reverse	5’ – CTC TCC ACC AGA AGG CTG AG – 3’
		Product size ~ 380 base pairs
Transgene	Forward	5’ – GCG GTC TGG CAG TAA AAA CTA TC – 3’
	Reverse	5’ – GTG AAA CAG CAT TGC TGT CAC TT – 3’
		Product size ~ 100 base pairs
Gbx2-CreER		
Wild type	Forward	5’ – AAG GTG TGG TTC CAG AAT CG – 3’
	Reverse	5’ – CTC TCC ACC AGA AGG CTG AG – 3’
		Product size ~ 380 base pairs
Transgene	Forward	5’ – GAT ATC TCA CGT ACT GAC GG – 3’
	Reverse	5’ – TGA CCA GAG TCA TCC TTA GC – 3’
		Product size ~ 300 base pairs

Table 5.2. PCR cycling parameters used for genotyping of genetic mice models.

This table summarizes the distinct PCR cycling parameters used for PCR genotyping of the various genetic mice models used in this study, as described in section 2.5.1..

Table 5.2. (Continued)

	Fezf2	*Ppargc1α*	*Ppargc1α (floxed)*	*Emx1-Cre*	*Gbx2-CreER*
Initialization	95 ^{o}C 5 minutes	94 ^{o}C 3 minutes	94 ^{o}C 3 minutes	95 ^{o}C 5 minutes	95 ^{o}C 5 minutes
Denaturation	94 ^{o}C 30 seconds	94 ^{o}C 30 seconds	94 ^{o}C 30 seconds	94 ^{o}C 30 seconds	94 ^{o}C 30 seconds
Annealing	57 ^{o}C 30 seconds	58 ^{o}C 30 seconds	58 ^{o}C 30 seconds	57 ^{o}C 30 seconds	57 ^{o}C 30 seconds
Extension	72 ^{o}C 30 seconds	72 ^{o}C 30 seconds	72 ^{o}C 30 seconds	72 ^{o}C 30 seconds	72 ^{o}C 30 seconds
Final extension	72 ^{o}C 1 minute	72 ^{o}C 2 minutes	72 ^{o}C 2 minutes	72 ^{o}C 1 minute	72 ^{o}C 1 minute
Number of cycles	30	35	35	30	30

5.1.2. Tissue collection and sectioning.

For embryonic tissue collection, timed pregnant mouse dams were first anesthetized with a lethal dose of Avertin (1.25% 2-2-2 tribromoethanol in 0.63% isomyl alcohol) and their deaths were ascertained by cervical dislocation. Embryos were then removed from the uterine horns by manual dissection. These embryos were anesthetized by hypothermia with ice for at least 3 minutes before decapitation. The whole heads were subsequently fixed in 4% paraformaldehyde (PFA) in phosphate buffer saline (PBS) at 4 ^{o}C overnight (for at least 16 hours), rinsed 3 times with 0.1 M PBS (pH 7.4) for at least 10 minutes each at 4 ^{o}C, before storing in 0.025% sodium azide in PBS (PBS-Azide). For postnatal tissue collection, pups that were P6 and younger were anesthetized by hypothermia with ice for at least 3 minutes; while pups that were P7 and older, including adult mice that were 2 months and older, were anesthetized with a lethal dose of Avertin. Anesthetized mice were perfused transcardially with PBS followed by 4% PFA. Brains were manually dissected, post-fixed in 4% PFA at 4 ^{o}C overnight, rinsed 3 times with PBS for at least 10 minutes each at 4 ^{o}C, and is stored in 0.025% PBS-Azide until sectioning. For the snap frozen *CamkIIα-Cre; Ppargc1α*$^{fl/fl}$ as well as *Ppargc1α*$^{fl/fl}$ littermate control brains, these brains were stored at -80 ^{o}C upon arrival, thawed only at room temperature (r.t.) when intended to be processed for downstream analysis, post-fixed in 4% PFA at 4 ^{o}C overnight, rinsed 3 times with PBS for at least 10 minutes each at 4 ^{o}C, and were sectioned immediately with cold PBS into 0.025% PBS-Azide. All brains were sectioned at 40 μm thickness with cold PBS either on a coronal or sagittal plane with a VT1000S vibrating microtome (Leica Microsystems). Floating sections were stored in PBS-Azide at 4 ^{o}C.

5.2. *In situ* hybridization.

5.2.1. *In situ* hybridization.

Nonradioactive colorimetric in situ hybridization (ISH) with antisense probes labeled with Digoxigenin-UTP (DIG-UTP) was utilized in accordance with previously published protocols. All clones used to produce probes for ISH were generated by reverse transcriptase-PCR (RT-PCR) on extracted RNA from murine cortices at various ages with specific primer sequences, as listed in Table 2.4.. DIG-labeled probes were generated with DIG RNA Labeling Kit (SP6/T7/T3) (Catalog number: 11175025910, Roche Applied Science, USA).

ISH procedures were carried out in RNase-free conditions. Floating brain sections were first mounted on Superfrost Plus slides (Catalog number: 12-550-15, Fisher Scientific, USA) in autoclaved deionised water (dd H_2O) and left to dry completely for a minimal time of at least 10 minutes at r.t.. Dried sections were rehydrated with cold PBS for 5 minutes, permeabilized in cold freshly prepared diluted Triton X-100 in distilled water (0.3% for embryonic tissue and 0.5% for postnatal and adult tissue, Catalog number: T9284-100ml, Sigma-Aldrich, USA) for 10 minutes, washed with cold PBS for 2 times at 5 minutes each, before further permeabilization with cold RIPA buffer (0.5% sodium deoxycholate, 150 mM autoclaved sodium chloride, 50 mM autoclaved Tris pH 8, 1 mM autoclaved EDTA, 1% Tergitol-type NP40, 0.1% sodium dodecyl sulfate in autoclaved dd H_2O) 2 times at 10 minutes each. Permeabilized sections were re-fixed in cold 4% PFA for 15 minutes, washed with cold PBS for 2 times at 5 minutes each and acetylated in a mixture of Triethanolamine Buffer (100 mM Triethanolamine, 0.4% acetic acid in autoclaved dd H_2O) and 0.25% acetic anhydride for 15 minutes at r.t. before washing with cold PBS for 3 times at 5 minutes each. Processed sections were then pre-hybridized for 1 hour at r.t. with hybridization solution [50% formamide, 5X saline sodium citrate, 5X Denhardts solution

(1μg/mL Ficoll 400, 1μg/mL Polyvinilpyrrolidone, 1μg/mL bovine serum albumin), 500 μg/mL salmon sperm DNA, 250 μg/mL yeast RNA in autoclaved dd H_2O] that was pre-warmed to 70 ^oC. Probes to be hybridized were diluted in hybridization solution to an empirically determined concentration ranging from 300 ng/mL to 1μg/mL and pre-warmed to 70 ^oC for 5 to 10 minutes before hybridization to processed sections with glass cover slips for incubation in a humidified chamber (50% formamide, 50% 5X saline sodium citrate) overnight at 70 ^oC. The following day, the sections were washed in freshly prepared post-hybridization solution (50% formamide, 2X saline sodium citrate, 0.1 Tween-20 in autoclaved dd H_2O), prewarmed to 70 ^oC for 2 times for 1 hour each in 70 ^oC, and subjected to further washes in MABT (100 mM malaeiic acid, 150 mM sodium chloride, 0.1% Tween-20 in autoclaved dd H_2O to pH 7.5) for 2 times at 15 minutes each at r.t.. They were then blocked in B2 solution (10% sheep serum in MABT) for 1 hour at r.t. before incubation with sheep polyclonal alkaline phosphatase-conjugated anti-DIG primary antibody diluted 1:2000 in B2 solution (Fab fragments, catalog number: 11093274910, Roche Applied Science, USA) overnight at 4 ^oC. The next day, the sections were rinsed in MABT for 2 times at 5 minutes each at r.t. before washing in freshly prepared B3 solution (100 mM autoclaved Tris pH 9.5, 50 mM autoclaved magnesium chloride, 100 mM autoclaved sodium chloride, 0.1% Tween-20 in autoclaved dd H_2O) for 30 minutes at r.t.. Alkaline phosphatase activity was detected by reaction with a mixture of filtered BCIP/NBT Liquid Substrate System (5-bromo-4-chloro-3'-indolyphosphate p-toluidine and nitro-blue tetrazolium chloride solution, catalog number: B1911, Sigma-Aldrich, USA) and 0.1% Tween-20 (Sigma-Aldrich) at r.t., where fresh solution was changed every 1 to 4 hours at r.t. or every 6 to 9 hours at 4 ^oC. The chromogenic reactions were allowed to continue until a desired empirically determined time point that ranged from 3 hours to more than 1 week. After which, the sections were washed in

0.1% Tween-20 (Sigma-Aldrich) in PBS for 3 times at 10 minutes each at r.t., rinsed quickly in autoclaved dd H_2O once at r.t., dried completely at r.t. for a minimum of 20 minutes, before mounting in water-based Fluoromount-G (Catalog number: 0100-01, SouthernBiotech, USA) with glass cover slips (Catalog number: 16004-312, VWR, USA) and nail polish for permanent storage at 4 ^{o}C.

5.2.2. *In situ* hybridization combined with immunohistochemistry.

ISH procedures were performed as described in 2.5.2.A. and following procedures for immunohistochemistry (IHC) after ISH were carried out at r.t. unless otherwise stated. Once the desired chromogenic signal was obtained, the sections were washed in 0.1% Tween-20 (Sigma-Aldrich) in PBS for 3 times at 10 minutes each, re-fixed in 4% PFA for 10 minutes, and rinsed in PBS for 3 times at 10 minutes each. Endogenous peroxidases were inactivated by incubating the sections in 0.5% hydrogen peroxide in ethanol for 30 minutes with agitation. Sections were then washed in PBS for 3 times at 2 minutes each, rinsed in 0.05% Tween-20 (Sigma-Aldrich) in PBS for 10 minutes, before blocking in Blocking solution (0.05% Tween-20, 20% serum in PBS) for 30 minutes. Sections were incubated with primary antibody diluted in 0.05% Tween-20 (Sigma-Aldrich) and 5% serum in PBS at 4 ^{o}C overnight. The following primary antibodies and their respective dilutions were used: rat anti-CTIP2, 1:1000 (Catalog number: AB18465, Abcam, USA), rabbit anti-CUX1 (CDP M-222), 1:100 (Catalog number: SC13024, Santa Cruz Biotechnology, USA), mouse anti-SATB2, 1:50 (Catalog number: AB51502, Abcam, USA), rabbit anti-PARVALBUMIN, 1:500 (Catalog number: PV25, Swant, USA), rabbit anti-OLIG2, 1:100 (Catalog number: 18953, Immuno-biological lab, USA), mouse anti-APC (AP-7, CC-1), 1:500 (Catalog number: OP80, EMD Millipore, USA), rabbit anti-S100β, 1:2000 (Catalog

number: ab41548, Abcam, USA). The next day, the sections were washed in Blocking solution for 3 times at 10 minutes each before incubating with relevant biotin-conjugated secondary antibody (Vector Laboratories, USA) diluted 1:200 in 0.05% Tween-20 (Sigma-Aldrich) and 5% serum in PBS for 1 to 2 hours. The following secondary biotinylated antibodies were used: goat anti-rat IgG (Catalog number: BA-9400), goat anti-rabbit IgG (Catalog number: BA-1000), goat anti-mouse IgG (Catalog number: BA-9200). The sections were then washed in 0.05% Tween-20 (Sigma-Aldrich) in PBS for 3 times at 10 minutes each before incubating with freshly prepared AB solution (1 drop of solution A and 1 drop of solution B in 5 mL of 0.05% Tween-20 in PBS mixed well and kept in dark for 30 minutes before usage, VectaStain Elite ABC kit, catalog number: PK-6100, Vector Laboratories, USA) for 1 hour. After which, the sections were washed in 0.05% Tween-20 (Sigma-Aldrich) in PBS for 3 times at 10 minutes each. Chromogenic reaction was allowed to developed by incubating sections with DAB solution (2 drops of buffer solution, 4 drops of DAB, 2 drops of hydrogen peroxidase in 5 mL of distilled H_2O mixed well and kept in dark before usage, DAB Peroxidase Substrate Kit, 3,3'-diaminobenzidine, catalog number: SK-4100, Vector Laboratories, USA) in the dark for an empirically determined duration that ranged from 2 to 30 minutes. Once the desired IHC signal was achieved, the chromogenic reaction was stopped by rinsing in distilled H_2O. After which, the sections were dried completely for a minimum of 20 minutes, before mounting in water-based Fluoromount-G (Catalog number: 0100-01, SouthernBiotech, USA) with glass cover slips (Catalog number: 16004-312, VWR, USA) and nail polish for permanent storage at 4 ^{o}C.

5.3. Histological staining.

5.3.1. Nissl staining.

Nissl staining was performed at r.t. unless otherwise stated. Floating sections were matched if necessary, and were mounted on Superfrost Plus slides (Catalog number: 12-550-15, Fisher Scientific, USA) in autoclaved deionised water (dd H_2O) and left to dry completely for at least 20 minutes. Sections were dehydrated in 70% ethanol for 2 to 3 minutes, 95% ethanol for 2 to 3 minutes and then 100% ethanol for 2 times for 2 to 3 minutes each before being immersed in xylene for at least 2 hours. After which, the sections were gradually rehydrated by being immersed in 100% ethanol for 2 times at 2 to 3 minutes each, 95% ethanol for 2 to 3 minutes, and then 70% ethanol for 2 to 3 minutes before they were rinsed in 50% ethanol for 2 to 3 minutes. Sections were washed in deionised water (ddH_2O) for 5 minutes and stained with filtered Cresyl Violet stain (0.2% cresyl violet, 0.5% acetic anhydrate, 0.01 M sodium acetate, 0.02 M sodium hydroxide in ddH_2O) for 2 to 5 minutes (determined empirically). Sections were then washed in ddH_2O for 1 minute, rinsed in 50% ethanol for 2 minutes, bled in 70% ethanol for 2 to 10 minutes, bled again in 90% ethanol for 2 to 10 minutes before being immersed in 100% ethanol for 2 times at 2 to 10 minutes each. The time taken for each bleeding step in a series of increasing ethanol washes was determined empirically and was dependent on the final color stained by the sections. After the desired color and stain were achieved, sections were immediately put in xylene for at least 2 hours, before being mounted in xylene-based DPX Mountant (Catalog number: 44581, Sigma-Aldrich, USA) with glass cover slips (Catalog number: 16004-312, VWR, USA) for permanent storage at 4 ^{o}C.

5.3.2. Neurosilver staining.

Neurosilver staining was performed at r.t. unless otherwise stated. Floating sections were matched if necessary, and were transferred into netwells (Catalog number: 07-200-212, Corning, USA). Control sections (Catalog number: PCS101, FD NeuroTechnologies, USA) were used in each experiment to act as positive controls for the staining. Neurosilver staining was carried out with the FD Neurosilver Kit II (Catalog number: PK301, FD NeuroTechnologies, USA) in accordance with the manufacturer's protocol. All sections were covered during incubation to prevent the reagents from splashing and vaporizing. Sections were also fully immersed in the solution involved and were incubated free floating with agitation. Sections were rinsed with Milli-Q water for 2 times for 5 minutes each and transferred into a mixture containing equal volumes of Solutions A and B for 2 times for 10 minutes each before being placed in a mixture consisting of equal volumes of Solutions A and B with Solution E (1 drop of Solution E for each 8 mL of a total volume of Solutions A and B) for 10 minutes. Sections were then transferred into a mixture of Solution C and Solution F (1 drop of Solution F for each 25 mL of Solution C) for 2 times for 2 minutes each. Incubation time with Solution C and F was determined empirically, and could be lengthened to decrease the background stain or shortened to increase the staining intensity. Sections were then rinsed in a mixture of Solution D and Solution F (1 drop of Solution F for each 25 mL of Solution D) for 5 minutes, washed in Milli-Q water for 2 times for 3 minutes each, immersed in diluted 1X Solution G in Milli-Q water for 2 times for 5 minutes each before being shaken in dark for 1 to 2 hours in diluted 1X Solution G. Sections were mounted in diluted 1X Solution G on Superfrost Plus slides (Catalog number: 12-550-15, Fisher Scientific, USA) and left to dry completely for at least 20 minutes in the dark. Sections were then cleared in xylene for 3 times for 3 minutes each before being mounted in xylene-based DPX Mountant

(Catalog number: 44581, Sigma-Aldrich, USA) with glass cover slips (Catalog number: 16004-312, VWR, USA) for permanent storage at 4 ^{o}C.

5.4. Immunohistochemistry.

5.4.1. Fluorescent immunohistochemistry.

Fluorescent IHC procedures were carried out at r.t. unless otherwise stated. Floating sections were matched, if necessary, and were transferred into netwells (Catalog number: 07-200-212, Corning, USA). Sections were washed in PBS for 3 times at 5 minutes each with agitation before blocking in Blocking buffer (0.3% bovine serum albumin, 8% serum, 0.3% Triton X-100 in PBS-Azide) for 1 hour with agitation. The sections were then incubated with primary antibody diluted appropriately in Blocking buffer overnight at 4 ^{o}C with agitation. The following primary antibodies and relevant dilutions were used: mouse anti-NeuN, 1:500 (Catalog number: MAB377, Millipore, USA), rabbit anti-CUX1 (CDP M-222), 1:100 (Catalog number: SC13024, Santa Cruz Biotechnology, USA), mouse anti-SATB2, 1:50 (Catalog number: AB51502, Abcam, USA), rat anti-CTIP2, 1:1000 (Catalog number: AB18465, Abcam, USA). rabbit anti-NEUROFILAMENT 200, 1:200 (Catalog number: N4142, Sigma-Aldrich, USA), rat anti-MBP a.a. 82-87, 1:100 (Catalog number: MAB386, Millipore, USA), rabbit anti-OLIG2, 1:100 (Catalog number: 18953, Immuno-biological lab, USA), rat anti-CD140a (or PDGF Receptor α chain), 1:100 (Catalog number: 558774, BD Pharmingen, USA) and mouse anti-APC (AP-7, CC-1), 1:500 (Catalog number: OP80, EMD Millipore, USA). The next day, sections were washed in PBS for 3 times at 10 minutes each with agitation before incubation with appropriate secondary antibodies (Molecular Probes Alexa series, Invitrogen, USA) diluted 1:750 in Blocking buffer for 2 hours with agitation. After which, the sections were counterstained for 4',6-diamidino-2-phenylindole (DAPI) diluted 1:50000 in PBS for 2 to 4 minutes with agitation before rinsing in PBS for 3 times at 10 minutes each with agitation. Sections were then mounted on Superfrost slides (Catalog number: 22-178-277, Fisher Scientific,

USA) in autoclaved deionised water (dd H_2O) and left to dry completely for a minimal time of at least 20 minutes in the dark. For confocal microscopy, the dried sections were mounted in water-based Fluoromount-G (Catalog number: 0100-01, SouthernBiotech, USA) or DAPI-Fluoromount-G if DAPI counterstain was not used prior (Catalog number: 0100-20, SouthernBiotech, USA) with glass cover slips (Catalog number: 16004-312, VWR, USA) and nail polish for permanent storage at 4 ^{o}C. For regular fluorescent microscopy, dried sections were mounted in xylene-based DPX Mountant (Catalog number: 44581, Sigma-Aldrich, USA) with glass cover slips (Catalog number: 16004-312, VWR, USA) for permanent storage at 4 ^{o}C.

5.4.2. Chromogenic immunohistochemistry.

Floating sections were matched, if necessary, and were transferred into netwells (Catalog number: 07-200-212, Corning, USA). Sections were washed in PBS for 3 times at 10 minutes each with agitation before inactivation of endogenous peroxidases. This inactivation step and subsequent procedures were performed in accordance to the IHC method after ISH, as described in 2.5.2.B. The following primary antibody and its dilution were used: rat anti-MBP a.a. 82-87, 1:100 (Catalog number: MAB386, Millipore, USA).

5.5. Quantification analysis

5.5.1. Quantification of distinct PN populations.

5 to 6 anatomically matched sections from each mutant mouse (n = 3 wild type, n = 3 *Ppargc1α*$^{-/-}$, n = 3 *Ppargc1α*$^{fl/fl}$ and n = 3 *Emx1-Cre; Ppargc1α*$^{fl/fl}$ mice at 2 months of age) were selected and immunostained for CUX1, SATB2 and CTIP2 as described in section 5.4.1.. Littermate controls were used in all quantifications. Quantification was done for cells in the primary motor, somatosensory aand visual area (n = 2 to 3 sections per area per animal) and positive cells were defined by comparing to control staining. Quantification was executed with the ImageJ software (Rasband, W.S., ImageJ, U. S. National Institutes of Health, Bethesda, Maryland, USA, http://imagej.nih.gov/ij/, 1997-2012.). Statistical analysis was achieved with the two tailed student's T test and p values were calculated with Microsoft Excel 2003 software.

5.5.2. Quantification of distinct MBP-positive vacuoles.

5 anatomically matched sections from each mutant mouse (n = 3 *Ppargc1α*$^{fl/fl}$ and n = 3 *Emx1-Cre; Ppargc1α*$^{fl/fl}$ mice at 2 months of age) were selected and immunostained for MBP as described in section 5.4.1.. Littermate controls were used in all quantifications. Quantification was done for cells in the primary motor, somatosensory aand visual area (n = 1 section per area per animal) and positive vacuoles were defined by comparing to control staining. The full cortical thickness was divided into 10 bins of equal area. Statistical analysis was achieved with the two tailed student's T test and p values were calculated with Microsoft Excel 2003 software.

5.5.3. Quantification of distinct oligodendrocyte populations.

5 anatomically matched sections from each mutant mouse (n = 3 *Ppargc1α*$^{fl/fl}$ and n = 3 *Emx1-Cre; Ppargc1α*$^{fl/fl}$ mice at 2 months of age) were selected and immunostained for OLIG2, PDGFRα and APC, as described in section 4.5.3.B.. Quantification was done for cells in the primary somatosensory area (n = 2 sections per animal, n = 3 animals per genotype) and positive cells were defined by comparing to control staining. The full cortical thickness was divided into 10 bins of equal area. An investigator blinded to the genotype of the samples quantified the number of positive cells in each bin. Statistical analysis was achieved with the two tailed student's T test and p values were calculated with Microsoft Excel 2003 software. Travis Hallett is currently confirming these quantifications by analyzing additional sections across more animals.

5.6. Gain-of-function analysis.

5.6.1. Vector constructs.

For gain-of-function analysis to test the overexpression of *Ppargc1α* in cortical progenitors, a control vector with a constitutively active CMV enhancer / β actin promoter driving an internal ribosomal entry site (IRES) was used (6). This construct was generated and generously given by Prof. Carlos Lois from the Department of Brain and Cognitive Sciences, Massachusetts Institute of Technology in Cambridge, Massachusetts, USA. For the *Ppargc1α* induction construct, PCR fragments of full length *Ppargc1α* cDNA with XhoI and HpaI restriction enzyme sites at its 5' and 3' ends respectively were generated from a pSport1 vector from Open Biosystems (Accession number: BC066868, clone ID: 30094033, catalog number: MMM1013-9201993, Thermo Scientific, USA), with AccuPrime Pfx DNA polymerase (Catalog number: 12344-024, Invitrogen, USA) in accordance with manufacturer's protocol. Primers for *Ppargc1α* were used, as shown in Table 5.3.. PCR fragments were cut with XhoI and HpaI (New England BioLabs, USA), ligated to similarly cut $Control^{GFP}$ vector with the Quick Ligation Kit (Catalog number: M2200L, New England BioLabs, USA) and transformed into Top10 competent cells. Clones were screened by restriction enzyme digest and sequenced with sequencing primers as described in Table 5.3.. A sequenced clone that is perfectly aligned to the murine *Ppargc1α* reference sequence BC066868.1 in both the sense and antisense orientations was selected for downstream analysis. This clone expressed *Ppargc1α* with a constitutively active CMV enhancer / β actin promoter and had a reporter IRES-EGFP ($Ppargc1\alpha^{GFP}$, Figure 3.7.A.).

Table 5.3. Cloning and sequencing primers used to generate the *Ppargc1α*^{GFP} construct.

This table summarizes the different cloning and sequencing primers used to generate the *Ppargc1α*^{GFP} construct, as described in section 5.6.1..

Table 5.3. (Continued)

Ppargc1α		
Cloning	Forward	5’ – AAATTTCTCGAGACCACCATGGCTTGGGACATGTGC – 3’
	Reverse	5’ – AAA TTT GTT AAC TTA CCT GCG CAA GCT TCT C – 3’
Sequencing	Forward	5’ – GCC AAC ACT CAG CTC AGC TAC – 3’
		5’ – TTG CAA GAC CGT GGT GCC – 3’
		5’ – AGG GAT GGC GAC TTC AGT AA – 3’
		5’ – GAG AAG CGG GAG TCT GAA AG – 3’
	Reverse	5’ – AAC AAT GGC AGG GTT TGT TC – 3’
		5’ – CCC TTT CTT GGT GGA GTG G – 3’
		5’ – TCA CTG TCA TCA AAT AGG CCA – 3’
		5’ – ACC AAC GTA AAT CAC ACG GC – 3’

5.6.2. *In utero* electroporation.

The day of vaginal plug by noon was designated as embryonic day 0.5 (E0.5). At E15.5, timed pregnant C57BL/6 wild type mouse dams were deeply anesthetized with Avertin by intraperitoneal injection, or with 2% isofluorane (Catalog number: 07-806-3204, Webster Vet, USA) by inhalation, and placed on a warm heating pat before, throughout and after the surgery during the recovery period. After a small incision was made at the midline of the anesthetized dam, a vertical midline laparotomy was carried out along the *linea alba* of the abdominal wall. This was followed by separation of the skin and abdominal wall by blunt dissection techniques on the intervening fascia. 690 nL of purified endotoxin-free DNA (1.5 to 2 μg/μL), mixed with 0.005% Fast Green FCF (Catalog number: F7258-25G, Sigma-Aldrich, USA) to enable easy visualization of DNA upon injection, were injected under ultrasound backscatter microscopy (Vevo 770, VisualSonics, USA) guidance into the lateral ventricle. Five pulses of 40 volts each of 50 ms duration at 1 second intervals were delivered into the progenitors of the ventricular zone at the desired orientation with 5 mm diameter CUY650-P5 platinum electrodes (Protech International, USA) and a Nepa Gene square wave electroporator (Catalog number: CUY21EDIT, Nepa Gene, Japan). DNA was delivered by *in utero* electroporation to non-sequential embryos along each horn, excluding the two embryos closest to the birth canal.

5.7. Neuronal metabolism analysis.

5.7.1. Tissue collection.

P14 and 2 month adult *Emx1-Cre; Ppargc1α*$^{fl/fl}$ and littermate control *Ppargc1α*$^{fl/fl}$ mice were terminated by cervical dislocation. Their brains were quickly removed by manual dissection and sectioned immediately at 999 μm thickness with cold PBS coronally with a VT1000S vibrating microtome (Leica Microsystems). Approximately 3 to 4 sections were obtained per brain. Tissue from the deep layers were collected with tissue punches of 0.35 mm diameter (Catalog number: 15070, Ted Pella Inc., USA) into a 1.5 mL eppendorf tube. These were immediately frozen with dry ice and stored at -80 ^{o}C before further downstream analysis. 8 tissue punches were collected per hemisphere with a total of 48 punches collected across 6 hemispheres of 3 sections (Figure 3.10.).

5.7.2. High performance liquid chromatography and mass spectrometry analysis.

Frozen tissue punches were resuspended with 2% acetonitrile in dd H_2O, centrifuged to collect the samples, and triturated by pipetting up and down slowly for 10 times before freezing on dry ice for 2 minutes. Samples were then thawed at r.t. for 3 minutes, further triturated by pipetting up and down for 12 times before being centrifugated at 5000 rpm for 10 minutes at 4 ^{o}C. Supernatant was removed, kept on dry ice and processed immediately for high performance liquid chromatography and mass spectrometry analysis by Mr. Kelly Chatman at the Small Molecule Mass Spectrometry Facility, FAS Center for System Biology, Harvard University in Cambridge, Massachusetts, USA. Detection and quantification of Lactate, Taurine, Creatine, and N-Acetyl-Aspartate were achieved by LC/MS/MS analysis performed with an Agilent (Agilent Technologies, Santa Clara, CA) 6460 triple-quadrupole LC/MS/MS system employing a novel

LC/MS/MS method. The ([M - H+] - / product ion) monitored via electrospray ionization in the negative ion mode with multiple reaction monitoring (MRM) were Lactate (89.02/43.1 amu), Taurine (130.06/41.1 amu), Creatine (124.0/80.0 amu) and N-Acetyl-Aspartate (174.04/88.0 amu). Mass spectrometer parameter settings were gas temp (350 °C), gas flow (12 L/min), nebulizer pressure (35 psi), sheath gas heater (400 °C), sheath gas flow (12 L/min), and capillary (4000V). An external standard curve mixture was prepared and analyzed at various concentrations ranging from 10 pg/uL to 1000 pg/uL and utilized for quantification. Reversed phase chromatography conditions with a Agilent Eclipse XDB-C18 5 uM 4.6 x 150 mm column were as follows: flow rate: 0.4 mLs/min; solvent A: 0.1% formic acid; solvent B: 0.1% formic acid in acetonitrile. The gradient was as follows: t = 0 min, 2% B; t = 5 min, 2% B; t = 10 min, 100% B; t = 11, 100%B; t = 11.1 min, 2% B; 3 minute equilibration. Concentrations for each compound were calculated and expressed in pg/mL. All experimental readings were then normalized to relevant creatine levels determined per experiment. Normalized readings were processed as a ratio of mutant over control. For P14 samples, n = 5 *Emx1-Cre; Ppargc1α*$^{fl/fl}$ and n = 3 littermate control *Ppargc1α*$^{fl/fl}$ murine samples were collected over 2 distinct experiments. For 2 month old adult samples, n = 7 *Emx1-Cre; Ppargc1α*$^{fl/fl}$ and n = 5 littermate control *Ppargc1α*$^{fl/fl}$ murine samples were collected over 3 different experiments. A two tailed student's T test was performed for comparative analysis based on the ratios obtained and significant values were calculated, as shown in section 3.3.11 and Figure 3.8..

5.8. Microscopy and image analysis.

Mounted sections were imaged on a Nikon 90i microscope (Catalog number: MVI 91933, Nikon Instruments, USA) with an XCite 120 illuminator (Catalog number: MVI 87541, EXFO, Canada) and Q-imaging 5 megapixel cooled CCD digital camera (Nikon Instruments, USA). Images were collected either in brightfield or fluorescence and analyzed with Volocity image analysis software (Version 6.0.1; Improvision Inc., USA).

Images were further processed with Adobe Photoshop/Illustrator software packages (CS5, Version 12.0.3, Adobe, USA).

References

1. Molyneaux BJ, Arlotta P, Menezes JR, Macklis JD. Neuronal subtype specification in the cerebral cortex. Nat Rev Neurosci. 2007 Jun;8(6):427-37.

2. Bayer SA, Altman J. Neocortical development. New York: Raven; 1991.

3. Rakic P. Mode of cell migration to the superficial layers of fetal monkey neocortex. J Comp Neurol. 1972 May;145(1):61-83.

4. Marin O, Rubenstein JL. A long, remarkable journey: Tangential migration in the telencephalon. Nat Rev Neurosci. 2001 Nov;2(11):780-90.

5. Arlotta P, Molyneaux BJ, Chen J, Inoue J, Kominami R, Macklis JD. Neuronal subtype-specific genes that control corticospinal motor neuron development in vivo. Neuron. 2005 Jan 20;45(2):207-21.

6. Molyneaux BJ, Arlotta P, Hirata T, Hibi M, Macklis JD. Fezl is required for the birth and specification of corticospinal motor neurons. Neuron. 2005 Sep 15;47(6):817-31.

7. Chen B, Schaevitz LR, McConnell SK. Fezl regulates the differentiation and axon targeting of layer 5 subcortical projection neurons in cerebral cortex. Proc Natl Acad Sci U S A. 2005 Nov 22;102(47):17184-9.

8. Chen B, Wang SS, Hattox AM, Rayburn H, Nelson SB, McConnell SK. The Fezf2-Ctip2 genetic pathway regulates the fate choice of subcortical projection neurons in the developing cerebral cortex. Proc Natl Acad Sci U S A. 2008 Aug 12;105(32):11382-7.

9. Chen JG, Rasin MR, Kwan KY, Sestan N. Zfp312 is required for subcortical axonal projections and dendritic morphology of deep-layer pyramidal neurons of the cerebral cortex. Proc Natl Acad Sci U S A. 2005 Dec 6;102(49):17792-7.

10. Rouaux C, Arlotta P. Fezf2 directs the differentiation of corticofugal neurons from striatal progenitors in vivo. Nat Neurosci. 2010 Nov;13(11):1345-7.

11. Rouaux C, Arlotta P. Direct lineage reprogramming of post-mitotic callosal neurons into corticofugal neurons in vivo. Nat Cell Biol. 2013 Feb;15(2):214-21.

12. Embryonic vertebrate central nervous system: Revised terminology. the boulder committee. Anat Rec. 1970 Feb;166(2):257-61.

13. Angevine JB,Jr, Sidman RL. Autoradiographic study of cell migration during histogenesis of cerebral cortex in the mouse. Nature. 1961 Nov 25;192:766-8.

14. Caviness VS,Jr, Takahashi T. Proliferative events in the cerebral ventricular zone. Brain Dev. 1995 May-Jun;17(3):159-63.

15. Rakic P. Neurons in rhesus monkey visual cortex: Systematic relation between time of origin and eventual disposition. Science. 1974 Feb 1;183(123):425-7.

16. O'Leary DD, Nakagawa Y. Patterning centers, regulatory genes and extrinsic mechanisms controlling arealization of the neocortex. Curr Opin Neurobiol. 2002 Feb;12(1):14-25.

17. Kasper EM, Lubke J, Larkman AU, Blakemore C. Pyramidal neurons in layer 5 of the rat visual cortex. III. differential maturation of axon targeting, dendritic morphology, and electrophysiological properties. J Comp Neurol. 1994 Jan 22;339(4):495-518.

18. Molnar Z, Cheung AF. Towards the classification of subpopulations of layer V pyramidal projection neurons. Neurosci Res. 2006 Jun;55(2):105-15.

19. Molnar Z, Metin C, Stoykova A, Tarabykin V, Price DJ, Francis F, et al. Comparative aspects of cerebral cortical development. Eur J Neurosci. 2006 Feb;23(4):921-34.

20. O'Leary DD, Koester SE. Development of projection neuron types, axon pathways, and patterned connections of the mammalian cortex. Neuron. 1993 Jun;10(6):991-1006.

21. Price DJ, Kennedy H, Dehay C, Zhou L, Mercier M, Jossin Y, et al. The development of cortical connections. Eur J Neurosci. 2006 Feb;23(4):910-20.

22. Kriegstein A, Noctor S, Martinez-Cerdeno V. Patterns of neural stem and progenitor cell division may underlie evolutionary cortical expansion. Nat Rev Neurosci. 2006 Nov;7(11):883-90.

23. Noctor SC, Martinez-Cerdeno V, Ivic L, Kriegstein AR. Cortical neurons arise in symmetric and asymmetric division zones and migrate through specific phases. Nat Neurosci. 2004 Feb;7(2):136-44.

24. Takahashi T, Nowakowski RS, Caviness VS,Jr. Mode of cell proliferation in the developing mouse neocortex. Proc Natl Acad Sci U S A. 1994 Jan 4;91(1):375-9.

25. Bertrand N, Castro DS, Guillemot F. Proneural genes and the specification of neural cell types. Nat Rev Neurosci. 2002 Jul;3(7):517-30.

26. Englund C, Fink A, Lau C, Pham D, Daza RA, Bulfone A, et al. Pax6, Tbr2, and Tbr1 are expressed sequentially by radial glia, intermediate progenitor cells, and postmitotic neurons in developing neocortex. J Neurosci. 2005 Jan 5;25(1):247-51.

27. Gohlke JM, Armant O, Parham FM, Smith MV, Zimmer C, Castro DS, et al. Characterization of the proneural gene regulatory network during mouse telencephalon development. BMC Biol. 2008 Mar 31;6:15.

28. Guillemot F. Cell fate specification in the mammalian telencephalon. Prog Neurobiol. 2007 Sep;83(1):37-52.

29. Guillemot F. Cellular and molecular control of neurogenesis in the mammalian telencephalon. Curr Opin Cell Biol. 2005 Dec;17(6):639-47.

30. Muzio L, DiBenedetto B, Stoykova A, Boncinelli E, Gruss P, Mallamaci A. Conversion of cerebral cortex into basal ganglia in Emx2(-/-) Pax6(Sey/Sey) double-mutant mice. Nat Neurosci. 2002 Aug;5(8):737-45.

31. Quinn JC, Molinek M, Martynoga BS, Zaki PA, Faedo A, Bulfone A, et al. Pax6 controls cerebral cortical cell number by regulating exit from the cell cycle and specifies cortical cell identity by a cell autonomous mechanism. Dev Biol. 2007 Feb 1;302(1):50-65.

32. O'Leary DD, Chou SJ, Sahara S. Area patterning of the mammalian cortex. Neuron. 2007 Oct 25;56(2):252-69.

33. Lai T, Jabaudon D, Molyneaux BJ, Azim E, Arlotta P, Menezes JR, et al. SOX5 controls the sequential generation of distinct corticofugal neuron subtypes. Neuron. 2008 Jan 24;57(2):232-47.

34. Alcamo EA, Chirivella L, Dautzenberg M, Dobreva G, Fariñas I, Grosschedl R, et al. Satb2 regulates callosal projection neuron identity in the developing cerebral cortex. Neuron. 2008 2/7;57(3):364-77.

35. Britanova O, de Juan Romero C, Cheung A, Kwan KY, Schwark M, Gyorgy A, et al. Satb2 is a postmitotic determinant for upper-layer neuron specification in the neocortex. Neuron. 2008 Feb 7;57(3):378-92.

36. Molyneaux BJ, Arlotta P, Fame RM, MacDonald JL, MacQuarrie KL, Macklis JD. Novel subtype-specific genes identify distinct subpopulations of callosal projection neurons. J Neurosci. 2009 Sep 30;29(39):12343-54.

37. Lodato S, Rouaux C, Quast KB, Jantrachotechatchawan C, Studer M, Hensch TK, et al. Excitatory projection neuron subtypes control the distribution of local inhibitory interneurons in the cerebral cortex. Neuron. 2011 Feb 24;69(4):763-79.

38. Lin J, Handschin C, Spiegelman BM. Metabolic control through the PGC-1 family of transcription coactivators. Cell Metab. 2005 Jun;1(6):361-70.

39. Spiegelman BM, Heinrich R. Biological control through regulated transcriptional coactivators. Cell. 2004 Oct 15;119(2):157-67.

40. Liu C, Lin JD. PGC-1 coactivators in the control of energy metabolism. Acta Biochim Biophys Sin (Shanghai). 2011 Apr;43(4):248-57.

41. Tiefenbock SK, Baltzer C, Egli NA, Frei C. The drosophila PGC-1 homologue spargel coordinates mitochondrial activity to insulin signalling. EMBO J. 2010 Jan 6;29(1):171-83.

42. Puigserver P, Wu Z, Park CW, Graves R, Wright M, Spiegelman BM. A cold-inducible coactivator of nuclear receptors linked to adaptive thermogenesis. Cell. 1998 Mar 20;92(6):829-39.

43. Kressler D, Schreiber SN, Knutti D, Kralli A. The PGC-1-related protein PERC is a selective coactivator of estrogen receptor alpha. J Biol Chem. 2002 Apr 19;277(16):13918-25.

44. Lin J, Puigserver P, Donovan J, Tarr P, Spiegelman BM. Peroxisome proliferator-activated receptor gamma coactivator 1beta (PGC-1beta), a novel PGC-1-related transcription coactivator associated with host cell factor. J Biol Chem. 2002 Jan 18;277(3):1645-8.

45. Andersson U, Scarpulla RC. Pgc-1-related coactivator, a novel, serum-inducible coactivator of nuclear respiratory factor 1-dependent transcription in mammalian cells. Mol Cell Biol. 2001 Jun;21(11):3738-49.

46. Puigserver P, Adelmant G, Wu Z, Fan M, Xu J, O'Malley B, et al. Activation of PPARgamma coactivator-1 through transcription factor docking. Science. 1999 Nov 12;286(5443):1368-71.

47. Knutti D, Kaul A, Kralli A. A tissue-specific coactivator of steroid receptors, identified in a functional genetic screen. Mol Cell Biol. 2000 Apr;20(7):2411-22.

48. Huss JM, Kopp RP, Kelly DP. Peroxisome proliferator-activated receptor coactivator-1alpha (PGC-1alpha) coactivates the cardiac-enriched nuclear receptors estrogen-related receptor-alpha and -gamma. identification of novel leucine-rich interaction motif within PGC-1alpha. J Biol Chem. 2002 Oct 25;277(43):40265-74.

49. Huss JM, Torra IP, Staels B, Giguere V, Kelly DP. Estrogen-related receptor alpha directs peroxisome proliferator-activated receptor alpha signaling in the transcriptional control of energy metabolism in cardiac and skeletal muscle. Mol Cell Biol. 2004 Oct;24(20):9079-91.

50. Kamei Y, Ohizumi H, Fujitani Y, Nemoto T, Tanaka T, Takahashi N, et al. PPARgamma coactivator 1beta/ERR ligand 1 is an ERR protein ligand, whose expression induces a high-energy expenditure and antagonizes obesity. Proc Natl Acad Sci U S A. 2003 Oct 14;100(21):12378-83.

51. Wu H, Kanatous SB, Thurmond FA, Gallardo T, Isotani E, Bassel-Duby R, et al. Regulation of mitochondrial biogenesis in skeletal muscle by CaMK. Science. 2002 Apr 12;296(5566):349-52.

52. Zhang Y, Ma K, Song S, Elam MB, Cook GA, Park EA. Peroxisomal proliferator-activated receptor-gamma coactivator-1 alpha (PGC-1 alpha) enhances the thyroid hormone induction of carnitine palmitoyltransferase I (CPT-I alpha). J Biol Chem. 2004 Dec 24;279(52):53963-71.

53. Shin DJ, Campos JA, Gil G, Osborne TF. PGC-1alpha activates CYP7A1 and bile acid biosynthesis. J Biol Chem. 2003 Dec 12;278(50):50047-52.

54. Wu Z, Puigserver P, Andersson U, Zhang C, Adelmant G, Mootha V, et al. Mechanisms controlling mitochondrial biogenesis and respiration through the thermogenic coactivator PGC-1. Cell. 1999 Jul 9;98(1):115-24.

55. Mootha VK, Lindgren CM, Eriksson KF, Subramanian A, Sihag S, Lehar J, et al. PGC-1alpha-responsive genes involved in oxidative phosphorylation are coordinately downregulated in human diabetes. Nat Genet. 2003 Jul;34(3):267-73.

56. Puigserver P, Rhee J, Lin J, Wu Z, Yoon JC, Zhang CY, et al. Cytokine stimulation of energy expenditure through p38 MAP kinase activation of PPARgamma coactivator-1. Mol Cell. 2001 Nov;8(5):971-82.

57. Heery DM, Kalkhoven E, Hoare S, Parker MG. A signature motif in transcriptional co-activators mediates binding to nuclear receptors. Nature. 1997 Jun 12;387(6634):733-6.

58. Wallberg AE, Yamamura S, Malik S, Spiegelman BM, Roeder RG. Coordination of p300-mediated chromatin remodeling and TRAP/mediator function through coactivator PGC-1alpha. Mol Cell. 2003 Nov;12(5):1137-49.

59. Borgius LJ, Steffensen KR, Gustafsson JA, Treuter E. Glucocorticoid signaling is perturbed by the atypical orphan receptor and corepressor SHP. J Biol Chem. 2002 Dec 20;277(51):49761-6.

60. Guan HP, Ishizuka T, Chui PC, Lehrke M, Lazar MA. Corepressors selectively control the transcriptional activity of PPARgamma in adipocytes. Genes Dev. 2005 Feb 15;19(4):453-61.

61. Puigserver P, Spiegelman BM. Peroxisome proliferator-activated receptor-gamma coactivator 1 alpha (PGC-1 alpha): Transcriptional coactivator and metabolic regulator. Endocr Rev. 2003 Feb;24(1):78-90.

62. Leone TC, Lehman JJ, Finck BN, Schaeffer PJ, Wende AR, Boudina S, et al. PGC-1alpha deficiency causes multi-system energy metabolic derangements: Muscle dysfunction, abnormal weight control and hepatic steatosis. PLoS Biol. 2005 Apr;3(4):e101.

63. Lin J, Wu PH, Tarr PT, Lindenberg KS, St-Pierre J, Zhang CY, et al. Defects in adaptive energy metabolism with CNS-linked hyperactivity in PGC-1alpha null mice. Cell. 2004 Oct 1;119(1):121-35.

64. Tiraby C, Tavernier G, Lefort C, Larrouy D, Bouillaud F, Ricquier D, et al. Acquirement of brown fat cell features by human white adipocytes. J Biol Chem. 2003 Aug 29;278(35):33370-6.

65. Olesen J, Kiilerich K, Pilegaard H. PGC-1alpha-mediated adaptations in skeletal muscle. Pflugers Arch. 2010 Jun;460(1):153-62.

66. Clayton DA. Replication and transcription of vertebrate mitochondrial DNA. Annu Rev Cell Biol. 1991;7:453-78.

67. Virbasius JV, Scarpulla RC. Activation of the human mitochondrial transcription factor A gene by nuclear respiratory factors: A potential regulatory link between nuclear and mitochondrial gene expression in organelle biogenesis. Proc Natl Acad Sci U S A. 1994 Feb 15;91(4):1309-13.

68. Lin J, Wu H, Tarr PT, Zhang CY, Wu Z, Boss O, et al. Transcriptional co-activator PGC-1 alpha drives the formation of slow-twitch muscle fibres. Nature. 2002 Aug 15;418(6899):797-801.

69. Lehman JJ, Barger PM, Kovacs A, Saffitz JE, Medeiros DM, Kelly DP. Peroxisome proliferator-activated receptor gamma coactivator-1 promotes cardiac mitochondrial biogenesis. J Clin Invest. 2000 Oct;106(7):847-56.

70. Arany Z, He H, Lin J, Hoyer K, Handschin C, Toka O, et al. Transcriptional coactivator PGC-1 alpha controls the energy state and contractile function of cardiac muscle. Cell Metab. 2005 Apr;1(4):259-71.

71. Russell LK, Mansfield CM, Lehman JJ, Kovacs A, Courtois M, Saffitz JE, et al. Cardiac-specific induction of the transcriptional coactivator peroxisome proliferator-activated receptor gamma coactivator-1alpha promotes mitochondrial biogenesis and reversible cardiomyopathy in a developmental stage-dependent manner. Circ Res. 2004 Mar 5;94(4):525-33.

72. St-Pierre J, Drori S, Uldry M, Silvaggi JM, Rhee J, Jager S, et al. Suppression of reactive oxygen species and neurodegeneration by the PGC-1 transcriptional coactivators. Cell. 2006 Oct 20;127(2):397-408.

73. Cui L, Jeong H, Borovecki F, Parkhurst CN, Tanese N, Krainc D. Transcriptional repression of PGC-1alpha by mutant huntingtin leads to mitochondrial dysfunction and neurodegeneration. Cell. 2006 Oct 6;127(1):59-69.

74. Weydt P, Pineda VV, Torrence AE, Libby RT, Satterfield TF, Lazarowski ER, et al. Thermoregulatory and metabolic defects in huntington's disease transgenic mice implicate PGC-1alpha in huntington's disease neurodegeneration. Cell Metab. 2006 Nov;4(5):349-62.

75. Zheng B, Liao Z, Locascio JJ, Lesniak KA, Roderick SS, Watt ML, et al. PGC-1alpha, a potential therapeutic target for early intervention in parkinson's disease. Sci Transl Med. 2010 Oct 6;2(52):52ra73.

76. Shin JH, Ko HS, Kang H, Lee Y, Lee YI, Pletinkova O, et al. PARIS (ZNF746) repression of PGC-1alpha contributes to neurodegeneration in parkinson's disease. Cell. 2011 Mar 4;144(5):689-702.

77. Zhao W, Varghese M, Yemul S, Pan Y, Cheng A, Marano P, et al. Peroxisome proliferator activator receptor gamma coactivator-1alpha (PGC-1alpha) improves motor performance and survival in a mouse model of amyotrophic lateral sclerosis. Mol Neurodegener. 2011 Jul 19;6(1):51,1326-6-51.

78. Liang H, Ward WF, Jang YC, Bhattacharya A, Bokov AF, Li Y, et al. PGC-1alpha protects neurons and alters disease progression in an amyotrophic lateral sclerosis mouse model. Muscle Nerve. 2011 Dec;44(6):947-56.

79. Brockington A, Heath PR, Holden H, Kasher P, Bender FL, Claes F, et al. Downregulation of genes with a function in axon outgrowth and synapse formation in motor neurones of the VEGFdelta/delta mouse model of amyotrophic lateral sclerosis. BMC Genomics. 2010 Mar 26;11:203,2164-11-203.

80. Witte ME, Nijland PG, Drexhage JA, Gerritsen W, Geerts D, van Het Hof B, et al. Reduced expression of PGC-1alpha partly underlies mitochondrial changes and correlates with neuronal loss in multiple sclerosis cortex. Acta Neuropathol. 2013 Feb;125(2):231-43.

81. Qin W, Haroutunian V, Katsel P, Cardozo CP, Ho L, Buxbaum JD, et al. PGC-1alpha expression decreases in the alzheimer disease brain as a function of dementia. Arch Neurol. 2009 Mar;66(3):352-61.

82. Christoforou A, Le Hellard S, Thomson PA, Morris SW, Tenesa A, Pickard BS, et al. Association analysis of the chromosome 4p15-p16 candidate region for bipolar disorder and schizophrenia. Mol Psychiatry. 2007 Nov;12(11):1011-25.

83. Gutsaeva DR, Carraway MS, Suliman HB, Demchenko IT, Shitara H, Yonekawa H, et al. Transient hypoxia stimulates mitochondrial biogenesis in brain subcortex by a neuronal nitric oxide synthase-dependent mechanism. J Neurosci. 2008 Feb 27;28(9):2015-24.

84. Chen SD, Lin TK, Yang DI, Lee SY, Shaw FZ, Liou CW, et al. Protective effects of peroxisome proliferator-activated receptors gamma coactivator-1alpha against neuronal cell death in the hippocampal CA1 subfield after transient global ischemia. J Neurosci Res. 2010 Feb 15;88(3):605-13.

85. Luo Y, Zhu W, Jia J, Zhang C, Xu Y. NMDA receptor dependent PGC-1alpha up-regulation protects the cortical neuron against oxygen-glucose deprivation/reperfusion injury. J Mol Neurosci. 2009 Sep;39(1-2):262-8.

86. Zhu HR, Wang ZY, Zhu XL, Wu XX, Li EG, Xu Y. Icariin protects against brain injury by enhancing SIRT1-dependent PGC-1alpha expression in experimental stroke. Neuropharmacology. 2010 Jul-Aug;59(1-2):70-6.

87. O'Donnell KC, Vargas ME, Sagasti A. WldS and PGC-1alpha regulate mitochondrial transport and oxidation state after axonal injury. J Neurosci. 2013 Sep 11;33(37):14778-90.

88. Xiang Z, Valenza M, Cui L, Leoni V, Jeong HK, Brilli E, et al. Peroxisome-proliferator-activated receptor gamma coactivator 1 alpha contributes to dysmyelination in experimental models of huntington's disease. J Neurosci. 2011 Jun 29;31(26):9544-53.

89. Cowell RM, Blake KR, Inoue T, Russell JW. Regulation of PGC-1alpha and PGC-1alpha-responsive genes with forskolin-induced schwann cell differentiation. Neurosci Lett. 2008 Jul 18;439(3):269-74.

90. Cowell RM, Talati P, Blake KR, Meador-Woodruff JH, Russell JW. Identification of novel targets for PGC-1alpha and histone deacetylase inhibitors in neuroblastoma cells. Biochem Biophys Res Commun. 2009 Feb 6;379(2):578-82.

91. Watkins J, Basu S, Bogenhagen DF. A quantitative proteomic analysis of mitochondrial participation in p19 cell neuronal differentiation. J Proteome Res. 2008 Jan;7(1):328-38.

92. Wareski P, Vaarmann A, Choubey V, Safiulina D, Liiv J, Kuum M, et al. PGC-1{alpha} and PGC-1{beta} regulate mitochondrial density in neurons. J Biol Chem. 2009 Aug 7;284(32):21379-85.

93. Lucas EK, Markwardt SJ, Gupta S, Meador-Woodruff JH, Lin JD, Overstreet-Wadiche L, et al. Parvalbumin deficiency and GABAergic dysfunction in mice lacking PGC-1alpha. J Neurosci. 2010 May 26;30(21):7227-35.

94. Cowell RM, Blake KR, Russell JW. Localization of the transcriptional coactivator PGC-1alpha to GABAergic neurons during maturation of the rat brain. J Comp Neurol. 2007 May 1;502(1):1-18.

95. Cheng A, Wan R, Yang JL, Kamimura N, Son TG, Ouyang X, et al. Involvement of PGC-1alpha in the formation and maintenance of neuronal dendritic spines. Nat Commun. 2012;3:1250.

96. Lucas EK, Dougherty SE, McMeekin LJ, Trinh AT, Reid CS, Cowell RM. Developmental alterations in motor coordination and medium spiny neuron markers in mice lacking pgc-1alpha. PLoS One. 2012;7(8):e42878.

97. Lucas EK, Markwardt SJ, Gupta S, Meador-Woodruff JH, Lin JD, Overstreet-Wadiche L, et al. Parvalbumin deficiency and GABAergic dysfunction in mice lacking PGC-1alpha. J Neurosci. 2010 May 26;30(21):7227-35.

98. Goldberg JL, Barres BA. The relationship between neuronal survival and regeneration. Annu Rev Neurosci. 2000;23:579-612.

99. Benn SC, Woolf CJ. Adult neuron survival strategies--slamming on the brakes. Nat Rev Neurosci. 2004 Sep;5(9):686-700.

100. Irmler M, Thome M, Hahne M, Schneider P, Hofmann K, Steiner V, et al. Inhibition of death receptor signals by cellular FLIP. Nature. 1997 Jul 10;388(6638):190-5.

101. Micheau O. Cellular FLICE-inhibitory protein: An attractive therapeutic target? Expert Opin Ther Targets. 2003 Aug;7(4):559-73.

102. Pitti RM, Marsters SA, Lawrence DA, Roy M, Kischkel FC, Dowd P, et al. Genomic amplification of a decoy receptor for fas ligand in lung and colon cancer. Nature. 1998 Dec 17;396(6712):699-703.

103. Hu Y, Benedict MA, Ding L, Nunez G. Role of cytochrome c and dATP/ATP hydrolysis in apaf-1-mediated caspase-9 activation and apoptosis. EMBO J. 1999 Jul 1;18(13):3586-95.

104. Bruey JM, Ducasse C, Bonniaud P, Ravagnan L, Susin SA, Diaz-Latoud C, et al. Hsp27 negatively regulates cell death by interacting with cytochrome c. Nat Cell Biol. 2000 Sep;2(9):645-52.

105. Cheng EH, Wei MC, Weiler S, Flavell RA, Mak TW, Lindsten T, et al. BCL-2, BCL-X(L) sequester BH3 domain-only molecules preventing BAX- and BAK-mediated mitochondrial apoptosis. Mol Cell. 2001 Sep;8(3):705-11.

106. Echtay KS, Roussel D, St-Pierre J, Jekabsons MB, Cadenas S, Stuart JA, et al. Superoxide activates mitochondrial uncoupling proteins. Nature. 2002 Jan 3;415(6867):96-9.

107. Gavier-Widen D, Stack MJ, Baron T, Balachandran A, Simmons M. Diagnosis of transmissible spongiform encephalopathies in animals: A review. J Vet Diagn Invest. 2005 Nov;17(6):509-27.

108. Namboodiri AM, Peethambaran A, Mathew R, Sambhu PA, Hershfield J, Moffett JR, et al. Canavan disease and the role of N-acetylaspartate in myelin synthesis. Mol Cell Endocrinol. 2006 Jun 27;252(1-2):216-23.

109. Martinez-Saez E, Shah S, Costa C, Fleminger S, Connor S, Bodi I. Adult onset leukodystrophy with neuroaxonal spheroids and demyelinating plaque-like lesions. Neuropathology. 2012 Jun;32(3):285-92.

110. Kidd D, Barkhof F, McConnell R, Algra PR, Allen IV, Revesz T. Cortical lesions in multiple sclerosis. Brain. 1999 Jan;122 (Pt 1)(Pt 1):17-26.

111. Beal MF, Brouillet E, Jenkins BG, Ferrante RJ, Kowall NW, Miller JM, et al. Neurochemical and histologic characterization of striatal excitotoxic lesions produced by the mitochondrial toxin 3-nitropropionic acid. J Neurosci. 1993 Oct;13(10):4181-92.

112. Baumann N, Pham-Dinh D. Biology of oligodendrocyte and myelin in the mammalian central nervous system. Physiol Rev. 2001 Apr;81(2):871-927.

113. Simons M, Trajkovic K. Neuron-glia communication in the control of oligodendrocyte function and myelin biogenesis. J Cell Sci. 2006 Nov 1;119(Pt 21):4381-9.

114. Emery B. Regulation of oligodendrocyte differentiation and myelination. Science. 2010 Nov 5;330(6005):779-82.

115. Richardson WD, Kessaris N, Pringle N. Oligodendrocyte wars. Nat Rev Neurosci. 2006 Jan;7(1):11-8.

116. Levison SW, Goldman JE. Both oligodendrocytes and astrocytes develop from progenitors in the subventricular zone of postnatal rat forebrain. Neuron. 1993 Feb;10(2):201-12.

117. Kessaris N, Fogarty M, Iannarelli P, Grist M, Wegner M, Richardson WD. Competing waves of oligodendrocytes in the forebrain and postnatal elimination of an embryonic lineage. Nat Neurosci. 2006 Feb;9(2):173-9.

118. Tekki-Kessaris N, Woodruff R, Hall AC, Gaffield W, Kimura S, Stiles CD, et al. Hedgehog-dependent oligodendrocyte lineage specification in the telencephalon. Development. 2001 Jul;128(13):2545-54.

119. Pringle NP, Richardson WD. A singularity of PDGF alpha-receptor expression in the dorsoventral axis of the neural tube may define the origin of the oligodendrocyte lineage. Development. 1993 Feb;117(2):525-33.

120. Levison SW, Goldman JE. Multipotential and lineage restricted precursors coexist in the mammalian perinatal subventricular zone. J Neurosci Res. 1997 Apr 15;48(2):83-94.

121. Levison SW, Young GM, Goldman JE. Cycling cells in the adult rat neocortex preferentially generate oligodendroglia. J Neurosci Res. 1999 Aug 15;57(4):435-46.

122. Luskin MB, McDermott K. Divergent lineages for oligodendrocytes and astrocytes originating in the neonatal forebrain subventricular zone. Glia. 1994 Jul;11(3):211-26.

123. Lu QR, Sun T, Zhu Z, Ma N, Garcia M, Stiles CD, et al. Common developmental requirement for olig function indicates a motor neuron/oligodendrocyte connection. Cell. 2002 Apr 5;109(1):75-86.

124. Lu QR, Yuk D, Alberta JA, Zhu Z, Pawlitzky I, Chan J, et al. Sonic hedgehog--regulated oligodendrocyte lineage genes encoding bHLH proteins in the mammalian central nervous system. Neuron. 2000 Feb;25(2):317-29.

125. Zhou Q, Wang S, Anderson DJ. Identification of a novel family of oligodendrocyte lineage-specific basic helix-loop-helix transcription factors. Neuron. 2000 Feb;25(2):331-43.

126. Zhou Q, Choi G, Anderson DJ. The bHLH transcription factor Olig2 promotes oligodendrocyte differentiation in collaboration with Nkx2.2. Neuron. 2001 Sep 13;31(5):791-807.

127. Zhou Q, Anderson DJ. The bHLH transcription factors OLIG2 and OLIG1 couple neuronal and glial subtype specification. Cell. 2002 Apr 5;109(1):61-73.

128. Takebayashi H, Nabeshima Y, Yoshida S, Chisaka O, Ikenaka K, Nabeshima Y. The basic helix-loop-helix factor olig2 is essential for the development of motoneuron and oligodendrocyte lineages. Curr Biol. 2002 Jul 9;12(13):1157-63.

129. Wegner M. A matter of identity: Transcriptional control in oligodendrocytes. J Mol Neurosci. 2008 May;35(1):3-12.

130. Qi Y, Cai J, Wu Y, Wu R, Lee J, Fu H, et al. Control of oligodendrocyte differentiation by the Nkx2.2 homeodomain transcription factor. Development. 2001 Jul;128(14):2723-33.

131. Stolt CC, Rehberg S, Ader M, Lommes P, Riethmacher D, Schachner M, et al. Terminal differentiation of myelin-forming oligodendrocytes depends on the transcription factor Sox10. Genes Dev. 2002 Jan 15;16(2):165-70.

132. Finzsch M, Stolt CC, Lommes P, Wegner M. Sox9 and Sox10 influence survival and migration of oligodendrocyte precursors in the spinal cord by regulating PDGF receptor alpha expression. Development. 2008 Feb;135(4):637-46.

133. Emery B, Agalliu D, Cahoy JD, Watkins TA, Dugas JC, Mulinyawe SB, et al. Myelin gene regulatory factor is a critical transcriptional regulator required for CNS myelination. Cell. 2009 Jul 10;138(1):172-85.

134. Dugas JC, Cuellar TL, Scholze A, Ason B, Ibrahim A, Emery B, et al. Dicer1 and miR-219 are required for normal oligodendrocyte differentiation and myelination. Neuron. 2010 Mar 11;65(5):597-611.

135. Zhao X, He X, Han X, Yu Y, Ye F, Chen Y, et al. MicroRNA-mediated control of oligodendrocyte differentiation. Neuron. 2010 Mar 11;65(5):612-26.

136. Shin D, Shin JY, McManus MT, Ptacek LJ, Fu YH. Dicer ablation in oligodendrocytes provokes neuronal impairment in mice. Ann Neurol. 2009 Dec;66(6):843-57.

137. Ye F, Chen Y, Hoang T, Montgomery RL, Zhao XH, Bu H, et al. HDAC1 and HDAC2 regulate oligodendrocyte differentiation by disrupting the beta-catenin-TCF interaction. Nat Neurosci. 2009 Jul;12(7):829-38.

138. He Y, Dupree J, Wang J, Sandoval J, Li J, Liu H, et al. The transcription factor yin yang 1 is essential for oligodendrocyte progenitor differentiation. Neuron. 2007 Jul 19;55(2):217-30.

139. Barres BA, Raff MC. Axonal control of oligodendrocyte development. J Cell Biol. 1999 Dec 13;147(6):1123-8.

140. Boiko T, Winckler B. Myelin under construction -- teamwork required. J Cell Biol. 2006 Mar 13;172(6):799-801.

141. Pedraza L, Huang JK, Colman DR. Organizing principles of the axoglial apparatus. Neuron. 2001 May;30(2):335-44.

142. Scherer SS, Arroyo EJ. Recent progress on the molecular organization of myelinated axons. J Peripher Nerv Syst. 2002 Mar;7(1):1-12.

143. Poliak S, Peles E. The local differentiation of myelinated axons at nodes of ranvier. Nat Rev Neurosci. 2003 Dec;4(12):968-80.

144. Salzer JL. Polarized domains of myelinated axons. Neuron. 2003 Oct 9;40(2):297-318.

145. Hsieh ST, Kidd GJ, Crawford TO, Xu Z, Lin WM, Trapp BD, et al. Regional modulation of neurofilament organization by myelination in normal axons. J Neurosci. 1994 Nov;14(11 Pt 1):6392-401.

146. Edgar JM, McLaughlin M, Yool D, Zhang SC, Fowler JH, Montague P, et al. Oligodendroglial modulation of fast axonal transport in a mouse model of hereditary spastic paraplegia. J Cell Biol. 2004 Jul 5;166(1):121-31.

147. Barres BA, Raff MC. Control of oligodendrocyte number in the developing rat optic nerve. Neuron. 1994 May;12(5):935-42.

148. Miller RH. Regulation of oligodendrocyte development in the vertebrate CNS. Prog Neurobiol. 2002 Aug;67(6):451-67.

149. Baron W, Colognato H, ffrench-Constant C. Integrin-growth factor interactions as regulators of oligodendroglial development and function. Glia. 2005 Mar;49(4):467-79.

150. Noble M, Murray K, Stroobant P, Waterfield MD, Riddle P. Platelet-derived growth factor promotes division and motility and inhibits premature differentiation of the oligodendrocyte/type-2 astrocyte progenitor cell. Nature. 1988 Jun 9;333(6173):560-2.

151. Richardson WD, Pringle N, Mosley MJ, Westermark B, Dubois-Dalcq M. A role for platelet-derived growth factor in normal gliogenesis in the central nervous system. Cell. 1988 Apr 22;53(2):309-19.

152. Raff MC, Lillien LE, Richardson WD, Burne JF, Noble MD. Platelet-derived growth factor from astrocytes drives the clock that times oligodendrocyte development in culture. Nature. 1988 Jun 9;333(6173):562-5.

153. Calver AR, Hall AC, Yu WP, Walsh FS, Heath JK, Betsholtz C, et al. Oligodendrocyte population dynamics and the role of PDGF in vivo. Neuron. 1998 May;20(5):869-82.

154. Wang S, Sdrulla AD, diSibio G, Bush G, Nofziger D, Hicks C, et al. Notch receptor activation inhibits oligodendrocyte differentiation. Neuron. 1998 Jul;21(1):63-75.

155. Hu QD, Ang BT, Karsak M, Hu WP, Cui XY, Duka T, et al. F3/contactin acts as a functional ligand for notch during oligodendrocyte maturation. Cell. 2003 Oct 17;115(2):163-75.

156. Demerens C, Stankoff B, Logak M, Anglade P, Allinquant B, Couraud F, et al. Induction of myelination in the central nervous system by electrical activity. Proc Natl Acad Sci U S A. 1996 Sep 3;93(18):9887-92.

157. Stevens B, Porta S, Haak LL, Gallo V, Fields RD. Adenosine: A neuron-glial transmitter promoting myelination in the CNS in response to action potentials. Neuron. 2002 Dec 5;36(5):855-68.

158. Coman I, Barbin G, Charles P, Zalc B, Lubetzki C. Axonal signals in central nervous system myelination, demyelination and remyelination. J Neurol Sci. 2005 Jun 15;233(1-2):67-71.

159. Charles P, Hernandez MP, Stankoff B, Aigrot MS, Colin C, Rougon G, et al. Negative regulation of central nervous system myelination by polysialylated-neural cell adhesion molecule. Proc Natl Acad Sci U S A. 2000 Jun 20;97(13):7585-90.

160. Amaral AI, Meisingset TW, Kotter MR, Sonnewald U. Metabolic aspects of neuron-oligodendrocyte-astrocyte interactions. Front Endocrinol (Lausanne). 2013;4:54.

161. van den Berg CJ, Garfinkel D. A stimulation study of brain compartments. metabolism of glutamate and related substances in mouse brain. Biochem J. 1971 Jun;123(2):211-8.

162. Gegelashvili G, Schousboe A. High affinity glutamate transporters: Regulation of expression and activity. Mol Pharmacol. 1997 Jul;52(1):6-15.

163. Gegelashvili G, Schousboe A. Cellular distribution and kinetic properties of high-affinity glutamate transporters. Brain Res Bull. 1998;45(3):233-8.

164. Norenberg MD, Martinez-Hernandez A. Fine structural localization of glutamine synthetase in astrocytes of rat brain. Brain Res. 1979 Feb 2;161(2):303-10.

165. Martinez-Hernandez A, Bell KP, Norenberg MD. Glutamine synthetase: Glial localization in brain. Science. 1977 Mar 25;195(4284):1356-8.

166. Sonnewald U, Westergaard N, Schousboe A, Svendsen JS, Unsgard G, Petersen SB. Direct demonstration by [13C]NMR spectroscopy that glutamine from astrocytes is a precursor for GABA synthesis in neurons. Neurochem Int. 1993 Jan;22(1):19-29.

167. Reubi JC, Van Der Berg C, Cuenod M. Glutamine as precursor for the GABA and glutamate trasmitter pools. Neurosci Lett. 1978 Nov;10(1-2):171-4.

168. Lee Y, Morrison BM, Li Y, Lengacher S, Farah MH, Hoffman PN, et al. Oligodendroglia metabolically support axons and contribute to neurodegeneration. Nature. 2012 Jul 26;487(7408):443-8.

169. Funfschilling U, Supplie LM, Mahad D, Boretius S, Saab AS, Edgar J, et al. Glycolytic oligodendrocytes maintain myelin and long-term axonal integrity. Nature. 2012 Apr 29;485(7399):517-21.

170. Moffett JR, Ross B, Arun P, Madhavarao CN, Namboodiri AM. N-acetylaspartate in the CNS: From neurodiagnostics to neurobiology. Prog Neurobiol. 2007 Feb;81(2):89-131.

171. Moffett JR, Namboodiri AM. Expression of N-acetylaspartate and N-acetylaspartylglutamate in the nervous system. Adv Exp Med Biol. 2006;576:7,26; discussion 361-3.

172. Namboodiri AM, Peethambaran A, Mathew R, Sambhu PA, Hershfield J, Moffett JR, et al. Canavan disease and the role of N-acetylaspartate in myelin synthesis. Mol Cell Endocrinol. 2006 Jun 27;252(1-2):216-23.

173. D'Adamo AF,Jr, Gidez LI, Yatsu FM. Acetyl transport mechanisms. involvement of N-acetyl aspartic acid in de novo fatty acid biosynthesis in the developing rat brain. Exp Brain Res. 1968;5(4):267-73.

174. D'Adamo AF,Jr, Yatsu FM. Acetate metabolism in the nervous system. N-acetyl-L-aspartic acid and the biosynthesis of brain lipids. J Neurochem. 1966 Oct;13(10):961-5.

175. Burri R, Steffen C, Herschkowitz N. N-acetyl-L-aspartate is a major source of acetyl groups for lipid synthesis during rat brain development. Dev Neurosci. 1991;13(6):403-11.

176. Mehta V, Namboodiri MA. N-acetylaspartate as an acetyl source in the nervous system. Brain Res Mol Brain Res. 1995 Jul;31(1-2):151-7.

177. Chakraborty G, Mekala P, Yahya D, Wu G, Ledeen RW. Intraneuronal N-acetylaspartate supplies acetyl groups for myelin lipid synthesis: Evidence for myelin-associated aspartoacylase. J Neurochem. 2001 Aug;78(4):736-45.

178. Ariyannur PS, Moffett JR, Manickam P, Pattabiraman N, Arun P, Nitta A, et al. Methamphetamine-induced neuronal protein NAT8L is the NAA biosynthetic enzyme: Implications for specialized acetyl coenzyme A metabolism in the CNS. Brain Res. 2010 Jun 4;1335:1-13.

179. Bhakoo KK, Pearce D. In vitro expression of N-acetyl aspartate by oligodendrocytes: Implications for proton magnetic resonance spectroscopy signal in vivo. J Neurochem. 2000 Jan;74(1):254-62.

180. Laplante M, Sabatini DM. mTOR signaling in growth control and disease. Cell. 2012 Apr 13;149(2):274-93.

181. Inoki K, Li Y, Xu T, Guan KL. Rheb GTPase is a direct target of TSC2 GAP activity and regulates mTOR signaling. Genes Dev. 2003 Aug 1;17(15):1829-34.

182. Tee AR, Manning BD, Roux PP, Cantley LC, Blenis J. Tuberous sclerosis complex gene products, tuberin and hamartin, control mTOR signaling by acting as a GTPase-activating protein complex toward rheb. Curr Biol. 2003 Aug 5;13(15):1259-68.

183. Inoki K, Li Y, Zhu T, Wu J, Guan KL. TSC2 is phosphorylated and inhibited by akt and suppresses mTOR signalling. Nat Cell Biol. 2002 Sep;4(9):648-57.

184. Manning BD, Tee AR, Logsdon MN, Blenis J, Cantley LC. Identification of the tuberous sclerosis complex-2 tumor suppressor gene product tuberin as a target of the phosphoinositide 3-kinase/akt pathway. Mol Cell. 2002 Jul;10(1):151-62.

185. Potter CJ, Pedraza LG, Xu T. Akt regulates growth by directly phosphorylating Tsc2. Nat Cell Biol. 2002 Sep;4(9):658-65.

186. Ma L, Chen Z, Erdjument-Bromage H, Tempst P, Pandolfi PP. Phosphorylation and functional inactivation of TSC2 by erk implications for tuberous sclerosis and cancer pathogenesis. Cell. 2005 Apr 22;121(2):179-93.

187. Roux PP, Ballif BA, Anjum R, Gygi SP, Blenis J. Tumor-promoting phorbol esters and activated ras inactivate the tuberous sclerosis tumor suppressor complex via p90 ribosomal S6 kinase. Proc Natl Acad Sci U S A. 2004 Sep 14;101(37):13489-94.

188. Lee DF, Kuo HP, Chen CT, Hsu JM, Chou CK, Wei Y, et al. IKK beta suppression of TSC1 links inflammation and tumor angiogenesis via the mTOR pathway. Cell. 2007 Aug 10;130(3):440-55.

189. Inoki K, Ouyang H, Zhu T, Lindvall C, Wang Y, Zhang X, et al. TSC2 integrates wnt and energy signals via a coordinated phosphorylation by AMPK and GSK3 to regulate cell growth. Cell. 2006 Sep 8;126(5):955-68.

190. Ma XM, Blenis J. Molecular mechanisms of mTOR-mediated translational control. Nat Rev Mol Cell Biol. 2009 May;10(5):307-18.

191. Zinzalla V, Stracka D, Oppliger W, Hall MN. Activation of mTORC2 by association with the ribosome. Cell. 2011 Mar 4;144(5):757-68.

192. Sarbassov DD, Guertin DA, Ali SM, Sabatini DM. Phosphorylation and regulation of Akt/PKB by the rictor-mTOR complex. Science. 2005 Feb 18;307(5712):1098-101.

193. Garcia-Martinez JM, Alessi DR. mTOR complex 2 (mTORC2) controls hydrophobic motif phosphorylation and activation of serum- and glucocorticoid-induced protein kinase 1 (SGK1). Biochem J. 2008 Dec 15;416(3):375-85.

194. Jacinto E, Loewith R, Schmidt A, Lin S, Ruegg MA, Hall A, et al. Mammalian TOR complex 2 controls the actin cytoskeleton and is rapamycin insensitive. Nat Cell Biol. 2004 Nov;6(11):1122-8.

195. Sarbassov DD, Ali SM, Kim DH, Guertin DA, Latek RR, Erdjument-Bromage H, et al. Rictor, a novel binding partner of mTOR, defines a rapamycin-insensitive and raptor-independent pathway that regulates the cytoskeleton. Curr Biol. 2004 Jul 27;14(14):1296-302.

196. Cunningham JT, Rodgers JT, Arlow DH, Vazquez F, Mootha VK, Puigserver P. mTOR controls mitochondrial oxidative function through a YY1-PGC-1alpha transcriptional complex. Nature. 2007 Nov 29;450(7170):736-40.

197. Puigserver P. Tissue-specific regulation of metabolic pathways through the transcriptional coactivator PGC1-alpha. Int J Obes (Lond). 2005 Mar;29 Suppl 1:S5-9.

198. Knutti D, Kralli A. PGC-1, a versatile coactivator. Trends in Endocrinology and Metabolism. 2001 10/1;12(8):360-5.

199. Tritos NA, Mastaitis JW, Kokkotou EG, Puigserver P, Spiegelman BM, Maratos-Flier E. Characterization of the peroxisome proliferator activated receptor coactivator 1 alpha (PGC 1alpha) expression in the murine brain. Brain Res. 2003 Jan 31;961(2):255-60.

200. Nieto M, Monuki ES, Tang H, Imitola J, Haubst N, Khoury SJ, et al. Expression of cux-1 and cux-2 in the subventricular zone and upper layers II-IV of the cerebral cortex. J Comp Neurol. 2004 Nov 8;479(2):168-80.

201. Woodworth MB, Custo Greig L, Kriegstein AR, Macklis JD. SnapShot: Cortical development. Cell. 2012 Nov 9;151(4):918,918.e1.

202. Shoemaker LD, Arlotta P. Untangling the cortex: Advances in understanding specification and differentiation of corticospinal motor neurons. Bioessays. 2010 Mar;32(3):197-206.

203. Markram H, Toledo-Rodriguez M, Wang Y, Gupta A, Silberberg G, Wu C. Interneurons of the neocortical inhibitory system. Nat Rev Neurosci. 2004 Oct;5(10):793-807.

204. Anastasiades PG, Butt SJ. Decoding the transcriptional basis for GABAergic interneuron diversity in the mouse neocortex. Eur J Neurosci. 2011 Nov;34(10):1542-52.

205. Wegner M. Expression of transcription factors during oligodendroglial development. Microsc Res Tech. 2001 Mar 15;52(6):746-52.

206. Lang J, Maeda Y, Bannerman P, Xu J, Horiuchi M, Pleasure D, et al. Adenomatous polyposis coli regulates oligodendroglial development. J Neurosci. 2013 Feb 13;33(7):3113-30.

207. Bhat RV, Axt KJ, Fosnaugh JS, Smith KJ, Johnson KA, Hill DE, et al. Expression of the APC tumor suppressor protein in oligodendroglia. Glia. 1996 Jun;17(2):169-74.

208. Langley ,O.Keith, Ghandour ,M.SaÃ¯d, Gombos ,Giorgio. Immunohistochemistry of cell markers in the central nervous system.

209. Cahoy JD, Emery B, Kaushal A, Foo LC, Zamanian JL, Christopherson KS, et al. A transcriptome database for astrocytes, neurons, and oligodendrocytes: A new resource for understanding brain development and function. J Neurosci. 2008 Jan 2;28(1):264-78.

210. Mullen RJ, Buck CR, Smith AM. NeuN, a neuronal specific nuclear protein in vertebrates. Development. 1992 Sep;116(1):201-11.

211. Porter AG, Janicke RU. Emerging roles of caspase-3 in apoptosis. Cell Death Differ. 1999 Feb;6(2):99-104.

212. Switzer RC,3rd. Application of silver degeneration stains for neurotoxicity testing. Toxicol Pathol. 2000 Jan-Feb;28(1):70-83.

213. Haigis MC, Yankner BA. The aging stress response. Mol Cell. 2010 Oct 22;40(2):333-44.

214. Kourtis N, Tavernarakis N. Cellular stress response pathways and ageing: Intricate molecular relationships. EMBO J. 2011 May 17;30(13):2520-31.

215. Kirkwood TB, Austad SN. Why do we age? Nature. 2000 Nov 9;408(6809):233-8.

216. Lin MT, Beal MF. Mitochondrial dysfunction and oxidative stress in neurodegenerative diseases. Nature. 2006 Oct 19;443(7113):787-95.

217. Rubinsztein DC. The roles of intracellular protein-degradation pathways in neurodegeneration. Nature. 2006 Oct 19;443(7113):780-6.

218. Trojanowski JQ, Walkenstein N, Lee VM. Expression of neurofilament subunits in neurons of the central and peripheral nervous system: An immunohistochemical study with monoclonal antibodies. J Neurosci. 1986 Mar;6(3):650-60.

219. Ma D, Li S, Lucas EK, Cowell RM, Lin JD. Neuronal inactivation of peroxisome proliferator-activated receptor gamma coactivator 1alpha (PGC-1alpha) protects mice from diet-induced obesity and leads to degenerative lesions. J Biol Chem. 2010 Dec 10;285(50):39087-95.

220. Gorski JA, Talley T, Qiu M, Puelles L, Rubenstein JL, Jones KR. Cortical excitatory neurons and glia, but not GABAergic neurons, are produced in the Emx1-expressing lineage. J Neurosci. 2002 Aug 1;22(15):6309-14.

221. Chen L, Guo Q, Li JY. Transcription factor Gbx2 acts cell-nonautonomously to regulate the formation of lineage-restriction boundaries of the thalamus. Development. 2009 Apr;136(8):1317-26.

222. Bostrom P, Wu J, Jedrychowski MP, Korde A, Ye L, Lo JC, et al. A PGC1-alpha-dependent myokine that drives brown-fat-like development of white fat and thermogenesis. Nature. 2012 Jan 11;481(7382):463-8.

223. Lu QR, Yuk D, Alberta JA, Zhu Z, Pawlitzky I, Chan J, et al. Sonic hedgehog--regulated oligodendrocyte lineage genes encoding bHLH proteins in the mammalian central nervous system. Neuron. 2000 Feb;25(2):317-29.

224. Meijer DH, Kane MF, Mehta S, Liu H, Harrington E, Taylor CM, et al. Separated at birth? the functional and molecular divergence of OLIG1 and OLIG2. Nat Rev Neurosci. 2012 Dec;13(12):819-31.

225. Richardson WD, Smith HK, Sun T, Pringle NP, Hall A, Woodruff R. Oligodendrocyte lineage and the motor neuron connection. Glia. 2000 Jan 15;29(2):136-42.

226. Hall A, Giese NA, Richardson WD. Spinal cord oligodendrocytes develop from ventrally derived progenitor cells that express PDGF alpha-receptors. Development. 1996 Dec;122(12):4085-94.

227. Butt AM, Hornby MF, Ibrahim M, Kirvell S, Graham A, Berry M. PDGF-alpha receptor and myelin basic protein mRNAs are not coexpressed by oligodendrocytes in vivo: A double in situ hybridization study in the anterior medullary velum of the neonatal rat. Mol Cell Neurosci. 1997;8(5):311-22.

228. Wrann CD, White JP, Salogiannnis J, Laznik-Bogoslavski D, Wu J, Ma D, et al. Exercise induces hippocampal BDNF through a PGC-1alpha/FNDC5 pathway. Cell Metab. 2013 Nov 5;18(5):649-59.

229. Jan YN, Jan LY. Branching out: Mechanisms of dendritic arborization. Nat Rev Neurosci. 2010 May;11(5):316-28.

230. Kumar V, Zhang MX, Swank MW, Kunz J, Wu GY. Regulation of dendritic morphogenesis by ras-PI3K-akt-mTOR and ras-MAPK signaling pathways. J Neurosci. 2005 Dec 7;25(49):11288-99.

231. Jaworski J, Spangler S, Seeburg DP, Hoogenraad CC, Sheng M. Control of dendritic arborization by the phosphoinositide-3'-kinase-akt-mammalian target of rapamycin pathway. J Neurosci. 2005 Dec 7;25(49):11300-12.

232. Dijkhuizen PA, Ghosh A. BDNF regulates primary dendrite formation in cortical neurons via the PI3-kinase and MAP kinase signaling pathways. J Neurobiol. 2005 Feb 5;62(2):278-88.

233. Saito T, Nakatsuji N. Efficient gene transfer into the embryonic mouse brain using in vivo electroporation. Dev Biol. 2001 Dec 1;240(1):237-46.

234. Moffett JR, Ross B, Arun P, Madhavarao CN, Namboodiri AM. N-acetylaspartate in the CNS: From neurodiagnostics to neurobiology. Prog Neurobiol. 2007 Feb;81(2):89-131.

235. Luyten PR, den Hollander JA. Observation of metabolites in the human brain by MR spectroscopy. Radiology. 1986 Dec;161(3):795-8.

236. Andrews H, White K, Thomson C, Edgar J, Bates D, Griffiths I, et al. Increased axonal mitochondrial activity as an adaptation to myelin deficiency in the shiverer mouse. J Neurosci Res. 2006 Jun;83(8):1533-9.

237. Hogan V, White K, Edgar J, McGill A, Karim S, McLaughlin M, et al. Increase in mitochondrial density within axons and supporting cells in response to demyelination in the Plp1 mouse model. J Neurosci Res. 2009 Feb;87(2):452-9.

238. Kiryu-Seo S, Ohno N, Kidd GJ, Komuro H, Trapp BD. Demyelination increases axonal stationary mitochondrial size and the speed of axonal mitochondrial transport. J Neurosci. 2010 May 12;30(19):6658-66.

239. Campbell GR, Mahad DJ. Mitochondrial changes associated with demyelination: Consequences for axonal integrity. Mitochondrion. 2012 Mar;12(2):173-9.

240. Campbell GR, Ohno N, Turnbull DM, Mahad DJ. Mitochondrial changes within axons in multiple sclerosis: An update. Curr Opin Neurol. 2012 Jun;25(3):221-30.

241. Zambonin JL, Zhao C, Ohno N, Campbell GR, Engeham S, Ziabreva I, et al. Increased mitochondrial content in remyelinated axons: Implications for multiple sclerosis. Brain. 2011 Jul;134(Pt 7):1901-13.

242. Kuramoto T, Kuwamura M, Tokuda S, Izawa T, Nakane Y, Kitada K, et al. A mutation in the gene encoding mitochondrial mg(2)+ channel MRS2 results in demyelination in the rat. PLoS Genet. 2011 Jan 6;7(1):e1001262.

243. Kuwamura M, Inumaki K, Tanaka M, Shirai M, Izawa T, Yamate J, et al. Oligodendroglial pathology in the development of myelin breakdown in the dmy mutant rat. Brain Res. 2011 May 10;1389:161-8.

244. Ohno N, Kidd GJ, Mahad D, Kiryu-Seo S, Avishai A, Komuro H, et al. Myelination and axonal electrical activity modulate the distribution and motility of mitochondria at CNS nodes of ranvier. J Neurosci. 2011 May 18;31(20):7249-58.

245. Canty AJ, Murphy M. Molecular mechanisms of axon guidance in the developing corticospinal tract. Prog Neurobiol. 2008 Jun;85(2):214-35.

246. Tolwani RJ, Cosgaya JM, Varma S, Jacob R, Kuo LE, Shooter EM. BDNF overexpression produces a long-term increase in myelin formation in the peripheral nervous system. J Neurosci Res. 2004 Sep 1;77(5):662-9.

247. Chan JR, Cosgaya JM, Wu YJ, Shooter EM. Neurotrophins are key mediators of the myelination program in the peripheral nervous system. Proc Natl Acad Sci U S A. 2001 Dec 4;98(25):14661-8.

248. Zhang JY, Luo XG, Xian CJ, Liu ZH, Zhou XF. Endogenous BDNF is required for myelination and regeneration of injured sciatic nerve in rodents. Eur J Neurosci. 2000 Dec;12(12):4171-80.

249. Cosgaya JM, Chan JR, Shooter EM. The neurotrophin receptor p75NTR as a positive modulator of myelination. Science. 2002 Nov 8;298(5596):1245-8.

250. Cellerino A, Carroll P, Thoenen H, Barde YA. Reduced size of retinal ganglion cell axons and hypomyelination in mice lacking brain-derived neurotrophic factor. Mol Cell Neurosci. 1997;9(5-6):397-408.

251. Djalali S, Holtje M, Grosse G, Rothe T, Stroh T, Grosse J, et al. Effects of brain-derived neurotrophic factor (BDNF) on glial cells and serotonergic neurones during development. J Neurochem. 2005 Feb;92(3):616-27.

252. Xiao J, Wong AW, Willingham MM, van den Buuse M, Kilpatrick TJ, Murray SS. Brain-derived neurotrophic factor promotes central nervous system myelination via a direct effect upon oligodendrocytes. Neurosignals. 2010;18(3):186-202.

253. Wong AW, Xiao J, Kemper D, Kilpatrick TJ, Murray SS. Oligodendroglial expression of TrkB independently regulates myelination and progenitor cell proliferation. J Neurosci. 2013 Mar 13;33(11):4947-57.

254. Song XY, Zhou FH, Zhong JH, Wu LL, Zhou XF. Knockout of p75(NTR) impairs re-myelination of injured sciatic nerve in mice. J Neurochem. 2006 Feb;96(3):833-42.

255. Zhang J, Nuebel E, Daley GQ, Koehler CM, Teitell MA. Metabolic regulation in pluripotent stem cells during reprogramming and self-renewal. Cell Stem Cell. 2012 Nov 2;11(5):589-95.

256. Cairns RA, Harris IS, Mak TW. Regulation of cancer cell metabolism. Nat Rev Cancer. 2011 Feb;11(2):85-95.

257. WARBURG O. On the origin of cancer cells. Science. 1956 Feb 24;123(3191):309-14.

258. Zhang J, Khvorostov I, Hong JS, Oktay Y, Vergnes L, Nuebel E, et al. UCP2 regulates energy metabolism and differentiation potential of human pluripotent stem cells. EMBO J. 2011 Nov 15;30(24):4860-73.

259. Panopoulos AD, Yanes O, Ruiz S, Kida YS, Diep D, Tautenhahn R, et al. The metabolome of induced pluripotent stem cells reveals metabolic changes occurring in somatic cell reprogramming. Cell Res. 2012 Jan;22(1):168-77.

260. Folmes CD, Nelson TJ, Martinez-Fernandez A, Arrell DK, Lindor JZ, Dzeja PP, et al. Somatic oxidative bioenergetics transitions into pluripotency-dependent glycolysis to facilitate nuclear reprogramming. Cell Metab. 2011 Aug 3;14(2):264-71.

Appendix / Chapter 6:

Fezf2 directs the differentiation of corticofugal neurons from mouse embryonic stem cells.

Author contribution: I started this work during my rotation in the laboratory. After I joined the laboratory, I collaborated with Dr. William Hendriks. We shared an equal collaboration in pilot molecular characterization of mESC-derived CLN and lentiviral transduction of cells undergoing aggregation. Besides this, with the input of Professor Paola Arlotta, I designed, performed and interpreted all the experiments detailed in this chapter except for the following: Dr. Bradley J. Molyneaux developed the method to label cortical PN intracellularly with subtype-specific markers and did the relevant FACS. Dr. Hsu-Hsin Chen developed the method to label nuclei of cortical PN with subtype-specific markers with Dr. Molyneaux and did the relevant FACS. She also quantified the number of layer specific CLN and generated the overexpressor mESC lines. Dr. Chiara Gerhardinger and Dr. Chen prepared the cDNA library from FACS-purified *Fezf2*$^{+}$/GFP^{+} cells for deep sequencing. Deep sequencing analysis will be done with Dr. Loyal Goff. I also performed the transplantation experiments with the assistance of Zachary Trayes-Gibson. I thank Dr. Hsu-Hsin Chen for her advice in this project.

Publication: These data will be published in another article that is distinct from Chapters 2 through 4.

6.1. Abstract.

The molecular signals that govern the development of distinct neuronal subtypes in the mammalian cerebral cortex are only beginning to be elucidated. Here, I focus on a specific subclass comprising corticospinal motor neurons (CSMN), a clinically relevant neuronal population that degenerates in Amyotrophic Lateral Sclerosis (ALS), and are permanently damaged in spinal cord injury (SCI).

With the identification of a series of neuronal subtype-specific genes that mark CSMN and other subcerebral projection neurons (SCPN) *in vivo,* it was notably discovered that the transcription factor *Forebrain Embryonic Zinc Finger 2 (Fezf2)* is necessary for the birth and early differentiation of all SCPN, including CSMN (i.e., *Fezf2*$^{-/-}$ mice lack SCPN in their cortex), and is sufficient to "fate-switch" otherwise fated progenitors and even early postmitotic neurons to generate deep layer corticofugal projection neurons (CfuPN), including CSMN.

The central role played by *Fezf2* in early SCPN differentiation led me to investigate whether cell-autonomous developmental signals that direct early SCPN development in the embryo could be used to selectively generate these neurons from dorsal telencephalic progenitors derived from mouse embryonic stem cells (mESC) or mouse induced pluripotent stem cells (miPSC) *in vitro*. I found that *Fezf2* overexpression, either by lentiviral transduction or by newly generated inducible mESC lines, represses callosal projection neuron (CPN) specific genes while inducing CfuPN specific signals. In addition, *Fezf2* induction also results in selective changes in axonal connectivity where subcortical and subcerebral projections through the internal capsule to targets like the thalamus and cerebral peduncle are favored instead of callosal interhemispheric connections. Therefore, *Fezf2* preferentially directs the differentiation of CfuPN from mouse embryonic stem cells.

6.2. Introduction.

Terminally differentiated fibroblasts can be reprogrammed into iPSC, which resemble ESC. Yamanaka and his group achieved a breakthrough in somatic reprogramming when they induced terminally differentiated mouse embryonic or adult fibroblasts to become miPSC by the ectopic expression of 4 transcription factors, namely *Oct4*, *Sox2*, *Klf4* and *cMyc* (1-3). These miPSC are reminiscent of mESC in terms of their morphology, marker gene expression and ability to form teratomas that can differentiate into various tissues (1-3). Their work was confirmed and extended by the Hochedlinger and Jaenisch laboratories, which showed that these miPSC could undergo global epigenetic remodeling into an ES-like state (4, 5). Not only can they generate chimaeras that are competent for germline transmission (4), miPSC can also produce viable and fertile adult mice through tetraploid complementation, thus passing the most stringent test for pluripotency (6, 7). Besides murine fibroblasts, other cell types, such as adult mouse hepatocytes and gastric epithelial cells, also have been directly reprogrammed to generate iPSC (8). The direct reprogramming of somatic cells by transcription factors therefore made possible the efficient production of a large quantity of ESC-like iPSC that can be used in disease modeling and chemical screens among other downstream applications.

Directed differentiation of ESC can generate dorsal telencephalic precursors and cortical neurons. ES cells can be directed to differentiate into different neuronal subtypes, including lower motor neurons (9), cerebellar neurons (10, 11), midbrain neurons and hindbrain neurons (12). Notably, Watanabe *et al.* showed that ESC can also be directed to differentiate into $Emx1^{+}Bf1^{+}Pax6^{+}$ dorsal telencephalic progenitors (DTP), when cultured in suspension under serum-free conditions and treated with Wnt and Nodal antagonists (Dkk1 and LeftyA) followed by Wnt3a treatment (13). Eiraku *et al.* improved the Watanabe method by using an efficient

three-dimensional aggregation culture to drive ESC to further differentiate into self-organized apico-basally polarized cortical neuroepithelial aggregates containing a core of DTP surrounded by cortical-like neurons (CLN) that are generated in a temporally controlled manner that mimics corticogenesis *in vivo* (14). Another study by Gaspard *et al.* showed similar results using a different protocol in which they directed the differentiation of adherent ESC monolayer cultures into *Otx1*$^{+}$*Pax6*$^{+}$ DTP before differentiating them into CLN under serum- and morphogen-free conditions, and in the presence of the Sonic hedgehog inhibitor cyclopamine (15, 16). Significantly, these studies verified previous work by Sally Temple and her group, indicating that the sequential timing of a generation of cortical PN from ES cells is "pre-programmed" and mimics the order of PN type generation from cortical progenitors in the embryo (17). However, in spite of this successful, sequential generation of different types of CLN, no one has managed to exclusively generate selected PN subtypes, particularly CSMN and other SCPN, *in vitro*.

Notably, prior work has shown that *Fezf2* is a key transcription factor that is necessary and mostly sufficient for the specification and early differentiation of SCPN, including CSMN *in vivo* (18-21). *Fezf2*$^{-/-}$ mice display a complete absence of CSMN as well as other SCPN, and lacked the corticospinal tract as well as all subcerebral projections (21). Absence of SCPN/CSMN is accompanied by the specification of additional CPN (19). Gain-of-function analysis showed that *Fezf2* overexpression in cortical progenitors fated to form the upper layer CPN "fate-switched" them to become neurons that not only express CfuPN-specific genes like *Ctip2*, *Sox5*, *Tle4* and *Tbr1*, but also extend axons subcortically (i.e., to the thalamus) and subcerebrally (i.e., to the cerebral peduncle) (21, 22). Notably, this switch of fate does not require neural progenitors of cortical fate (23). Our laboratory has recently demonstrated that *Fezf2* expression alone is sufficient to direct the differentiation of CfuPN ectopically within the

niche of the striatum from striatal progenitors *in vivo* (23). More remarkably, besides neural progenitors, *Fezf2* alone is able to instruct lineage reprogramming of early postmitotic upper layer CPN to become CfuPN by changing their molecular characteristics as well as axonal connectivity from intracortical targets to subcortical and subcerebral targets like the SC (24). Therefore, *Fezf2* is a critical transcriptional regulator that is sufficient to induce CfuPN, including SCPN/CSMN-specification.

Since *Fezf2* plays a central role in the specification of CSMN and other SCPN *in vivo* (18-24) and mESC-derived DTP and CLN have already taken initial steps committed to a cortical neuron fate (13-16), I hypothesize that *Fezf2* overexpression in DTP and/or CLN derived from mESC or miPSC can selectively direct their differentiation into CfuPN, including SCPN/CSMN *in vitro*. Before testing this hypothesis, I molecularly characterized the various DTP and CLN types derived from mESC and miPSC, using combinatorial marker analysis and deep sequencing analysis following fluorescence-activated cell sorting (FACS) purification. I found that distinct layer specific neurons are generated and a more in-depth expression profile by deep sequencing analysis is currently ongoing for future comparative analysis with *bona fide* SCPN at various developmental ages. This molecular characterization is important to gauge our present limits of generating cortical PN types *in vitro* and will serve as a benchmark for future improvements to current protocols. To test my hypothesis, I derived DTP and/or CLN from the aggregation culture and induced *Fezf2* by lentiviral transduction or by using newly generated doxycycline inducible mESC lines. I found that *Fezf2* overexpression represses CPN specific genes like *Satb2* while it induces CfuPN specific genes like *Mu-crystallin*. Expression profiling of *Fezf2* induced cells by deep sequencing is currently ongoing and is important for comparative analysis with *bona fide* SCPN at various developmental ages as well as CLN generated with

current methods. Axonal connectivity analysis of transplanted *Fezf2* induced cells revealed that *Fezf2* expressing cells preferentially develop subcortical and subcerebral projections through the internal capsule to the thalamus or even cerebral peduncle but not callosal interhemisphereic connections via the corpus callosum. Taken together, I conclude that *Fezf2* preferentially directs the differentiation of CfuPN from mESC.

6.3. Results.

6.3.1. Molecular characterization of mESC/miPSC-derived DTP and CLN from monolayer or aggregation culture.

mESC can be directed to differentiate into DTP and CLN either by monolayer culture under serum- and morphogen-free conditions, and in the presence of the Sonic hedgehog inhibitor cyclopamine (15, 16), or by aggregation culture where they self-organize into apico-basally polarized cortical neuroepithelial aggregates containing a core of DTP surrounded by CLN (13, 14). Coculture of mESC with murine stromal cell line MS5 can also generate CLN (25). Although they can project to various subcortical structures when transplanted into early postnatal pups (14-16, 25), it is still unknown how closely mESC/miPSC-derived CLN resemble *bona fide* cortical PN at the molecular level. Understanding the differences and similarities between CLN and *bona fide* CfuPN/CSMN will not only allow us to gauge our present limits of generating cortical PN types *in vitro* and create a benchmark for future improvements to current protocols, but it will more importantly enable us to identify additional cell-autonomous signals that can be manipulated to further instruct mESC/miPSC into SCPN/CSMN.

6.3.1.A. Monolayer culture.

I am fortunate to have established collaboration with Professor Konrad Hochedlinger (Department of Stem Cell and Regenerative Biology, Harvard University) who has kindly provided me with several lines of miPSC (A1, A2 and A3 lines) that were derived from adult male fibroblasts as well as several lines of mESC (A4, A5 and A6 lines). Using these cell lines, I have molecularly characterized mESC/miPSC-derived DTP and CLN from the monolayer culture. I differentiated mESC (A5, n = 1) and miPSC (A2, n = 1; A3, n = 1) into CLN by plating them as a monolayer before differentiating them into DTP and CLN under serum- and

morphogen-free conditions for 12 days, and in the presence of the Sonic hedgehog inhibitor cyclopamine from day 2 to 10 of differentiation, as shown in Figure 6.1.A. (15, 16). DIV refers to day of differentiation. Although marker analysis confirmed prior published results that monolayer culture can generate $NESTIN^+$ progenitors by DIV 14 and $TUJ1^+$ neurons by DIV 21, I found that specific generation of $PAX6^+$ DTP and $CTIP2^+$ or $SATB2^+$ CLN is inefficient and deviates significantly from previously reported percentages (Figures 6.1.B. to 6.1.C., data not shown for PAX6). Many cells also continue to express the pluripotency marker OCT3/4 at DIV 21 (data not shown). These results, as compared to my results from the aggregation culture described in section 6.3.1.B., indicate that the latter is a more efficient system to drive neural differentiation towards DTP and CLN. Therefore, I chose to focus on the more robust aggregation culture to derive DTP/CLN from mESC/miPSC for the rest of my studies.

6.3.1.B. Aggregation culture.

In addition to the monolayer culture, I have also molecularly characterized mESC/miPSC-derived DTP and CLN from the aggregation culture. I differentiated mESC (A5, n = 3) and miPSC (A1, n = 1; A2, n = 1; A3, n = 1) into CLN by culturing them in suspension to form 3D aggregates under serum-free conditions, and treating them with Wnt and Nodal antagonists (Dkk1 and LeftyA) followed by Wnt3a treatment, as shown in Figure 6.2.A. (14). I analyzed the identity of mESC/miPSC-derived progenitors and neurons at DIV 11 and 18 by immunocytochemistry (ICC) and ISH for pluripotent marker OCT3/4, early neural progenitor marker NESTIN, forebrain progenitor marker BF1, dorsal telencephalic marker PAX6, early and mature pan-neuronal markers TUJ1 and NeuN, and somatodendritic marker MAP2. I found that the aggregation culture is efficient in driving differentiation as few mESC/miPSC remain

Figure 6.1. Molecular characterization of mESC/miPSC-derived DTP and CLN from monolayer culture.

(A) Schematic for monolayer culture. DTP and CLN were preferentially generated by DIV 14 and 21 respectively. DIV refers to day of differentiation. This figure is adapted from (15, 16).

(B) While many $NESTIN^+$ progenitors were generated by DIV 14, few of them are $PAX6^+$ (data not shown). This result differs significantly from previously reported percentages (15, 16).

(C) Although many $TUJ1^+$ immature neurons were generated at DIV 21, few are $CTIP2^+$ or $SATB2^+$. This result varies considerably from previously reported percentages (15, 16).

Figure 6.1. (Continued)

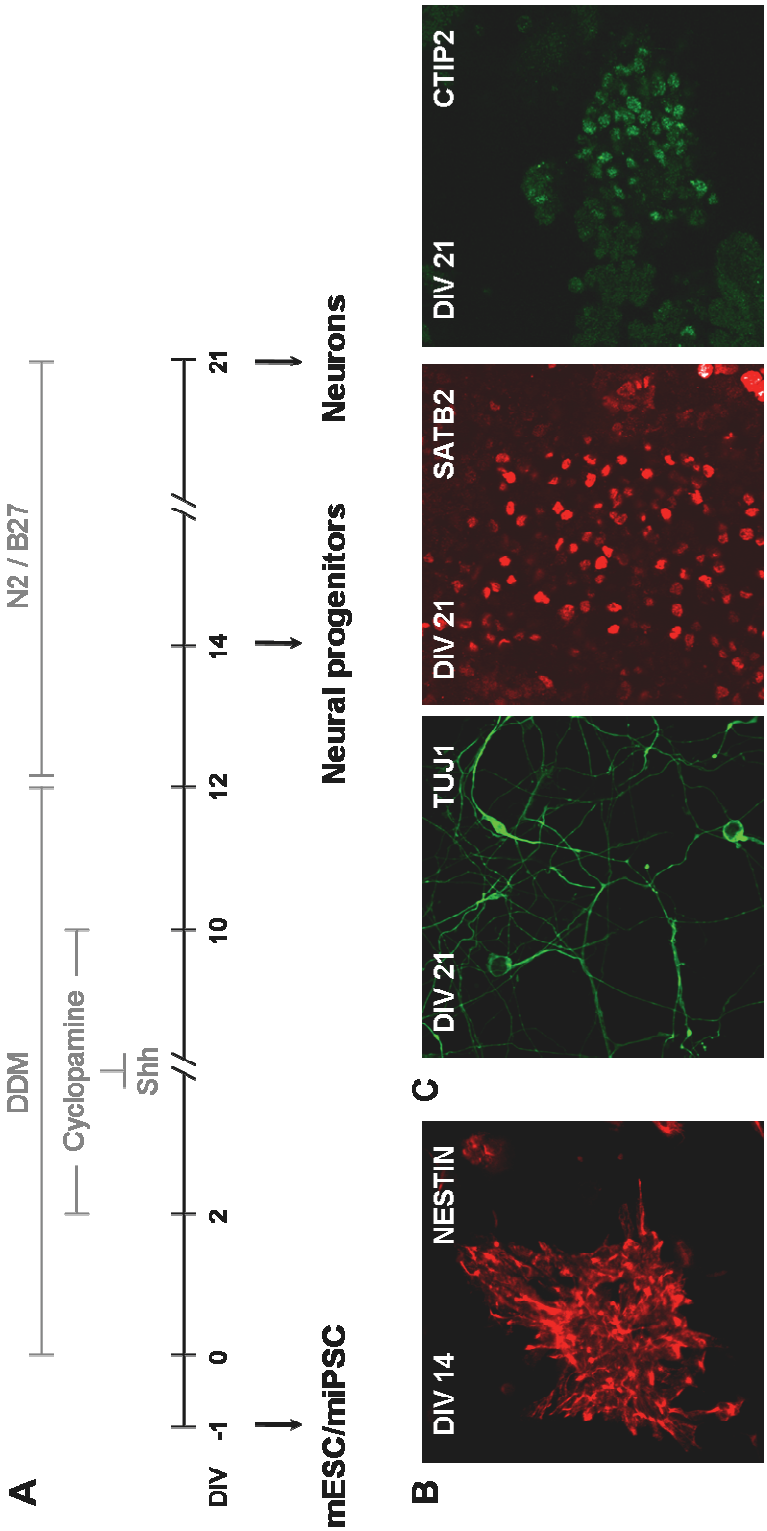

Figure 6.2. Molecular characterization of mESC/miPSC-derived DTP and CLN from aggregation culture.

(A) Schematic for aggregation culture. DTP and CLN were preferentially generated by DIV 11 and 18 respectively. DIV refers to day of differentiation. This figure is adapted from (14).

(B and E) Few mESC/miPSC remained pluripotent ($OCT3/4^{+}$) by DIV 11 and virtually none were pluripotent by DIV 18.

(C and F) mESC/miPSC differentiated into $NESTIN^{+}$ progenitors as early as DIV 11 and continue to do so till DIV 18.

(D and G) $MAP2^{+}$ neurons were generated as early as DIV 11 and were produced till DIV 18.

Scale bars: 10 μm (B – G).

Figure 6.2. (Continued)

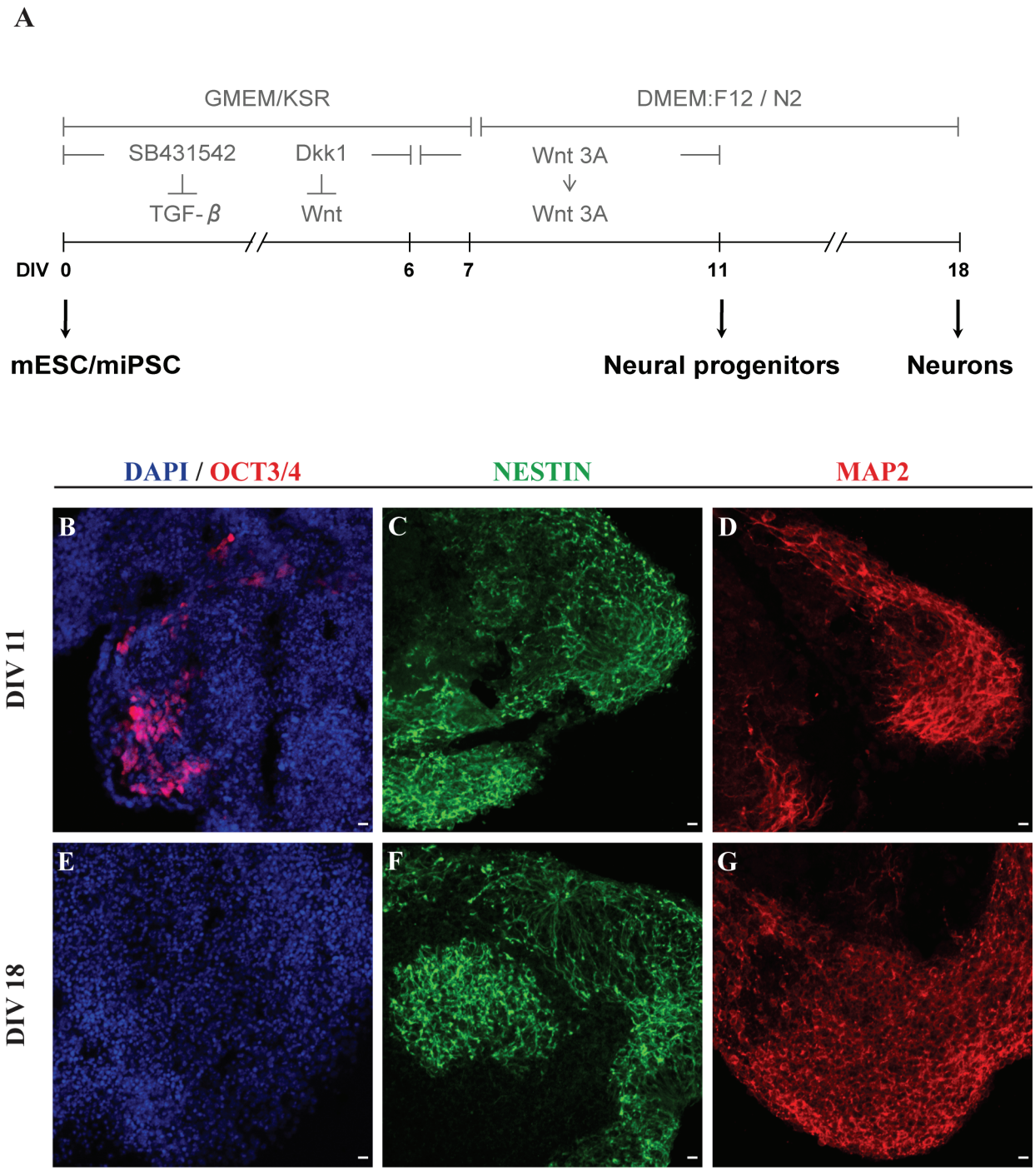

pluripotent (OCT3/4$^+$) by DIV 11 and virtually none are pluripotent by DIV 18 (Figures 6.2.B. and 6.2.E.). mESC/miPSC also differentiate into NESTIN$^+$ progenitors and MAP2$^+$ neurons as early as DIV 11 (Figures 6.2.C. and 6.2.D.) and persist till DIV 18 (Figures 6.2.F. and 6.2.G.). Further analysis also revealed that BF1$^+$/PAX6$^+$ dorsal forebrain progenitors can self-organize within an aggregate into distinct proliferative cores surrounded by NeuN$^+$/TUJ1$^+$ neurons from DIV 11 to DIV 18 (Figures 6.3.A. to 6.3.L.).

In addition, I tested for the expression of the following CfuPN specific markers: SOX5 (expressed in layer V/VI) (26), CTIP2 (expressed at high levels in layer V and low levels in layer VI) (27) and *Fezf2* (expressed at high levels in layer V and low levels in layer VI) (18, 20, 21); SCPN-specific markers: BHLHB5 (expressed in layers II/III and layer V) (28), MU-CRYSTALLIN (expressed in layer V) (27) and *Clim1* (expressed in layer V) (27); CPN specific markers: CUX1 (expressed in layers II/III) (29), SATB2 (expressed in all layers) (30, 31), LHX2 (expressed in layers II/III) (32, 33) and BRN2 (expressed in layers II/III and V) (34, 35); and corticothalamic PN (CThPN) specific markers that are expressed at high levels in layer VI: TBR1 (36, 37), TLE4 (38) and ZFPM2/FOG2 (39). Combinatorial marker analysis is not only necessary to identify CfuPN/SCPN, but also crucial to define the extent of differentiation into specific neuronal subtypes and to investigate the possible acquisition of mixed identity. Combinatorial marker analysis demonstrated that mESC/miPSC can robustly differentiate into cortical plate-like cells that are TBR1$^+$CTIP2$^+$ from DIV 11 to DV 18 (Figures 6.4.A. to 6.4.I.). Further qualitative analysis at DIV 18 revealed that the majority of CLN are single positive for cortical layer specific genes such as TLE4 (highly expressed in layer VI CThPN), CTIP2 (highly expressed in layer V SCPN) and SATB2 (highly expressed in CPN across all cortical layers) (Figures 6.5.B. to 6.5.E.). Occasional double positive cells that are TLE4$^+$CTIP2$^+$,

Figure 6.3. mESC/miPSC-derived neural progenitors and postmitotic neurons occupy distinct domains within an aggregate.

(A – F) $BF1^+$ forebrain progenitors can self-organize within an aggregate into distinct proliferative cores surrounded by $NeuN^+$ neurons from DIV 11 to DIV 18. Boxes indicate areas where high magnification images are taken. High magnification analysis showed that the progenitors and neurons are distinct populations.

(G – L) Similar to what is observed in (A – F), $PAX6^+$ dorsal telecephalic progenitors can self-organize within an aggregate into proliferative cores surrounded by $TUJ1^+$ immature neurons from DIV 11 to DIV 18. Boxes indicate areas where high magnification images are taken. High magnification analysis showed that the progenitors and neurons are different populations. Scale bars: 10 μm (A – L, including inserts).

Figure 6.3. (Continued)

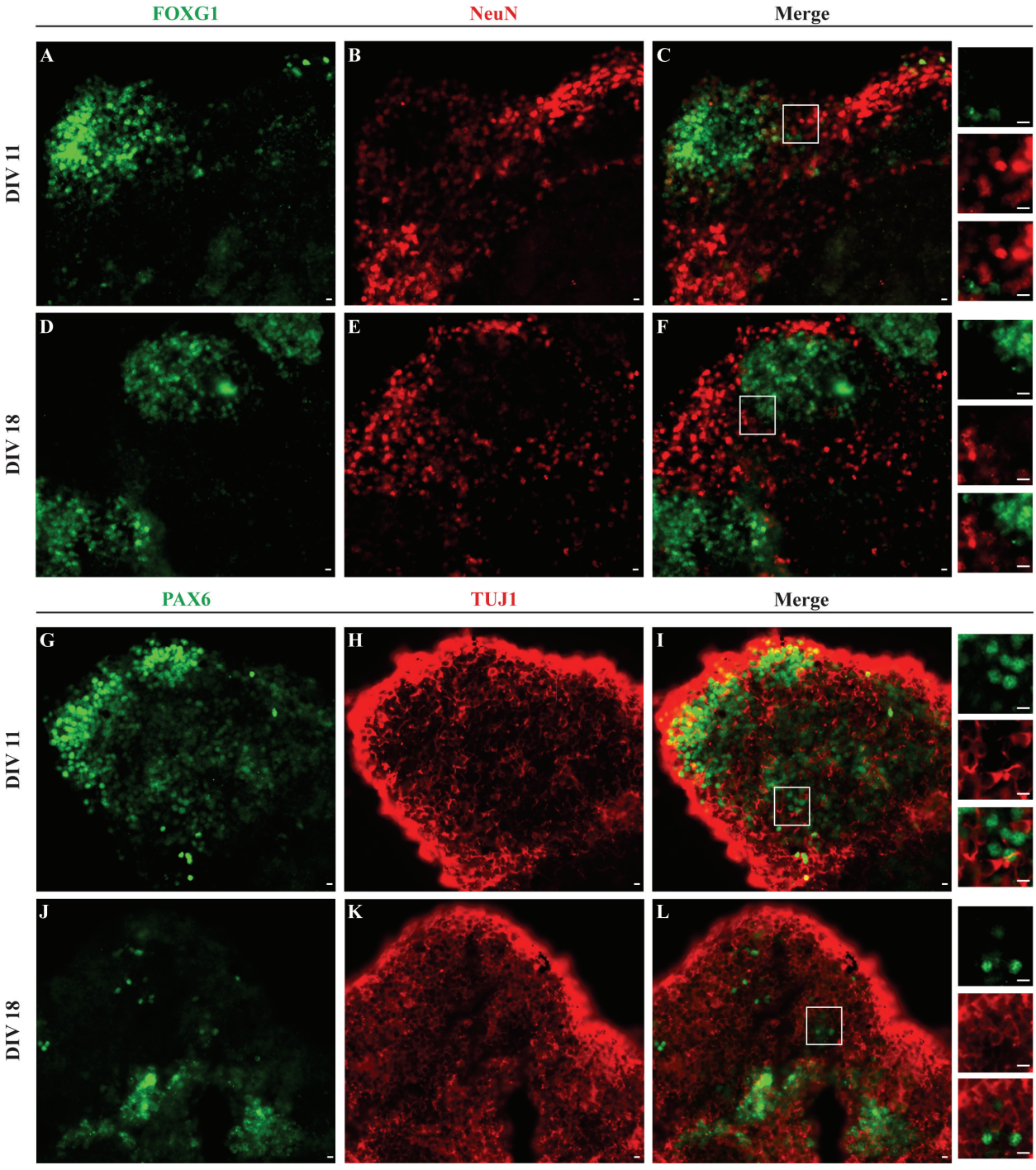

Figure 6.4. Cortical plate-like neurons are generated from mESC and miPSC at early and late stages of differentiation.

(A) At E13.5, $TBR1^{+}CTIP2^{+}TUJ1^{+}$ cortical plate-like neurons occupy the more superficial layers, above the proliferative zone consisting of the subventricular and ventricular zone that reside adjacent to the lateral ventricle (LV).

(B – I) mESC/miPSC can robustly differentiate into cortical plate-like neurons that are $TBR1^{+}CTIP2^{+}TUJ1^{+}$ from DIV 11 (B – E) to DV 18 (F – I). Scale bars: 100 μm (A), 10 μm (B – I).

Figure 6.4. (Continued)

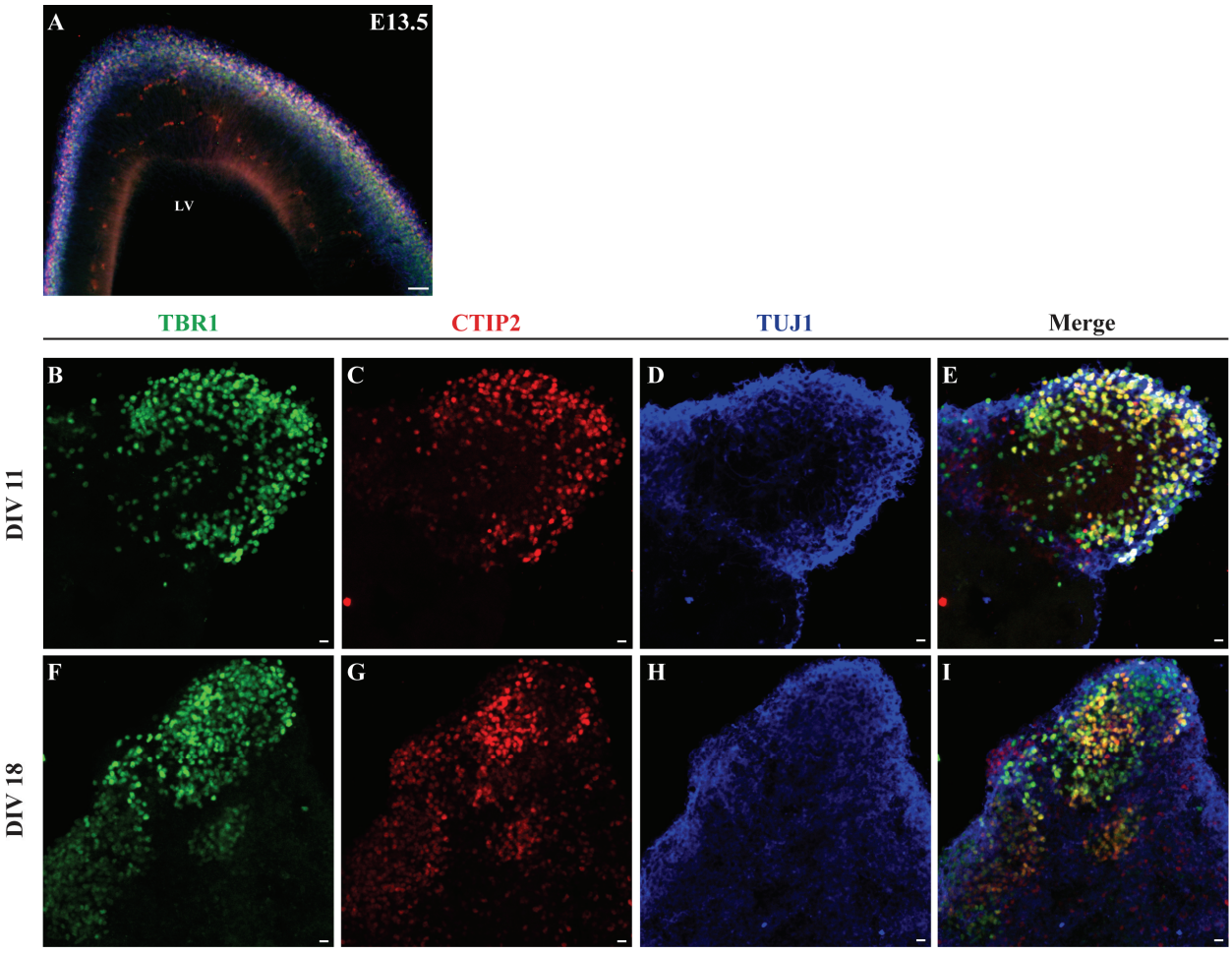

Figure 6.5. Distinct layer-specific CLN are generated from mESC and miPSC at early and late stages of differentiation.

(A) At E17.5, distinct layer-specific cortical neurons that are predominantly $TLE4^+$ or $CTIP2^+$ or $SATB2^+$ are generated and have migrated from the proliferative zone to occupy their destined layers in an "inside-out" fashion where later born neurons migrate past earlier born neurons to occupy more superficial layers.

(B – E) Majority of CLN are single positive for cortical layer specific genes such as TLE4 (highly expressed in layer VI CThPN), CTIP2 (highly expressed in layer V SCPN) and SATB2 (highly expressed in CPN across all cortical layers). Occasional double positive cells that are $TLE4^+CTIP2^+$, $TLE4^+SATB2^+$ and $CTIP2^+SATB2^+$ cells as well as rare triple positive cells that are $TLE4^+CTIP2^+SATB2^+$ are also found (data not shown).

(F) Quantitative analysis by Dr. Hsu-Hsin Chen ascertained the results in (B – E) and showed that among the single positive cells, $TLE4^+$ cells have the highest proportion followed by $CTIP2^+$ cells with $SATB2^+$ cells having the lowest proportion. Scale bars: 100 μm (A), 10 μm (B – E).

Figure 6.5. (Continued)

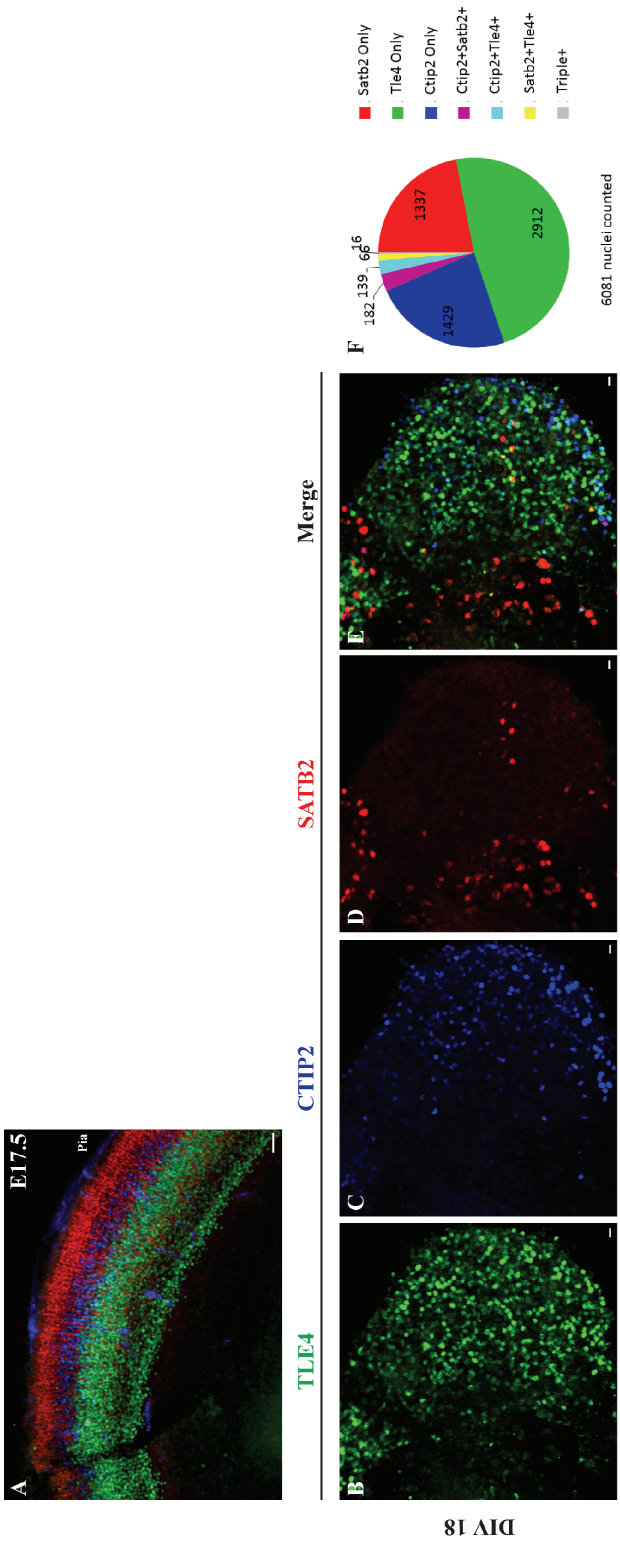

TLE4^{+}SATB2^{+} and CTIP2^{+}SATB2^{+} cells as well as rare triple positive cells that are TLE4^{+}CTIP2^{+}SATB2^{+} are also found (data not shown). Quantitative analysis by Dr. Hsu-Hsin Chen ascertained these results and showed that among the single positive cells, TLE4^{+} cells have the highest proportion followed by CTIP2^{+} cells with SATB2^{+} cells having the lowest proportion (Figure 6.5.F.). Thus, the aggregation culture can produce significant numbers of cortical plate-like cells as well as CLN that can successful segregate layer specific marker genes. Of relevant interest, to understand if the aggregation culture can generate layer V SCPN like cells, I have isolated the CTIP2^{+} cells and nuclei by FACS for ongoing expression profiling by deep sequencing, as described in section 6.3.2.. Future comparative analysis with *bona fide* SCPN that has been profiled with similar methods by Dr. Bradley J. Molyneaux and Dr. Hsu-Hsin Chen will be imperative to understand how similar or different these cells are in terms of their molecular identities and to provide the field with a much needed framework to understand and enhance present directed differentiation protocols.

Moreover, CfuPN/SCPN-specific marker analysis also showed that mESC/miPSC can differentiate into ZFPM2^{+}SOX5^{+} cells that are more similar to layer VI CThPN rather than layer V SCPN like ZFPM2^{-}SOX5^{+} cells (data not shown). CPN specific marker analysis further determined that SATB2^{+} and CUX1^{+}BRN2^{+} cells are generated by DIV 18 but not earlier at DIV 11 (data not shown). In all, these data support previous reports that mESC/miPSC-derived CLN undergoing aggregation are generated in a temporally controlled manner that mimics corticogenesis *in vivo*.

To determine if CLN identity is dependent on maintaining the 3D structure and to facilitate combinatorial marker analysis and quantification, I dissociated the aggregates, replated the cells as a monolayer at DIV 10, and performed similar marker analysis at DIV 11 and DIV

18, as shown in Figure 6.6.A.. My results revealed that CLN maintain their identity as a monolayer where $TUJ1^+$ immature neurons are either single or double positive for TBR1 and/or CTIP2 at DIV 11 and DIV 18 (Figures 6.6.B. to 6.6.E, data not shown for DIV 18). Combinatorial analysis with layer specific markers further showed that the majority of cells are $TLE4^+$ cells followed by a substantial number of $CTIP2^+$ cells with $SATB2^+$ cells having the lowest proportion at DIV 18 (Figures 6.6.F. to 6.6.I.). Thus, dissociated mESC/miPSC-derived CLN do maintain their identity in a monolayer after an initial period of aggregation. This characterization is important because lentiviral transduction to overexpress *Fezf2* prove to be efficient only when cells are in a monolayer and not in aggregates, as described in section 6.3.3.. Although replated cells from aggregates behave as a monolayer shortly after dissociation, they exhibit a tendency to cluster and form "clumps" in cultures as they differentiate, ultimately resulting in a multilayer culture with areas of different cellular densities by DIV 18 (data not shown), which makes unbiased quantification of distinct layer specific CLN problematic.

In all, my molecular characterization of DTP and CLN derived from either monolayer or aggregation cultures showed that the aggregation culture is a more robust system to generate these cell types of interest. Qualitative combinatorial marker analysis revealed that the aggregation culture can generate cortical plate-like cells that are $TBR1^+CTIP2^+$ as well as layer specific CLN that singly express markers like TLE4, CTIP2 and SATB2, a result that is further supported by quantitative analysis. I also demonstrated that dissociated mESC/miPSC-derived CLN can maintain their identity in a monolayer after an initial period of aggregation. Ongoing expression profiling of $CTIP2^+$ cells and nuclei from the aggregation culture, as described in section 6.3.2., will provide insights on how these cells resemble SCPN *in vivo*.

Figure 6.6. Dissociated mESC/miPSC-derived CLN maintain their identity in a monolayer after initial period of aggregation.

(A) Schematic of dissociation after an initial period of aggregation.

(B – E) 1 day after dissociation, many $TUJ1^+$ immature neurons continue to be either single or double positive for TBR1 and CTIP2. This is in line with what is observed in aggregates, as shown in Figure 6.4..

(F – I) 10 days after dissociation, distinct populations of layer-specific CLN that are single, double or triple positive for TLE4, CTIP2, and SATB2 were formed. Proportions of single positive cells are in agreement with what is observed in aggregates, as shown in Figure 6.5., where majority of cells are $TLE4^+$ cells followed by a substantial number of $CTIP2^+$ cells with $SATB2^+$ cells having the lowest proportion at DIV 18. Scale bars: 10 μm (B – I).

Figure 6.6. (Continued)

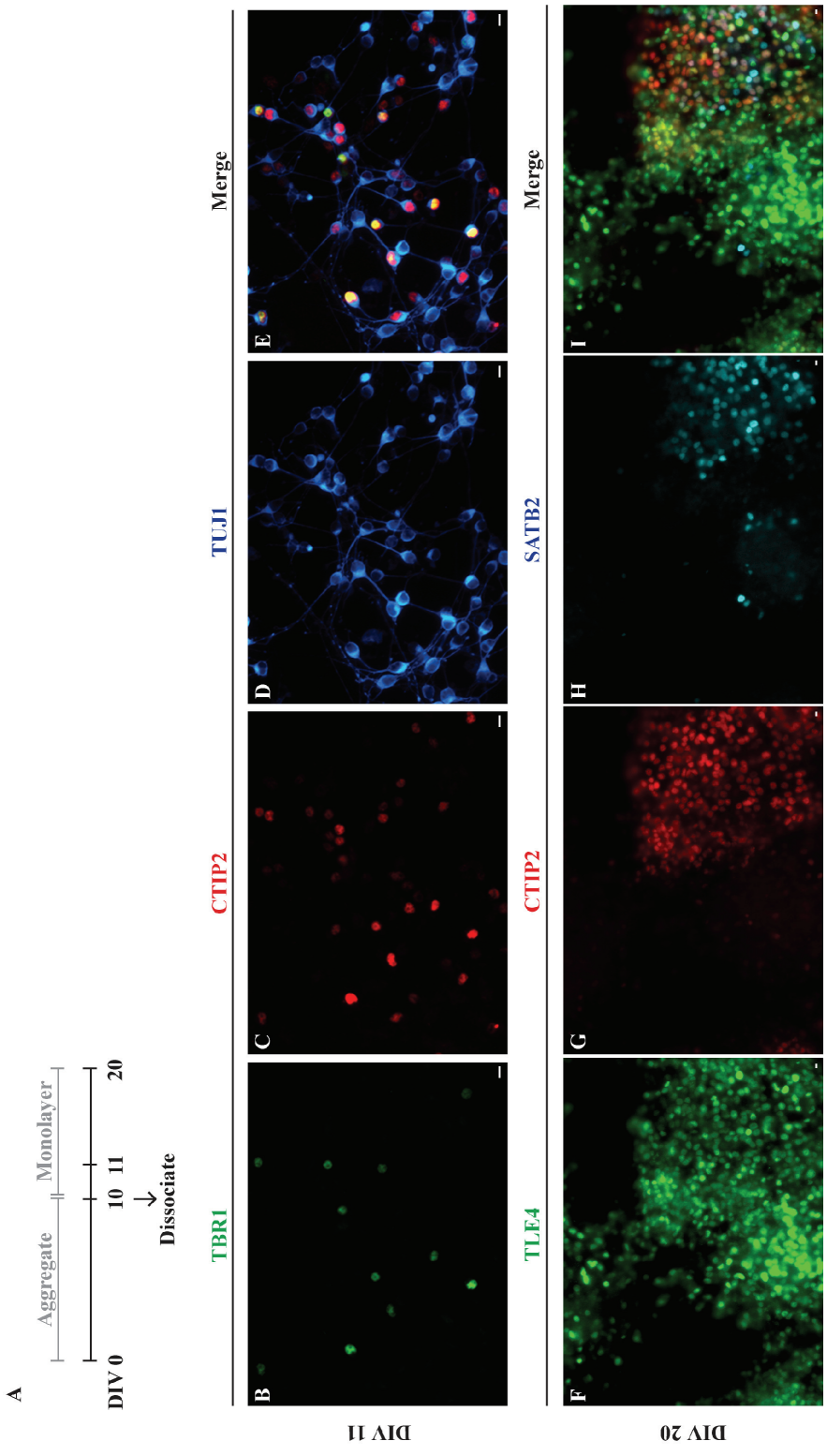

6.3.2. Population-specific FACS purification of mESC-derived CLN.

This work was done in collaboration with Dr. Bradley J Molyneaux, a post-doctoral fellow, and Dr. Hsu-Hsin Chen, an instructor in our laboratory.

To understand how mESC-derived CLN compare to *bona fide* cortical PN subtypes, it is crucial to isolate and molecularly profile different CLN populations in addition to performing qualitative marker gene analysis. This work is currently limited by the lack of reporter mESC lines that can delineate specific CLN classes. However, Dr. Molyneaux recently developed a method to label cortical PN intracellularly using a combination of subtype-specific antibodies like *Ctip2*, *Tle4* and *Satb2*, and isolate them by FACS (unpublished data). Together with Dr. Chen, he also developed a similar method to mark nuclei extracted from cortical PN (unpublished data). Both methods enable us not only to overcome the cellular heterogeneity of mESC-derived CLN that confounds gene expression profiling, but also to develop an unbiased quantitative approach to determine the proportions of different CLN subtypes *in vitro*.

To quantify and purify the heterogeneous cell populations derived *in vitro*, I enzymatically or chemically dissociated DIV18 mESC-derived neural aggregates into single cells, and stained them with subtype-specific antibodies including CTIP2 and SATB2 (n = 3). Flow cytometry analysis revealed that the percentages of $CTIP2^+$ and $SATB2^+$ cells are highly variable between independent experiments, which are not observed in my ICC results (data not shown). This is likely due to inconsistent dissociation of these aggregates into a single cell suspension. To optimize the cellular dissociation of these aggregates, I tried various mechanical, chemical (Neurocult) and enzymatic (Papain, Accutase, Accumax, TrypLE Express and Trypsin-EDTA) protocols but could not arrive at a robust reproducible method. To circumvent this problem, I extracted nuclei from these aggregates and stained them with similar primary and

secondary antibodies before flow cytometry analysis (n = 1). Pilot data showed that $CTIP2^{+}$ (~36%) and $SATB2^{+}$ (~23%) cell populations are distinguished with this method (data not shown). Consistent with ICC results, combinatorial analysis revealed 2 populations that are $CTIP2^{high}SATB2^{+}$ or $CTIP2^{low}SATB2^{-}$ (data not shown). I have since purified $CTIP2^{+}$ cells as well as nuclei from DIV 18 mESC-derived neural aggregates by FACS, extracted their RNA and assessed their quality with a bioanalyzer. Dr. Chen has prepared the cDNA library and the samples have been sent for Illumina HiSeq-based deep sequencing. Deep sequencing analysis will be done in collaboration with Dr. Loyal Goff, a post-doctoral fellow in the laboratory of Professor John Rinn (Department of Stem Cell and Regenerative Biology, Harvard University). The molecular profiles of these mESC-derived CLN populations will be compared to those of E15.5 and E16.5 cortical PN subtypes that have been purified and profiled by Dr. Molyneaux and Dr. Chen (unpublished data).

6.3.3. Lentiviral transduction of dissociated mESC/miPSC-derived DTP and CLN instead of aggregates is efficient and induces neuronal differentiation.

6.3.3.A. Lentiviral transduction of miPSC undergoing aggregation is inefficient.

This work was done in collaboration with Dr. William Hendriks, Head of iPS Genome Editing Service at the Harvard Stem Cell Institute.

Dr. William Hendriks, together with Dr. Caroline Rouaux in our laboratory, made an expression construct that contains the *Fezf2* transgene downstream of an *eGFP* reporter gene and a "self-cleaving" T2A peptide sequence. I refer to this construct as $LV^{CMV\text{-}Fezf2}$ (Figure 6.7.A.) and the control vector as $LV^{CMV\text{-}GFP}$. To determine whether miPSC undergoing aggregation can

Figure 6.7. Lentiviral transduction of mESC/miPSC undergoing aggregation is inefficient.

(A) Lentiviral constructs and schematic of lentiviral transduction.

(B – D) Immunostaining for GFP on cross sections of untransduced mock aggregates and aggregates transduced with either $LV^{CMV\text{-}Fezf2}$ or $LV^{CMV\text{-}GFP}$ collected at DIV 3 revealed the segregation of *Fezf2*$^+$/GFP$^+$ cells to the outermost position of the aggregate.

(E – G) ISH for *Fezf2* confirmed the results in (B – D) where *Fezf2*$^+$ cells are located at the periphery of the aggregate. Scale bars: 100 μm (B – G).

Figure 6.7. (Continued)

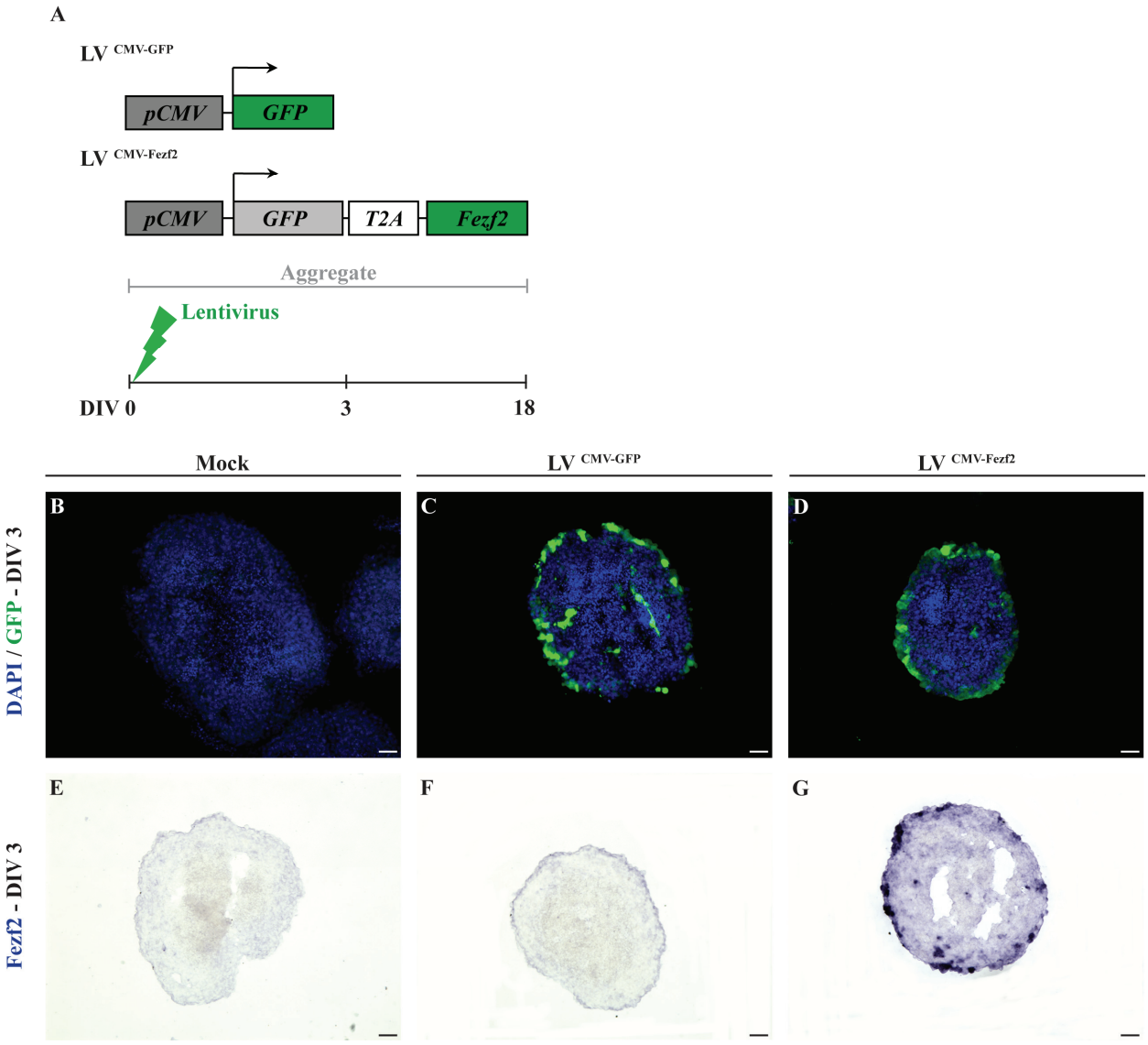

be efficiently transduced with lentivirus expressing $LV^{CMV\text{-}Fezf2}$ or $LV^{CMV\text{-}GFP}$, I transduced miPSC (A3, n = 3) with either $LV^{CMV\text{-}Fezf2}$ or $LV^{CMV\text{-}GFP}$ at DIV 0 and analyzed GFP expression at day 3 and day 18 of differentiation. Fluorescent live microscopy analysis showed that *Fezf2*$^+$/GFP$^+$ transduced aggregates expressed eGFP and maintained its expression for at least 18 days into differentiation (data not shown). However, immunostaining for GFP on cross sections of untransduced mock aggregates and aggregates transduced with either $LV^{CMV\text{-}Fezf2}$ or $LV^{CMV\text{-}GFP}$ collected at DIV 3 revealed the segregation of *Fezf2*$^+$/GFP$^+$ cells to the outermost position in the aggregate (Figures 6.7.B. to 6.7.D.). *In situ* hybridization (ISH) for *Fezf2* showed similar results where *Fezf2* induced cells are present only at the periphery of an aggregate in $LV^{CMV\text{-}Fezf2}$ transduced cells but not $LV^{CMV\text{-}GFP}$ transduced and mock untransduced cells (Figures 6.7.E. to 6.7.G.). To determine whether the transduction efficiency could be improved, together with Dr. Hendriks, I tested different multiplicities of infection (MOI) ranging from 500 to 2,000. We found that the GFP$^+$ cells segregate to the outermost surface of the aggregate at day 3 of differentiation, regardless of the MOI used (data not shown). Our transduction protocol involved transducing miPSC as dissociated, single-cell suspensions and incubating them with virus through aggregation for at least 16 hours. To test if we could increase the number of transduced cells in the aggregate by using another transduction protocol, we transduced a monolayer of miPSC cultured on gelatin-coated dishes before dissociating them for aggregation. We obtained high transduction efficiencies (more than 90%) for miPSC transduced as a monolayer and formed aggregates that consist of mostly transduced cells (more than 90%) at day 0 of differentiation (data not shown). Yet, immunostaining for GFP on cross sections of GFP- and *Fezf2*-transduced aggregates at DIV 3 still show the segregation of GFP$^+$ cells (data not shown). This suggests that the transgene may be silenced in transduced cells located at the core of the

aggregate but not in cells residing at the periphery. It is also possible that non-transduced cells proliferate at a much higher rate than transduced cells and form the core of the aggregates, thus segregating the less proliferative, transduced cells to the periphery. We conclude that lentiviral transduction of miPSC undergoing aggregation is inefficient and highly variable.

6.3.3.B. Lentiviral transduction of dissociated mESC/miPSC-derived DTP and CLN as a monolayer is efficient and induces neuronal differentiation.

As shown in section 6.3.3.B., lentiviral transduction of mESC/miPSC undergoing neural aggregation is inefficient, as transduced cells would segregate to the outermost periphery of the aggregate. Since dissociated mESC/miPSC-derived CLN do maintain their identity in a monolayer after an initial period of aggregation, in order to improve lentiviral transduction of DTP/CLN from neural aggregates, I first differentiated A5 mESC by culturing them in suspension to form 3D aggregates for 10 days and chemically dissociated these aggregates before replating them as a monolayer on fibronectin/laminin/poly-D-lysine coated coverslips for lentiviral transduction on DIV 11, as shown in Figure 6.8.B.. I used lentiviruses expressing LV^{GFP}, LV^{Fezf2}, LV^{2AGFP}, $LV^{Fezf2/Ngn2}$ or $LV^{Fezf2/Mash1}$ (Figure 6.8.A.), and performed marker gene analysis as described in section 6.3.1.B. at DIV 16 and 20. I found a high proportion of cells to be transduced (more than 50% by observation), regardless of the type of lentivirus used (Figures 6.8.C. to 6.8.J., data not shown for DIV 16). This indicates that lentiviral transduction of dissociated cells from aggregates is efficient. Molecular analysis also showed that most transduced cells become $TUJ1^+$ or $NeuN^+$ neurons (Figures 6.8.C. to 6.8.J., data not shown for DIV 16). Thus, lentiviral transduction of mESC-derived DTP/CLN is efficient and does not inhibit neural differentiation. Moreover, combining proneural genes like *Ngn2* and *Mash1* with

Figure 6.8. Lentiviral transduction of dissociated mESC/miPSC-derived DTP and CLN as a monolayer is efficient and induces neuronal differentiation.

(A) Lentiviral constructs made.

(B) Schematic of lentiviral transduction of dissociated mESC/miPSC-derived DTP and CLN after an initial period of aggregation.

(C – J) Lentiviral transduction is efficient as more than 50% of cells by observation were transduced, regardless of the lentivirus used. It also does not inhibit neural differentiation as lentivirally transduced cells are neuronal in morphology and are $TUJ1^+$ (C – F) and $NeuN^+$ (G – J). Scale bars: 10 μm (C – J).

Figure 6.8. (Continued)

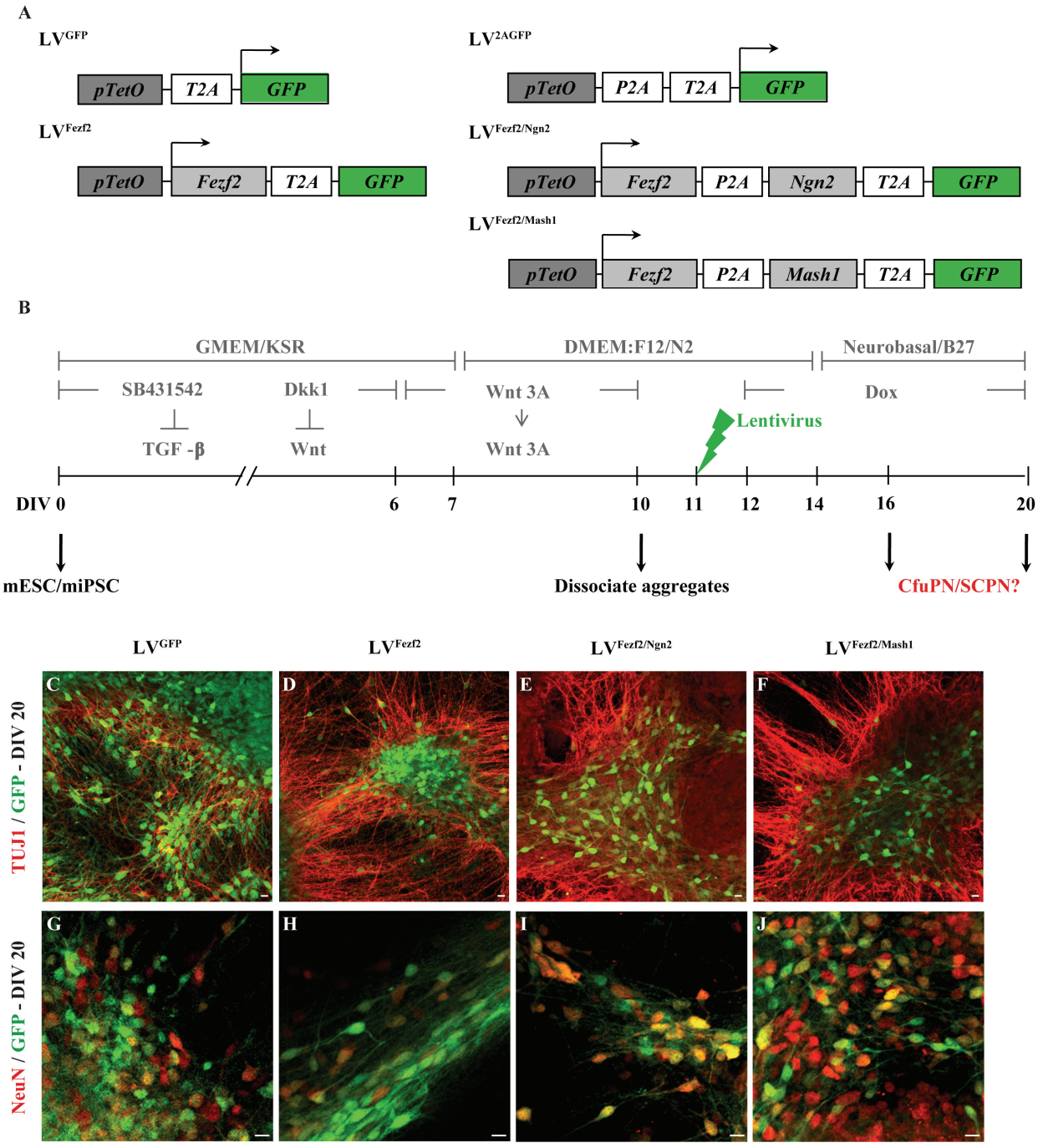

Fezf2 also did not seem to significantly enhance neural differentiation (data not shown). Hence, I only utilized LV^{Fezf2} and LV^{GFP} constructs for the remaining experiments.

6.3.4. *Fezf2* overexpressor mESC lines efficiently express transgene upon doxycycline induction.

6.3.4.A. Generation of doxycycline-inducible *Fezf2*-overexpressor mESC line.

This work was done in collaboration with Dr. Hsu-Hsin Chen.

Efficient lentiviral transduction of mESC/miPSC-derived DTP/CLN *in vitro* relies on successful dissociation of neural aggregates into a monolayer. Often, inconsistent dissociation results in a multilayer culture with clumps of cells, which affects the transduction efficiency at different parts of the culture. Moreover, random lentiviral integration may undermine the differentiation capability of some infected cells. To address these limitations, Dr. Hsu-Hsin Chen generated doxycycline-inducible *Fezf2*-overexpressor mESC lines (with or without *Gfp/tdTomato* reporter) targeted to the HPRT locus, using a recently developed Inducible Cassette Exchange (ICE) system (40) (Figure 6.9.B.). She generated targeting constructs using Gateway compatible shuttle vectors (41) (Figures 6.9.A. and 6.9.C.). I utilized these overexpressor lines for subsequent experiments: (i) *GFP* line that only expresses GFP to act as a control cell line, (ii) $Fezf2^{IRESGFP}$ line that expresses *Fezf2* and a GFP reporter and (iii) $Fezf2^{IREStdTomato}$ line that expresses *Fezf2* and a tdTomato reporter.

6.3.4.B. *Fezf2* overexpressor mESC lines efficiently express transgene upon doxycycline induction.

To test that trangene activation is tightly regulated by doxycycline administration, I differentiated the *GFP*, $Fezf2^{IRESGFP}$ and $Fezf2^{IREStdTomato}$ lines by culturing them in suspension to

Figure 6.9. *Fezf2* overexpressor mESC lines efficiently express transgene upon doxycycline induction.

(A) Creation of targeting constructs with heterologous loxP sites by Gateway-recombination.

(B) A schematic of the Inducible Cassette Exchange (ICE) system. *Cre*-mediated recombination in the A2LoxCre mESC line resulted in the insertion of the transgene under a *TetO* promoter targeted to the HPRT locus. Figure A and B are adapted from (40).

(C) Targeting constructs (with/without GFP/tdTomato reporter). Figure C is adapted from (41).

(D – G) ICC for GFP showed that the newly generated overexpressor mESC lines efficiently express transgene only upon doxycycline (Dox) induction. – Dox indicates no Dox addition while + Dox indicates the addition of Dox from DIV 10 to DIV 18. Scale bars: 100 μm (D – G).

Figure 6.9. (Continued)

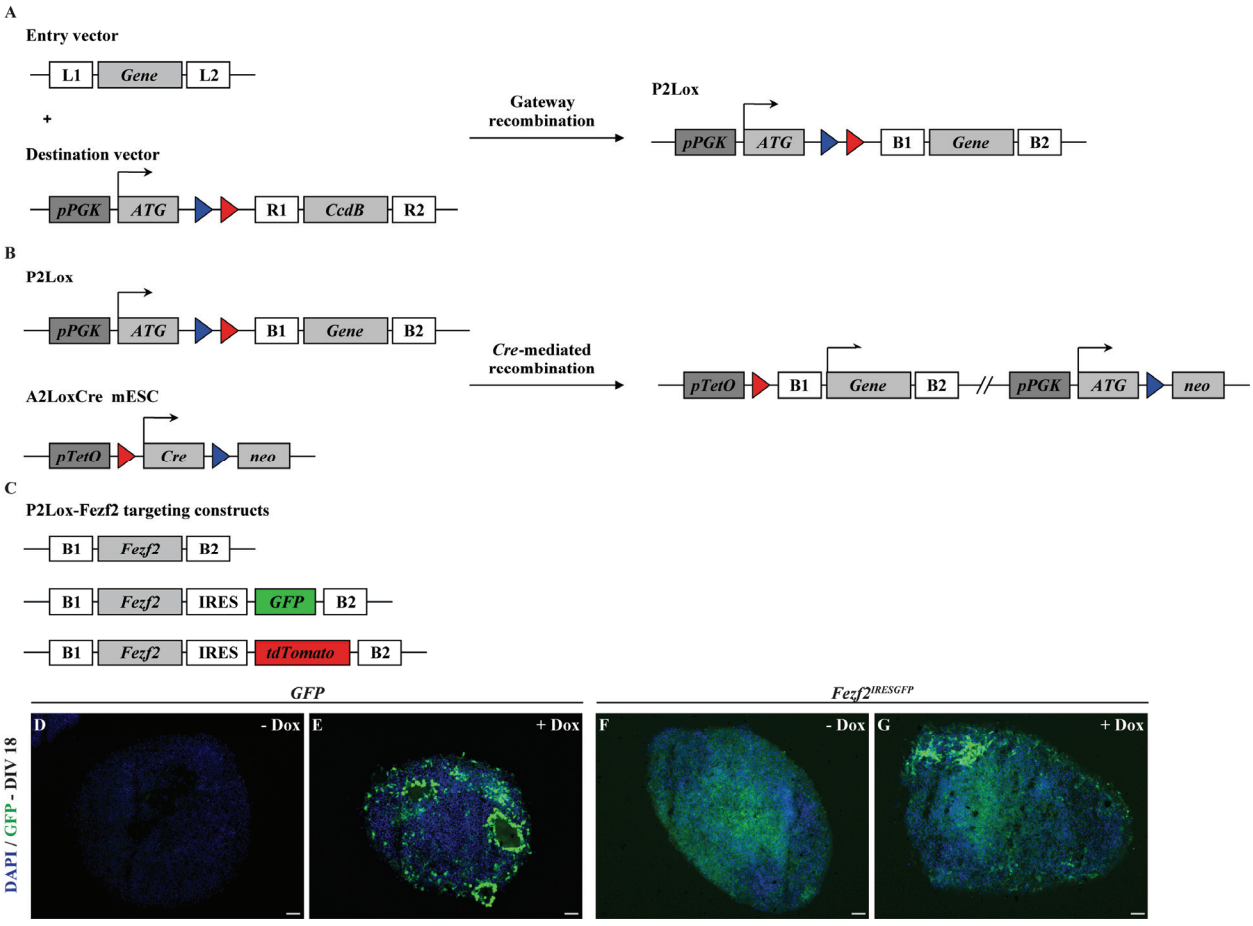

form 3D aggregates for 10 days before adding doxycycline from DIV 10 to DIV 18. Immunostaining on cross-sections of uninduced and induced aggregates for GFP showed that transgene expression is only induced upon doxycycline addition and not otherwise (Figures 6.9.D. to 6.9.G.). Hence, these overexpressor lines can efficiently express transgene upon doxycycline induction. Interestingly, some cells in the aggregate—particularly cells organized to form the core of an aggregate—do not express the transgene upon doxycycline administration. Subsequent marker analysis, as described in sections 6.3.5. and 6.3.6., showed that these cells also do not express any marker of interest, which led me to speculate that these cells are unhealthy, dying cells that may have silenced the HPRT locus.

6.3.5. *Fezf2* induced cells repress certain CPN specific genes.

6.3.5.A. Lentiviral transduction.

I hypothesize that *Fezf2* overexpression in DTP and/or CLN derived from mESC or miPSC can selectively direct their differentiation into CfuPN, including SCPN/CSMN *in vitro*. If this hypothesis is true, I expect *Fezf2* induction to repress CPN specific genes. To test this hypothesis, I first differentiated A5 mESC by culturing them in suspension to form 3D aggregates for 10 days and chemically dissociated these aggregates before replating them as a monolayer on fibronectin/laminin/poly-D-lysine coated coverslips for lentiviral transduction on DIV 11, as shown in Figure 6.10.A. (n = 3). Doxycycline was added from DIV 12 to DIV 20 for a period of 8 days to maintain transgene expression. I used lentiviruses expressing LV^{Fezf2} or LV^{GFP} (Figure 6.10.A.), and stained for CPN specific marker SATB2 (30, 31) at DIV 20. Strikingly, I discovered that *Fezf2* induced cells do not coexpress SATB2, while control GFP induced cells do (Figures 6.10.B. to 6.10.G.). This is consistent with previous work in our

Figure 6.10. *Fezf2* induced cells repress SATB2, a CPN specific marker.

(A) Lentiviral constructs and a schematic of lentiviral transduction.

(B – G) *Fezf2* induced cells (white arrows) do not coexpress SATB2, a marker that is expressed in CPN across all cortical layers. These cells segregate away from mock untransduced cells that are $SATB2^+$. In contrast, GFP induced cells coexpress SATB2 and are clustered together with $SATB2^+$ cells.

(H) Overexpressor mESC lines and a schematic illustrating transgene induction by doxycycline (Dox) addition.

(I – N) Similar to results obtained in (B – G), *Fezf2* induced cells (white arrows) do not coexpress SATB2 while GFP induced cells do. Likewise, *Fezf2* induced cells segregate away from $SATB2^+$ cells while GFP induced cells cluster together with $SATB2^+$ cells. Scale bars: 50 μm (B – G and I – N), 10 μm (inserts).

Figure 6.10. (Continued)

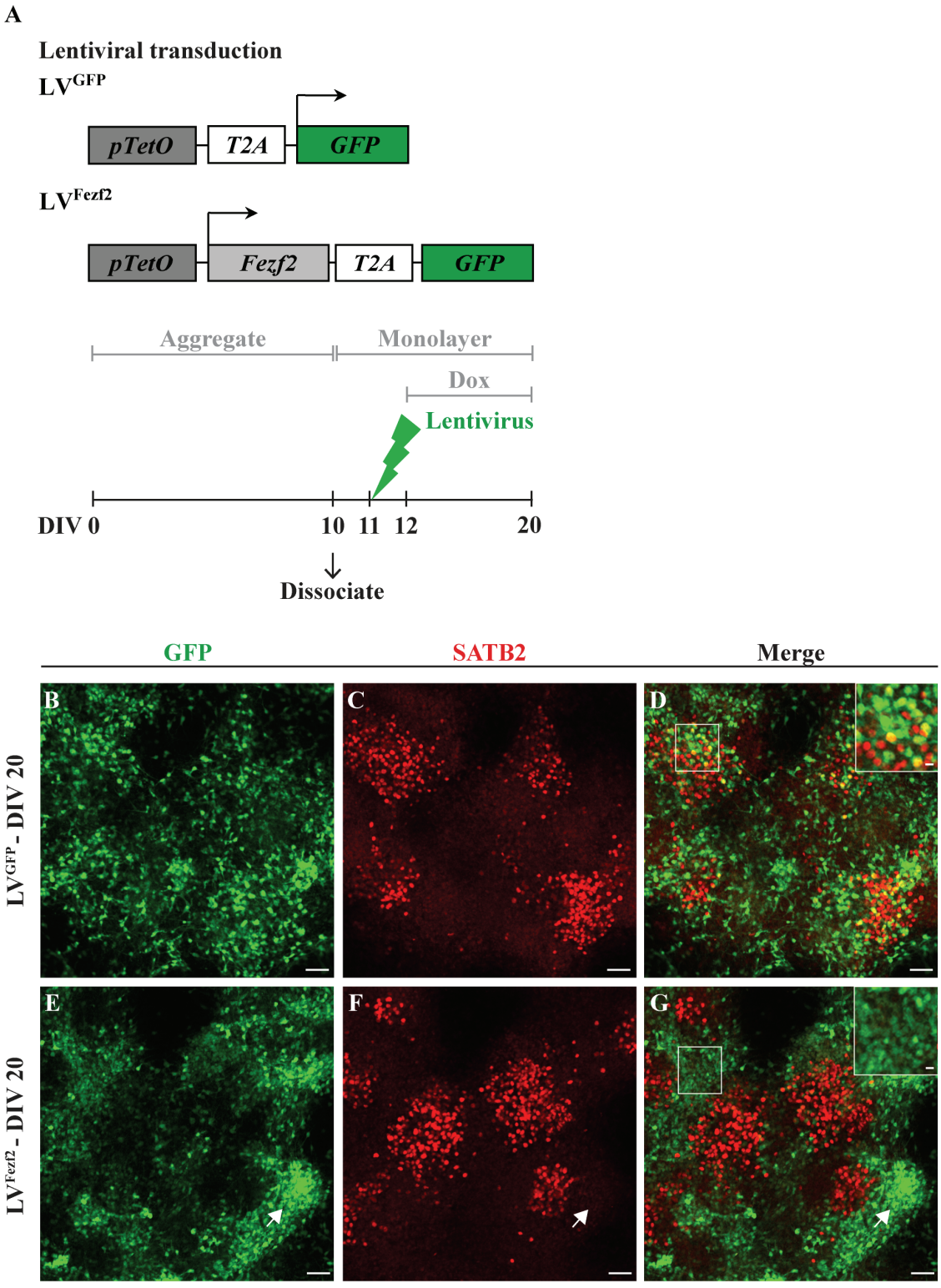

Figure 6.10. (Continued)

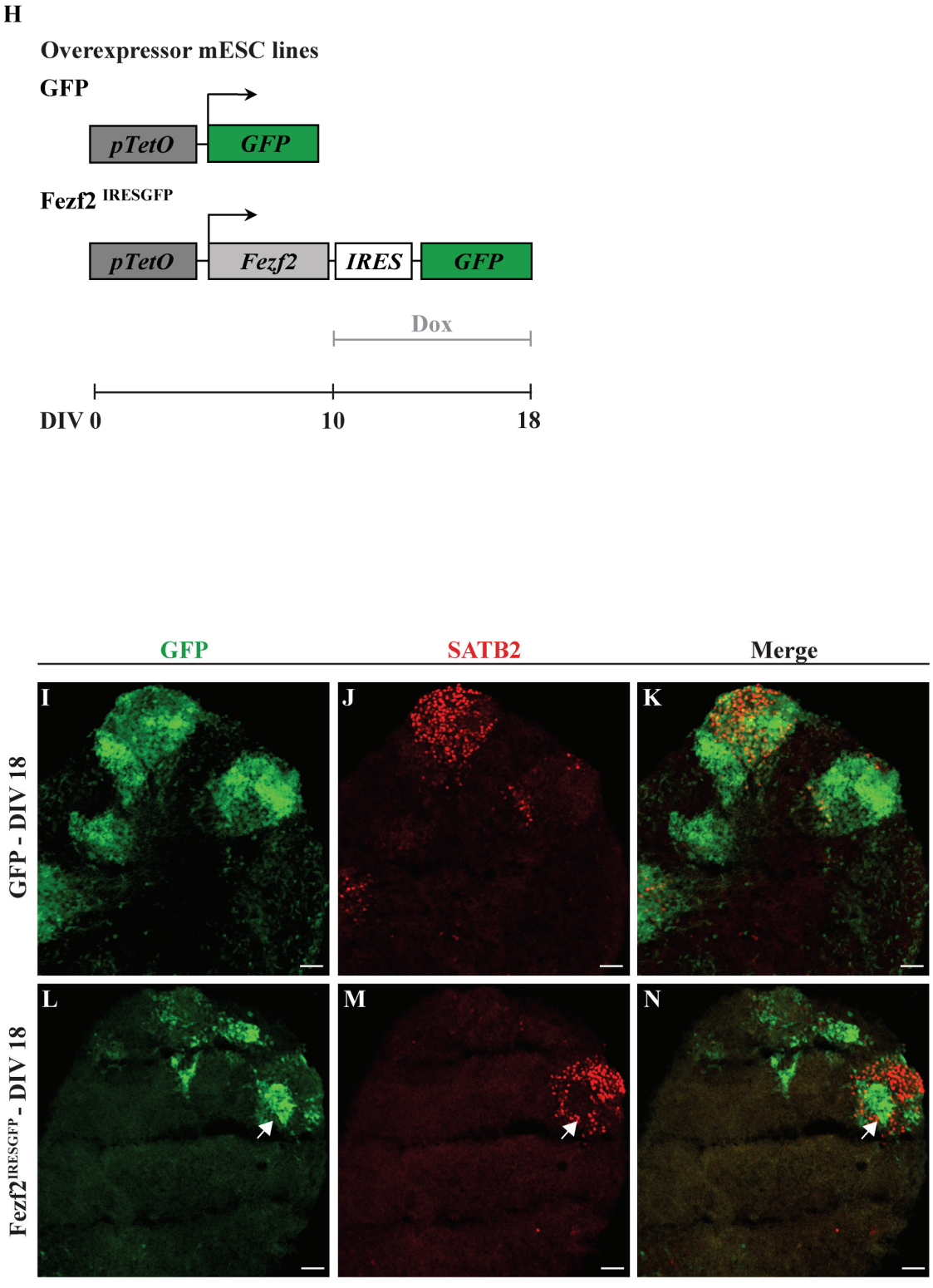

laboratory, which demonstrated that *Fezf2* overexpression represses CPN specific marker SATB2 in cortical progenitors that normally generate upper layer CPN *in vivo* (22). Hence, *Fezf2* overexpressing cells repress CPN specific marker SATB2.

To quantify the different CLN populations upon *Fezf2* overexpression with an unbiased method, as described in section 6.3.2., I dissociated the infected culture at DIV 20 into a single cell suspension, then fixed, permeabilized and stained them intracellularly with subtype-specific markers like CTIP2 and SATB2, and analyzed them by flow cytometry analysis (n = 3). Similar to what is observed in section 6.3.2., the percentages of $CTIP2^+$ and $SATB2^+$ cells are highly variable between independent experiments, which is likely caused by inconsistent dissociation of these cells that tend to form clumps by DIV 20 (data not shown). To circumvent this limitation, I repeated the experiment on nuclei extracted from transduced cells (n = 1). I found that the amount of transduced cells needed for such analysis is much greater than is experimentally feasible. Hence, future quantification may need to rely on the biased method of quantifying cells of interest within a selected field of interest.

6.3.5.B. Overexpressor mESC lines.

To ascertain the results shown in section 6.3.5.A., I differentiated the *GFP*, $Fezf2^{IRESGFP}$ and $Fezf2^{IREStdTomato}$ lines by culturing them in suspension to form 3D aggregates for 10 days before adding doxycycline from DIV 10 to DIV 18 for a period of 8 days to maintain transgene expression, similar to what was performed with lentiviral transduction (Figure 6.10.H.). ICC for CPN specific marker SATB2 at DIV 18 revealed similar results where *Fezf2* induced cells do not coexpress SATB2, while control GFP induced cells do (Figures 6.10.I. to 6.10.N., data not shown for $Fezf2^{IREStdTomato}$ line). Therefore, these results further confirm that *Fezf2* overexpressing cells repress CPN specific marker SATB2. ISH for *PlxnD1*, a marker that is

expressed at high levels in CPN of layer IV and Va and at low levels in CPN of upper layers II/III (42), also showed that *Fezf2* induced cells express *PlxnD1* at low levels, as compared to GFP control cells that express *PlxnD1* at high levels (data not shown). In contrast, ISH for *Dkk3*, a marker that is expressed at high levels in CPN of deep cortical layer VI (42), did not reveal any observable differences between *Fezf2* and control GFP induced cells (data not shown). Hence, these data show that *Fezf2* induced cells can repress CPN specific genes like SATB2 and *PlxnD1* but not *Dkk3*. It is also likely that ISH analysis is not sensitive enough to detect a few fold difference in gene expression as quantitative PCR (qPCR) analysis in section 6.3.5.C. revealed a reduction in *Dkk3* mRNA expression in FACS-purified *Fezf2* induced cells. Hence, a comprehensive expression profile by deep sequencing and subsequent comparative analysis will enable us to better determine the full extent of this repression mediated by *Fezf2*.

6.3.5.C. Expression profiling of FACS-purified *Fezf2* induced cells.

To understand the full extent of *Fezf2* mediated repression of CPN specific genes, I differentiated the *GFP* and *Fezf2*^{IRESGFP} lines by culturing them in suspension to form 3D aggregates for 10 days before adding doxycycline from DIV 10 to DIV 18 for a period of 8 days to maintain transgene expression (n = 1 experiment for each clone, n = 2 clones for each line). At DIV 12 and DIV 18, I dissociated the aggregates with 0.05% Trypsin and purified the *Fezf2*$^{+}$/GFP^{+} cells by FACS (Figure 6.11.A.). qPCR analysis on extracted RNA of purified *Fezf2*$^{+}$/GFP^{+} cells that were induced at DIV 9 and isolated at DIV 11 showed that *Fezf2* induced cells have significant induction of *Fezf2* (fold change ~ 177), as compared to control GFP induced cells (Figure 6.11.B). Similar analysis for CPN specific genes like *Satb2* and *Dkk3* showed that *Fezf2* induced cells significantly downregulate the mRNA expression of these genes (*Satb2*: fold change ~ -2.7; *Dkk3*: fold change ~ 6.0), as compared to control GFP induced cells

Figure 6.11. FACS-purified *Fezf2* induced cells repress certain CPN specific genes while inducing CfuPN specific markers.

(A) Schematic illustrating the purification of *Fezf2*$^{+}$/GFP^{+} cells from overexpressor mESC lines by FACS for expression profiling by deep sequencing analysis.

(B – F) qPCR analysis on extracted RNA of purified *Fezf2*$^{+}$/GFP^{+} cells that were induced at DIV 9 and isolated at DIV 11 (48 hours of transgene induction) showed that *Fezf2* induced cells has significant upregulation of *Fezf2* (fold change ~ 177), as compared to control GFP induced cells (B). Similar analysis for CPN specific genes like *Satb2* and *Dkk3* showed that *Fezf2* induced cells significantly downregulate the mRNA expression of these genes (*Satb2*: fold change ~ -2.7; *Dkk3*: fold change ~ 6.0), as compared to that of control GFP cells (C – D). In contrast, qPCR analysis for CfuPN specific genes like *Mu-crystallin* and *Pcp4* showed that *Fezf2* induced cells significantly upregulate the mRNA expression of these genes (*Mu-crystallin*: fold change ~ 5.9; *Dkk3*: fold change ~ 5.8), as compared to control GFP induced cells (E – F).

Figure 6.11. (Continued)

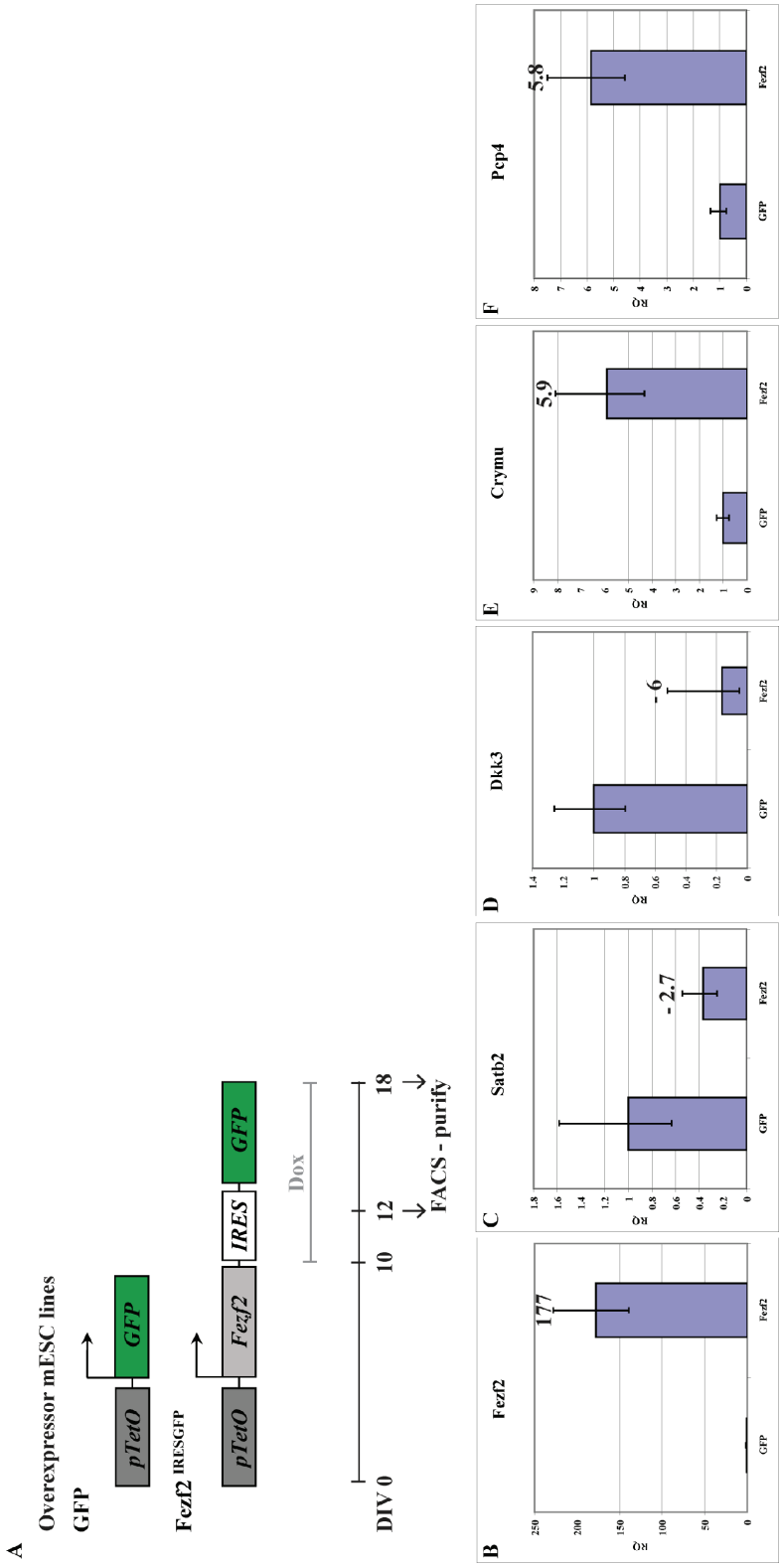

(Figures 6.11.C. and 6.11.D.). In agreement with results shown in sections 6.3.5.A. and 6.3.5.B., these data show that *Fezf2* overexpression can repress certain CPN specific genes in mESC/miPSC-derived neurons. To understand the full extent of *Fezf2* repression of CPN specific genes, I have since purified DIV 12 and DIV 18 $Fezf2^{+}$/GFP^{+} cells (n = 2 clones per line). Dr. Chiara Gerhardinger and Dr. Chen have prepared the cDNA library from RNA extracted from purified cells. The samples have been sent for Illumina HiSeq-based deep sequencing. Deep sequencing analysis will be done in collaboration with Dr. Loyal Goff, a post-doctoral fellow in the laboratory of Professor John Rinn (Department of Stem Cell and Regenerative Biology, Harvard University). The molecular profiles of these $Fezf2^{+}$/GFP^{+} cells will be compared to that of E15.5 and E16.5 cortical PN subtypes that have been purified and profiled by Dr. Molyneaux (unpublished data).

6.3.6. *Fezf2* induced cells upregulate some CfuPN specific genes.

6.3.6.A. Lentiviral transduction.

I hypothesize that *Fezf2* overexpression in DTP and/or CLN derived from mESC or miPSC can selectively direct their differentiation into CfuPN, including SCPN/CSMN *in vitro*. To test this hypothesis, I first differentiated A5 mESC by culturing them in suspension to form 3D aggregates for 10 days and chemically dissociated these aggregates before replating them as a monolayer on fibronectin/laminin/poly-D-lysine coated coverslips for lentiviral transduction on DIV 11, as shown in Figure 6.10.A. (n = 3). Doxycycline was added from DIV 12 to DIV 20 for a period of 8 days to maintain transgene expression. I used lentiviruses expressing LV^{Fezf2} or LV^{GFP} (Figure 6.10.A.), and collected the cells for both ICC as well as qPCR analysis at DIV 20. Although both *Fezf2* and GFP induced cells express TLE4, a CThPN specific marker (38), I

found that *Fezf2* induced cells repress the expression of CTIP2, a marker that is expressed at high levels in SCPN and low levels in CThPN (27), while control GFP induced cells do not (data not shown). The repression of CTIP2 is supported by previous studies done in our laboratory where CTIP2 is induced at low proportions in *Fezf2* reprogammed neurons, as compared to other markers like TLE4 and *Mu-crystallin* (24). Remarkably, qPCR analysis for *Mu-crystallin*, a marker that is expressed at high levels in SCPN and at lower levels in CThPN (27), and *Pcp4*, a marker that is expressed at high levels in SCPN (27), showed that *Fezf2* overexpression in lentivirally transduced mESC-derived neurons upregulates the mRNA expression of these genes (*Mu-crystallin*: fold change ~ 12.8; *Pcp4*: fold change ~ 2.2), as compared to mock untransduced as well as control GFP induced cells (Figures 6.12.A. and 6.12.B.). Hence, these data show that *Fezf2* expressing cells can express or upregulate certain CfuPN specific markers with the exception of CTIP2. Comprehensive expression profiling of *Fezf2* induced cells will provide insights on the full extent of *Fezf2* mediated induction of CfuPN selective genes.

6.3.6.B. Overexpressor mESC lines.

To ascertain the results shown in section 6.3.6.A., I differentiated the *GFP*, *Fezf2*^{IRESGFP} and *Fezf2*^{IREStdTomato} lines by culturing them in suspension to form 3D aggregates for 10 days before adding doxycycline from DIV 10 to DIV 18 for a period of 8 days to maintain transgene expression, similar to what was performed with lentiviral transduction (Figure 6.10.H.). ISH for CfuPN specific markers *Mu-crystallin* and *Pcp4* at DIV 18 showed that *Fezf2* induced cells upregulate mRNA expression of *Mu-crystallin*, while control GFP induced cells do not (Figure 6.12.C. to 6.12.D., data not shown for *Fezf2*^{IREStdTomato} line). In contrast, I did not detect any observable difference between *Pcp4* mRNA expression between *Fezf2* and GFP induced cells (data not shown). It is likely that ISH analysis is not sensitive enough to detect a two-or three-

Figure 6.12. *Fezf2* induced cells upregulate some CfuPN specific genes.

(A – B) qPCR analysis showed that *Fezf2* induced cells upregulate mRNA expression of CfuPN specific genes like *Mu-crystallin* and *Pcp4* while control GFP induced cells and mock untransduced cells do not.

(C – D) Similar to results obtained in (A – B), ISH for *Mu-crystallin* on DIV 18 aggregates derived from overexpressor mESC lines (*GFP* and *Fezf2*^{IRESGFP}) showed that *Fezf2* induced cells upregulate *Mu-crystallin* mRNA expression (arrows), as compared to control GFP induced cells. Scale bars: 100 μm (C – D).

Figure 6.12. (Continued)

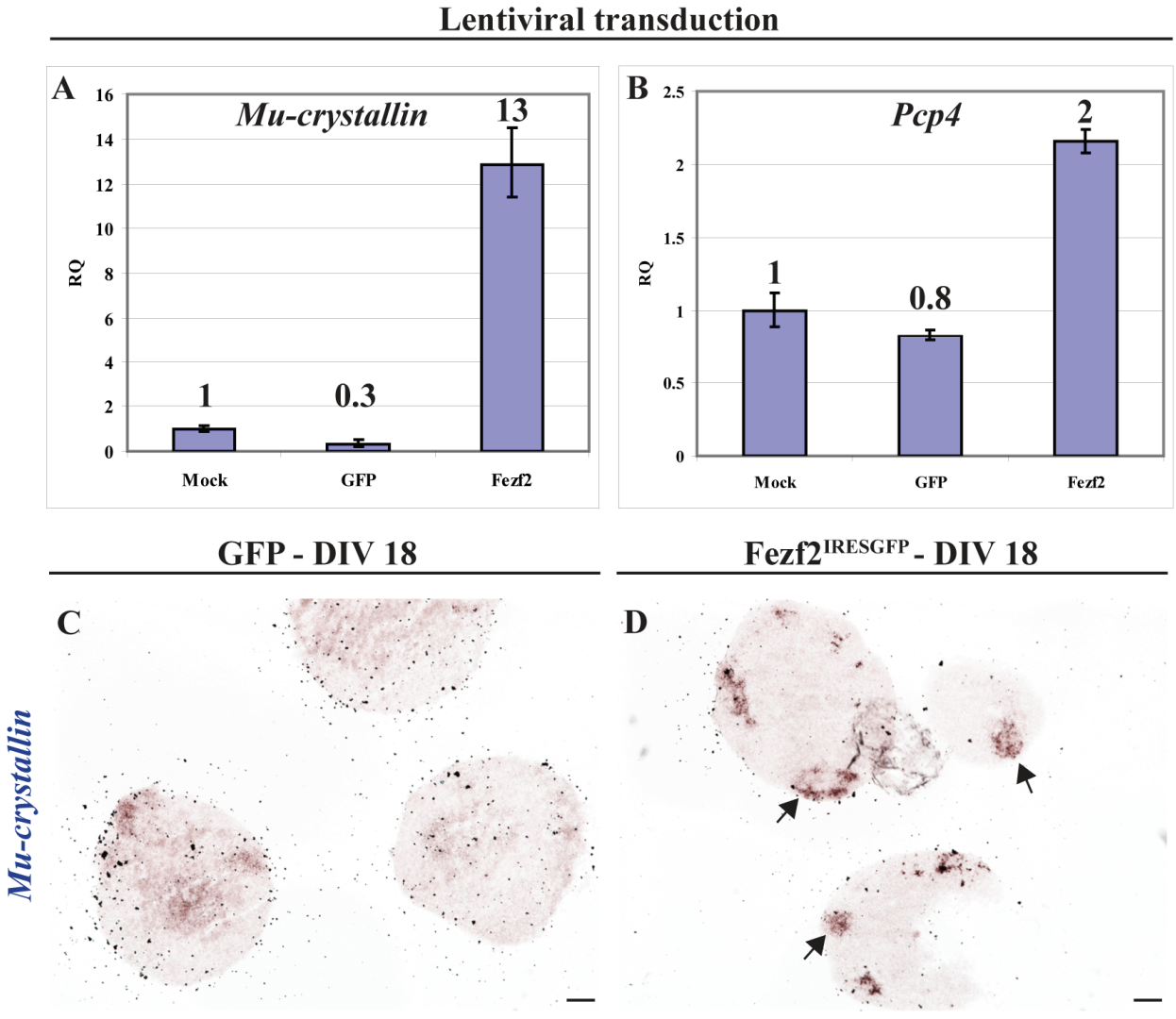

fold difference in gene expression; therefore, a comprehensive expression profile by deep sequencing and subsequent comparative analysis will enable us to better determine the full extent of this upregulation mediated by *Fezf2*.

6.3.6.C. Expression profiling of FACS-purified *Fezf2* induced cells.

To understand the full extent of *Fezf2* mediated repression of CPN specific genes, I differentiated the *GFP* and *Fezf2*^{IRESGFP} lines by culturing them in suspension to form 3D aggregates for 10 days before adding doxycycline from DIV 10 to DIV 18 for a period of 8 days to maintain transgene expression (n = 1 experiment for each clone, n = 2 clones for each line). At DIV 12 and DIV 18, I dissociated the aggregates with 0.05% Trypsin and purified the *Fezf2*$^{+}$/GFP^{+} cells by FACS (Figure 6.11.A.). qPCR analysis on extracted RNA of purified *Fezf2*$^{+}$/GFP^{+} cells that were induced at DIV 9 and isolated at DIV 11 showed that *Fezf2* induced cells have significant induction of *Fezf2* (fold change ~ 177), as compared to control GFP induced cells (Figure 6.11.B). qPCR analysis for CfuPN specific genes like *Mu-crystallin* and *Pcp4* showed that *Fezf2* induced cells significantly upregulate the mRNA expression of these genes (*Mu-crystallin*: fold change ~ 5.9; *Pcp4*: fold change ~ 5.8), as compared to control GFP induced cells (Figures 6.11.E. and 6.11.F.). Therefore, these data showed that purified *Fezf2* induced cells can significantly upregulate CfuPN/SCPN-specific genes. In agreement with results shown in sections 6.3.6.A. and 6.3.6.B., these data show that *Fezf2* overexpression can induce certain CfuPN/SCPN-specific genes in mESC-derived neurons. To understand the full extent of *Fezf2* upregulation of CfuPN specific genes, I have since purified DIV 12 and DIV 18 *Fezf2*$^{+}$/GFP^{+} cells (n = 2 clones per line). Dr. Chiara Gerhardinger and Dr. Chen have prepared the cDNA library from RNA extracted from purified cells. The samples have been sent for Illumina HiSeq-based deep sequencing. Deep sequencing analysis will be done in collaboration

with Dr. Loyal Goff, a post-doctoral fellow in the laboratory of Professor John Rinn (Department of Stem Cell and Regenerative Biology, Harvard University). The molecular profiles of these *Fezf2*$^{+}$/GFP^{+} cells will be compared to those of E15.5 and E16.5 cortical PN subtypes that have been purified and profiled by Dr. Molyneaux (unpublished data).

6.3.7. Transplanted *Fezf2* induced cells project preferentially through the internal capsule to subcortical and subcerebral targets and rarely develop callosal interhemispheric connections.

To determine if *Fezf2* induced cells preferentially project to subcortical or subcerebral targets, I transduced dissociated A5 mESC-derived DTP/CLN with lentivirus expressing LV^{Fezf2}, and transplanted enzymatically-dissociated *Fezf2* induced neurons into the cortex of P3 *Fezf2*$^{-/-}$ and their littermate wild type control pups. Transgene induction is maintained by administrating doxycycline to nursing dams. At 1 to 4 weeks after transplantation, I stained for GFP to detect *Fezf2*$^{+}$/GFP^{+} cell soma in the cortex and *Fezf2*$^{+}$/GFP^{+} axonal projections. Strikingly, at 4 weeks after transplantation, I found many *Fezf2* induced cells to be alive and organized into a clump emanating dendrites and axonal projections, many of which were organized into axonal bundles of the internal capsule with long distance projections to subcortical targets like the thalamus and subcerebral targets like the cerebral peduncle (Figures 6.13.A. to 6.13.E., n = 4 animals). Notably, I detected that *Fezf2* induced cells rarely project across the corpus callosum to the contralateral hemisphere (Figure 6.13.F., n = 4 animals). Examination of *Fezf2* induced cells that were transplanted near or at the corpus callosum further ascertained this result (n = 3 animals). In these cases, I observed few callosal interhemispheric connections by *Fezf2* induced cells (Figure 6.13.F.). This is in contrast to published work where mock or control GFP^{+} cells develop

Figure 6.13. *Fezf2* induced cells project preferentially through the internal capsule to subcortical and subcerebral targets and rarely develop callosal interhemispheric connections.

(A – F) At 4 weeks after transplantation, immunostaining for GFP revealed that *Fezf2* induced cells are organized into a clump emanating dendrites (A) and axonal projections, many of which are organized into axonal bundles of the internal capsule (B – C) with long distance projections to subcortical targets like the thalamus (E) and subcerebral targets like the cerebral peduncle (CP) (D). In contrast, transplanted *Fezf2* induced cells rarely project via the corpus callosum (CC) to the contralateral hemisphere (F). Dotted lines indicate boundaries of described structure. Scale bars: 50 μm (C – D).

Figure 6.13. (Continued)

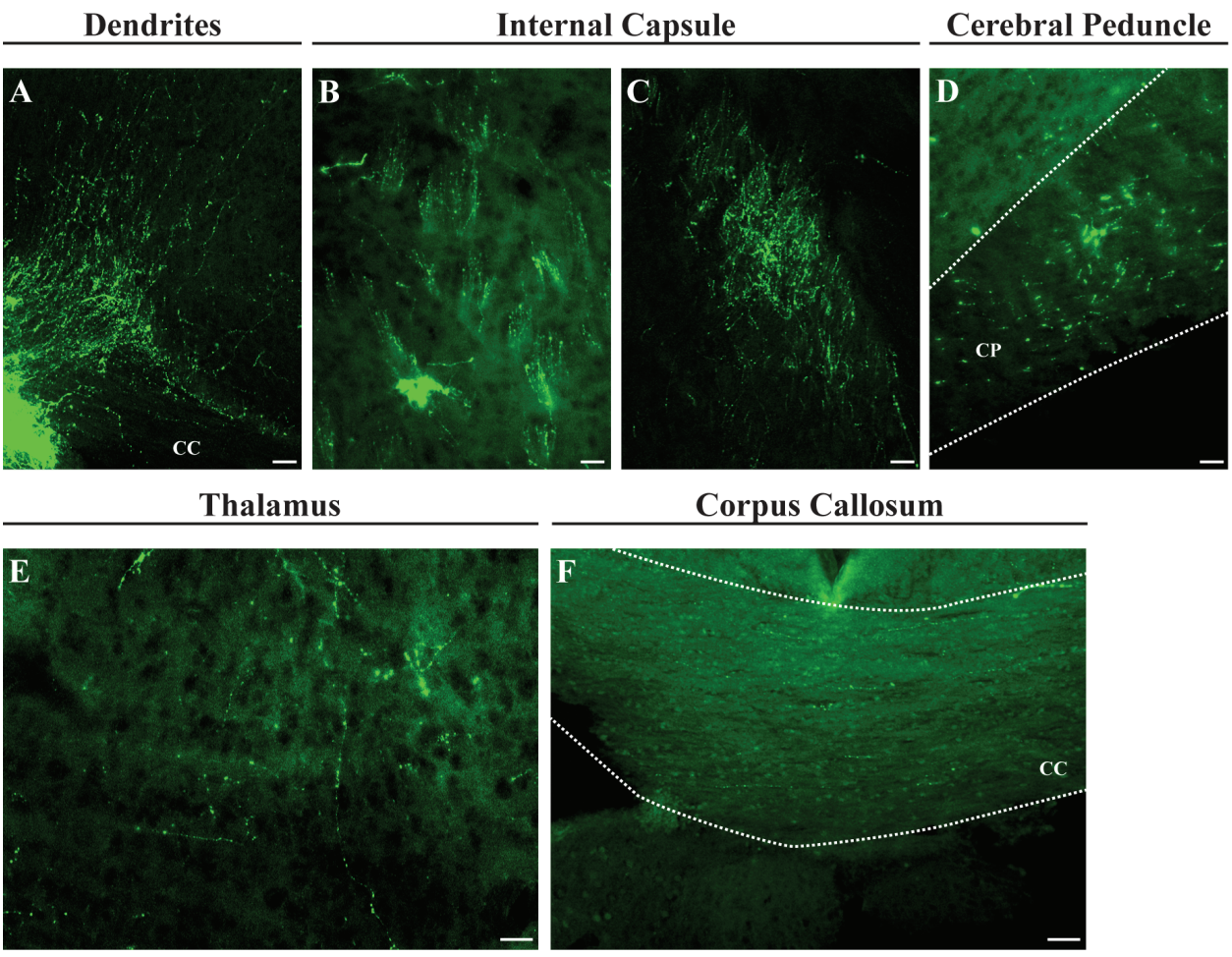

significantly observable axonal extensions via the corpus callosum to the contralateral hemisphere (14-16). Transplantations with cells that are lentivirally transduced with control lentivirus expressing LV^{GFP} are ongoing and necessary to confirm the above results. In all, and in accordance with the results obtained by the molecular analysis shown in sections 6.3.5. and 6.3.6., these data support that *Fezf2* induced cells repress CPN specific genes while upregulating CfuPN selective genes. This molecular change mediated by *Fezf2* is reflected in similar changes to the axonal connectivity where *Fezf2* induced cells project preferentially through the internal capsule to subcortical and subcerebral targets and rarely develop callosal interhemispheric connections.

6.4. Discussion.

By using combinatorial marker analysis as well as expression profiling, I molecularly characterized DTP and CLN derived from mESC and/or miPSC from two established protocols—the monolayer culture (15, 16) as well as the aggregation culture (13, 14). Combinatorial molecular analysis is not only necessary to identify neuronal subclasses like CfuPN/SCPN, but also crucial to defining the extent of differentiation into specific neuronal subtypes and to investigating the possible acquisition of mixed identity. I found that the aggregation culture is more robust and reproducible in generating DTP and CLN than the monolayer culture. I also discovered that the aggregation method can produce significant numbers of $TBR1^{+}CTIP2^{+}$ cortical plate-like cells as well as CLN that can successful segregate layer specific marker genes like *Tle4*, *Ctip2* and *Satb2*. Expression profiling of these distinct layer specific CLN is ongoing and is imperative to advance our current knowledge on how similar or different these *in vitro* mESC/miPSC-derived CLN are to *bona fide* SCPN. It also enables the field to develop a defined benchmark upon which future directed differentiation experiments can improve.

The central role played by transcription factor *Fezf2* in early SCPN differentiation (18-24) led me to investigate whether cell-autonomous developmental signals that direct early SCPN development in the embryo can be used to selectively generate these neurons from mESC/miPSC-derived DTP and CLN *in vitro*. Here, I report that *Fezf2* can preferentially direct the differentiation of CfuPN like neurons from mESC/miPSC-derived DTP and CLN. *Fezf2* does so by repressing certain CPN specific genes like *Satb2* and *PlxnD1* while upregulating some CfuPN specific genes such as *Mu-crystallin* and *Pcp4*. The full extent of *Fezf2* mediated repression and induction of subtype-specific genes is currently being investigated by expression

profiling with deep sequencing followed by comparative analysis with molecular profiles of early embryonic *bona fide* SCPN. The change in the molecular identity of *Fezf2* induced cells is reflected in the changes to their axonal connectivity where these cells preferentially project their axons through the internal capsule to subcortical and subcerebral targets like the thalamus and cerebral peduncle, which is in line with *Fezf2's* upregulation of CfuPN specific genes. Notably, in agreement with *Fezf2's* repression of CPN specific genes, these cells rarely connect via the corpus callosum to the contralateral hemisphere.

mESC and/or miPSC can be directed to generate diverse populations of DTP and CLN, yet this diversity is not as well understood as that of *bona fide* neurons in the cortex. Understanding neuronal diversity is important to comprehend the limits of directed differentiation and the reproducibility of producing distinct neuronal subclasses *in vitro*. In the cerebral cortex, the huge diversity of progenitors and neurons is tightly controlled and organized both temporally and spatially (38). Hence, it becomes possible to classify different populations of neurons by their birthdates, laminar positions, molecular identities as well as axonal connectivity (38). In contrast, this cannot be achieved in the dish where different cellular populations are generated concurrently and are organized randomly. Though cells differentiated via the aggregation culture maintain a 3D structure that resembles a "mini-cortex" *in vivo*, it is also different. Notably, the layer specific CLN generated are predominantly of a deep layer identity and less of an upper layer II/III CPN identity. Single cell sequencing has been proposed to allow gauging of neuron diversity *in vivo* (43, 44), but its feasibility for *in vitro* studies remains uncertain due to the inherent problems of reproducibility between experiments. I argue that population-based analyses may be a better method to obtain knowledge of the neuronal diversity generated *in vitro*. Neuronal subtype identity is often defined not by a single marker,

but by a combination of distinct genes. Hence, population-based analyses are limited by the availability of reliable antibodies, a problem that must be solved before neuronal diversity in the dish can be accounted for.

I have shown that cell-intrinsic signals like *Fezf2* that are developmentally relevant can be manipulated to instruct mESC/miPSC-derived DTP and CLN to become more CfuPN-like in terms of their molecular identities as well as axonal connectivity. It remains to be tested whether other genes, whether in combination with *Fezf2* or not, can also be utilized. Current knowledge of cell-autonomous signals that control definitive aspects of CfuPN/SCPN continues to restrict our manipulation in the dish. Therefore, discovering novel effectors of SCPN development continues to be an area of interest.

6.5. Materials and Methods.

6.5.1. Cell culture.

Several lines of miPSC (A1, A2 and A3 lines) that were derived from adult male fibroblasts as well as several lines of mESC (A4, A5 and A6 lines) were generated and generously given by Professor Konrad Hochedlinger from the Harvard Department of Stem Cell and Regenerative Biology, Harvard University in Boston, Massachusetts, USA. mESC and/or miPSC were grown on gelatin-coated dishes with irradiated mouse embryonic fibroblasts (MEF) in mESC medium (Knockout DMEM, 15% fetal bovine serum, 2 mM Glutamax, 100 U / mL Penicillin/Streptomycin, 1X MEM non essential amino acids and 1 X 10^3 units ESGRO / mL), and were passaged every 2 to 3 days with 0.25% Trypsin. Dissociated mESC and/or miPSC were preplated on gelatin-coated dishes to preferentially remove MEF before being subcultured to initiate differentiation experiments. Monolayer culture was performed according to previously described methods outlined in (15, 16) while aggregation culture was done in accordance with published protocols described in (13, 14). At desired timepoints, aggregates were washed in PBS and fixed in 4% PFA for 1 hour at r.t. before being rinsed in PBS overnight. The next day, aggregates were immersed in 30% sucrose and in OCT for 1 hour before being frozen in OCT on dry ice and stored at -80 ^{o}C. Aggregates were serially sectioned at 20 μm thickness on the cryostat before downstream analysis.

6.5.2. Fluorescent Immunohistochemistry.

Fluorescent immunohistochemistry procedures were carried out as described in relevant sections of Chapter 2. The following primary antibodies and relevant dilutions were used: mouse anti-OCT3/4, 1:250 (Catalog number: BDB611202, BD Transduction Laboratories, USA),

mouse anti-NESTIN, 1:200 (Catalog number: 556309, BD Biosciences, USA), rabbit anti-BF1, 1:1000 (Catalog number: SCFAB, StemCulture Inc, USA), rabbit anti-PAX6, 1:1000 (Catalog number: PRB-278P, Covance, USA), mouse anti-TUJ1, 1:1000 (Catalog number: MMS-435P, Covance, USA), mouse anti-NeuN, 1:500 (Catalog number: MAB377, Millipore, USA), mouse anti-MAP2, 1:500 (Catalog number: M1406-.2ML, Sigma-Aldrich, USA), goat anti-SOX5, 1:500 (Catalog number: 17329, Santa Cruz Biotechnology, USA), rat anti-CTIP2, 1:1000 (Catalog number: AB18465, Abcam, USA), goat anti-BHLHB5 (E-17), 1:500 (Catalog number: sc-6045, Santa Cruz Biotechnology, USA), mouse anti-MU CRYSTALLIN, 1:100 (Catalog number: AB54669, Abcam, USA), rabbit anti-CUX1 (CDP M-222), 1:100 (Catalog number: SC13024, Santa Cruz Biotechnology, USA), mouse anti-SATB2, 1:50 (Catalog number: AB51502, Abcam, USA), goat anti-LHX2, 1:200 (Catalog number:SC-19344, Santa Cruz Biotechnology, USA), goat anti-BRN2, 1:200 (Catalog number: SC-6029, Santa Cruz Biotechnology, USA), rabbit anti-TBR1, 1:1000 (a gift from Professor Robert Hevner, University of Washington, USA), rabbit anti-ZFPM2/FOG2, 1:500 (Catalog number: SC-10755, Santa Cruz Biotechnology, USA).

6.5.3. *In situ* hybridization.

Nonradioactive colorimetric in situ hybridization was executed as described in relevant sections of Chapter 2.

6.5.4. Lentiviral transduction.

Lentivirus production and transduction were carried out in accordance with previously published methods (45).

6.5.5. qPCR analysis.

TaqMan qPCR analysis was carried out in accordance with the manufacturer's protocol. The following primer sets are used: Mouse *Fezf2* (Catalog number: 4448892, ID: Mm01320619_m1, Invitrogen, USA), mouse *Satb2* (Catalog number: 4331182, ID: Mm00507331_m1, Invitrogen, USA), mouse *Dkk3* (Catalog number: 4331182, ID: Mm00443800_m1, Invitrogen, USA), mouse *Mu-crystallin* (Catalog number: 4331182, ID: Mm00516679_m1, Invitrogen, USA) and mouse *Pcp4* (Catalog number: 4331182, ID: Mm00500973_m1, Invitrogen, USA)

6.5.6. Transplantation.

Transduced A5 mESC-derived DTP/CLN with lentivirus expressing LV^{Fezf2} were dissociated enzymatically with Accutase for 20 to 30 minutes at 37 ^{o}C. Dissociated cells were resuspended in Optimem and mixed with 0.005% Fast Green FCF (Catalog number: F7258-25G, Sigma-Aldrich, USA) to enable easy visualization of cells upon injection. P3 pups were anesthetized by hypothermia with ice for at least 3 minutes before 1 μl of cell suspension at an approximate density of 5 to 10 X 10^4 cells / μl (total of 5 to 10 X 10^4 cells per animal) was injected into the cortex by a glass microcapillary over 3 minutes. Transgene was induced and maintained by administrating doxycycline (2 mg / mL) to nursing dams. 4 weeks after transplantation, the cortex was dissected, fixed and sectioned at 40 μm thickness with cold PBS either on a coronal or sagittal plane with a VT1000S vibrating microtome (Leica Microsystems). Floating sections were stored in PBS-Azide at 4 ^{o}C.

6.5.7. Microscopy and image analysis.

Microscopy and image analysis were performed as described in relevant sections of Chapter 2.

6.6. References.

1. Takahashi K, Okita K, Nakagawa M, Yamanaka S. Induction of pluripotent stem cells from fibroblast cultures. Nat Protoc. 2007;2(12):3081-9.

2. Takahashi K, Yamanaka S. Induction of pluripotent stem cells from mouse embryonic and adult fibroblast cultures by defined factors. Cell. 2006 Aug 25;126(4):663-76.

3. Okita K, Ichisaka T, Yamanaka S. Generation of germline-competent induced pluripotent stem cells. Nature. 2007 Jul 19;448(7151):313-7.

4. Maherali N, Sridharan R, Xie W, Utikal J, Eminli S, Arnold K, et al. Directly reprogrammed fibroblasts show global epigenetic remodeling and widespread tissue contribution. Cell Stem Cell. 2007 Jun 7;1(1):55-70.

5. Wernig M, Meissner A, Foreman R, Brambrink T, Ku M, Hochedlinger K, et al. In vitro reprogramming of fibroblasts into a pluripotent ES-cell-like state. Nature. 2007 Jul 19;448(7151):318-24.

6. Zhao XY, Li W, Lv Z, Liu L, Tong M, Hai T, et al. iPS cells produce viable mice through tetraploid complementation. Nature. 2009 Sep 3;461(7260):86-90.

7. Boland MJ, Hazen JL, Nazor KL, Rodriguez AR, Gifford W, Martin G, et al. Adult mice generated from induced pluripotent stem cells. Nature. 2009 Sep 3;461(7260):91-4.

8. Aoi T, Yae K, Nakagawa M, Ichisaka T, Okita K, Takahashi K, et al. Generation of pluripotent stem cells from adult mouse liver and stomach cells. Science. 2008 Aug 1;321(5889):699-702.

9. Wichterle H, Lieberam I, Porter JA, Jessell TM. Directed differentiation of embryonic stem cells into motor neurons. Cell. 2002 Aug 9;110(3):385-97.

10. Salero E, Hatten ME. Differentiation of ES cells into cerebellar neurons. Proc Natl Acad Sci U S A. 2007 Feb 20;104(8):2997-3002.

11. Su HL, Muguruma K, Matsuo-Takasaki M, Kengaku M, Watanabe K, Sasai Y. Generation of cerebellar neuron precursors from embryonic stem cells. Dev Biol. 2006 Feb 15;290(2):287-96.

12. Lee SH, Lumelsky N, Studer L, Auerbach JM, McKay RD. Efficient generation of midbrain and hindbrain neurons from mouse embryonic stem cells. Nat Biotechnol. 2000 Jun;18(6):675-9.

13. Watanabe K, Kamiya D, Nishiyama A, Katayama T, Nozaki S, Kawasaki H, et al. Directed differentiation of telencephalic precursors from embryonic stem cells. Nat Neurosci. 2005 Mar;8(3):288-96.

14. Eiraku M, Watanabe K, Matsuo-Takasaki M, Kawada M, Yonemura S, Matsumura M, et al. Self-organized formation of polarized cortical tissues from ESCs and its active manipulation by extrinsic signals. Cell Stem Cell. 2008 Nov 6;3(5):519-32.

15. Gaspard N, Bouschet T, Herpoel A, Naeije G, van den Ameele J, Vanderhaeghen P. Generation of cortical neurons from mouse embryonic stem cells. Nat Protoc. 2009;4(10):1454-63.

16. Gaspard N, Bouschet T, Hourez R, Dimidschstein J, Naeije G, van den Ameele J, et al. An intrinsic mechanism of corticogenesis from embryonic stem cells. Nature. 2008 Sep 18;455(7211):351-7.

17. Shen Q, Wang Y, Dimos JT, Fasano CA, Phoenix TN, Lemischka IR, et al. The timing of cortical neurogenesis is encoded within lineages of individual progenitor cells. Nat Neurosci. 2006 Jun;9(6):743-51.

18. Chen B, Schaevitz LR, McConnell SK. Fezl regulates the differentiation and axon targeting of layer 5 subcortical projection neurons in cerebral cortex. Proc Natl Acad Sci U S A. 2005 Nov 22;102(47):17184-9.

19. Chen B, Wang SS, Hattox AM, Rayburn H, Nelson SB, McConnell SK. The Fezf2-Ctip2 genetic pathway regulates the fate choice of subcortical projection neurons in the developing cerebral cortex. Proc Natl Acad Sci U S A. 2008 Aug 12;105(32):11382-7.

20. Chen JG, Rasin MR, Kwan KY, Sestan N. Zfp312 is required for subcortical axonal projections and dendritic morphology of deep-layer pyramidal neurons of the cerebral cortex. Proc Natl Acad Sci U S A. 2005 Dec 6;102(49):17792-7.

21. Molyneaux BJ, Arlotta P, Hirata T, Hibi M, Macklis JD. Fezl is required for the birth and specification of corticospinal motor neurons. Neuron. 2005 Sep 15;47(6):817-31.

22. Lodato S, Rouaux C, Quast KB, Jantrachotechatchawan C, Studer M, Hensch TK, et al. Excitatory projection neuron subtypes control the distribution of local inhibitory interneurons in the cerebral cortex. Neuron. 2011 Feb 24;69(4):763-79.

23. Rouaux C, Arlotta P. Fezf2 directs the differentiation of corticofugal neurons from striatal progenitors in vivo. Nat Neurosci. 2010 Nov;13(11):1345-7.

24. Rouaux C, Arlotta P. Direct lineage reprogramming of post-mitotic callosal neurons into corticofugal neurons in vivo. Nat Cell Biol. 2013 Feb;15(2):214-21.

25. Ideguchi M, Palmer TD, Recht LD, Weimann JM. Murine embryonic stem cell-derived pyramidal neurons integrate into the cerebral cortex and appropriately project axons to subcortical targets. J Neurosci. 2010 Jan 20;30(3):894-904.

26. Lai T, Jabaudon D, Molyneaux BJ, Azim E, Arlotta P, Menezes JR, et al. SOX5 controls the sequential generation of distinct corticofugal neuron subtypes. Neuron. 2008 Jan 24;57(2):232-47.

27. Arlotta P, Molyneaux BJ, Chen J, Inoue J, Kominami R, Macklis JD. Neuronal subtype-specific genes that control corticospinal motor neuron development in vivo. Neuron. 2005 Jan 20;45(2):207-21.

28. Joshi PS, Molyneaux BJ, Feng L, Xie X, Macklis JD, Gan L. Bhlhb5 regulates the postmitotic acquisition of area identities in layers II-V of the developing neocortex. Neuron. 2008 Oct 23;60(2):258-72.

29. Nieto M, Monuki ES, Tang H, Imitola J, Haubst N, Khoury SJ, et al. Expression of cux-1 and cux-2 in the subventricular zone and upper layers II-IV of the cerebral cortex. J Comp Neurol. 2004 Nov 8;479(2):168-80.

30. Alcamo EA, Chirivella L, Dautzenberg M, Dobreva G, Fariñas I, Grosschedl R, et al. Satb2 regulates callosal projection neuron identity in the developing cerebral cortex. Neuron. 2008 2/7;57(3):364-77.

31. Britanova O, de Juan Romero C, Cheung A, Kwan KY, Schwark M, Gyorgy A, et al. Satb2 is a postmitotic determinant for upper-layer neuron-specification in the neocortex. Neuron. 2008 Feb 7;57(3):378-92.

32. Bulchand S, Subramanian L, Tole S. Dynamic spatiotemporal expression of LIM genes and cofactors in the embryonic and postnatal cerebral cortex. Dev Dyn. 2003 Mar;226(3):460-9.

33. Nakagawa Y, Johnson JE, O'Leary DD. Graded and areal expression patterns of regulatory genes and cadherins in embryonic neocortex independent of thalamocortical input. J Neurosci. 1999 Dec 15;19(24):10877-85.

34. McEvilly RJ, de Diaz MO, Schonemann MD, Hooshmand F, Rosenfeld MG. Transcriptional regulation of cortical neuron migration by POU domain factors. Science. 2002 Feb 22;295(5559):1528-32.

35. Sugitani Y, Nakai S, Minowa O, Nishi M, Jishage K, Kawano H, et al. Brn-1 and brn-2 share crucial roles in the production and positioning of mouse neocortical neurons. Genes Dev. 2002 Jul 15;16(14):1760-5.

36. Bulfone A, Smiga SM, Shimamura K, Peterson A, Puelles L, Rubenstein JL. T-brain-1: A homolog of brachyury whose expression defines molecularly distinct domains within the cerebral cortex. Neuron. 1995 Jul;15(1):63-78.

37. Hevner RF, Shi L, Justice N, Hsueh Y, Sheng M, Smiga S, et al. Tbr1 regulates differentiation of the preplate and layer 6. Neuron. 2001 Feb;29(2):353-66.

38. Molyneaux BJ, Arlotta P, Menezes JR, Macklis JD. Neuronal subtype-specification in the cerebral cortex. Nat Rev Neurosci. 2007 Jun;8(6):427-37.

39. Tiveron MC, Hirsch MR, Brunet JF. The expression pattern of the transcription factor Phox2 delineates synaptic pathways of the autonomic nervous system. J Neurosci. 1996 Dec 1;16(23):7649-60.

40. Iacovino M, Bosnakovski D, Fey H, Rux D, Bajwa G, Mahen E, et al. Inducible cassette exchange: A rapid and efficient system enabling conditional gene expression in embryonic stem and primary cells. Stem Cells. 2011 Oct;29(10):1580-8.

41. Mazzoni EO, Mahony S, Iacovino M, Morrison CA, Mountoufaris G, Closser M, et al. Embryonic stem cell-based mapping of developmental transcriptional programs. Nat Methods. 2011 Nov 13;8(12):1056-8.

42. Molyneaux BJ, Arlotta P, Fame RM, MacDonald JL, MacQuarrie KL, Macklis JD. Novel subtype-specific genes identify distinct subpopulations of callosal projection neurons. J Neurosci. 2009 Sep 30;29(39):12343-54.

43. Evrony GD, Cai X, Lee E, Hills LB, Elhosary PC, Lehmann HS, et al. Single-neuron sequencing analysis of L1 retrotransposition and somatic mutation in the human brain. Cell. 2012 Oct 26;151(3):483-96.

44. Iourov IY, Vorsanova SG, Yurov YB. Single cell genomics of the brain: Focus on neuronal diversity and neuropsychiatric diseases. Curr Genomics. 2012 Sep;13(6):477-88.

45. Caiazzo M, Dell'Anno MT, Dvoretskova E, Lazarevic D, Taverna S, Leo D, et al. Direct generation of functional dopaminergic neurons from mouse and human fibroblasts. Nature. 2011 Jul 3;476(7359):224-7.